The Dissertation Committee for Cliff Andrew Jones Certifies that this is the approved version of the following Dissertation:

A Method for Developing the True Stress-Strain Relationship for Structural Steels Based on Tension Coupon Tests

Committee:

Michael Engelhardt, Co-Supervisor

Eric Williamson, Co-Supervisor

Todd Helwig

Patricia Clayton

Eric Taleff

A Method for Developing the True Stress-Strain Relationship for Structural Steels Based on Tension Coupon Tests

by

Cliff Andrew Jones

Dissertation

Presented to the Faculty of the Graduate School of

The University of Texas at Austin

in Partial Fulfillment

of the Requirements

for the Degree of

Doctor of Philosophy

The University of Texas at Austin

December 2019

Dedication

To my family and friends who supported me over the years and allowed me the space and time to pursue this degree; and most especially to my lovely wife, Rebecca, who has always supported, encouraged, inspired and, most importantly, believed in me.

Acknowledgements

This research would not have been possible without the support and creative thoughts and input from my co-advisors – Michael Engelhardt and Eric Williamson – my additional committee members – Todd Helwig, Patricia Clayton, and Eric Taleff – and the University of Texas at Austin. In addition, I owe a deep debt of gratitude and much of the credit for the finite element analysis techniques used to develop the recommendations presented in this dissertation to my colleagues and former co-workers at Protection Engineering Consultants (PEC): Matt Barsotti, Eric Sammarco, and Michalis Hadjioannou. Their encouragement, thoughtful analysis, constructive criticism, and generously given guidance played an instrumental role in allowing me to develop, refine, condense, and clarify this approach. My sincerest appreciation and thanks go out to each and every one of them.

Abstract

A Method for Developing the True Stress-Strain Relationship for Structural Steels Based on Tension Coupon Tests

Cliff Andrew Jones, Ph.D.

The University of Texas at Austin, 2019

Co-Supervisors: Michael Engelhardt & Eric Williamson

Predicting the uniaxial stress-stress response of ductile metals like structural steel can provide valuable insight into a broad range of engineering problems. Despite a wide body of research covering more than a century, the approach and guidance related to developing the true stress-strain relationship for ductile metals—specifically structural steels—continues to change and evolve. In particular, guidance related to accurate prediction of the onset of necking and post-necking response remains a topic of ongoing research and capturing these effects remains a challenge to researchers and engineers.

The research presented in this dissertation was undertaken to extend the body of knowledge in this area. Particular emphasis is placed on developing a true stress-strain relationship for structural steels that is capable of capturing the onset of necking and post-necking behavior up to fracture. In addition, as standard tension coupon load-deformation data are often the only available information from which to develop such a model, the processes and guidance presented in this dissertation require only that input information. Therefore, advanced experimental approaches and measurement techniques are not required to leverage the guidance presented herein. This path was chosen in the hopes of

providing guidance that would be broadly applicable to a wide range of problems, industries, research, and practicing professionals.

This dissertation proposes a method for developing a true stress-strain relationship for structural steels that can be directly used in predictive finite element analysis (FEA) models using three-dimensional (3D) solid elements. The result of this research indicate that such a model should be able to reproduce the experimental results of the tension test quite accurately, providing validation and verification of the assumed material definition. Additionally, three derivative rules are presented. These rules were distilled from existing research and provide simple guidelines for capturing necking, maintaining computational stability and uniqueness, and prohibiting post-necking cold-drawing behavior. The rules are incorporated into the recommended process for developing the true stress-strain relationship for structural steels; however, they are also presented separately so they can easily be incorporated into alternate methods for defining such a constitutive relationship.

Finally, while this research has furthered the understanding of the true stress-strain relationship of structural steels, particularly in predicting necking and post-necking behavior, there is still considerable room for additional research on this topic. For example, automation, incorporating error minimizing techniques, and adding local and material-level and microstructural phenomena (e.g., void formation, growth and coalescence) each offer great potential for extending and improving the recommendations presented in this dissertation. Thus, while this effort has intentionally maintained a limited focus, it is the authors hope that it serves others as one more small step toward accurate prediction of the load-deformation behavior of structural steels and other ductile metals.

Table of Contents

List of Tables

List of Figures

List of Variables

δ	Incremental deformation
Δ	Deformation measured during tensile testing
ε	True strain
$\dot{\varepsilon}$	True strain rate
ε_f	Engineering strain at tension rupture (failure strain)
ε_i	General increment of true strain
ε_{max}	True strain at maximum engineering stress, s_{max}
ε_{pi}	Plastic true strain value used in LS-DYNA where "i" is any integer
ε_{pl}	True strain at the proportionality limit
ε_{sh}	True strain at the onset of strain hardening
ε_y	True strain at yield
$d\boldsymbol{\varepsilon}$	General strain increment tensor
σ	True stress
σ_f	True stress at tension rupture (failure)
σ_i	General increment of true stress
σ_{LB}	Lower bound post-necking true stress-strain relationship
σ_{max}	True stress at maximum engineering stress, s_{max}
σ_{pi}	Plastic true stress value used in LS-DYNA where "i" is any integer
σ_{pl}	True stress at the proportional limit
σ_{sh}	True stress at the onset of strain hardening
σ_{UB}	Upper bound post-necking true stress-strain relationship
σ_y	True stress at yield
$d\boldsymbol{\sigma}$	General stress increment tensor
$d\sigma/d\varepsilon$	First derivative of the true stress-strain relationship Rate of material strain hardening
$\delta\sigma$	Incremental change in stress
$d^2\sigma/d\varepsilon^2$	Second derivative of the true stress-strain relationship
A	Current cross-sectional area including effects of deformation
A_o	Initial undeformed cross-sectional area

δA	Incremental change in area
dA/A	Rate of geometric softening
C_i	General or arbitrary constant, where "i" is an integer
E	Engineering elastic modulus
E_{max}	Engineering modulus at the onset of necking (equal to zero)
$E_{max\text{-}true}$	True modulus at the onset of necking
E_{sh}	Engineering strain hardening modulus
$E_{sh\text{-}true}$	True strain hardening modulus
E_{true}	True elastic modulus
F	Force
dF	Incremental change in force
L	Current length including effects of deformation
L_o	Initial undeformed length
P	Measured load during tension test
P_{max}	Maximum measured load during tension test
R	Radius of curvature at the center of the neck
T	Temperature
T_G	Glass transition temperature for polymeric materials
a	Radius of a cylindrical coupon specimen at the neck Half-width of a two-dimensional flat coupon specimen at the neck
e	Engineering strain
$\dot{e}$	Engineering strain rate
e_f	Engineering strain at tension rupture (failure strain)
e_{max}	Engineering strain at maximum engineering stress, s_{max}
e_{pl}	Engineering strain at the proportionality limit
e_{sh}	Engineering strain at the onset of strain hardening
e_y	Engineering strain at yield
δe	Arbitrary increment of engineering strain
r_0	Equilibrium (atomic) spacing for two isolated atoms
R^2	Coefficient of determination

s	Engineering stress
s_f	Engineering stress at tension rupture (failure)
s_{max}	Maximum engineering stress
s_{pl}	Engineering stress at the proportionality limit
s_{sh}	Engineering stress at the onset of strain hardening
s_y	Engineering yield stress
δs	Arbitrary increment of engineering stress
t	Time
t_i	Current thickness including effects of deformation
t_o	Initial undeformed thickness
v_{xh}	Cross-head velocity during tension testing
w	Function weighting variable used in curve fitting
w_i	Current width including effects of deformation
w_o	Initial undeformed width

1 INTRODUCTION

1.1 INTRODUCTION

The ability to understand and predict the uniaxial stress-stress response of ductile metals such as structural steel plays an important role in a broad range of industries and applications. While modeling the elastic and pre-necking inelastic stress-strain response is of primary interest in many engineering applications, predicting and modeling the onset of necking and the behavior beyond necking is also of interest in some applications. For example, there is increasing interest in predicting the initiation and propagation of ductile fracture in metals using advanced finite element analysis (FEA). Such analyses generally require that the stress-strain curve for the material be accurately characterized in the form of a true stress-strain relationship from the start of loading up to the initiation of fracture. True stress-strain relationships are generally derived from engineering stress-strain curves developed from tension coupon tests. Deriving the true stress-strain relationship from an engineering stress-strain curve prior to necking is straightforward. However, predicting the onset of necking and deriving the true stress-strain curve from an engineering stress-strain curve after necking can be significantly more challenging, and is the subject of the research reported in this dissertation.

This research effort seeks to improve the understanding and prediction of the onset of necking and the post-necking response of structural steels in tension; particularly for cases where only data from a standard coupon tension test are available. While complex methods of testing and measuring the post-necking tension response can be undertaken, standard tension coupon tests in accordance with ASTM E8 (American Society for Testing and Materials, 2016), and other similar standard methodologies, are normally the sole test performed. As a result, information available to develop a material true stress-strain

relationship for computational analysis are limited to basic coupon geometry and load-deformation data. Thus, this research was undertaken assuming only standard tension coupon test information is available to develop the true stress-strain relationship for a structural steel, which can then be used in FEA models. While a similar approach may be able to be applied to other ductile metals like aluminum and copper, additional investigation is recommended prior to extending the conclusions of this research to alternate materials.

The following sections describe in greater detail the need for additional research on this topic, as well as the basic objectives of this work in Section 1.2. Next, a brief summary of potential areas for application of the findings of this research is presented in Section 1.3, followed by a summary of the applicability and basic assumptions inherent in this research work in Section 1.4. Finally, Section 1.5 provides an outline of this dissertation including a brief summary of the content of each chapter.

1.2 RESEARCH NEED AND OBJECTIVES

While extensively studied, the onset of necking and post-necking response of ductile metals in tension is still not fully understood. Within the current body of research, oversimplification and inaccurate or imprecise assumptions about post-necking behavior have resulted in errors in modeling and simulation, which, in turn, result in errors in observations and conclusions drawn from these analytical and computational models. In addition, research on ductile material behavior is ongoing and there are many opportunities for incorporation and combination of these efforts to align and leverage the breadth and depth of their findings. Thus, this research work was undertaken to address some of these shortcomings and improve the engineering understanding of and ability to computationally predict post-necking response. In particular, the primary objective of this research was to

provide clear and detailed guidance on developing the constitutive true stress-strain relationship for the most common scenario where the only available data for comparison are the load-displacement and undeformed coupon dimensions from a standard coupon tension test.

The research presented herein is intended to inform the process of developing a true stress-strain relationship for use in FEA models using solid elements. Such a constitutive material relationship can then be used to develop a model capable of reproducing the experimental results of the tension test quite accurately and precisely, providing validation and verification of the assumed material definition. Eventually, the approach could, through additional research, be adapted to alternate element formulations and modeling approaches, and further improved through incorporating lessons learned from research on microstructural response and local necking in sheet metals. In its current form, however, the guidance and conclusions presented in this dissertation still have the potential for immediate application to a variety of areas as described in Section 1.3.

1.3 POTENTIAL AREAS FOR APPLICATION AND USE

Due to the broad use of structural steel across a variety of industries, the recommendations and conclusions of this research have the potential for immediate wide-ranging application. The following sections discuss a few key areas where there is current need for improved guidance in developing material constitutive relationships for structural steels, and where the results of this research could be directly applied. As noted, the focus of the research reported in this dissertation is on structural steel. However, the methods developed in this research can likely be applied to other ductile metals like aluminum and copper, with experimental verification and possible modification. Thus, the following

sections discuss possible applications of this research both for structural steel and for other ductile metals.

1.3.1 Structural Engineering

There are applications of the findings of this research to the field of structural engineering. In particular, where structural engineers attempt to understand the post-elastic response of structural metals, the derivative rules of Chapter 3 and the methodology for developing the true stress-strain relationship for computational modeling in Chapter 4, could prove useful. Applications include forensic and failure analysis, inelastic member buckling, and crushing of thin-walled structures. In addition, structural analysis problems where large plastic deformations or failure are expected can benefit from the work presented in this dissertation. These include prediction of partial or total collapse (i.e., progressive and disproportionate collapse), performance based seismic analysis, and analysis for other extreme loads such as those that might occur as a result of blast, impact, penetration, or perforation.

1.3.2 Metal Forming

Metal forming refers to the process of fashioning metal parts through mechanical manipulation and deformation. Often, these processes involve a variety of tactics to shape and plastically deform metals including compressive forming techniques like rolling, extrusion, die forming, forging, indenting, stamping and explosive forming; tension techniques such as stretching, expanding, and recessing; and combined tension and compression forming techniques such as die drawing, deep drawing, hot forming, superplastic forming, spinning, and bulging. These processes rely on a precise and accurate understanding of the non-linear post-elastic response of metals. As such, they can benefit from the improved understanding of the true stress-strain relationship for structural steels

presented in this dissertation; particularly for developing, modifying, and calibrating processes through analysis models, such as FEA.

1.3.3 Automotive Manufacturing and Crashworthiness

Due to the extensive use of sheet metal in automotive manufacturing, the value discussed in Section 1.3.2 for metal forming also applies to the automotive manufacturing industry. In addition, crashworthiness relies on understanding the buckling and failure of sheet metal materials, as well as plastic deformation of various parts and systems within the frame. As such, prediction relies on an in depth understanding of non-linear response of metals. Therefore, the conclusions and methodologies presented in this paper could be directly applied to improving the speed and accuracy of the developed material true stress-strain relationships for analysis of automotive manufacturing processes and crashworthiness.

1.4 Applicability and Inherent Assumptions

The methodology and proposed rules are intended to be used when developing the true stress-strain relationships for structural steels but are also expected to be applicable to other ductile metals such as aluminum and copper with additional validation and verification. This dissertation is not intended to provide guidance, however, for brittle structural materials (e.g., glass, concrete and stone), ductile non-metallic materials (e.g., plastics and polymers) or other non-structural metals and materials. In addition, this dissertation focuses specifically on developing true stress-strain relationships for use in FEA using three-dimensional (3D) solid continuum elements from load-deformation information obtained in a standard coupon tension test. Use of alternate element formulations is recommended as a topic for future research in Section 6.3.2, and discussed briefly in Appendix Section B.4. Finally, certain behaviors were neglected in the

development of the recommendations presented in this dissertation. These neglected behaviors are discussed in Section 2.4.

Because the presented approach is meant to be broadly applicable to a range of problems, and utilize only the load deformation data from a coupon tension test, it does not require advanced measurement techniques or specialized equipment, although these topics are discussed briefly in Section 2.9.3. In addition, the models proposed for analysis were developed for standard FEA using commercially available software and typical simplifying assumptions including material isotropy, continuum solid element formulations, and material homogeneity.

It is possible that the methods and recommendations presented in this dissertation could be improved by applying these more complex approaches; however, that would defeat the overall goal of broad applicability and the requirement for only standard tension test data and coupon geometry as the inputs, and standard FEA software and techniques as the means of developing the true stress-strain relationship. Though, incorporation of some of these more advanced techniques and lessons learned through their application is recommended in the discussion of future work and research in Section 6.3.

1.5 DISSERTATION OUTLINE

The introductory material to this dissertation includes a table of contents, followed by a list of figures and tables. Next, a list of variables is provided. These variables are used throughout this dissertation. For clarity, equations developed and presented in this dissertation generally use a single unique variable for each quantity or property. Where possible, repetition of variables for multiple quantities and properties was avoided. For cases where variables are repeated, the definition should be made clear through context.

Chapter 1 provides the introduction to this dissertation followed by a brief summary of the need for, and objectives of, this research. Next, the applicability of the presented methodology is briefly discussed, followed by this section, which provides an outline of this dissertation and a brief summary of the contents of each chapter.

Chapter 2 provides a brief introduction to engineering and true stress and strain, a summary of the typical response of ductile metals during a standard coupon tension test, and a detailed summary of the broad range of literature reviewed as part of this research. Reviewed and cited references including textbooks, journal papers, technical presentations, websites, and college course materials. Related research is generally organized by topic, rather than chronologically, to provide a clearer picture of the context and relationships between various published research related to material response of ductile metals. As a result, references may appear multiple times in different sections of this chapter. In addition, due to the extensive history of research on necking and post-necking response of ductile metals, there are surely many published works that were not cited. These works were omitted for brevity only and their omission does not imply a lack of importance.

Chapter 3 presents theoretical support for three proposed derivative "rules" that should be obeyed when developing the true stress-strain relationship for ductile structural steel in tension for use in an FEA model using 3D elements. Each derivative rule and its theoretical basis is described in detail in this section, along with the math associated with its derivation and development. At the chapter's conclusion, the three rules are collected and re-presented together to illustrate their simplicity and similarity.

Chapter 4 illustrates the step-by-step method of developing the true stress-strain relationship for use in FEA. For clarity, the experimental stress-strain curve is divided into five zones of response, with each discussed individually. The zones of response include (I) linear elastic, (II) nonlinear elastic, (III) yield plateau, (IV) strain-hardening, and (V) strain

softening. For each zone, guidance is provided for developing the true stress-strain relationship within each zone. In addition, guidance is provided for the transitions between zones including constraints when using mathematical functions to fit the various zones of response. This chapter also includes the math and derivations underlying the recommendations and, where possible, provides simple equations for various key quantities used to define the true stress-strain relationship.

Chapter 5 provides an example case for developing the true stress-strain relationship for finite element analysis using the methodology from Chapter 4. The only inputs are the engineering stress-strain relationship calculated directly from a load-deformation curve from a steel tension coupon test, and the coupon geometry. Considerable efforts were applied to refine the developed relationship in order to demonstrate the level of accuracy that can be achieved through application of the methodologies proposed in this dissertation.

The remainder of this dissertation provides summary and supporting background information. Chapter 6 summarizes the basic conclusions of this research effort, along with a discussion of future work related to post-necking response of structural steels and other ductile metals in tension. Appendix A provides background information on experimental data used throughout this dissertation to illustrate different features of measured load-deformation and engineering stress-strain curves. Appendix B provides a summary of key information related to the FEA models used in this dissertation. The sections include a brief and informal discussion of several topics including the model geometry, boundary conditions, element formulations, solver controls and settings, the material model, the load application process, outputs and model interrogation, and fracture. The information is provided specifically for use in LS-DYNA and LS-PrePost, the software packages used to develop and document this approach; however, the main points of discussion are generally

applicable to any similar commercially available finite element analysis software (e.g. ABAQUS, ANSYS and others). Finally, a list of references cited throughout this dissertation, denoted using parentheses in the following format "(Author(s), Year of Publication)," is provided at the end of this dissertation.

2 BACKGROUND

2.1 INTRODUCTION

This chapter provides essential background information about ductile metals focusing on structural steels. General characteristics are described in Section 2.2. Response to uniaxial loading in tension is presented in Section 2.3, which is followed by a discussion of neglected behaviors (i.e., those intentionally ignored) in Section 2.4. Next, the atomic structure of ductile metals is briefly introduced and discussed in Section 2.5 within the context of response to tension loads and deformations, followed by a discussion of engineering and true stress and strain, including a summary of the typical features of the engineering stress-strain curve for ductile metals in Section 2.6. Section 2.7 includes a discussion of true stress and strain in the context of uniaxial tension. Sections 2.8 and 2.9 describe a range of published research including analytical, numerical and experimental studies focused on the investigation, interpretation, and prediction of the tension response and true stress-strain relationship for ductile metals, with a focus on accurately predicting the onset of necking and post-necking behavior. Finally, Section 2.10 briefly discusses tension response of select non-metallic materials and concluding remarks for the chapter are included in Section 2.11.

2.2 DUCTILE METALS

In the context of this dissertation, the term *ductile metals* refers to metallic materials that exhibit significant inelastic (plastic) deformation prior to failure. This description includes both pure metals, as well as ferrous and nonferrous metallic alloys. Examples include iron, copper, lead, tin, and aluminum, as well as their many alloys, like steel, brass, and bronze. Provided the pure metal or alloy undergoes significant plastic deformation prior to failure in tension, including necking, it is considered a ductile metal in the context

of this dissertation and the following discussion. Although the discussion broadly applies to all ductile metals, it was developed with a focus on structural steels.

2.3 Uniaxial Response of Ductile Metals

Included in this section is a qualitative discussion of the response of ductile metals to uniaxial tension loading, including a brief discussion of the microstructure of ductile metals and its effect on observed tension response, which is addressed in greater detail in Section 2.5. Because the focus of this dissertation is on capturing this response analytically using only data from a standard tension test, the discussion of atomic microstructure effects has been purposefully simplified to provide context without delving too deeply into the nuances of the topic. For additional information on the uniaxial response of ductile metals and the effects on the atomic microstructure, a variety of academic texts are available (Beer, Johnston, Jr., & DeWolf, 2002) (Boresi & Schmidt, 2003) (Callister, Jr., 2007) (Ugural & Fenster, 2003) (Boyer, 1987) (Courtney, 1990) (Hayden, Moffatt, & Wulff, 1965).

Ductile metals, which include steel, aluminum and copper, are characterized by their ability to yield and deform plastically at normal environmental temperatures (e.g., room temperature). When subject to uniaxial loading at normal temperatures, they initially respond elastically, where deformation is linearly proportional to the applied load and recoverable upon unloading. After the linear-elastic range, a ductile metal loaded in uniaxial tension will typically yield, deforming plastically. The majority of deformation occurring after the onset of yield is inelastic, or “plastic”, and non-recoverable. Shearing stresses are primarily responsible for plastic deformation and failure of ductile materials. In contrast, normal stresses are primarily responsible for the failure of brittle (non-ductile) materials (Beer, Johnston, Jr., & DeWolf, 2002).

After a certain maximum value of load has been reached, a local instability occurs in the ductile metal under uniaxial tension loading. This local instability occurs when the ability of the material to harden can no longer keep up with the reduction in section necessitated by conservation of volume. This initiation of local instability is referred to as the onset of necking Figure 2-1. After necking has occurred, the load carrying capacity of the specimen begins to drop, and these lower loads are capable of elongating the specimen further until rupture finally occurs.

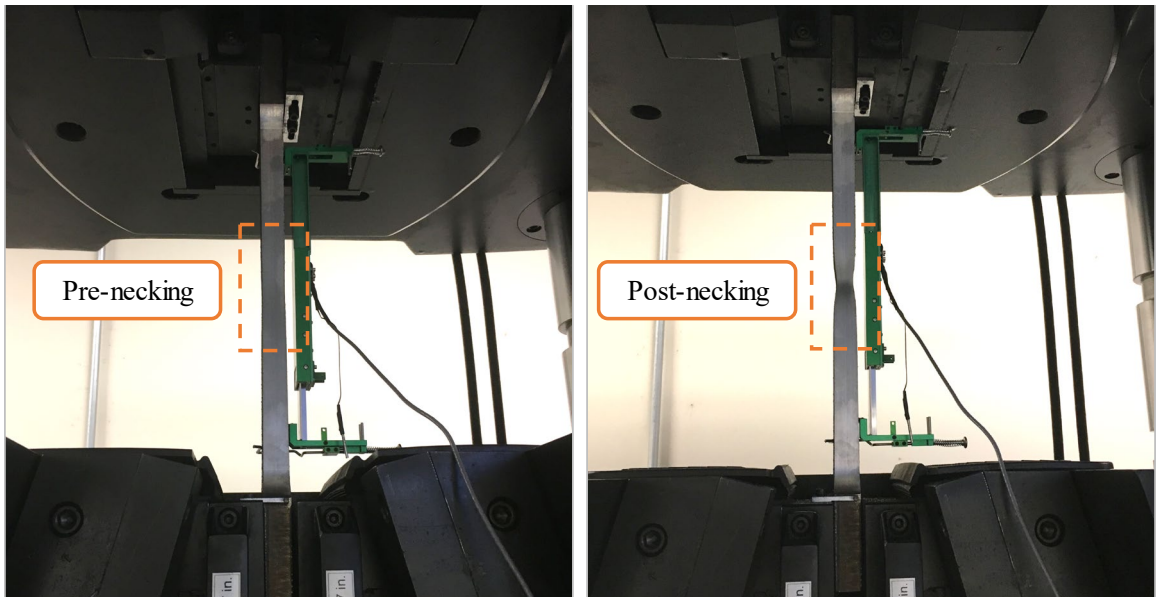

Figure 2-1: Steel Coupon Necking in Tension

An illustrative example of the load-deformation response observed in a typical tension test is presented in Figure 2-2, highlighting the elastic and inelastic (or plastic) ranges of response, as well as the onset of necking, and pre- and post-necking ranges of response. This curve is intentionally not drawn to scale and is intended to illustrate typical features exhibited by ductile metal materials, specifically mild carbon steel. It should be noted that not all features will be present in the data generated by any given ductile metal

test. For example, many non-steel ductile metals do not exhibit a well-defined yield plateau.

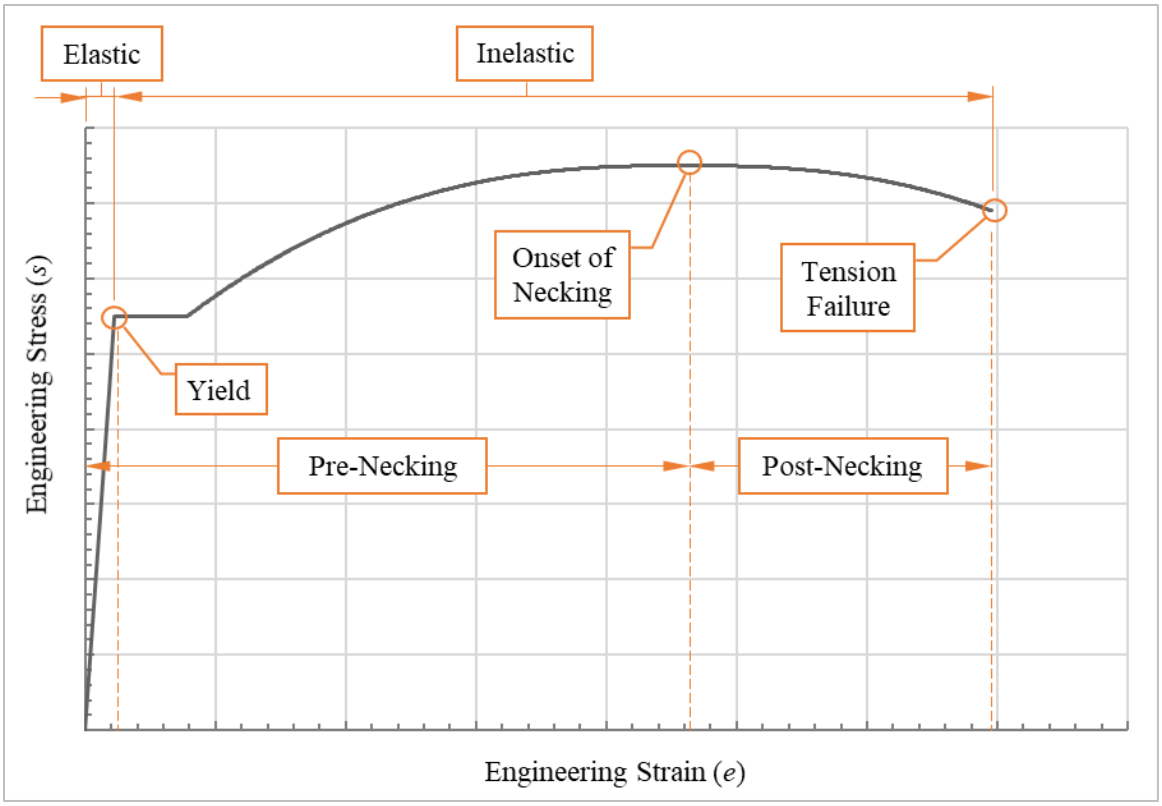

Figure 2-2: Idealized Engineering Stress-Strain Curve for Ductile Metal in Uniaxial Tension (Not to Scale)

2.4 NEGLECTED BEHAVIORS

To focus the overall scope of this study, certain behaviors, modes of response, and other complicating factors were intentionally neglected. The following paragraphs briefly summarize these cases, providing justification for neglecting them in this study. The list is not intended to be complete or exhaustive; rather, it focuses on the most commonly cited phenomena in the literature related to stress-strain response of ductile materials, that may

manifest error in the proposed "rules" and recommendations presented in this dissertation for capturing material-level response of ductile metals.

Anelasticity and creep are neglected in this study. Anelasticity is the term that refers to time-dependent elastic response of materials. Creep is a typically permanent time-dependent plastic response of a material. Creep deformations often occur as a result of long-term exposure to stresses below yield and/or high temperatures. These phenomena were neglected due to the long-term nature of these phenomena and the breadth of influencing factors impacting creep and inelastic response. In addition, because the focus of this work is on necking and post-necking response, behaviors that typically manifest just prior to failure, long-term effects like anelasticity and creep are typically not significant contributors to behavior in this regime.

Strain-rate effects are also neglected in this study. Materials deformed such that their strains change quickly can exhibit strain-rate effects. Most commonly, strain-rate effects in ductile metals are characterized by increasing stiffness and perceived strength as the rate of change in stress and strain are increased. For materials loaded slowly or those that bear static loads, strain-rate effects are insignificant and often neglected. Conversely, materials loaded extremely quickly from impact, blast, seismic, or other rapidly applied or changing load, will often exhibit strain-rate effects. To capture strain-rate effects in a computational model, material stiffness, often captured by the modulus of elasticity or other post-yield modulus, and strength, including yield, ultimate, or other, as appropriate, will be increased when compared to the same material loaded statically or quasi-statically. Strain-rate effects are typically captured by applying a standard amplification relationship to static properties. The recommendations in this dissertation neglect these rate-dependent behaviors, assuming they can be incorporated, as required, using standard approaches.

Temperature effects and thermal properties are neglected in this study. Temperature can affect the elastic and plastic properties of ductile metals. Increasing temperature often manifests decreased material strength and stiffness and vice-versa. Temperature effects were neglected to ensure the conclusions developed in this study remain concise. Like strain-rate effects, temperature effects and thermal properties are typically applied to scale static values; thus, it is assumed they can be incorporated, as required, using standard approaches.

2.5 Atomic Structure and Microstructure Behavior of Ductile Metals

To provide context for the discussion of microstructural post-necking phenomena in Section 2.9.4, the following sections provide an introduction to, and summary of, the atomic structure of ductile metals and their response to elastic and inelastic deformations. On a microstructure level, metals are crystalline solids, meaning their atoms exhibit an orderly arrangement, unlike amorphous materials like glass. The general crystalline atomic structure of ductile metals is introduced and discussed in Section 2.5.1. The subsequent sections, 2.5.2 and 2.5.3, describe the atomic and microscopic response of ductile metals to elastic and inelastic deformations, respectively. The information presented is intentionally simplified to convey the basic concepts of metallic materials and their structure. Additional information on the atomic structure and microstructure behavior of ductile metals can be found in a variety of sources (Callister, Jr., 2007) (Askeland & Fulay, 2004) (Askeland, Fulay, & Wright, 2011).

2.5.1 Atomic Crystalline Structure of Ductile Metals

Typical ductile metals like steel, copper, and aluminum exhibit a crystalline atomic structure. Crystalline materials have a regular, repeating, orderly, three-dimensional atomic structure. Their atoms are joined together through atomic bonds; for metals, these are

generally metallic bonds where valence electrons — those that occupy the outermost shell of electrons — are not bound to any particular atom. Rather, the valence electrons are shared, drifting freely throughout the metallic material. These shared electrons, commonly referred to as a "sea" or "cloud" of electrons, shield the positively charged ion cores formed by the nuclei and remaining non-valence electrons from their otherwise repulsive electrostatic forces bonding the system together. Due to their atomic bonding arrangement and sea of electrons, metallic bonds are generally non-directional in nature.

Ductile metals exhibit a variety of relatively simple crystalline structures. The simplest repeating unit within a crystalline structure is referred to as a unit cell. The unit cell geometry varies depending on the material and a range of other factors, including temperature and the formation process. The atoms of ductile metals tend to pack together tightly due to the nature of the metallic bonds, forming three typical crystal structures, face-centered cubic (FCC), body centered cubic (BCC), and hexagonal close-packed (HCP). Idealized representations of these typical crystalline structures are illustrated in Figure 2-3.

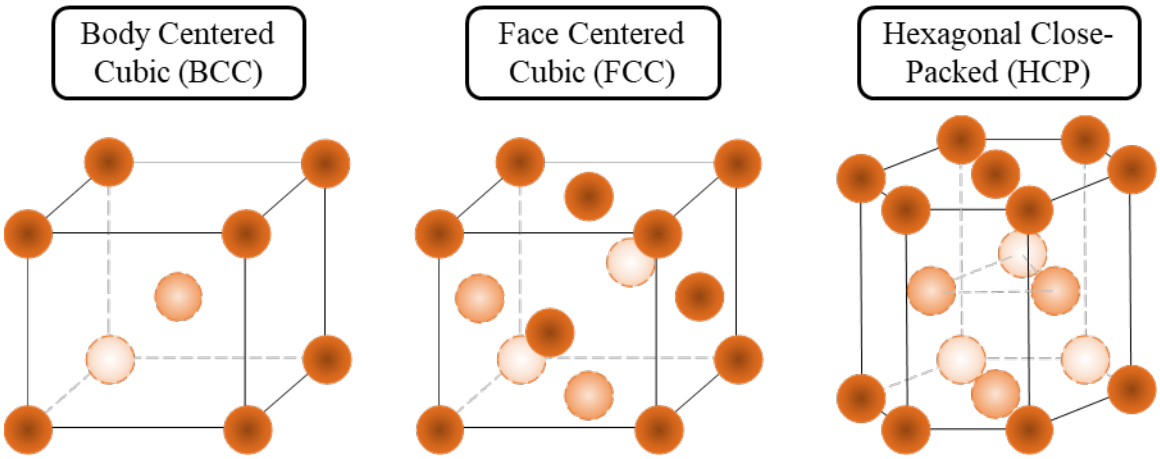

Figure 2-3: Typical Unit Crystal Structures for Ductile Metals

Some properties of crystalline solids, such as ductility, are influenced by their crystal structure. The response of these structures depends upon the number of slip systems,

which are essentially preferred planes upon which deformation and movement of atoms can occur, inherent in the system. For example, BCC and FCC structures have a relatively large number of slip systems; specifically, 12 or more. Conversely, HCP systems have between three and six. As a result, HCP structured metals are much more brittle than those with BCC or FCC structures. Table 2-1 provides a list of common metals and their atomic structure. Note that many common brittle metals like cadmium, cobalt, titanium, and zinc typically exhibit an HCP structure.

Table 2-1: Crystal Structures of Common Metals (Callister, Jr., 2007)

Metal	Crystal Structure	Metal	Crystal Structure
Aluminum	FCC	Molybdenum	BCC
Cadmium	HCP	Nickel	FCC
Chromium	BCC	Platinum	FCC
Chromium	HCP	Silver	FCC
Copper	FCC	Tantalum	BCC
Gold	FCC	Titanium	HCP
Iron	BCC	Tungsten	BCC
Lead	FCC	Zinc	HCP

Steel can exhibit both FCC and BCC structures depending on the manufacturing process and alloying elements used; thus, it is called a polymorphic material. Polymorphism, or allotropy, refers to materials that have more than one crystal structure. Another example is iron, which has a BCC crystal structure at room temperature, but transitions to a FCC crystal structure when subject to higher temperatures in excess of approximately 900^{o}C (Callister, Jr., 2007).

In addition, alloying elements, impurities, and other defects can influence the crystal structure and affect material properties. As a result, these idealized unit cells and crystals can exhibit a range of variations that can influence their physical properties. While

a detailed discussion of microstructure defects is beyond the scope of this dissertation, it is important to note that, due to their extremely small size, high volume, and relatively random distribution within most ductile metals, the resulting properties can typically be assumed to be homogeneous for most engineering applications.

These crystalline structures form the basis for the atomic structure of ductile metals. Although it is possible to develop single large crystals with uniform structure, it is extremely difficult and rare. Thus, most standard forming and processing techniques develop ductile metals that are polycrystalline. Polycrystalline materials are made up from many small crystals, often referred to as grains. These grains are localized regions of similar crystalline orientation and abut each other along grain boundaries. The shape, size, type, and distribution of grains all influence material response. Similar to defects, due to their typically small size, high volume, and relatively random distribution within most ductile metals, the resulting material properties can typically be assumed as homogeneous for most engineering applications. For reference, Figure 2-4 is an image illustrating crystalline grains within a stainless steel specimen.

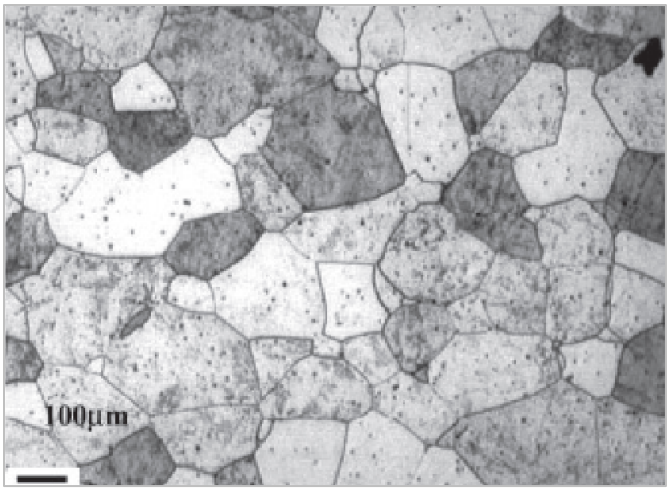

Figure 2-4: Crystalline Grains in Stainless Steel (Askeland, Fulay, & Wright, 2011)

The mechanical response of ductile metals to stresses is generally some combination of deformation and movement within the atomic unit crystalline cell, movement within crystalline grains, movement and changes precipitated at imperfections, and interactions among grains. While these topics have been extensively studied, and documented, the following sections provide a simple overview of the general mechanisms by which metals deform elastically and inelastically, in Sections 2.5.2 and 2.5.3, respectively. These discussions are intended only to provide context to later discussions of microstructure response. Ultimately, for engineering analysis, these mechanisms of microstructural movement are generally neglected and replaced by simpler models capturing their aggregate effects, like engineering stress and strain, which is described in Section 2.6, and true stress and strain, as discussed in Section 2.7.

2.5.2 Elastic Deformation of Ductile Metal Materials

Elastic deformation is characterized by a change in shape due to applied stress that is recovered when the applied stress is removed. During elastic deformation, intermolecular bonds are stretched, resulting in small changes in interatomic spacing, but no permanent change to the material or its internal microstructure occurs. As a result, elastic deformations are recoverable upon unloading.

The perceived stiffness while undergoing elastic deformation is characterized by the modulus of elasticity, E, which is also known as the elastic modulus or Young's modulus. The value of this parameter is proportional to the slope of the interatomic force-separation curve at the equilibrium spacing, r_0, where the equilibrium spacing refers to the interatomic separation distance where attractive and repulsive forces balance in the absence of outside forces. As shown in Figure 2-5, for two isolated atoms at the equilibrium separation distance, net force is zero (i.e., attractive and repulsive forces balance), and the potential energy is at a minimum. For typical atoms, the equilibrium spacing is

approximately about 0.3 nm (Callister, Jr., 2007). In Figure 2-6, the elastic response is illustrated on an idealized load-deformation curve representative of a typical ductile metal coupon tested in tension. Note that, relative to the total deformation capacity, the elastic response is quite small. In addition, it has been extended for illustration purposes. In reality, it is often much shorter, encompassing less than one percent of the total deformation capacity of ductile metals.

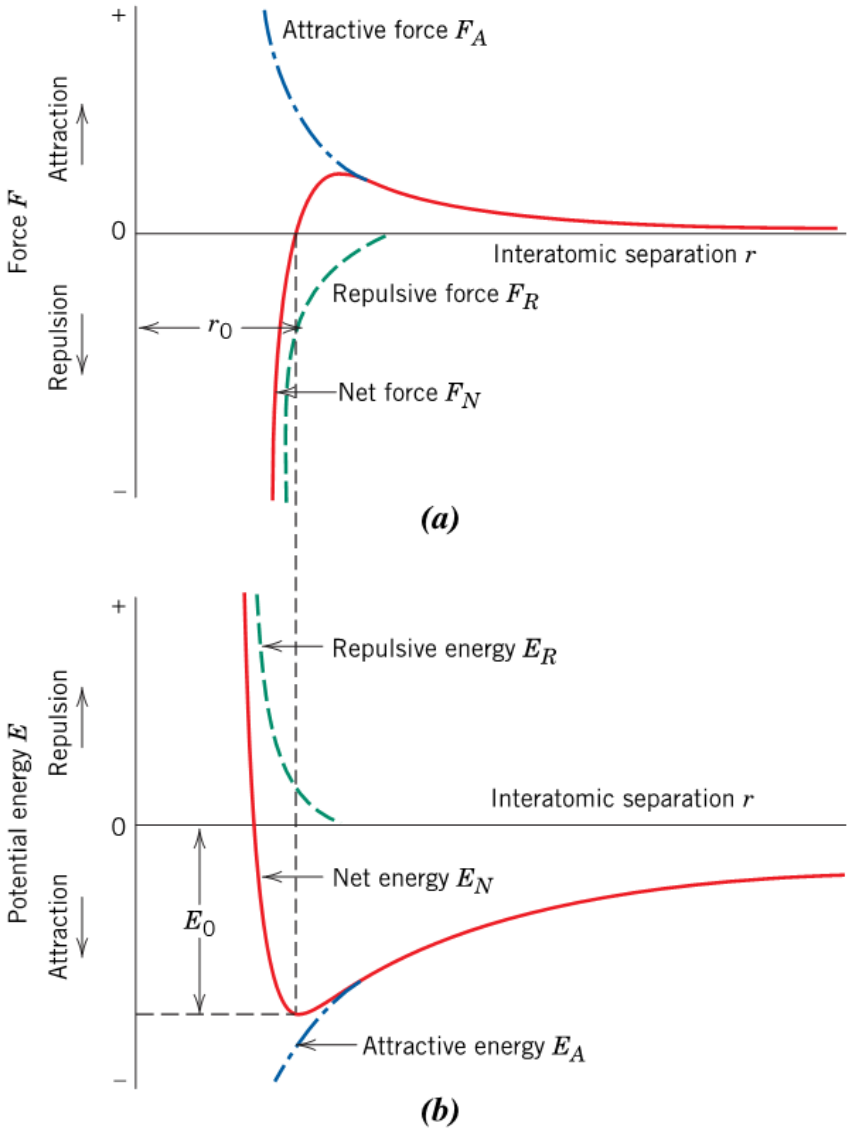

Figure 2-5: (a) Net Force and (b) Potential Energy Relationships for Two Isolated Atoms (Callister, Jr., 2007)

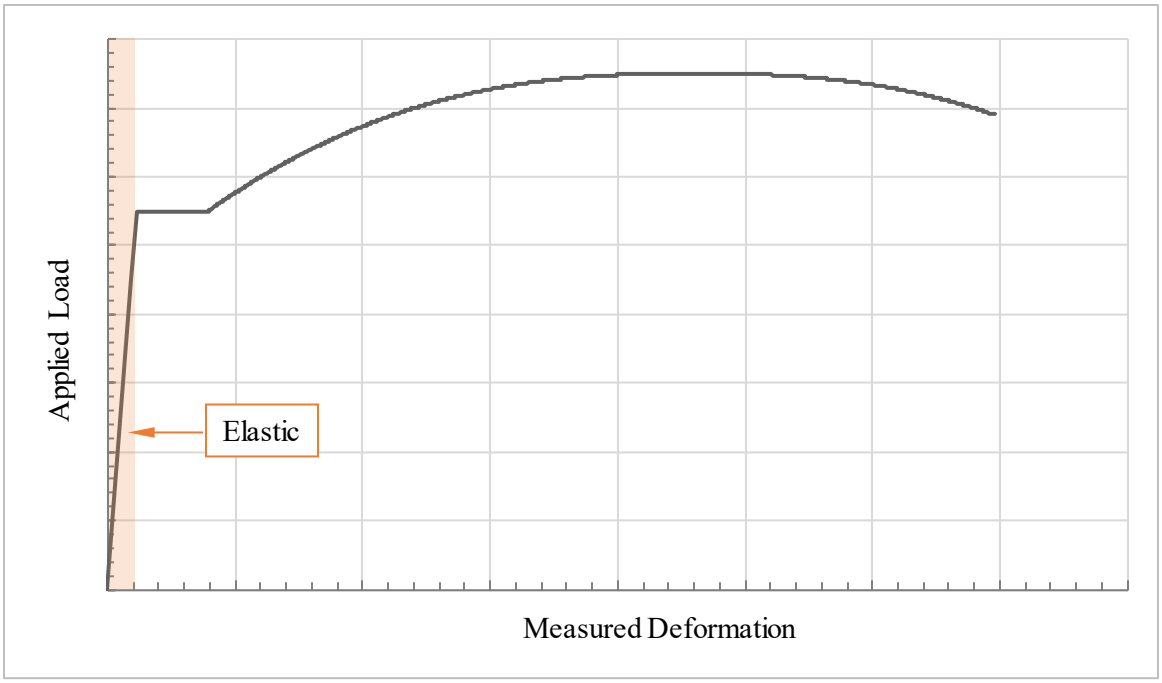

Figure 2-6: Elastic Deformation Regime for Idealized Load-Deformation Curve

Thus, as the response in the elastic deformation regime can be approximated by treating the material like a simple spring with stiffness equal to the elastic modulus, *E*. However, when sufficient stress is applied to permanently deform a material, the stretching of intermolecular bonds is no longer the only way in which the material deforms. This permanent deformation is called inelastic or plastic deformation. Inelastic deformation is the result of a variety of deformation mechanisms within the material, which are described in the following section.

2.5.3 Inelastic Deformation of Ductile Metal Materials

Inelastic deformation, also called plastic deformation, is caused by stresses large enough to cause permanent deformation in a material. As the name suggests, these permanent deformations remain even after loads are removed. For ductile metals, the bulk of the deformation capacity is a result of their ability to deform inelastically, as illustrated in Figure 2-7.

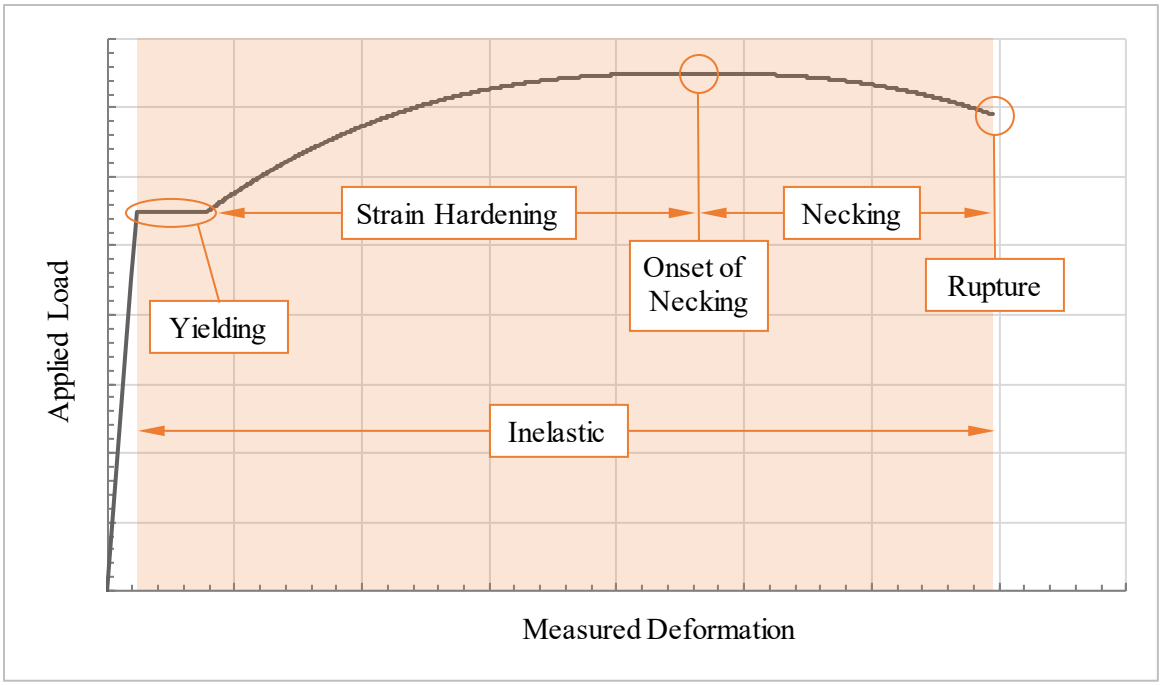

Figure 2-7: Inelastic Deformation Regime for Idealized Load-Deformation Curve

Inelastic deformation is a result of several different microstructural movement mechanisms that break and shift atomic bonds within the material. Note that, while the stress required to completely break the atomic bonds can be quite high, the stress required to shift them is much lower (Askeland, Fulay, & Wright, 2011). Inelastic deformation is essentially this shifting of atomic bonds and it occurs along preferential low-strength planes of movement within and between crystals, such as along grain boundaries or other defects within the crystalline structure. As noted previously for defects and grains, due to the random orientation and relatively uniform distribution of these "slip" planes, the observed properties of most ductile metal materials appear non-directional or isotropic in nature (Dieter, Jr., 1961).

One example of inelastic deformation is yielding (see Figure 2-7). During yielding, the specimen undergoes large deformations relative to the change in applied load, caused at the microstructure level by slippage along oblique surfaces due primarily to shearing

stresses. This process results in breaking molecular and atomic bonds with original atom neighbors and reforming bonds with new neighbors. Thus, during yielding, the crystalline microstructure is permanently changed, and most of the post-yield deformation is plastic and not recoverable upon unloading.

Plastic deformation during yielding occurs as a result of slip within the crystalline structure that typically begins at imperfections in the crystal lattice. Because slip does not occur simultaneously at all locations, deformation appears discontinuous on the microscopic level of crystalline grains. The overall effect at a macro-level, however, is often approximated by a perfectly plastic solid. As deformation continues, a locking of these dislocations can occur, resulting in strain hardening, which is observed as an increase in stiffness of the material. This strain hardening process is generally assumed to occur up to the point of necking, causing slip at higher and higher levels of stress.

At a certain point, the load will reach a maximum. This maximum load is referred to as the onset of necking, as shown in Figure 2-7. Beyond this point, deformations will concentrate in a reduced area causing a local reduction in section, called necking (see Figure 2-1). As the specimen necks, the measured load will decrease until rupture occurs. During this necking response, another deformation mechanism contributes to the observed material deformation — void nucleation, growth, and coalescence. During void nucleation, growth, and coalescence, small cavities form, which are called microvoids or simply voids. With increased deformation, these voids grow. As they increase in size, they begin to join, eventually forming a crack across the specimen. Ultimately, the process ends in tension rupture when the crack grows to the point where the edges are completely sheared. This process is illustrated in Figure 2-8 and discussed in additional detail in Section 2.9.4.2.

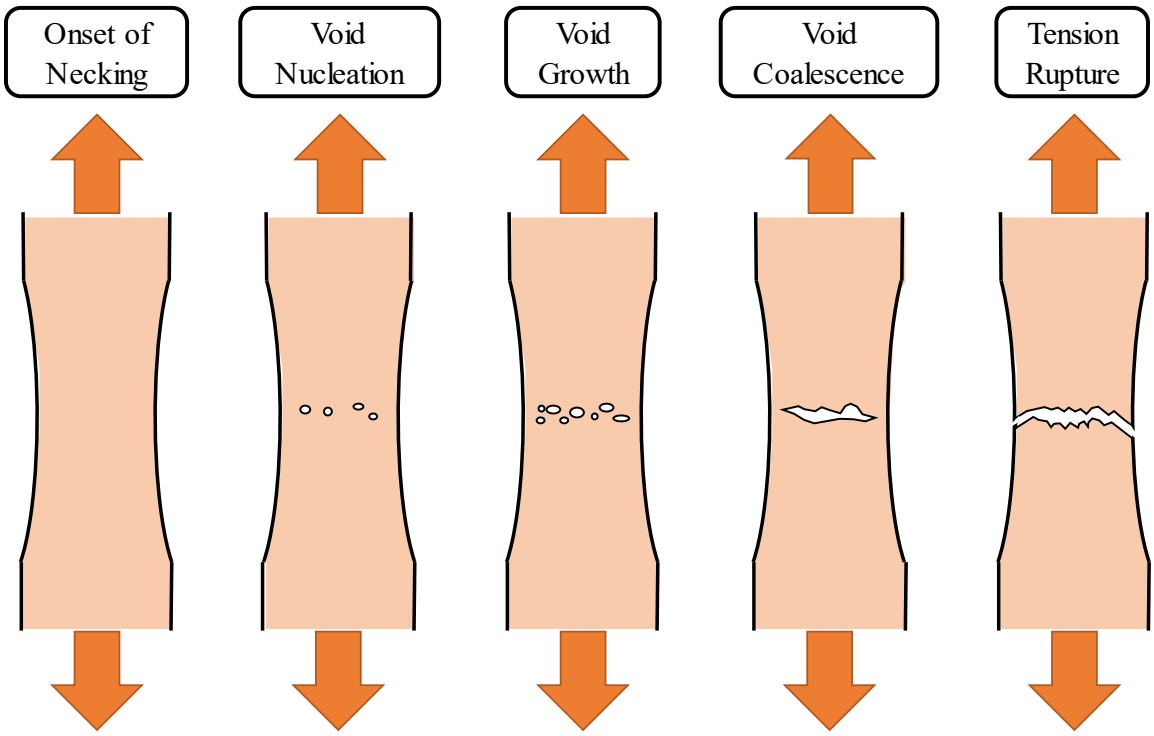

Figure 2-8: Void Nucleation, Growth, and Coalescence

Note that void nucleation, growth, and coalescence is just one mechanism for deformation after necking. Slip within the crystal microstructure still occurs during this regime of response. In fact, slip is the dominant mode of response early in the necking regime because voids are still quite small and relatively few in number (Askeland, Fulay, & Wright, 2011). However, as the specimen approaches rupture and voids become more numerous and larger, the dominant deformation mechanism shifts toward voids, until the point of rupture where the deformation is nearly entirely the result of void growth and coalescence (Benzerga, Leblond, Needleman, & Tvergaard, 2016).

Now that typical uniaxial tension testing procedures and deformation characteristics of ductile metals have been introduced, simplifying approximations of these process can be considered. The following sections describe two different approximation levels for material response under uniaxial loading — engineering and true stress and

strain. The engineering stress-strain relationship, presented in Section 2.6, is the most commonly used approximation for material response. It is nearly exact for elastic response; however, it can become quite inaccurate, particularly at large deformations, due to its underlying simplifying assumptions. The true stress-strain relationship, which provides a more thorough and complex approximation than engineering stress-strain, is described in Section 2.7. True stress-strain directly accounts for the specimen deformation in its derivation. Thus, it provides a more precise model of material behavior under large deformations. The true stress-strain relationship is the focus of this dissertation.

2.6 ENGINEERING STRESS AND STRAIN

Engineering stress and strain are the most common way engineers communicate the strength and deformation characteristics of ductile metal materials. These characteristics, often denoted as mechanical properties, are particularly important when determining the structural response of materials to imposed loads and deformations. For typical ductile metals, the engineering stress-strain relationship is determined through standard laboratory tests of specially fabricated specimens. The simplest and most common test used to develop mechanical properties for ductile metals is the coupon tension test. Properties determined from a standard coupon tension test are often used to develop mechanical properties that characterize material response in tension as well as compression, shear, torsion and combined states of stress and deformation.

Tension testing of ductile metals is typically performed in accordance with the *ASTM E8 – Standard Test Methods for Tension Testing of Metallic Materials* (American Society for Testing and Materials, 2016), or, more specifically for steels, *ASTM A370 – Standard Test Methods and Definitions for Mechanical Testing of Steel Products* (American Society for Testing and Materials, 2015). Per these standards, a tension coupon,

often referred to as a “dogbone” specimen due to the shape, is developed with standardized dimensions prescribed in the associated test standard. An example using nomenclature from the aforementioned tension test standards is provided in Figure 2-9. These tension coupons are intentionally shaped to provide wide ends that can be easily gripped and pulled during testing, along with a narrow center section within which all plastic deformation will be confined.

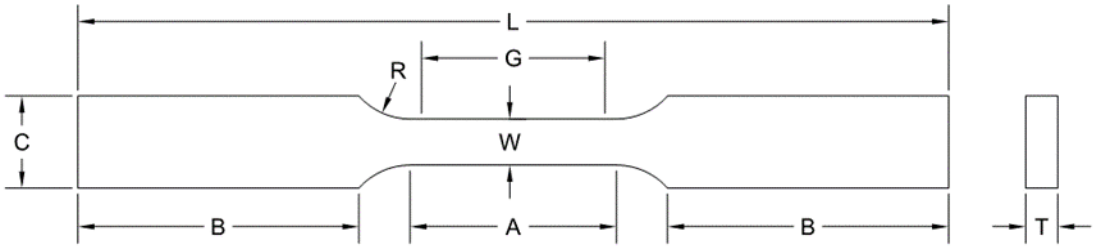

Figure 2-9: Generalized Tension Coupon Geometry

where G = Gauge Length

W = Width

T = Thickness

R = Radius of Fillet (minimum)

L = Overall Length (minimum)

A = Length of Reduced Parallel Section (minimum)

B = Length of Grip Section (minimum)

C = Width of Grip Section (approximate)

Applied load is typically measured using a load cell built into the testing machine, and displacement is typically measured using an extensometer. An extensometer is an instrument that measures elongation of the coupon over the gauge length (“G” in Figure 2-9). There are many types of extensometers available including contact (those that attach directly to the test specimen) and non-contact (those that optically track deformations

without touching the test specimen). Figure 2-10 is an image of a contact extensometer, the most common type used in tension testing of ductile metals. The extensometer is attached to a steel coupon during a tension test. Detailed information on tensile testing and typical stress-strain curves for engineering materials is available in engineering literature (Boyer, 1987) (Davis, 2004) (ASM International, 2002).

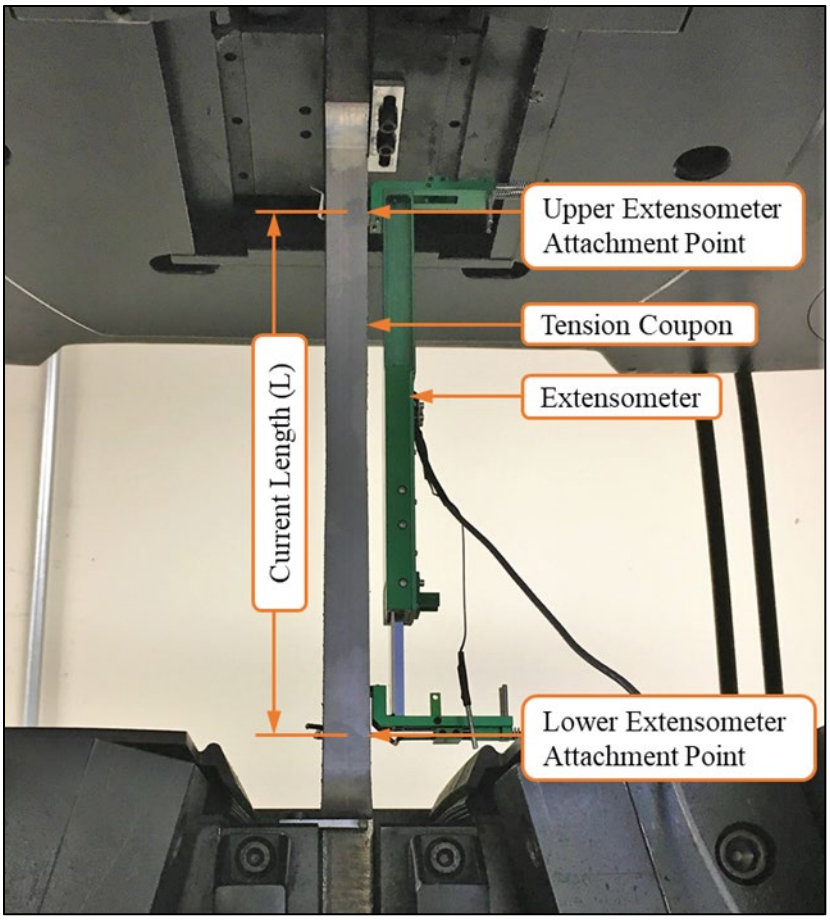

Figure 2-10: Tension Coupon during Testing showing Contact Extensometer

Measured load data from a tension test can be converted to engineering stress, *s*, using Equation 2-1. Similarly, deformation data can be converted to engineering strain, *e*, using Equation 2-2. The units for engineering stress are load per unit area. Because

measured deformation (change in length, Δ) is divided by the initial length to calculate engineering strain, strain is a dimensionless quantity.

$$s = \frac{P}{A_o} \qquad \text{Equation 2-1}$$

$$e = \frac{L - L_o}{L_o} = \frac{\Delta}{L_o} \qquad \text{Equation 2-2}$$

where P = Measured load

A_o = Initial cross-sectional area of the specimen

L = Current length measured by the extensometer

L_o = Initial length measured by the extensometer

Δ = Deformation measured by the extensometer

These standard conversions are used to develop the engineering stress-strain (s-e) relationship, and they are also used to determine mechanical properties of the material, which are often called engineering properties. These engineering properties can then be used in design, including properties such as elastic modulus, E, yield stress, s_y, strain hardening modulus, E_{sh}, ultimate strength, s_{max}, and rupture strain, e_f. The engineering stress-strain relationship is commonly plotted with stress on the ordinate axis and strain on the abscissa, as illustrated in Figure 2-11.

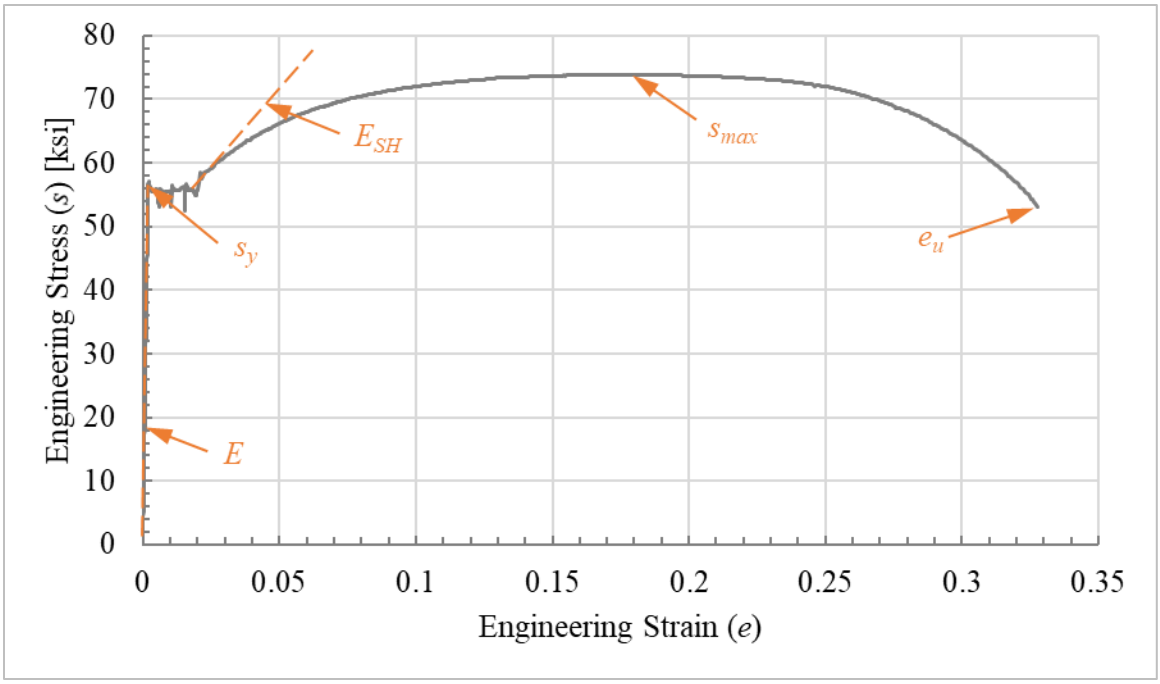

Figure 2-11: Typical Ductile Metal Engineering Stress-Strain Curve

To obtain the engineering stress-strain diagram for ductile metal materials, a tensile test, described in earlier in this section, is the most common approach (Beer, Johnston, Jr., & DeWolf, 2002). It should also be noted that different tensile tests conducted on the same material will yield different results. Differences between tests can be small or vary widely depending on the circumstances. These variances are due to a range of factors, such as minor changes in geometry and precise cross-sectional dimensions of the specimen, out-of-straightness of the sample in the test machine, variability in material properties throughout the sample, relative location of the necked region within the gauge length, rate of loading and deformation during the test, and many other sources as discussed in more detail in Section 2.6.1. Many of these variances manifest particularly clearly in the post-ultimate branch of the curve, after the onset of necking. Figure 2-12 and Figure 2-13 illustrate the variability between measured engineering stress-strain curves for coupons with the same geometry and materials, ASTM A992 Gr. 50 structural steel and ASTM

A653 cold-formed sheet metal, respectively. Data used in these figures were derived from work by others (Hadjioannou, 2015). Refer to Appendix A for additional information on the experimental data presented throughout this dissertation.

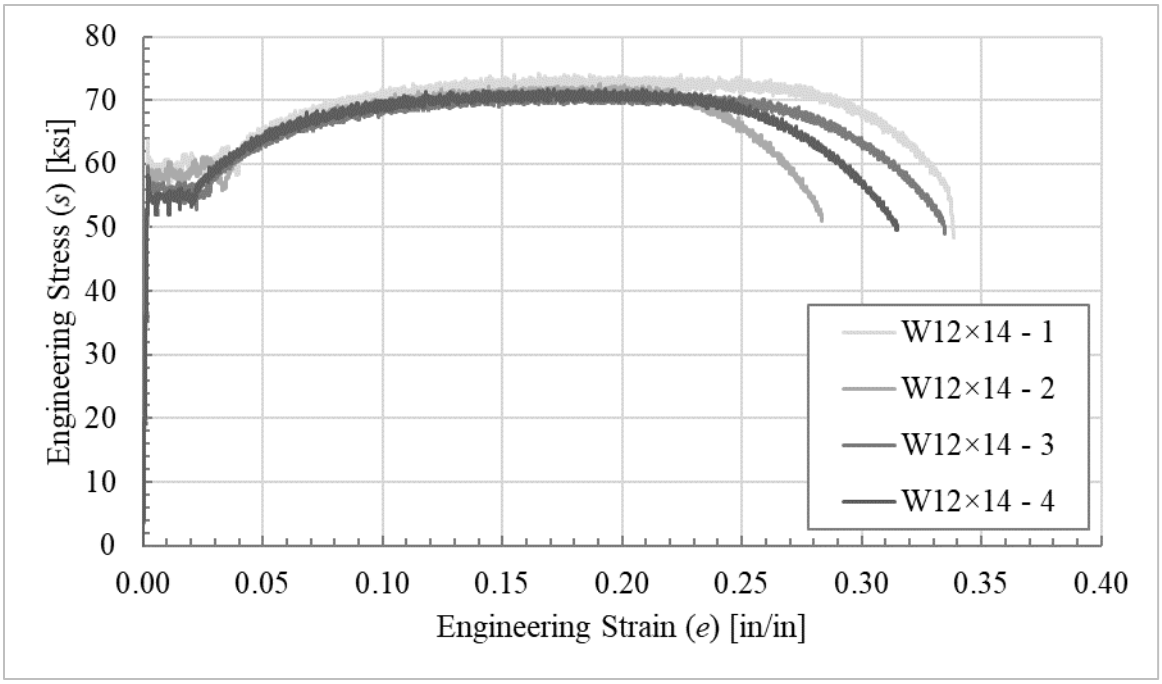

Figure 2-12: Engineering Stress-Strain Curves for ASTM A992 Gr. 50

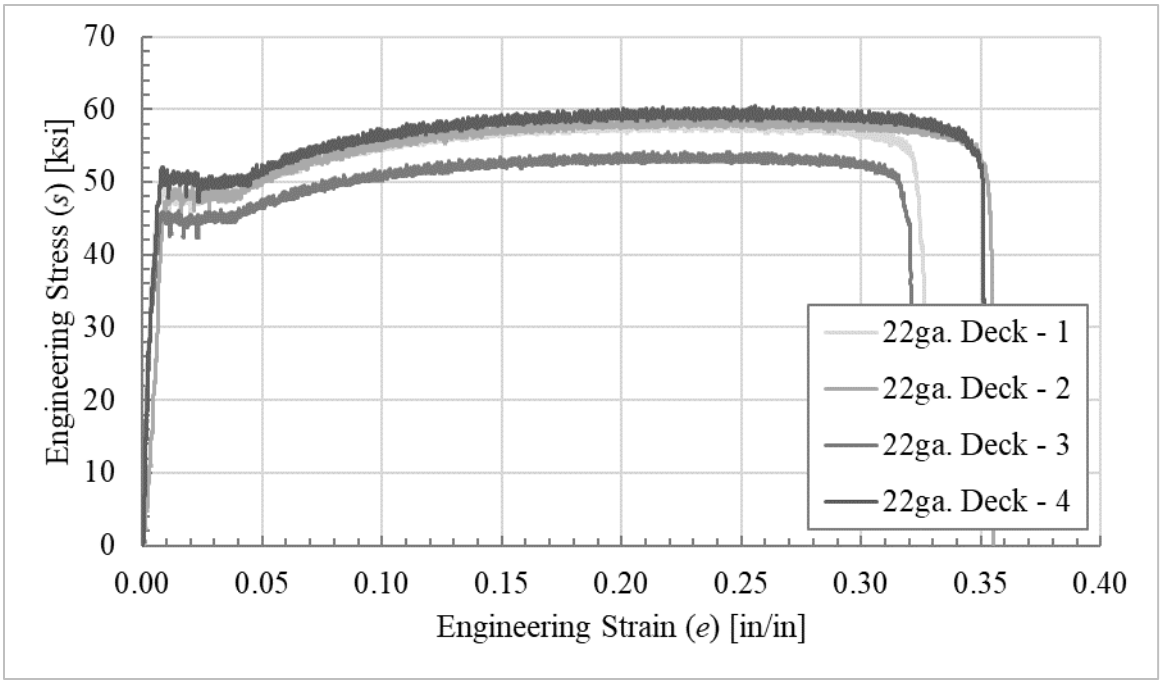

Figure 2-13: Engineering Stress-Strain Curves for ASTM A653

In addition to the variabilities described previously, variability in the engineering stress-strain relationship can manifest from differences in material fabrication and processing. While beyond the scope of this study, the hot-rolling process of structural steel specimens like W-shapes causes varied residual stresses and material microstructure resulting in varied material properties due to the effects of boundary conditions (e.g. proximity to free edges or other portions of the cross-section) and relative rates of cooling. For example, the experimental data presented in Figure 2-12 for A992 steel combines the results of a series of coupons cut from the web and flange of the donor section. In this particular case, a W12×14 beam is divided to show the beam web coupon *s*-*e* curves in Figure 2-14, separate from the flange coupons in Figure 2-15. Similarly, Figure 2-16 shows the beam and web coupons together for a W6×9 section. Data used in these figures were derived from work by others (Hadjioannou, 2015).

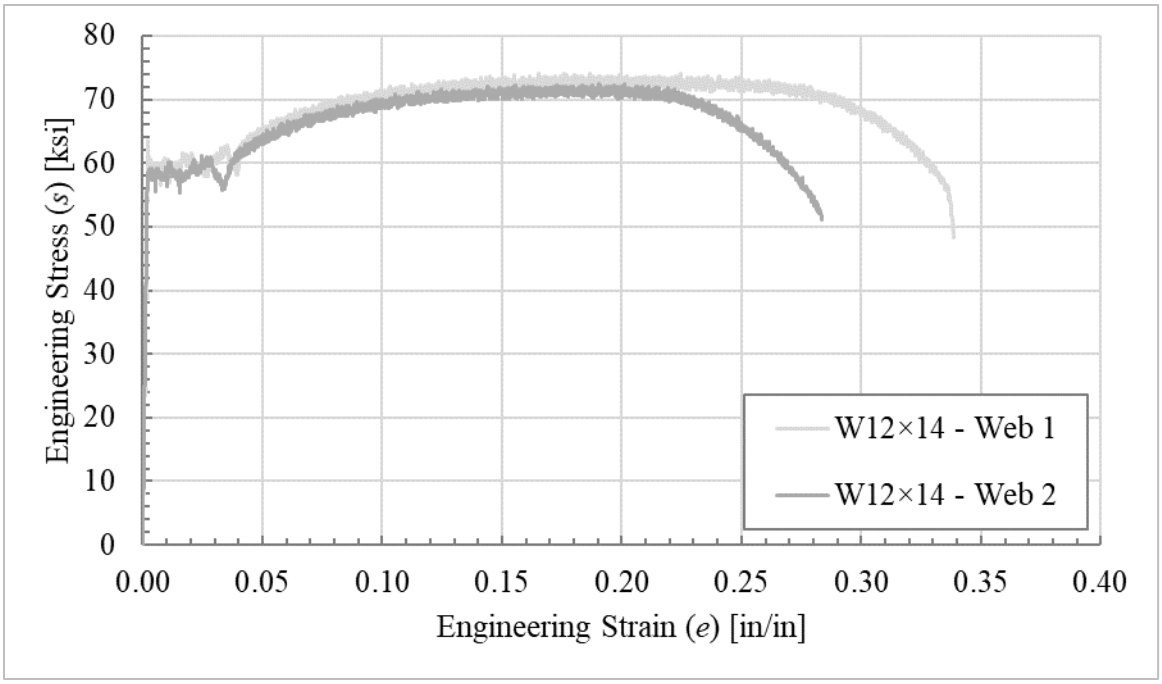

Figure 2-14: Engineering Stress-Strain Curves from W12×14 Section – Web

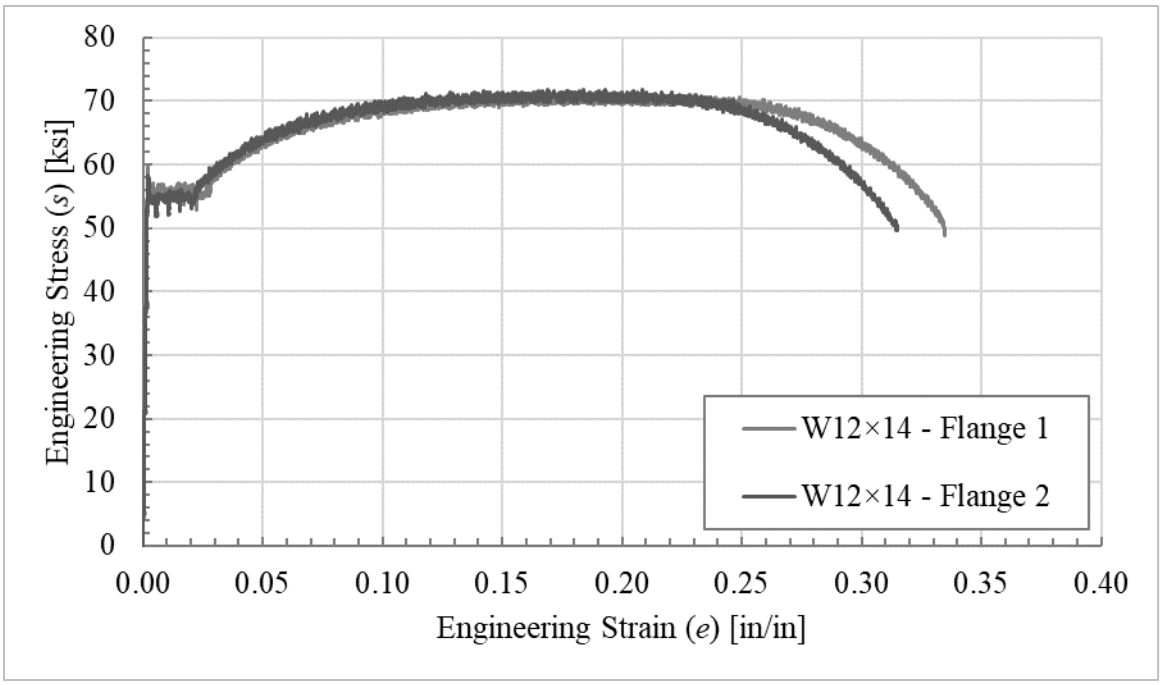

Figure 2-15: Engineering Stress-Strain Curves from W12×14 Section – Flange

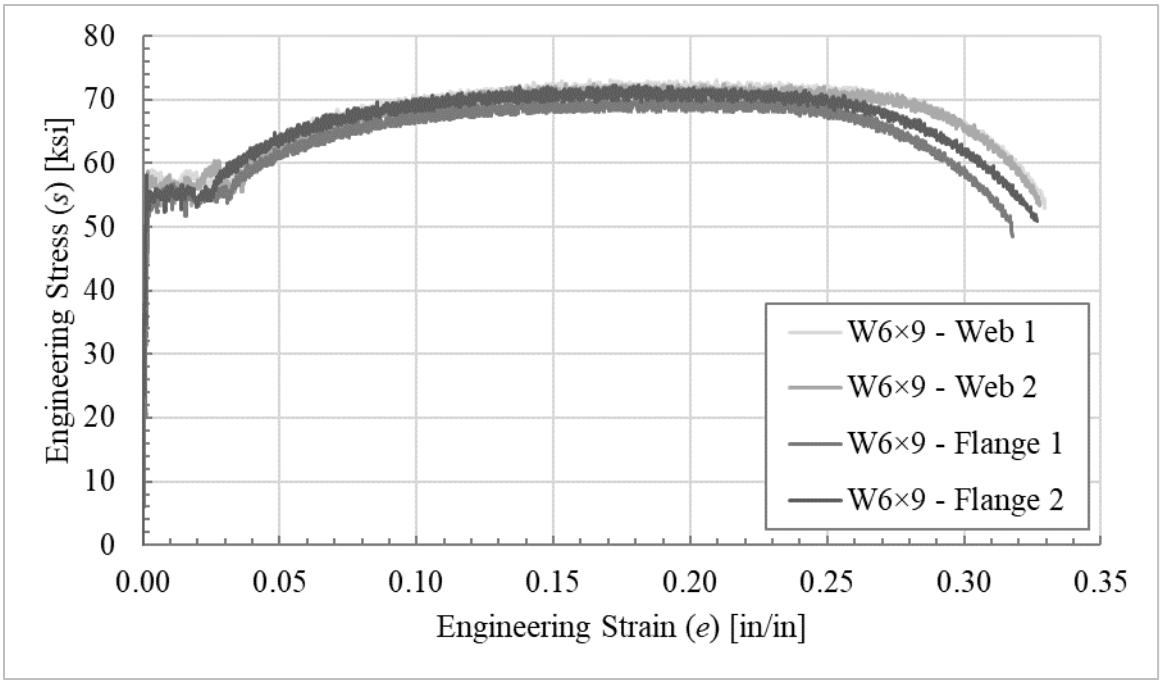

Figure 2-16: Engineering Stress-Strain Curves from W6×9 Section

In most engineering applications, permitted performance of structural materials like ductile metals is limited to the early linear-elastic portion of their engineering stress-strain relationship. In certain unique circumstances, such as localized plastic zones within structural members designed for high seismic loads, metal forming, or design for extreme loads like blast, impact, or disproportionate collapse, materials are allowed to undergo some level of controlled plastic deformation; however, post-necking response is rarely, if ever, intended to occur in engineered systems. Therefore, engineering stress and strain are the primary way in which engineers present material properties and information for analysis and design of structural components and systems. Thus, engineering stress and strain provide adequate resolution and clarity for most problems.

In unique cases where material failure must be considered, or large plastic strains are expected, the use of the engineering stress-strain relationship in predictive analysis, can produce significant errors. In these problems, a more precise and accurate definition of

material behavior is warranted, and the true stress and strain, as introduced in Section 2.6.1, can be used to provide a more accurate estimate of real material behavior using advanced analysis techniques like finite element analysis (FEA) with solid three-dimensional (3D) elements. Examples of scenarios in which post-necking response of ductile metals plays a critical role include but are not limited to fracture modeling, manufacturing, processing, forming of metals, crashworthiness and impact analysis, forensic engineering, and material failure analysis.

Aside from the differences described in the previous paragraphs, engineering stress-strain relationships for a ductile metal material experiencing uniaxial tension will differ from the same material undergoing compression. When cross-sectional changes are explicitly included in the derivation of stress and strain, however, as done with the "true" versions of these quantities, uniaxial loading in either direction—tension or compression—produce the same true stress and strain relationship, as demonstrated in Figure 2-17.

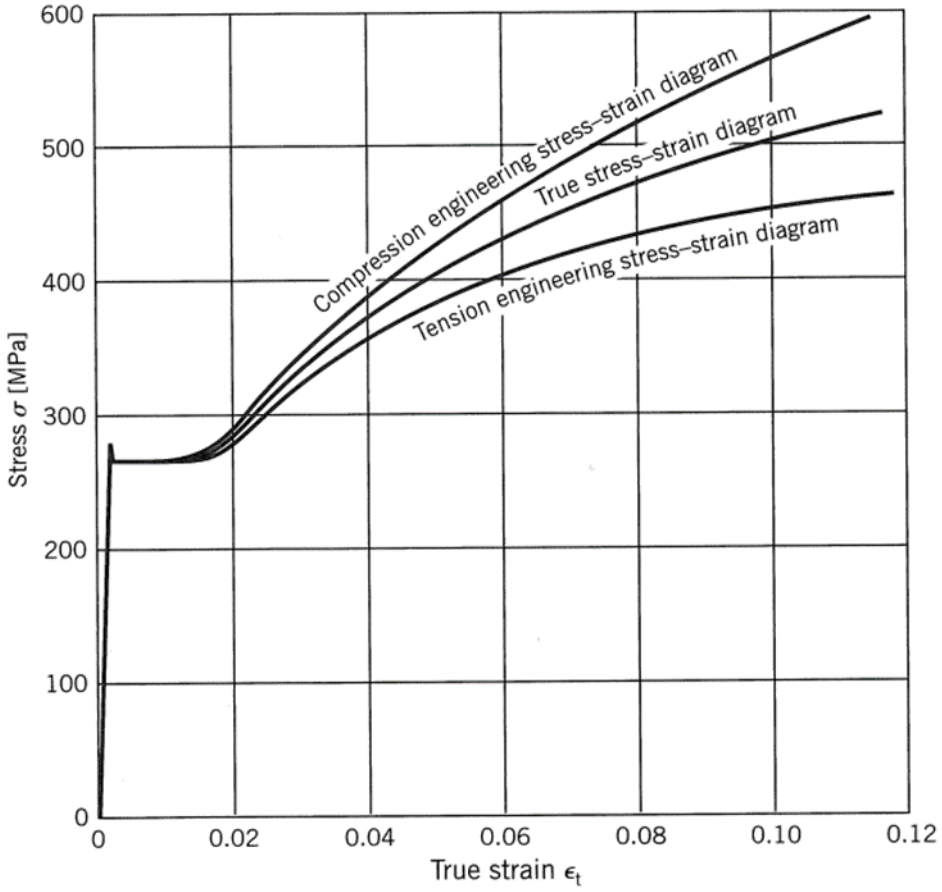

Figure 2-17: Comparison of Engineering Stress-Strain Diagrams with the True Stress-Strain Diagram for Structural Steel (Boresi & Schmidt, 2003)

2.6.1 Variability and Uncertainty in Standard Tension Tests

While load-deformation data and the resulting engineering stress-strain data derived from coupon tension tests are directly measured quantities, it is important to understand and acknowledge that considerable variability, uncertainty, and inaccuracy is inherent in the data itself. Thus, use of these data has the potential to introduce these sources of variability into predictive models. Variability in tests is a result of numerous material, human, methodology, equipment, and ambient condition factors, as shown in Figure 2-18.

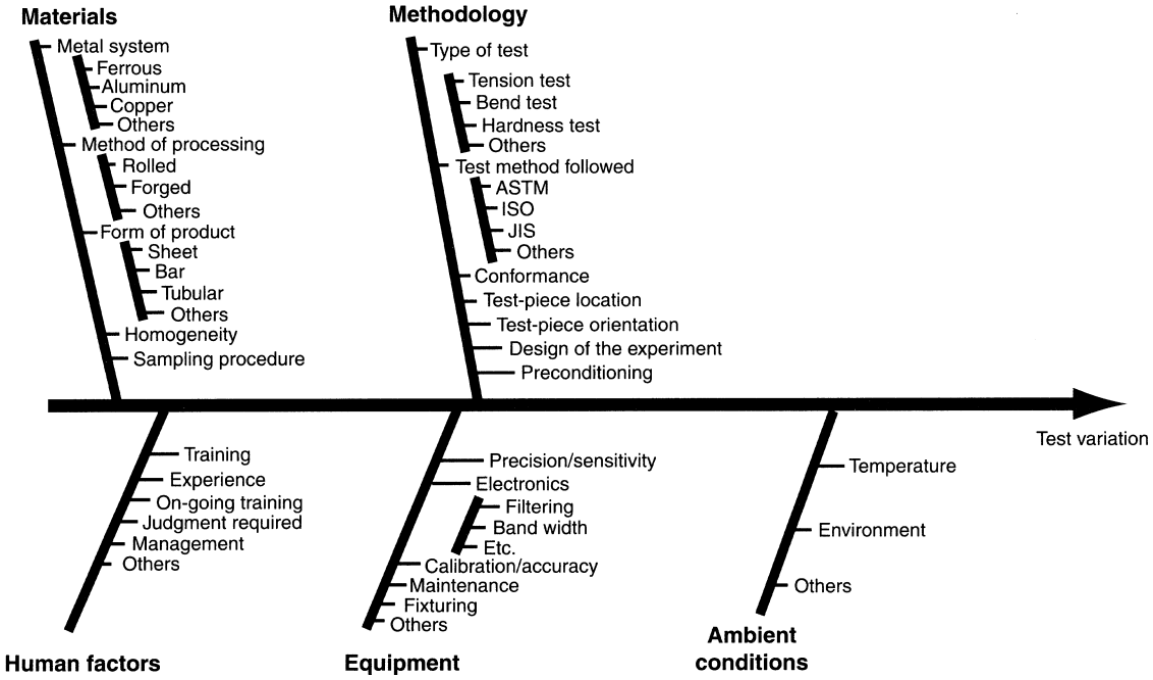

Figure 2-18: Sources of Variability in Mechanical Test Results (Davis, 2004)

Uncertainty is introduced by the simple fact that the results of a single or small subset of material tests are extrapolated to the response of larger volumes and quantities of that material. For example, a single flange and coupon test may be used to develop the material model for a single beam, or several, all the steel in a building, or even all steel of a certain type used across a range of cases. This extrapolation effect introduces variability due to uncertainty. Considering that uncertainty, along with the myriad of sources of variability inherent in experimental testing discussed previously and illustrated in the tension test data presented in Section 2.6, it can be argued that precision in fit of the true stress-strain relationship is often not necessary due to the small sample size of test results often available when developing a material true stress-strain relationship for computational analysis. As a result, judgement should be exercised when using these data and determining and appropriate level of fit for a given case.

Finally, there is also frequently some level of inaccuracy inherent in test data. One source may be improper procedures, such as testing at too high a strain rate. Others include unintended bending induced by coupon misalignment (discussed in more detail in Section 4.3.1 and illustrated in Figure 4-6), grip seating and slip, improper alignment of the extensometer, improper scaling of test data, and possibly other factors. These inaccuracies should be avoided wherever possible; however, while efforts may be undertaken to control them, it is often difficult or even impossible to eliminate them entirely. In addition, there may be no opportunity to control inaccuracies, as may be the case when using data prepared by an outside test lab, extracted from a published reference, or some other similar outside source. In these cases, similarly to the recommendation for addressing uncertainty and variability, the data should be viewed as generally representative; however, precise fit is often not warranted.

Therefore, in light of the information presented on variability, uncertainty, and inaccuracy, it is generally a best practice to avoid excessive focus on precision of fit when developing the true stress-strain relationship for computational analysis. Instead, fitting key points and features will often provide adequate fidelity for most applications. For demonstration purposes, the example case presented in Chapter 5 was developed with the goal of high precision and accuracy of fit. However, this level of effort and precision is generally not recommended as it is often unnecessary and can lead to a perception that the numerical predictions are more accurate than they are likely to realistically be.

2.7 TRUE STRESS AND STRAIN

True stress, like engineering stress, is a measure of the load per unit area in a material. Unlike engineering stress, true stress considers the dynamically changing cross section including Poisson's effect and conservation of volume of the tested material. By

including these effects, the relationship between measured load and deformation during a tension test and true stress, σ, and true strain, ε, become more complex. Along with this more complex relationship, however, true stress and strain are more descriptive of the physical stresses and strains within the material and can be used to accurately predict large plastic deformations in ductile metals, specifically, when using advanced computational methods like finite element analysis (FEA).

Thus, to accurately capture large deformations in material-level numerical models like FEA, the material true stress-strain relationship must typically be determined. For strains up to the ultimate strength of a material, a standard analytical relationship exists to convert engineering stress-strain data to true stress and strain as described in Section 2.7.1. At the onset of necking, a balance exists between the rate of material hardening and the rate of geometric softening that occurs as a result of conservation of volume of the elongating material, as discussed in Section 2.7.2. Finally, Section 2.7.3 presents the true stress-strain (σ- ε) relationship after the onset of necking which is often the most difficult to capture and is the primary focus of this dissertation.

2.7.1 True Stress-Strain Relationship Before Necking

Prior to necking, a standard relationship exists for converting load and deformation measured in a standard coupon tension test, or engineering stress and strain, to true stress and strain. This conversion assumes uniform stress in the reduced section of the tension coupon (often called gauge length (see Figure 2-9)) and small dimensional change in an incompressible material, often referred to as conservation of volume. From these assumptions, load-deformation data or engineering stress-strain data can be converted to true stress-strain using Equation 2-3 and Equation 2-4, respectively, where s and e represent engineering stress and strain, respectively, and σ and ε represent true stress and strain, respectively. Due to the natural log relationship shown in Equation 2-4, true strain is

commonly referred to as logarithmic strain in technical publications and engineering literature. (Dieter, Jr., 1961) (ASM International, 2002) (Callister, Jr., 2007)

$$\sigma = \frac{P}{A} = s(1 + e)$$ Equation 2-3

$$\varepsilon = \frac{L - L_o}{L} = \ln(1 + e)$$ Equation 2-4

Prior to necking, the physical tension coupon specimen, from which the true stress-strain relationship is determined, exhibits nearly uniform deformation and cross-sectional area change, over the entire gauge length. Therefore, the assumptions made in the derivation of the standard relationships (e.g., uniform cross-section and uniform strain in the reduced parallel section) remain valid within what is usually an acceptable range of error.

An additional potential for error results from the assumption of conservation of volume or incompressibility, which can be expressed as an assumption of Poisson's ratio equal to 0.50. This assumption is incorrect for elastic deformations where the standard Poisson's ratio, typically around 0.20 to 0.3 for most ductile metals, is appropriate. Most finite element analysis software will allow for the use of an elastic Poisson's ratio to accurately capture the relationship between orthogonal strains prior to plastic deformation where the assumption of conservation of volume is introduced, and the value for Poisson's ratio is typically assumed to change to 0.50. For large plastic strains in typical ductile metals, the proportion of strain resulting from elastic deformation is quite small relative to total strain. Thus, the assumption of incompressibility, even when applied to the full range of response, including the elastic regime, results in minimal error that is typically acceptable in computational models.

2.7.1.1 True Stress-Strain Relationships in Tension and Compression

While the focus of this dissertation is the true stress-strain relationship in tension, it is important to understand the difference between tension and compression true stress-strain relationships. To illustrate this relationship, consider an ideal isotropic material where the true stress-strain relationship is exactly the same in tension and in compression up to the onset of necking as shown in Figure 2-22. The relationship is limited to pre-necking strains so the standard analytical conversions from engineering to true stress and strain shown in Equation 2-3 and Equation 2-4 can be applied.

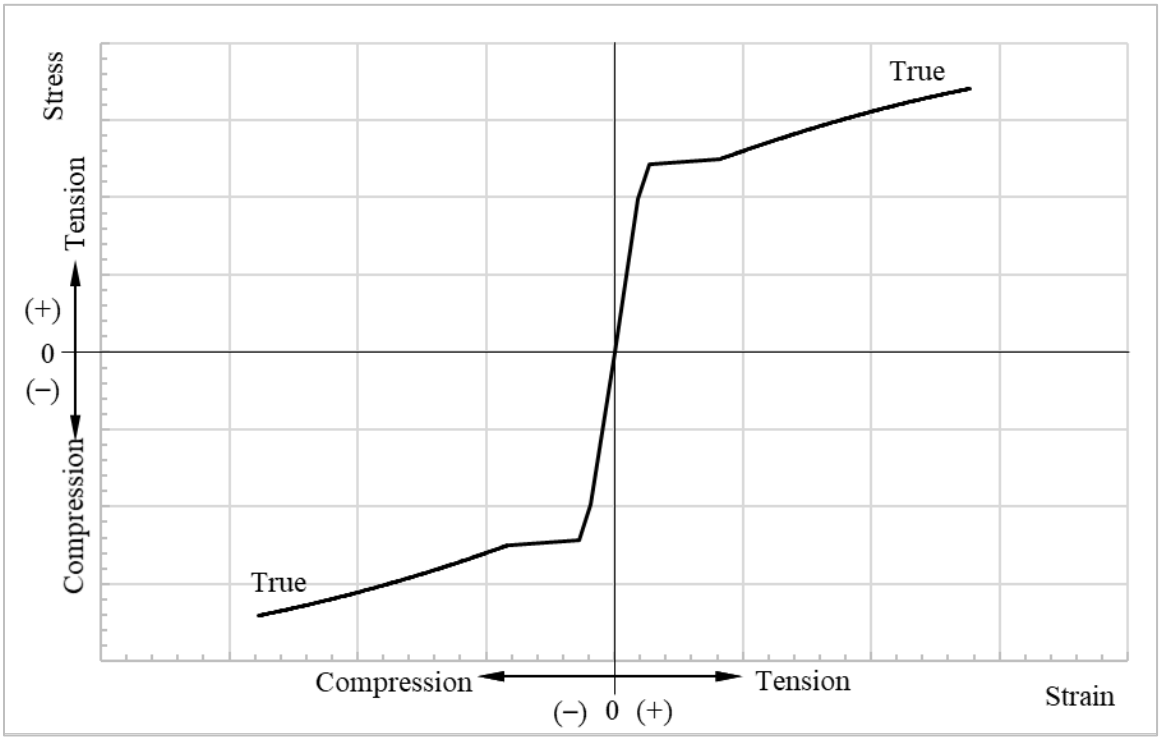

Figure 2-19: Tension-Compression True Stress-Strain Relationship for Ideal Isotropic Material

By applying the conversions in Equation 2-3 and Equation 2-4, and taking care to maintain signs—positive for tension stresses and deformations, and negative for compression stresses and deformations—the engineering stress-strain relationship can be

determined in tension and compression. As previously shown in Figure 2-17, and further illustrated for this ideal isotropic material in Figure 2-20, when plotted together the true stress-strain relationship lies above the engineering relationship in the tension region. The opposite occurs in compression, where the true stress-strain curve lies below the engineering relationship. For additional clarity, the three relationships—true, engineering compression, and engineering tension—are illustrated in the same quadrant in Figure 2-21 by taking the absolute value of all stress and strain values. Note the similarity to the previously presented Figure 2-17.

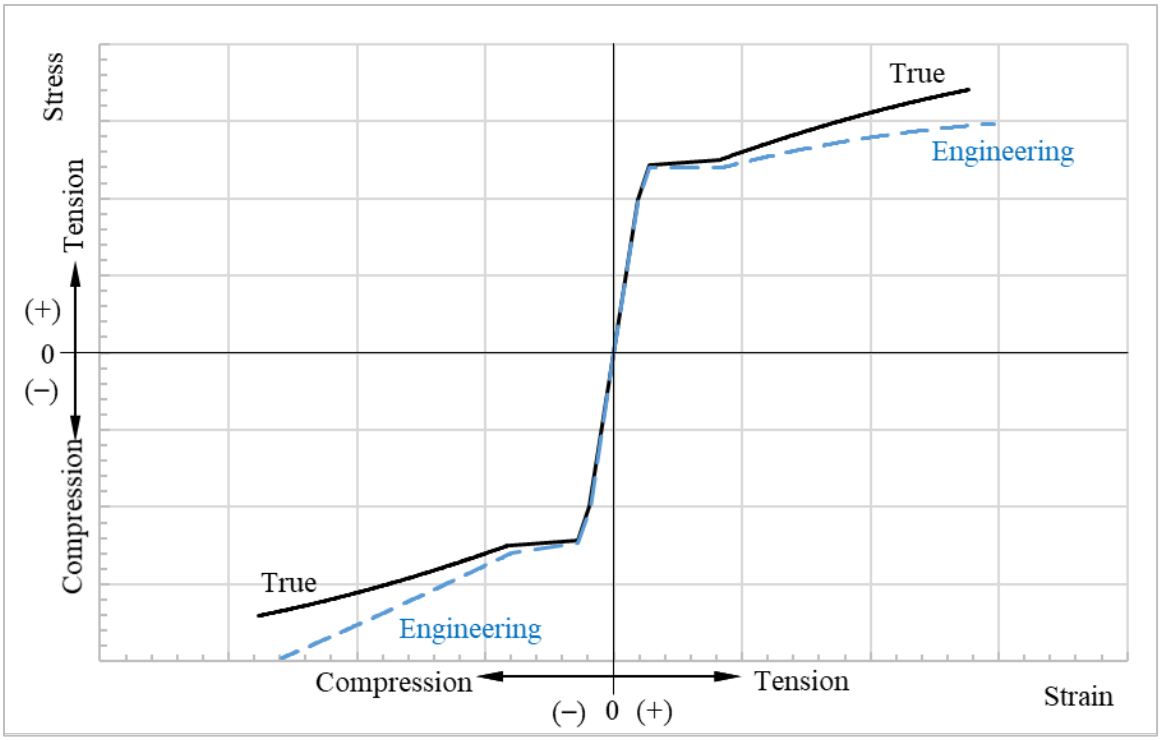

Figure 2-20: Tension and Compression Engineering Stress-Strain Relationships for Ideal Isotropic Material

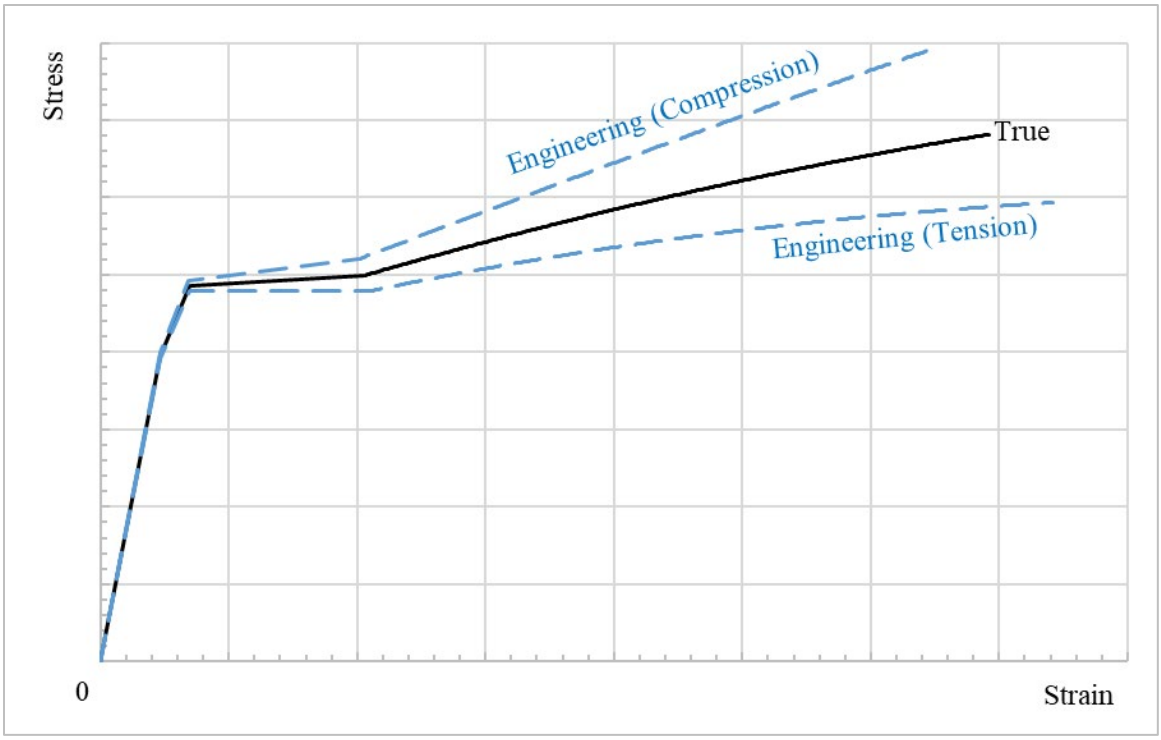

Figure 2-21: Comparison of Engineering Tension and Compression Stress-Strain Relationships for Ideal Isotropic Material

This discussion was provided to illustrate the differences that result from the application of the pre-necking analytical conversion from true stress-strain to engineering stress-strain for tension and compression. The remainder of this dissertation will focus on tension response only, with particular emphasis on necking and post-necking response. Thus, squashing, buckling, and other phenomena associated with compression response of ductile materials is not covered.

2.7.2 True Stress-Strain Relationship at Necking

Physically, necking is most commonly observed in ductile metals as the manifestation of a local instability in the cross-section of a tension coupon; it begins at ultimate load and ends at rupture of the specimen. Necking is characterized by relatively large amounts of localized deformation and strain in a disproportionately small region of

the material, resulting in a prominent decrease in cross-sectional area in the region of the neck (Bridgman, 1952). Figure 2-22 illustrates a steel coupon during a tension test with the necked region enlarged for clarity.

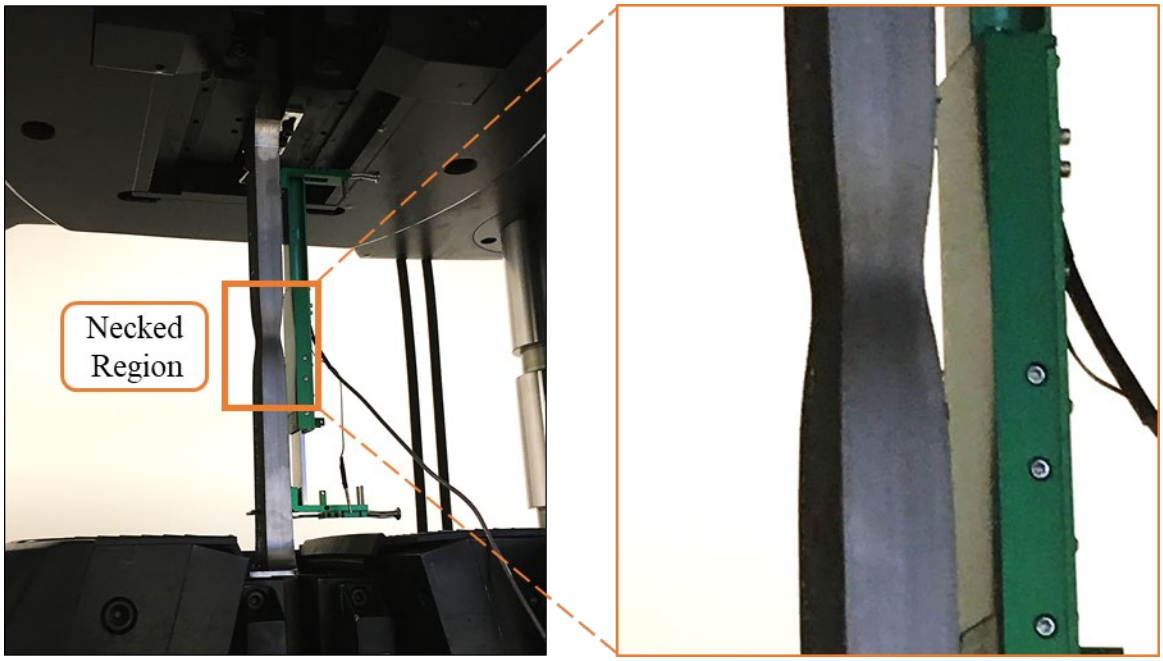

Figure 2-22: Tension Coupon during Necking

For metals with lower levels of deformation prior to failure in tension, necking may be relatively minimal and even difficult to observe visually. Cast or wrought iron are examples of relatively brittle metals that undergo little post-yield plastic deformation in a tension test, resulting in little evidence of necking. In contrast, highly ductile metals like copper, pure gold, or a range of metals at high temperatures, can often undergo large deformations and exhibit significant necking prior to fracture in tension. Figure 2-23 shows the simplified fracture shape of (a) a brittle metal, (b) a semi-ductile metal, and (c) a perfectly ductile metal. Failure and fracture response of ductile metals is beyond the scope of this dissertation; inclusion of this information is only intended to demonstrate the qualitative difference in observed necking between materials with a range of ductilities.

Ductile metals considered in this dissertation generally exhibit failure most like the semi-ductile example, undergoing some necking prior to fracture in tension.

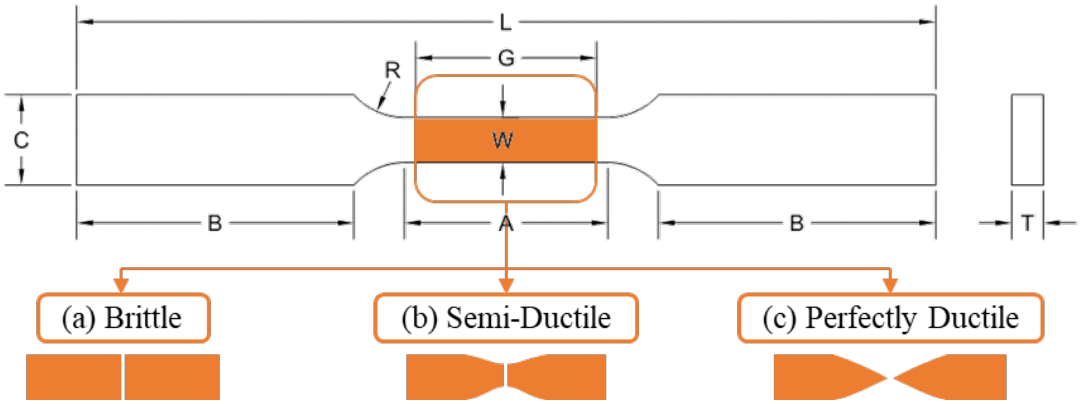

Figure 2-23: Qualitative Neck Shapes at Fracture for Varying Levels of Ductility

At the precise onset of necking, the previously summarized pre-necking analytical relationship between engineering and true stress and strain (see Section 2.7.1) remains valid. Beyond this point, however, the assumption of uniform strain no longer applies due to localization of strains within the gauge length, as manifested in the necking region. Continuing to use these relationships will result in accumulation of error with increasing strains beyond the onset of necking. Therefore, a different approach must be used to define the relationship after necking.

At the precise instant of the onset of necking, a unique relationship exists between the rate at which the material strain-hardens and the rate at which the material softens as a result of conservation of volume. This relationship identifying the onset of necking was first developed and published by Armand Considère in 1885 and is often referred to as Considère's construction (Considère, 1885).

Considère's construction uses the relationship between the true stress and strain for a material and its first derivative, or slope, to predict the onset of necking. By comparing

these relationships, one can simply determine if necking behavior will be exhibited by a given material and precisely predict when it will occur.

When plotted on the same axes, necking materials will have a point at which the engineering stress-strain curve and its first derivative, a plot of the slope, will intersect prior to the fracture strain. The onset of necking occurs precisely at this point as shown in Figure 2-24. Considère's construction is described in greater detail in Section 2.8. In addition, it is discussed in the context of proposed rules for developing true stress-strain relationships for ductile metals in Chapter 3.

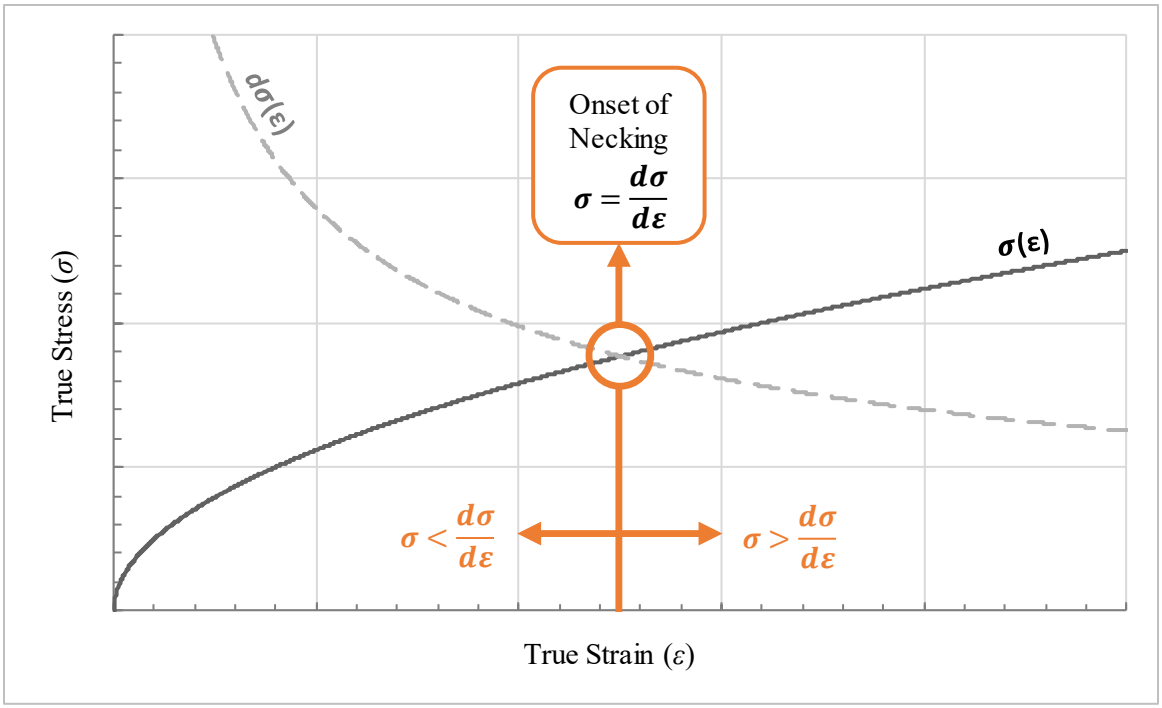

Figure 2-24: True Stress-Strain Relationship at the Onset of Necking

2.7.3 True Stress-Strain Relationship after Necking

After the onset of necking, strains localize, and the relationship between stress and strain within the gauge length of a tension coupon becomes much more complex due to non-uniformity of stresses and strains. As a result, simple analytical relationships like those

presented in Section 2.7.1 are no longer valid. Significant research effort has been conducted to develop analytical, experimental, and hybrid approaches to determining the true stress-strain relationship in this post-necking domain. Due to the complex nature of the post-necking true stress-strain relationship, however, there is still no general consensus on a singular approach to determining the post-necking true stress-strain relationship. As a result, it is one of the primary focuses of this dissertation as discussed in the following sections and chapters.

Previous research related to post-necking response of ductile metals has been extensive and broad. A cross-section of the available published research related to and focusing on the prediction of necking and post-necking response of ductile metals is presented in the following sections. Section 2.8 focuses on research related to the onset of necking, and Section 2.9 of this dissertation discusses published research related to post-necking response of metals. In addition, Section 2.10 is included to provide a brief discussion of the response of non-metallic materials exhibiting cold-drawing behavior, a phenomenon not observed in ductile metals. While these sections discuss a broad selection of published research on these topics, due to the breadth and large volume of research, it is not intended to be an all-inclusive literature review. Only those references considered essential to the research presented in this dissertation are included.

2.8 Research Related to the Onset of Necking in Ductile Metals

The topic of necking and post-necking response of ductile metals has been the subject of extensive research. However, accurate prediction of the onset necking was known as early as 1885. Nonetheless, many research publications fail to recognize this fact or its importance. In fact, some researchers claim that prediction of the onset of necking *a priori* is not possible (Joun, Choi, Eom, & Lee, 2007). Others go so far as to entirely

contradict the physical and analytical relationship characterizing the onset of necking stating, for example, that "*there is no definite relation between dF/dL=0* [the slope of the load-deformation relationship at maximum load in tension] *and the onset of necking,*" (Shen & Jones, 1993).

Despite these dissenting opinions, most researchers acknowledge the general relationship between the true stress-strain response and its first derivative at the onset of necking first published by Considère. The following subsections describe, in detail, the basic observations and assumptions underpinning the work of Armand Considère (Section 2.8.1), and Considère's Construction and the importance of this relationship to predicting the onset of necking (Section 2.8.2). Afterward, Section 2.8.3 discusses the pervasive but incorrect claim that a geometric or material imperfection is required for the initiation of necking in FEA models. This subsection includes examples of this claim in currently published research as well as a summary of the common modeling errors that necessitate the use of imperfections to computationally induce necking.

2.8.1 Basis for Analytical Relationships at Necking

Qualitatively, necking in tension for ductile metals is affected by three primary factors: (1) local variations in properties, (2) Poisson's effect, and (3) material strain hardening. The first factor dictates, to some extent, where necking will occur and is the reason that necking in real tension coupon specimens appears to occur randomly within the reduced coupon section (i.e., the gauge length, *G*, in Figure 2-9) of a standard tension coupon. The latter factors, (2) and (3), affect the stability of the neck. In FEA, where material properties are traditionally assumed to be perfectly uniform, necking should always be predicted at the center of the specimen where stresses are highest, as discussed in more detail in Section 4.3.6. Thus, in computational simulations, the onset of necking is

affected by only two factors, the reduction in section from Poisson's effect or conservation of volume, and the rate at which the material hardens.

A given incremental deformation of a tension coupon, δ, manifests an incremental change in material strength (i.e., change in true stress, $\delta\sigma$). This phenomenon is often referred to as strain hardening, or material hardening, and it typically occurs along with an incremental change (reduction) in cross-sectional area caused by Poisson's effect and conservation of volume (δA), which results in a perceived softening. This behavior caused by a reduction in load-bearing cross-section is often referred to as geometric softening. For any incremental deformation, δ, where the effect of material hardening is greater than the effect of geometric softening, the coupon remains stable. Thus, deformation causes a uniform stress increase in the reduced section of the coupon. However, when this balance is reversed and the rate of geometric softening outpaces the rate of material hardening, the section becomes locally unstable.

As a result of this instability, a neck forms, characterized by a confined region within the gauge length where stresses and strains localize. This phenomenon was analytically captured by Armand Considère in 1885 (Considère, 1885), where he noted that the onset of necking can be defined as the point at which the rate of material hardening, and the rate of geometric softening, are equal, resulting in a critical balance between these competing hardening and softening effects.

In addition, through observation of the load-deformation data from a standard tension test, or the derived engineering stress-strain relationship, it is clear that a local maximum occurs in the engineering stress, s, at the onset of necking because the onset of necking is coincident with the maximum load carried in a ductile metal tension coupon. As a point of maximum load and local maximum, the onset of necking is characterized by a point on the load-deformation plot or engineering stress-strain relationship where the slope

is zero, as highlighted in Figure 2-24 for data from two different tension tests by others (Hadjioannou, 2015). This observation, coupled with the understanding of competing hardening and softening effects discussed in the prior paragraphs, is of critical importance to the derivation of Considère's Construction described in Section 2.8.2.

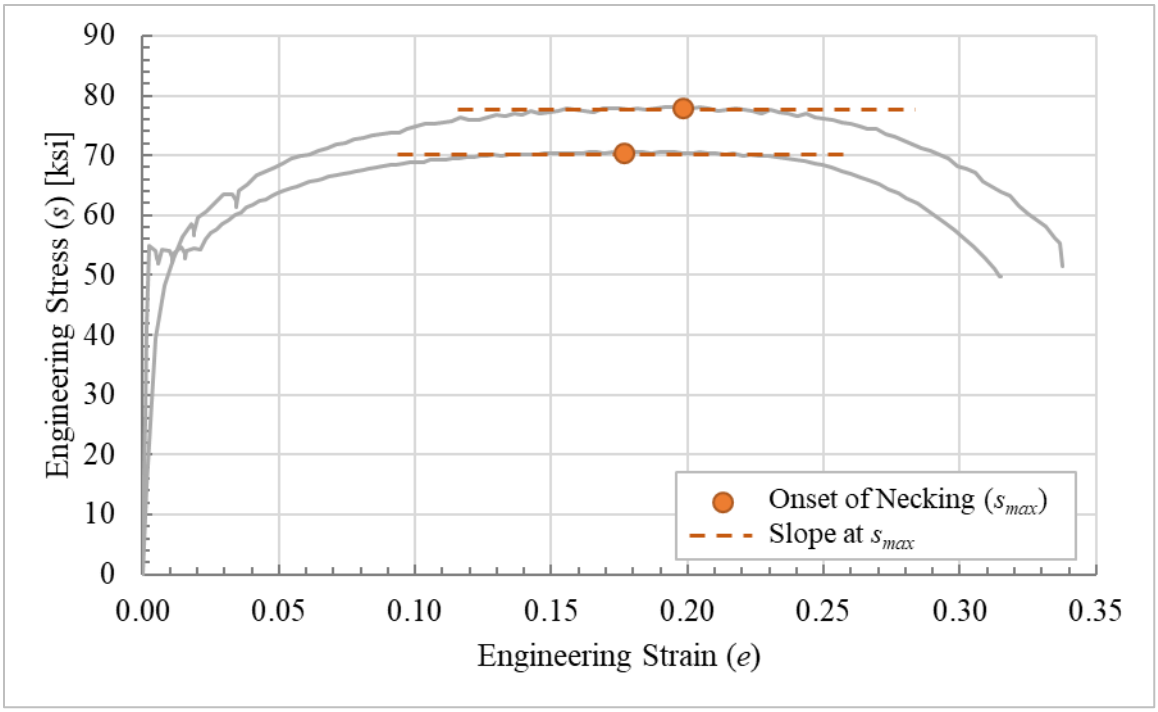

Figure 2-25: Local Maximum and Zero Slope at the Onset of Necking

2.8.2 Considère's Construction

The following paragraphs provide is a summary of the work of Armand Considère and its importance to predicting the onset of necking. It should be noted that this summary was developed based on review of other published works that reference the original work published by Considère because the original work is in French and was unavailable when writing this dissertation. Accordingly, some differences may be present if the derivation and conclusions presented later are compared against the original cited work.

Considère's work focused on an analytical study of the state of stress at the onset of necking. Specifically, he developed an analytical relationship that captures the onset of necking by making simplifying assumptions, such as stress and strain uniformity in the reduced section of a standard tension coupon, isometric and homogeneous material properties, and incompressible material behavior. By making these assumptions and observing and analyzing the physical phenomena that affect the stability of the coupon just prior to the onset of necking, Considère was able to show a distinct change between the rate of material hardening and geometric softening that occurs precisely at the onset of necking.

As stated previously, the competing actions identified that affect stability of the neck are the rate of material hardening and the rate of geometric softening. These actions can be represented by the change in stress for a given increment of strain as shown in Equation 2-5, and the change in cross-sectional area for a given increment of strain as shown in Equation 2-6, for material hardening and geometric softening, respectively.

$$A\left(\frac{d\sigma}{d\varepsilon}\right) \qquad \text{Equation 2-5}$$

$$\sigma\left(\frac{dA}{d\varepsilon}\right) \qquad \text{Equation 2-6}$$

Prior to necking, when stresses and strains are uniform in the reduced section of the coupon, the change in measured force measured during testing is influenced by both of these actions. To determine the incremental material hardening effect on measured force, it can be multiplied by the current area. Similarly, the rate of material softening can be multiplied by the current stress to capture its effect on the change in measured force. Combining these effects yields Equation 2-7, which captures the relative change in force,

dF, for a given strain increment, $d\varepsilon$. In this equation, σ represents the true stress in the material, A is the cross-sectional area of the reduced section of the coupon (including deformation effects), $dA/d\varepsilon$ is the incremental geometric softening, and $d\sigma/d\varepsilon$ is the material hardening.

$$dF = \sigma\left(\frac{dA}{d\varepsilon}\right) + A\left(\frac{d\sigma}{d\varepsilon}\right) \qquad \text{Equation 2-7}$$

At the onset of necking, as previously noted, the slope of the load-deformation relationship is zero. Thus, the incremental change in force, captured by the first derivative of the load-displacement function determined in testing, is also equal to zero. Therefore, by setting *dF* in Equation 2-7 equal to zero, the equation can be evaluated at the onset of necking.

Evaluating this relationship at the onset of necking yields the relationship between material hardening and geometric softening illustrated in Equation 2-8. Through algebraic manipulation and application of conservation of volume, this relationship reduces to Equation 2-9, which is the most common presentation of Considère's Construction.

$$\sigma\left(\frac{dA}{d\varepsilon}\right) = -A\left(\frac{d\sigma}{d\varepsilon}\right) \quad \textit{at the onset of necking} \qquad \text{Equation 2-8}$$

$$\sigma = \frac{d\sigma}{d\varepsilon} \quad \textit{at the onset of necking} \qquad \text{Equation 2-9}$$

The detailed derivation of the relationship presented in Equation 2-9 is provided in Section 3.2, along with additional discussion of its importance in predicting necking and developing the true stress-strain relationship for 3D FEA of ductile metals and other similar computational analysis approaches.

2.8.3 Necking Initiation by Geometric Imperfection

While this section is probably best suited toward a discussion of common errors and issues encountered when attempting to capture necking and post-necking response in computational analyses (e.g., 3D FEA), such a study is beyond the scope of this dissertation. Nonetheless, due to the prevalence of this belief across a range of industries and current research areas, and the importance of accurate necking prediction to many fields of engineering and science, it is presented briefly in the following paragraphs. This discussion is provided to clarify the typical reasons this belief still exists in academia and across the engineering research community. In addition, the discussion includes simple recommendations to remedy the errors that necessitate geometric imperfections to computationally simulate the initiation of necking in tension.

Despite the existence of Considère's Construction, a simple relationship established long ago, many researchers and academics still believe initial geometric or material model imperfections must be introduced to initiate necking analytically or in a computational model. More precisely, a pervasive belief exists that perfect uniformity and homogeneity of materials, coupled with perfect coupon geometry, does not allow for the stress or strain localization that manifests the unstable condition characterizing the onset of necking (Tvergaard, Needleman, & Lo, 1981) (Shen & Jones, 1993) (Brünig, 1998) (Zhang, Hauge, Ødegard, & Thaulow, 1999) (Kamaya, Kitsunai, & Koshiishi, 2015).

First, the general observation that perfect materials and geometry will not permit necking initiation in a computational or analytical model is, in fact, valid and true, provided that some other condition does not exist to force non-uniformity in stresses and strains predicted in the section. As a result, some researchers believe that a geometric imperfection (e.g., slight section reduction at a key point), or material imperfection (e.g., slight variation in material definition at one or more points in the model) must be introduced into an

analytical or computational model for necking to occur. Consequently, there are some who avoid leveraging the benefits of symmetry and who go to great lengths to introduce and calibrate these imperfections in their model to match test data. Examples include Tvergaard et al. (Tvergaard, Needleman, & Lo, 1981), Shen and Jones (Shen & Jones, 1993), Brünig (Brünig, 1998), Zhang et al. (Zhang, Hauge, Ødegard, & Thaulow, 1999), and Kamaya et al. (Kamaya, Kitsunai, & Koshiishi, 2015). Each of these researchers makes several critical simplifications that oversimplify the analysis to the point where they create a scenario in which necking cannot occur.

In reality, however, if such a perfect material (i.e., one with homogeneous and isometric properties) existed, and such a perfect test specimen could be manufactured (i.e., one that was geometrically perfect), and such a perfect test could be performed where no local variations could occur, necking would still occur for two reasons. First, by the nature of the coupon geometry (illustrated previously in Figure 2-9), the wider gripped ends provide dilatational (i.e., shear) restraint to the ends of the coupon test region. This restraint creates a stress and strain gradient within the reduced section. Similarly, the act of gripping the ends of the coupon provides dilatational restraint to the ends, resulting in a similar gradient within the ends of the coupon specimen. Thus, the reason simulated coupon tension models fail to neck is the lack of shear restraint within the model. This restraint can be captured by physically modeling the wider ends of the coupon or by applying appropriate boundary constraints to the ends in a sub-model that includes only the reduced section of the coupon. This error appears to underly many of the analytical or computational studies that claim necking must be initiated through some assumed geometric or material imperfection.

If applied correctly, the effect of dilatational restraining boundary conditions creates slight stress and strain gradients along the length of the modeled coupon, as well as

through the cross-section. These gradients provide the "imperfection" in the stress and strain predictions within the analytical or computational model necessary to manifest necking. It should also be mentioned that, when using symmetry through the plane of necking, dilatational shear restraints should not be applied to the end where the symmetry condition occurs as there is no such restraint at that boundary in the actual specimen. Additional discussion of the gradients developed through application of proper boundary conditions is provided in Section 4.3.6.

2.9 RESEARCH ON NECKING AND POST-NECKING TRUE STRESS AND STRAIN RELATIONSHIPS FOR DUCTILE METALS

Accurately capturing the true stress-strain curve for steel has been a topic of consideration in the engineering world for decades. Early researchers used experimental approaches requiring precise measurement of the dimensions of the neck throughout the test. They then developed true stress-strain curves from this experimental data using conversion factors, developed through detailed analytical studies involving a range of simplifying assumptions, including uniform distribution of stress and strain across planar sections through the neck, cut perpendicular to the direction of applied loading. Thus, these early correction factor approaches neglected any variation in stresses and strains within a given section that develop after the onset of necking. Bridgman developed one of the earliest correction factor approaches for cylindrical and flat (two-dimensional) specimens. near the middle of the 20th century. His work went on to inspire renewed interest in the onset of necking and post-necking response, providing an analytical framework for the works of many later researchers.

After Bridgman, researchers have continued studying the post-necking response of ductile metals in tension, developing improved analytical correction factor techniques to determine the material true stress-strain relationship. Early approaches considered simple

cylindrical coupons with radially symmetrical circular cross-sections. Later, these circular coupon calibration approaches were extended to thin plate coupons, and then thick plate and rectangular coupons. More recently, a variety of other methods were developed to apply, calibrate, and scale these analytical approaches, including incorporation of FEA models to aid in the process.

In parallel with many of these later efforts, several researchers began using more advanced testing and physical measurement approaches to measure the deformed shape and strain profile within the neck. These efforts included the use of special cameras to precisely track deformations through digital image correlation (DIC) (see Section 2.9.3.1), fractography and scanning electron microscopy (SEM) (see Section 2.9.3.2), and X-ray diffraction (see Section 2.9.3.3), among others. At present, while these experimental techniques have shown considerable promise, they typically require the use of complex, specialized, and expensive equipment that is far more advanced than what is typically used in the typical ASTM engineering stress-strain coupon tests. As a result, they are generally impractical in most situations.

Another more recent approach to determining the true stress-strain relationship for ductile metals involves the use of advanced FEA models, coupled with iterative-corrective solvers and other computational data analysis and processing approaches (see Section 2.9.2). This approach uses the iterative solver to minimize the relative error between the FEA predicted material response and a measured stress-strain relationship developed directly using data from a standard tension test or other means (e.g., fitting a target idealized stress-strain relationship). Due to the rapidly decreasing cost of computational hardware and software, these techniques show considerable promise and potential for widespread application and use.

The techniques employed by these researchers are most like the approach recommended in this dissertation in Chapter 4. As discussed in the recommendations for future work in Section 6.3, there is potential for additional improvement of these approaches through application of more advanced data processing techniques applied in the error minimization approaches.

The following sections provide a brief description and summary of the broad range of research associated with developing the true stress-strain relationship for ductile metals, with particular focus on accurately capturing the onset of necking and post-necking response, up to failure. While it is not an exhaustive list of all available research, it provides a detailed summary of a range of the developed approaches within the context described previously, as well as cited works that can be referenced for additional information.

2.9.1 Early Analytical Research on Post-Necking Response of Ductile Metals

Between the early works related to the onset of necking by Considère and the middle of the 20th century, little notable research related to the onset of necking and post-necking response of ductile metals was published. That changed, however, with Bridgman's publication of *Studies in Large Plastic Flow and Fracture* (Bridgman, 1952). This publication provided many new analytically derived insights into post-necking response of ductile materials, as discussed in Section 2.9.1.1, and it laid the groundwork for later research by Needleman (Needleman, 1972), Shen and Jones (Shen & Jones, 1993), Ling (Ling, 1996), and many others, as discussed in Section 2.9.1.2.

2.9.1.1 Bridgman's Study of Necking and Post-Necking Behavior

In 1952, Harvard University Professor P.W. Bridgman published *Studies in Large Plastic Flow and Fracture* (Bridgman, 1952). This extensive text covers a range of topics beginning with a detailed study of the effect of non-uniformities in stress at the neck of a

tension specimen and concluding with a broad range of studies on hydrostatic pressure effects on tension, compression, punching, drawing, and other mechanical properties of both ductile and brittle materials. Of particular relevance to this dissertation are his early portions of this publication discussing his analytical study of the onset of necking and stress non-uniformities in the neck of a tension specimen.

This necking study discusses several levels of increasing complexity of approximation of the material stress-strain relationship for ductile metals in tension. The simplest level, referred to as the zero level, is the engineering stress-strain relationship. At this level, stresses are calculated based on the initial undeformed cross-section area, A_o, neglecting cross-sectional deformation. Although useful, Bridgman indicates this level of approximation "does not offer a very fundamental correlation with what is going on within the tensile specimen." Specifically, the stresses and strains calculated are not indicative of the true behavior of the material due to the level of simplification.

The next more complex level of approximation, referred to as the first approximation, assumes an average uniform distribution of stress across a given section within the necked region, but directly uses the actual cross-section area, A, of the specimen in the derivation. This approach is similar to the standard pre-necking engineering to true stress-strain conversions given in Equation 2-3 and Equation 2-4. This approximation requires running measurements of both load and actual cross-sectional area within the neck, which can be challenging to measure, particularly for non-cylindrical specimens. In addition, for the first approximation, Bridgman notes that the resulting true stress-strain relationship "continues rising to fracture." While this comment is not given particular emphasis, it is an important observation noted in this early work, which is necessitated for numerical stability as discussed further in Section 3.3. The discussion of the first approximation concludes by noting that "average stress across the neck is not adequate to

describe all the significant physical phenomena, including the phenomena of fracture." This final statement alludes to the fact that this level of approximation does not adequately capture the coupon response between the onset of necking and fracture.

The next and final level of complexity, termed the second approximation, seeks to capture the non-uniform stress and strain distribution within the neck to a degree that is capable of accurately capturing the peak value of these quantities occurring at the center of the specimen, where fracture is ultimately initiated. The second approximation is the focus of Bridgman's work although he acknowledges this approximation requires "complete determination of the contour of the specimen at points remote from the neck, as well as in the neighborhood of the neck," which he later recognizes as difficult to accomplish in a real test. Thus, his development of the second approximation focuses on the peak stresses and strains at the center of the neck and makes some basic assumptions about the general neck shape, characterizing it by a single parameter. This parameter is the radius of curvature of the circle osculating the profile at the neck, as illustrated in Figure 2-26. In addition, his derivation is further simplified by developing it for a cylindrical coupon specimen, allowing for radial symmetry to be used, as discussed later in this section.

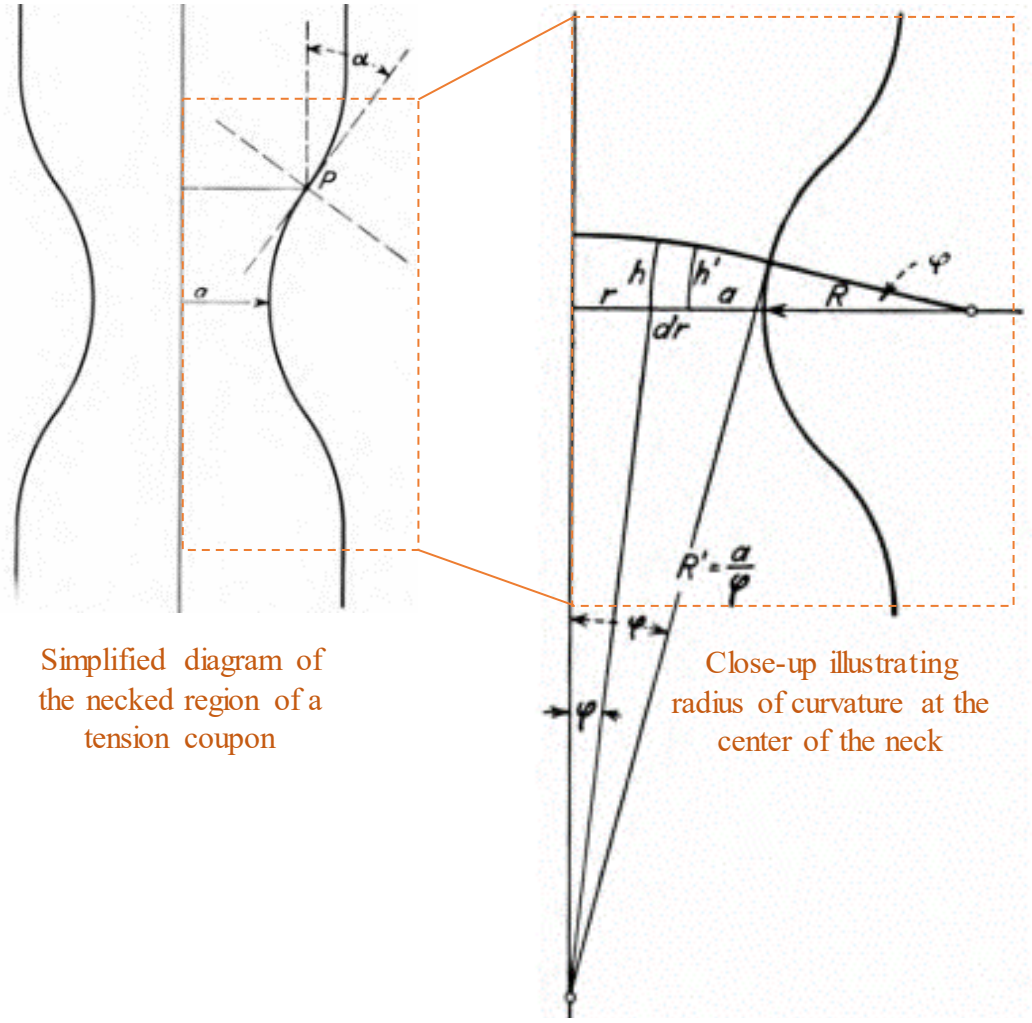

Figure 2-26: Radius of Curvature at the Center of the Neck (Bridgman, 1952)

Through an application of several simplifying assumptions including radial symmetry, symmetry about the center of the neck, and a necked geometry that can be approximated as circular, along with application of appropriate boundary conditions, the von Mises plasticity function for ideal plastic materials and plastic flow theory are applied and mathematically manipulated to develop a correction function for the first approximation, frequently referred to as Bridgman's correction. This corrected first approximation was developed as an attempt to convert the first approximation to the second, capturing the non-uniformity of stresses and strains within the neck. The Bridgman

correction for cylindrical specimens takes the form shown in Equation 2-10, where a represents the radius of the neck in a cylindrical specimen and R refers to the radius of curvature of the neck, as illustrated previously in Figure 2-26.

$$\frac{1}{\big(1+2(R/a)\big)\ln\big(1+(a/2R)\big)} \qquad \text{Equation 2-10}$$

A similar approach was used to develop the correction factor for two-dimensional (2D) flat specimens. The derivation for 2D specimens follows a similar process, but the resulting correction factor is a bit more complex, as illustrated in Equation 2-11. In this relationship, R still represents the radius of curvature at the neck, but rather than radius, a represents the half-width of the 2D specimen.

$$\frac{1}{\sqrt{1+2(R/a)}\ln\Big(1+(a/R)+\sqrt{(2a/R)}\sqrt{1+(a/2R)}\Big)-1} \qquad \text{Equation 2-11}$$

Each of these corrections is intended to capture the peak stress which, as his derivation showed, occurs along the centerline of the specimen. Bridgman's correction factors are shown graphically for a range of values of (a / R) in Figure 2-27. For both cases, cylindrical and two-dimensional flat specimens, when this ratio approaches zero, which would be the case in prior to necking, the correction factor is equal to 1.0. As necking begins, the value of (a / R) increases, and with it, the correction factor decreases. Thus, the first approximation where stress is assumed uniform across a given section within the neck is an overestimate of the true maximum stress in the specimen. As noted by Bridgman, values are reported to a value of (a / R) equal to 4.0 because "if the specimen is pulled to higher strains… the neck loses its geometrical regularity… [because] individual grains monopolize the cross section." In essence, the correction no longer applies beyond this limiting value of (a / R).

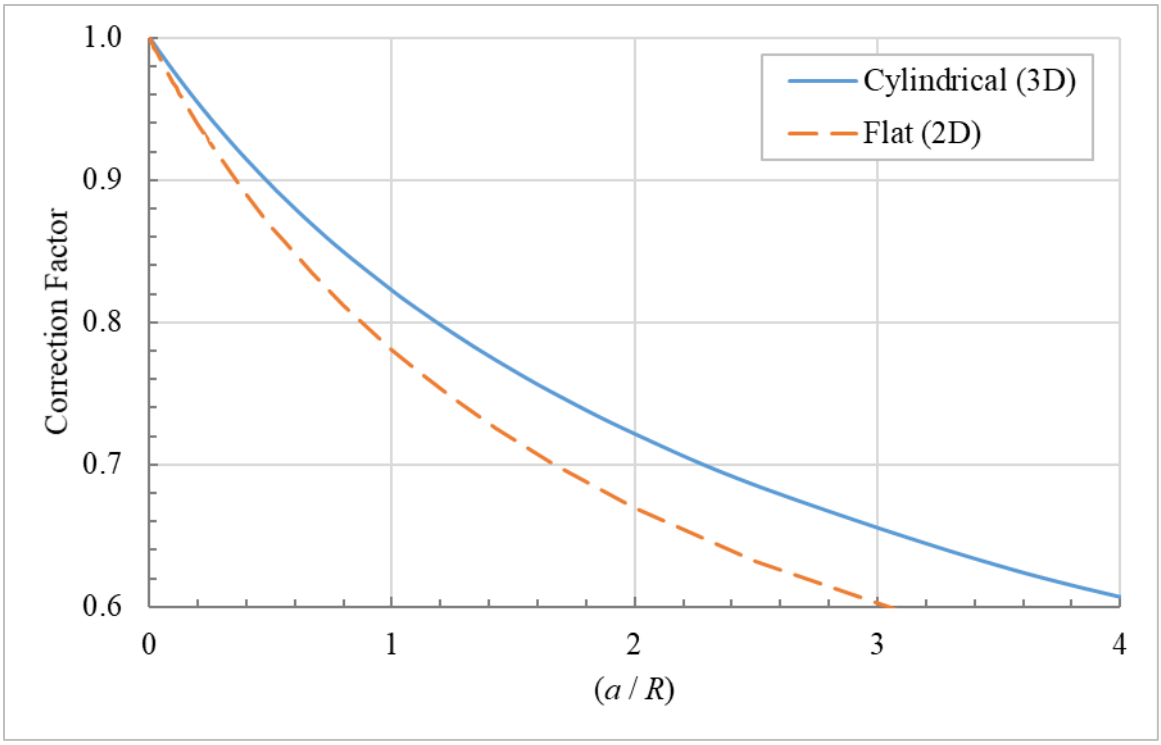

Figure 2-27: Bridgman's Correction Factor

These correction factors, developed for cylindrical and 2D flat specimens, provide significant value within the context of these idealized specimen types. As discussed in Section 2.9.1.2, however, the Bridgman correction factors can exhibit shortcomings and inaccuracies when applied to thin and thick plate coupons, rectangular specimens, and ductile metal materials other than steel, such as copper.

2.9.1.2 Later Analytical Studies

Bridgman's work inspired renewed interest in research related to the onset of necking and post-necking response of ductile metals in tension, serving as the starting point for further development by a broad range of researchers. These researchers refined his works and identified limitations inherent in the assumptions and approaches recommended in *Studies in Large Plastic Flow and Fracture* (Bridgman, 1952). The work of these researchers is discussed in the following paragraphs.

Shortly after Bridgman published his text, Chen (Chen W. H., 1971) published the results of an analytical study on necking building on Bridgman's work investigating the non-uniformities of stress and strain that occur within the neck. Chen's research focused on incorporating the stress distribution in the entire specimen, not just at the neck, as well as the complete load history, effects of plastic unloading, and the effects of changes in geometry that occur during necking. Though, this approach relied on the assumption of an initial imperfection in the surface of the specimen. The imperfection was introduced as a slight reduction in the cross-sectional area at the center of the specimen. As a result, Chen's analysis did not consider necking as a bifurcation from a state of uniform stress. Instead, necking occurs due to a pre-existing localization caused by a reduction in cross-sectional area. With these assumptions, Chen developed and contrasted two cylindrical bar models: one that is geometrically perfect and one with an initial imperfection, as illustrated in Figure 2-28.

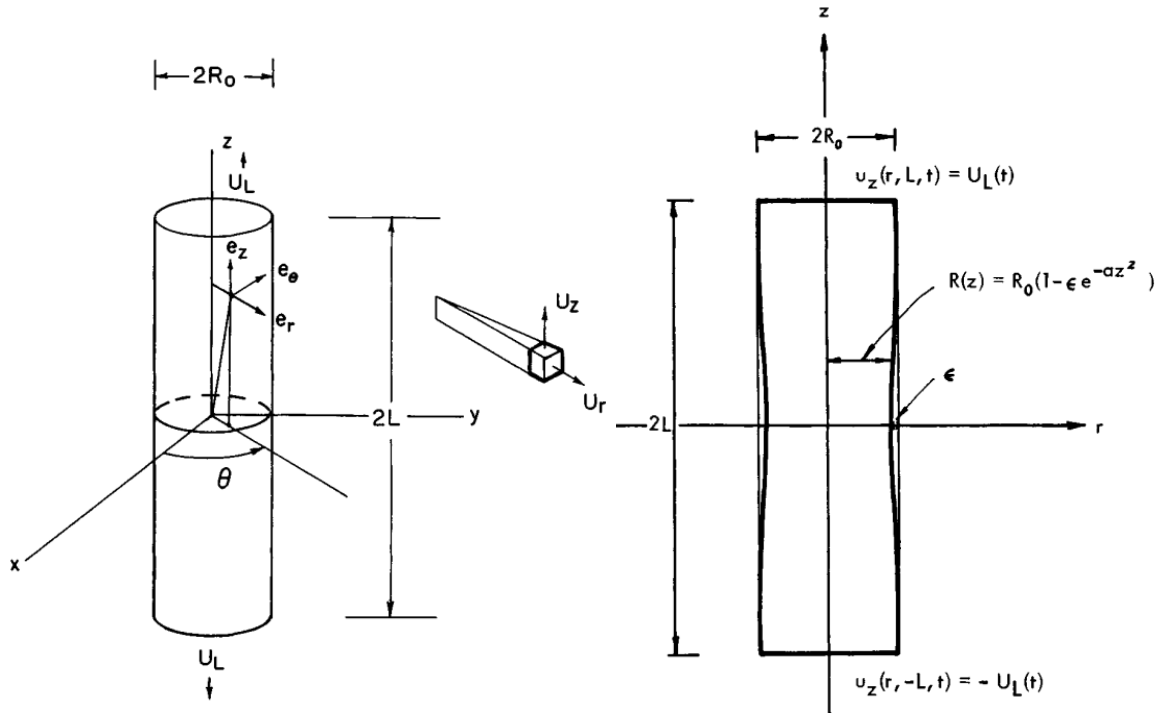

Figure 2-28: Chen's Perfect (left) and Imperfect (right) Bar Models (Chen W. H., 1971)

To simplify the analysis, radial symmetry of each specimen was assumed, allowing for the use of a simplified two-dimensional FEA model for both the perfect and imperfect cylindrical bars. The results of Chen's study show the initially perfect specimen will not neck; however, this result appears to be a consequence of omitting the shear restraint at the ends of the modeled section, discussed previously in Section 2.8.3. Thus, due to the noted deviation of the perfect model from the target post-necking relationship, the remainder of the study focused on the imperfect bar model. The results produced using the two FEA models, shown in Figure 2-29, were then compared and contrasted.

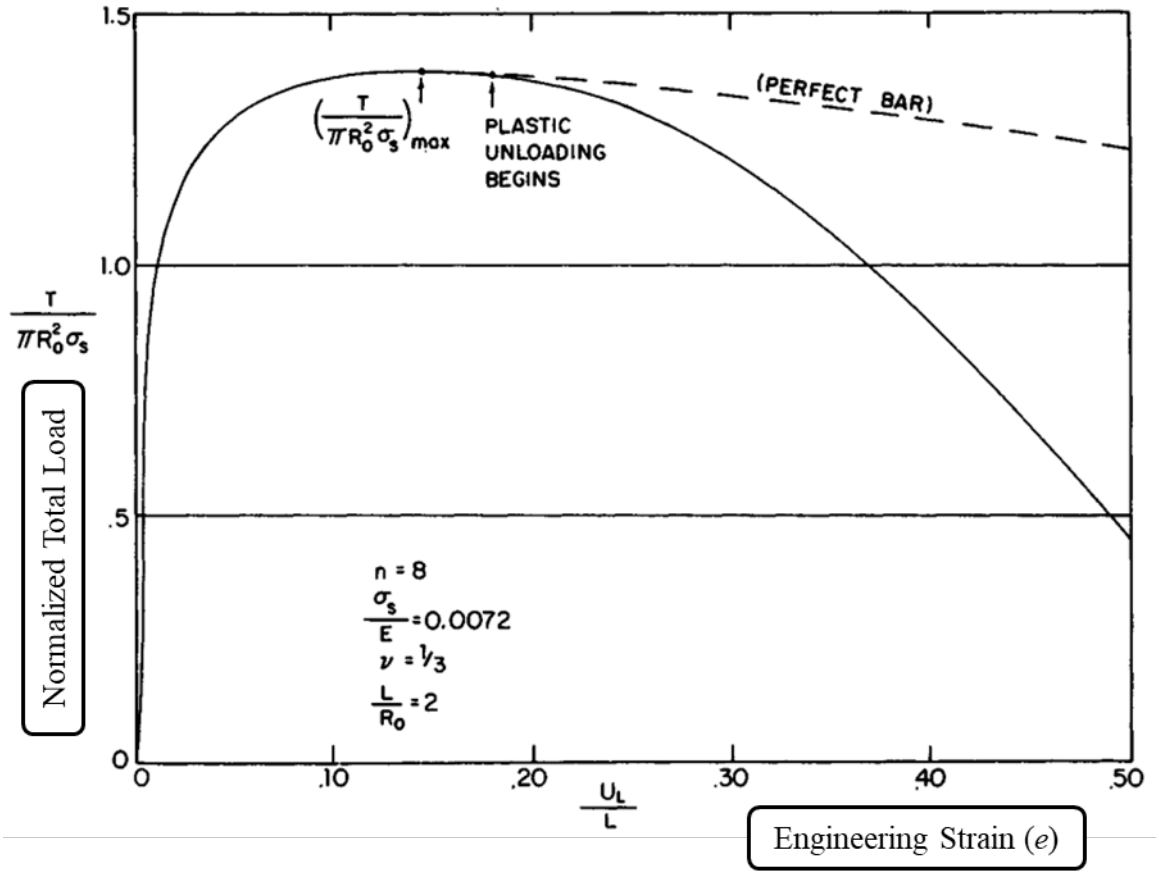

Figure 2-29: Comparison of Perfect and Imperfect Bar Models (Chen W. H., 1971)

While the imperfect bar model generally predicts a load-strain relationship similar to what is commonly observed for a ductile metal coupon in tension, the lack of sufficient post-necking softening in the perfect model is a likely the result of imprecise assumptions, particularly with regard to the simplification of boundary constraints. In addition, closer inspection of Chen's model indicates the predicted peak stress values occur away from the centerline of the specimen, as illustrated in Figure 2-30. Thus, the results of Chen's model deviate considerably from the behavior predicted by Bridgman. which indicate peak stresses occurring at the center of the coupon.

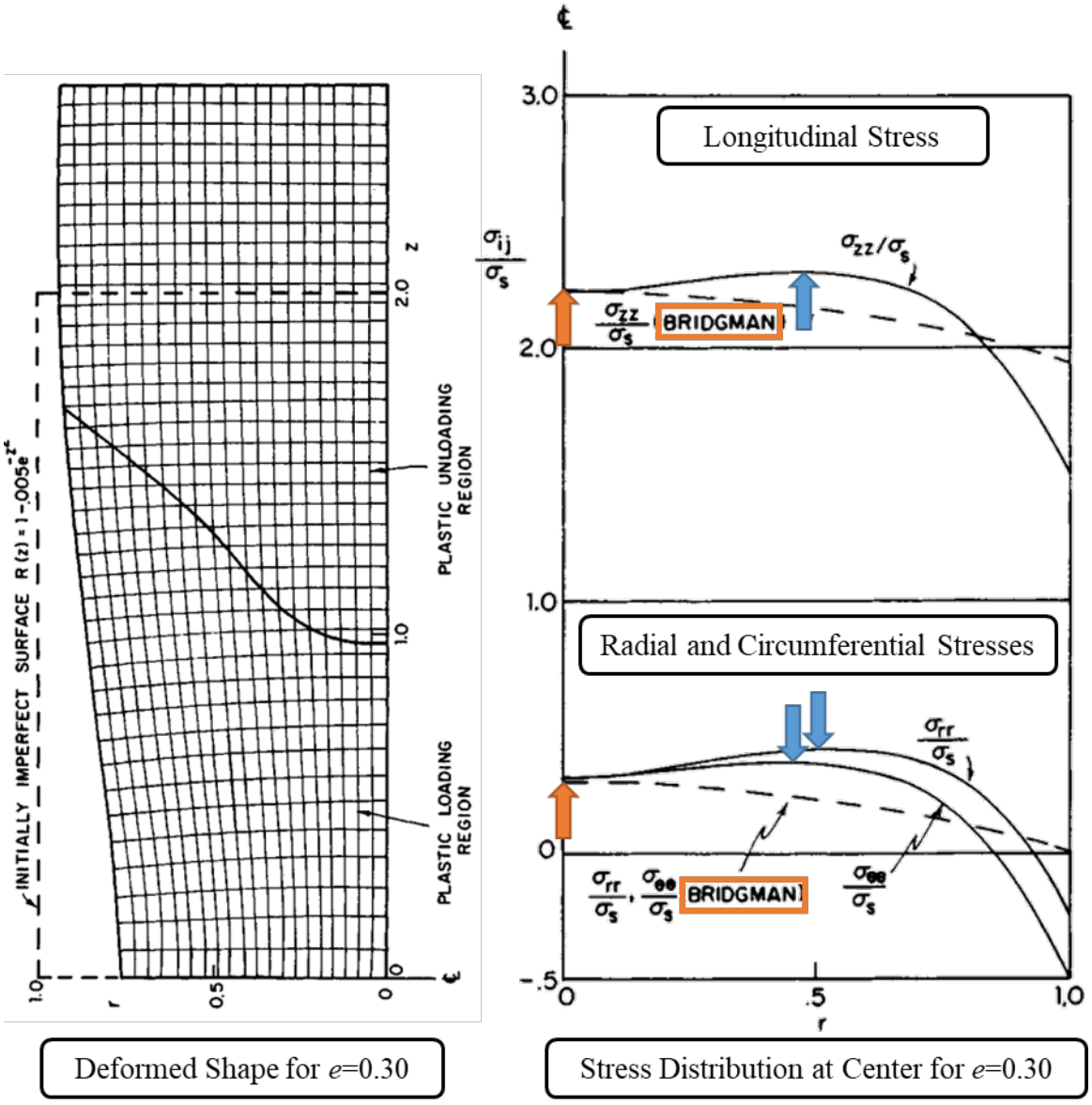

Figure 2-30: Chen Comparison of Stress Distribution in Neck to Bridgman Formulae (Chen W. H., 1971)

Finally, only a single assumed initial imperfection was considered in this study, which obscures the relative effect of the geometry and location of the imperfection. While the paper notes that "the results are not sensitive to the magnitude of [the initial imperfection]", the study does not provide substantive support for this conclusion 9e.g., a

sensitivity study of the assumed imperfection characteristics). Considering an extreme scenario where a large initial imperfection relative to the specimen radius was assumed, it is likely the results would show the results were in fact related to the magnitude of the initial imperfection. Further, as demonstrated by later researchers, coupon FEA model predictions do depend on the assumed initial imperfection (Tvergaard, Needleman, & Lo, 1981) (Shen & Jones, 1993).

Next, Needleman (Needleman, 1972) produced a similar numerical study on necking in cylindrical bars, building upon Bridgman's work through the application of the finite element method. Needleman's study considers the effects of end restraint, noting that a shear free end restraint will result in uniform uniaxial stress for all values of extension, as discussed in Section 2.8.3. Thus, by considering the effects of shear restraints at the ends of the specimen, referred to as a "cemented end-condition," along with the assumption of incompressible material, axisymmetric deformation, symmetry about the midplane of the specimen, and application of the principle of virtual work, Needleman further refined the analytical work by Bridgman. Figure 2-31 compares the stresses within the center of the neck predicted by Needleman's modified behavior model and Bridgman's formulae. Note Needleman's higher predicted stresses at the center of the specimen relative to Bridgman.

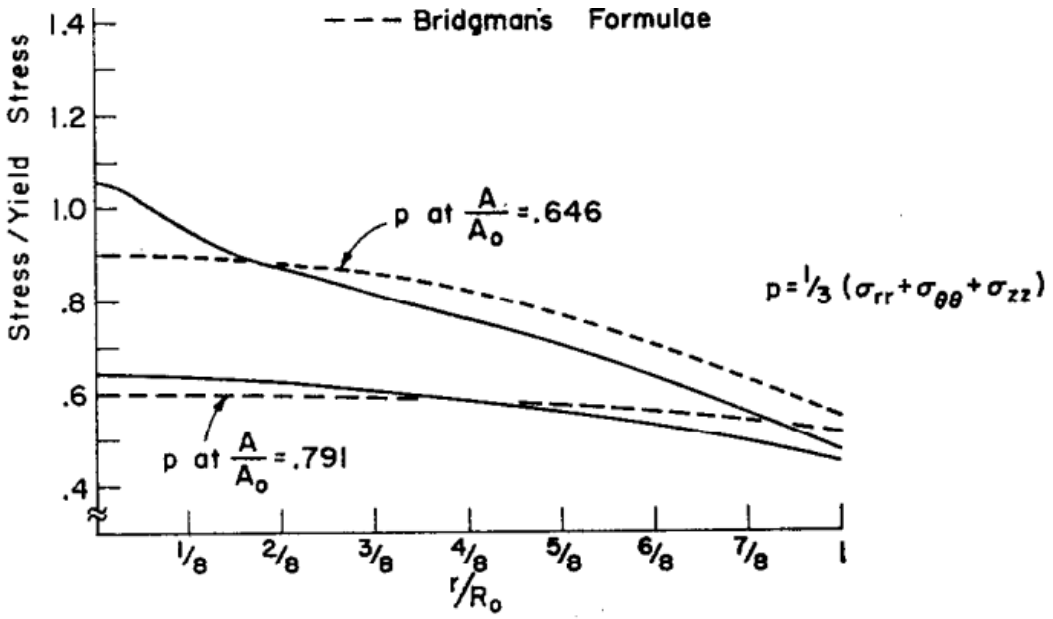

Figure 2-31: Needleman Comparison of Stress Distribution in Neck to Bridgman Formulae (Needleman, 1972)

Later, researchers employed finite element analysis (FEA) models to extend the analytical results developed for circular bar specimens and two-dimensional (2D) flat specimens, developed by Bridgman and Needleman, to thin plate specimens with finite thickness. Specifically, Tvergaard et al. (Tvergaard, Needleman, & Lo, 1981) and Zhang et al. (Zhang, Hauge, Ødegard, & Thaulow, 1999) were able to computationally reproduce the shear banding failure observed in necking and rupture of tested specimens. Though, initial imperfections were used to initiate necking in the models developed in these studies, failing to incorporate the "cemented end-condition" used by Needleman (Needleman, 1972). These studies concluded that the shear banding (i.e., necking) pattern predicted for thin plate specimens was indeed dependent on the assumed initial inhomogeneity, contrasting one of the main conclusions presented by Chen (Chen W. H., 1971), discussed previously.

Cabezas and Celentano (Cabezas & Calentano, 2004) further refined the work on thin plate specimens through finite element analysis. Beginning with a cylindrical specimen, they derived the material true stress-strain relationship and adapted it for thin plate specimen of similar material. While it is not explicitly noted, there is no indication that initial imperfections were used to initiate necking in their computational models. Cabezas' and Celentano's model-predicted behaviors were reasonable, although somewhat imprecise when compared to experimental results. The primary reason for this inaccuracy appears to be the use of a simple power law function to capture the full true stress-strain relationship. Ultimately, Cabezas and Celentano developed a refined correction factor for thin plate specimens based on the area ratio for a thin plate specimen, shown in Equation 2-12, eliminating the need to measure the profile of the neck during testing.

$$\frac{A_0}{A} = \frac{t_0 \cdot w_0}{t_i \cdot w_i} \qquad \text{Equation 2-12}$$

The majority of the preceding work was performed and developed considering the behavior of ductile steel test specimens. In contrast, Celentano et al. (Celentano, Cabezas, & Garcia, 2005) and Garcia-Garino et al. (Garcia-Garino, Gabaldon, & Goicolea, 2006) investigated Bridgman's correction (Bridgman, 1952) applied to copper and aluminum coupons, respectively. Celentano et al. concluded that the standard Bridgman corrections are not accurate for copper, so they developed an alternative correction based on experimental data. A comparison of the Bridgman correction against experimental data for both steel and copper is provided in Figure 2-32. Garcia-Garino et al. concluded that the Bridgman correction was sufficiently accurate for aluminum. The observed deviation of certain materials from Bridgman's correction is generally attributed to differences in necking strains (Tegart, 1966).

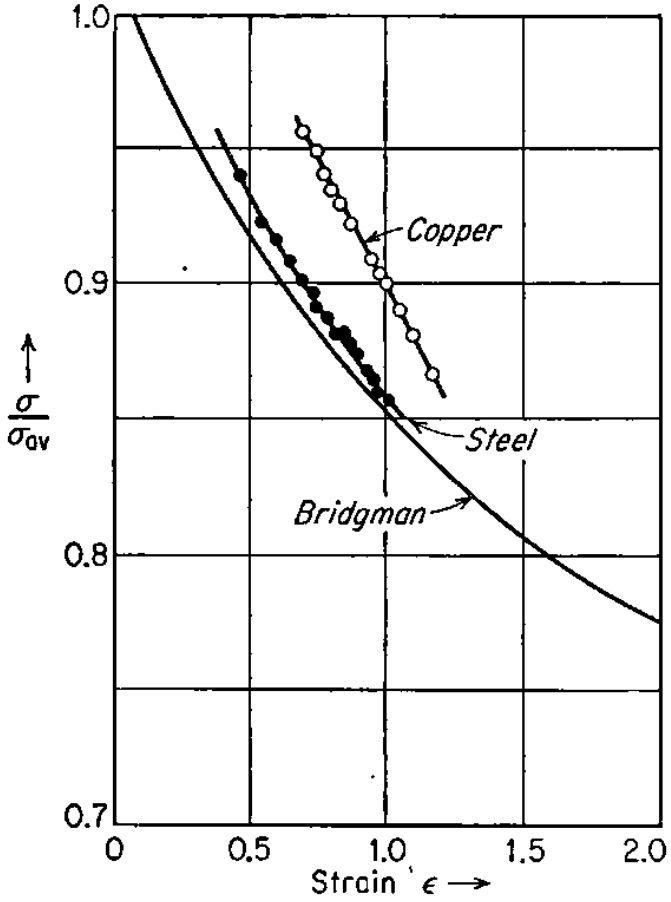

Figure 2-32: Bridgman Correction Factor Comparison for Steel and Copper (Marshall & Shaw, 1952)

Many other researchers built on Bridgman's analytical work, including Shen and Jones (Shen & Jones, 1993), Ling (Ling, 1996), Choung and Cho (Choung & Cho, 2008), and Majzoobi et al. (Majzoobi, Fariba, Pipelzadeh, & Hardy, 2015). Each contributed their own modification and interpretation of his correction to the first approximation of the stress-strain relationship. In addition, many applied other analytical, computational, and experimental methods and techniques to extend, modify, develop and adapt these simple analytical correction approaches. In particular, with the relatively recent advances in computing power and experimental techniques, the recent trend in research on necking and

post-necking response of ductile metals has shifted away from purely analytical relationships toward computational modeling and simulation, iterative fitting and error minimizing methods, and advanced experimental and measurement techniques, as discussed in the following sections.

2.9.2 Iterative Computational Techniques for Evaluating Post-Necking Behavior

Researchers are taking advantage of recent advances in computing techniques and newly available computational resources to investigate post-necking response of ductile metals in tension. In particular, coupling FEA with automated error minimization is proving to be a popular approach to investigating the post-necking response of ductile metals in tension. While early researchers used FEA models to validate analytically derived relationships for necking and post-necking response, as discussed in Section 2.9.1.2, more recently these models have been coupled with iterative programs in an attempt to more rapidly and precisely determine the true stress-strain relationship from tension test data. The iterative approach used by these researchers to develop the true stress-strain relationship varies to some extent, but generally follows the steps illustrated in the flow chart shown in Figure 2-33.

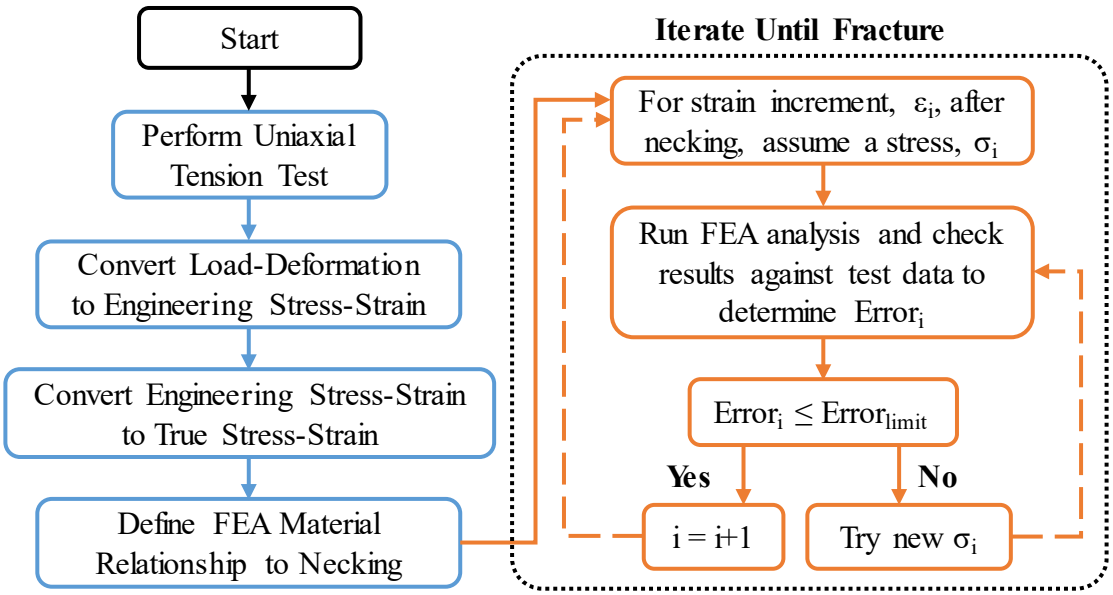

Figure 2-33: General Iterative Approach to Determine the True Stress-Strain Relationship

This iterative approach is used to minimize the error between experimental results and those predicted in computational simulation and has been used by a range of researchers including Zhang and Li (Zhang & Li, 1994), Joun et al. (Joun, Eom, & Lee, 2008), Tao et al. (Tao, Zhang, & Tong, 2009), Kamaya et al. (Kamaya, Kitsunai, & Koshiishi, 2015), and Wang et al. (Wang, Xu, Ren, & Wang, 2016). Early researchers typically used it with simple models and relatively large strain increments. With recent advances in computing power and speed, simulations and iterative techniques have become much more complex and precise, allowing for many more iterations with lower error tolerance and smaller strain increments. The basic process adopted by Wang et al. (Wang, Xu, Ren, & Wang, 2016), referred to by the authors as the "experimental-numerical combined method," or ENM, is similar to that applied by other researchers and is illustrated in Figure 2-34. Results from Wang et al. using this approach are illustrated in Figure 2-35 alongside those developed using the "traditional analytical method," or TAM, which refers to the use of the standard pre-necking true stress and strain relationships (see Equation 2-3

and Equation 2-4) and Bridgman's correction (see Section 2.9.1.1) for post-necking response. Note the high quality of the fit using ENM, with the exception of the portion immediately preceding failure.

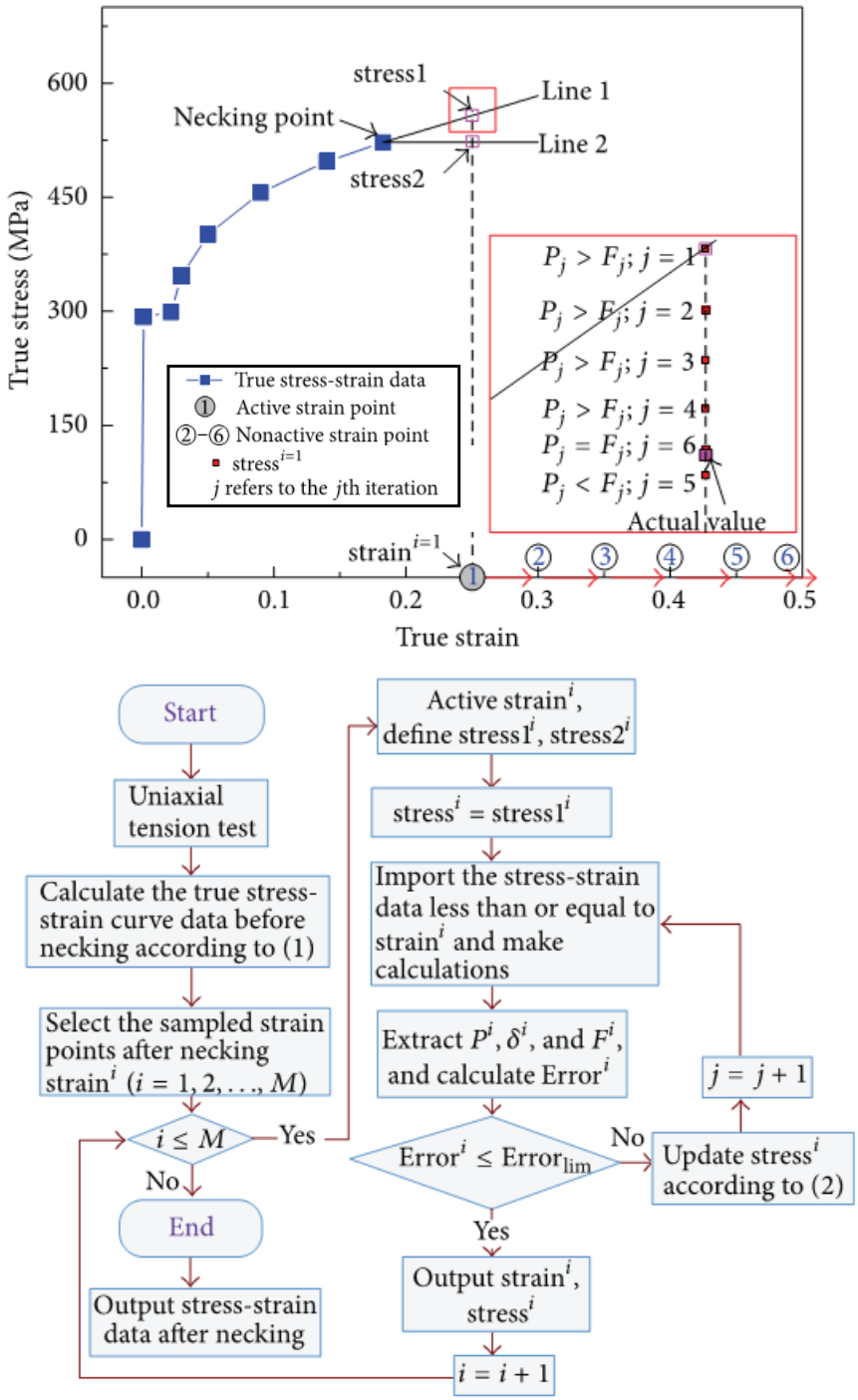

Figure 2-34: Summary of the Experimental-Numerical Combined Method (ENM) (Wang, Xu, Ren, & Wang, 2016)

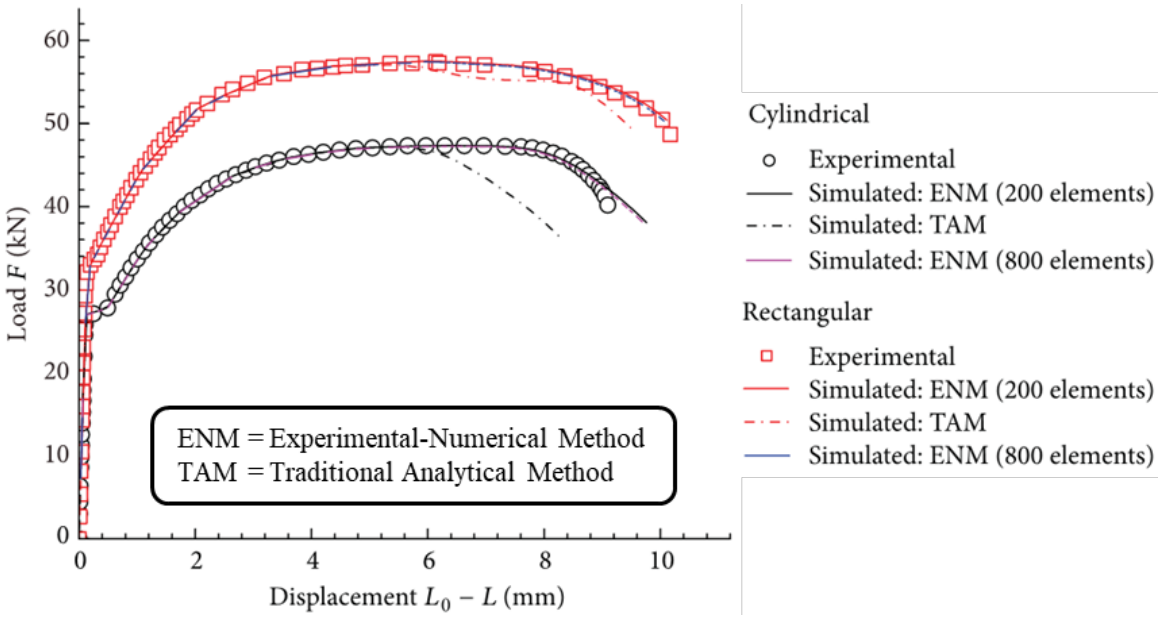

Figure 2-35: Results using Iterative Error Minimizing Technique (Wang, Xu, Ren, & Wang, 2016)

As it is currently applied, the iterative error minimizing technique typically seeks only to provide a best fit to the data. Thus, with increased computing power and the ability to choose extremely fine strain increments and small error tolerances, it is possible that application of such a procedure produces nearly perfect correlation between simulation and experiment. However, such an approach is subject to errors because it could end up fitting the noise or natural experimental variability, rather than the underlying trend. As a result, the true stress-strain relationship developed may not be accurate and may produce inaccurate or spurious results when applied to another model.

Nonetheless, the iterative error minimization approach does show considerable promise. In particular, through application of simple rules to help guide the iterative procedure, the likelihood of fitting noise can be reduced. Thus, as recommended for future research in Section 6.3.6, the derivative rules proposed in Chapter 3 could be incorporated

into the iterative process to improve the speed of convergence and reduce the likelihood of fitting spurious noise in the experimental data.

2.9.3 Experimental Techniques for Evaluating Post-Necking Behavior

In addition to the analytical and computational approaches described in the preceding sections, necking and the post-necking behavior of ductile metals in tension has also been extensively studied using advanced experimental techniques. These experimental techniques have been used as an alternative or, more often, to compliment and inform analytical and computational approaches. While there is value in these approaches, their use was intentionally avoided and omitted when developing the rules and methodologies presented in this dissertation, because the primary focus was to develop the true stress-strain relationship from only load-deformation data and geometry information from a standard coupon tension test, as discussed in Section 1.2. Nevertheless, there is value to understanding the state of the practice in experimental techniques related to the study of necking and post-necking response of ductile metals in tension and considering the observations and conclusions developed through this research. Thus, the following sections provide a brief summary of some of the more prevalent experimental techniques applied to develop the true stress-strain relationship for ductile metals in tension.

2.9.3.1 Digital Image Correlation (DIC)

Digital image correlation, or DIC, is a technique used to optically track strains over a select region of the coupon throughout tension testing. The basic process is illustrated in Figure 2-36. As shown, a "speckle" pattern is applied to the surface of the specimen and one or more digital cameras are used to track the movement of this pattern. Then, those images are processed using special computer software to compute the relative strains across the surface. A variety of techniques for DIC are available at the current time, including a

range of visual speckle patters, image processing software and techniques, and the use of one or multiple cameras (sometimes referred to as stereo DIC).

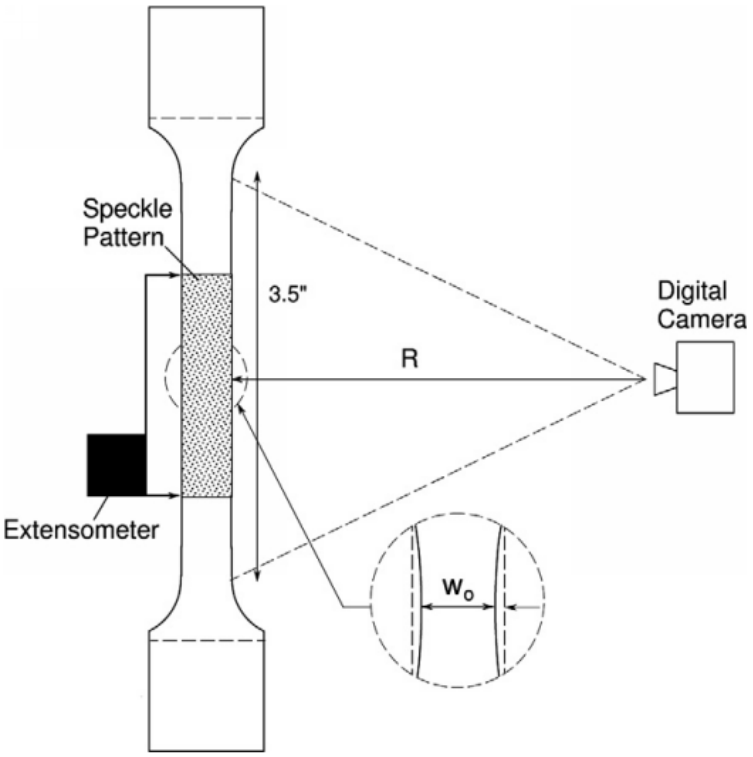

Figure 2-36: Strain Visualization using Digital Image Correlation (DIC) (Tardif & Kyriakides, 2012)

DIC is widely used to study the strain profile in the neck by many researchers including Kim et al. (Kim, Serpantié, Barlat, Pierron, & Lee, 2013), Kamaya et al. (Kamaya, Kitsunai, & Koshiishi, 2015), Scheider et al. (Scheider, Brocks, & Cornec, 2004), Duan et al. (Duan, Jain, Metzger, & Wilkinson, 2007), Choung and Cho (Choung & Cho, 2008), Tao et al. (Tao, Zhang, & Tong, 2009), Coppieters et al. (Coppieters, Cooreman, Sol, Van Houtte, & Debruyne, 2011), Tardif and Kyriakides (Tardif & Kyriakides, 2012), and Coppieters and Kuwabara (Coppieters & Kuwabara, 2014), among many others. The benefit of DIC is it allows the strain profiles to be physically measured

and studied without the simplifications and the assumptions required to facilitate analytical approaches, or inherent in computational simulations.

Of note, through application of DIC, Scheider et al. (Scheider, Brocks, & Cornec, 2004) were able to develop some of the first accurate predictions of the behavior of thick plate, or rectangular, coupon specimens. Prior to the work by Scheider et al., thick plate rectangular geometries were generally avoided due to difficulty in analytically capturing the complex deformed shape at the neck analytically. Specifically, a cross-section through the neck of a rectangular specimen takes a "bow-tie" shape, as illustrated in Figure 2-37. This bow-tie geometry is difficult to study analytically due to the lack of the radial or 2D symmetry used to develop the analytical relationships for circular and flat specimens, respectively. Thus, the application of DIC aided in the development of some of the earliest predictive models of thick plate and rectangular tension coupons. An example comparison of the tested and simulated load versus width reduction for a rectangular specimen is provided in Figure 2-38. Note that the fit is fairly accurate over the range considered, although the data deviate beyond the limits presented due to, in the author's words, the inability of "purely elastic-plastic simulation" to predict unstable failure of the section.

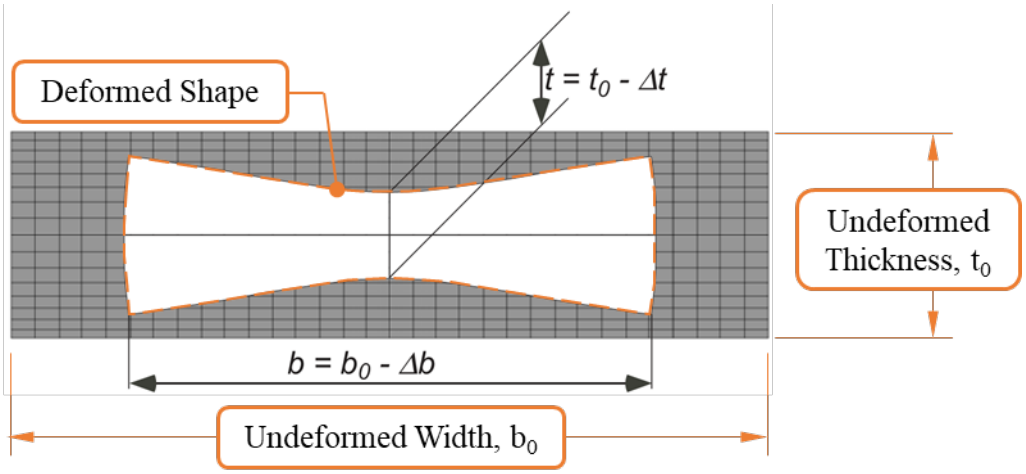

Figure 2-37: Deformed Shape Thick Plate Specimen after Necking (Scheider, Brocks, & Cornec, 2004)

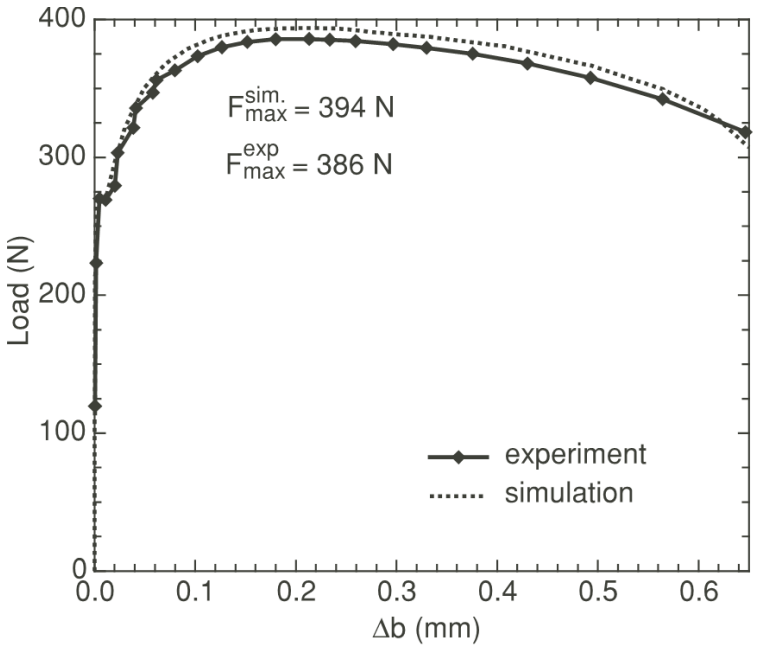

Figure 2-38: Load versus Width Reduction Comparison of Test and Simulation (Scheider, Brocks, & Cornec, 2004)

While it shows great promise as an experimental measuring technique, DIC is subject to two primary shortcomings. First, due to the visual nature of the approach, only measurements of surface strains are captured. Thus, it provides no quantitative information

for strains within the section, which are often the drivers of behavior, particularly failure. Second, the strain measurements using DIC have somewhat limited resolution, typically controlled by the speckle pattern and the process of its application to the specimen. An example of the relative resolution of strain data is provided in Figure 2-39. Note the pixelated presentation of the strain fringe plots indicating the relative noisiness of the data, suggesting significant variability and likely imprecision in the measured strains. Though, with advances in technology, the latter shortcoming is expected to become much less significant in the future.

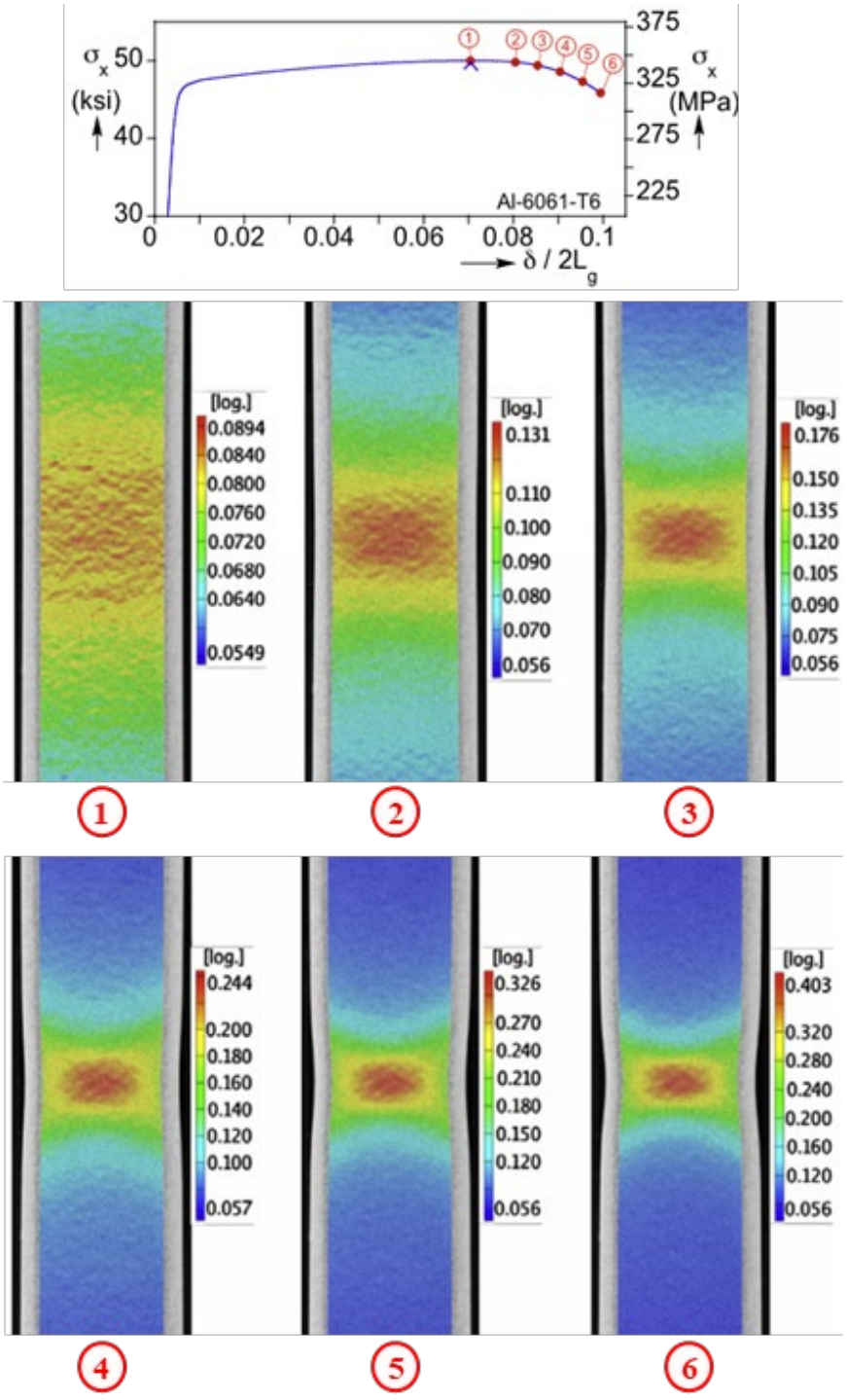

Figure 2-39: Surface Strains Measured using Digital Image Correlation (DIC) (Tardif & Kyriakides, 2012)

2.9.3.2 Fractography and Scanning Electron Microscopy (SEM)

Fractography refers to the study of fracture surfaces of a material. To visually amplify and study the fracture surface and phenomena like void nucleation, growth, and coalescence discussed in Section 2.9.4.2, transmission electron microscopy (TEM), and, more recently, scanning electron microscopy (SEM), are often employed. TEM preceded SEM. Due to the limitations of TEM, SEM technology is currently the standard approach used to study the fracture surface of ductile metals. SEM is useful in fractography, as it allows for a large depth of field and high magnifications, typically from 5,000× to 10,000× (Campbell, 2012). The basic elements of an SEM are illustrated in Figure 2-40.

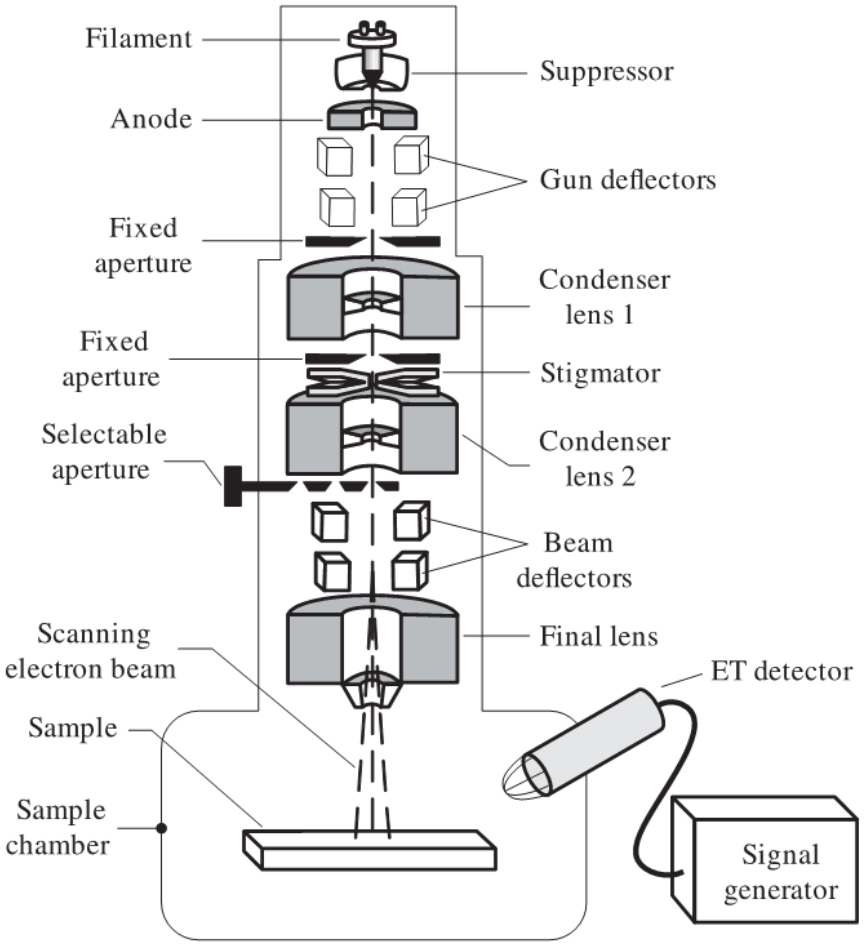

Figure 2-40: Basic Elements of an SEM (McEvily, 2013)

SEM is used to study the fracture surface of ductile metal tension coupons by the following researchers: Wouters and Froyen (Wouters & Froyen, 1996), Thomason (T, 1998), Duan et al. (Duan, Jain, Metzger, & Wilkinson, 2007), Ramazani et al. (Ramazani, Schwedt, Aretz, Prahl, & Bleck, 2013), Momoh et al. (Momoh, Donatus, & Alaneme, 2016), and Cheng et. al (Cheng, Hu, Choi, & Sun, 2017), among many others. This widespread use is because an SEM produces extremely detailed images of the area of failure allowing for close inspection to identify flaws, granular structure, voids, fracture types, and many other features within the facture surface. Examples of fracture surface images produced with SEM are provided in Figure 2-41.

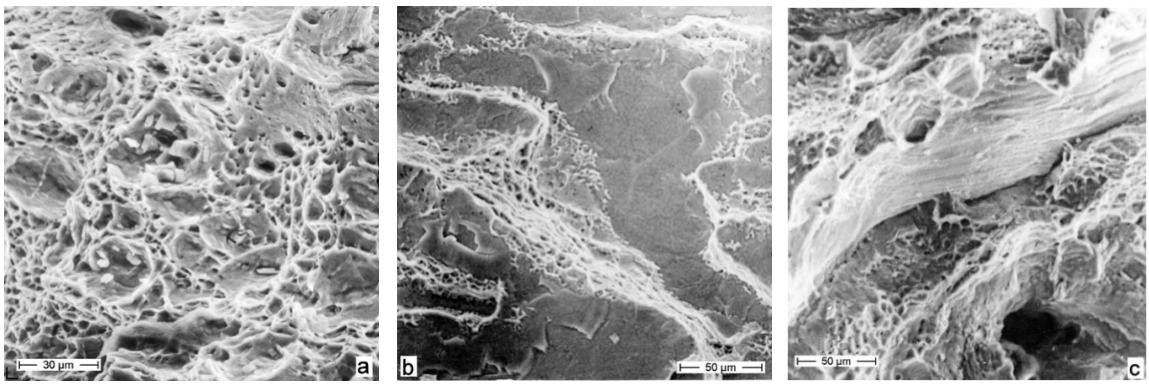

Figure 2-41: Fracture Surface Images of Steels developed using SEM (Möser, 1987)

Due to the cost of SEM equipment and the time and effort associated with processing specimens for imaging, it is often impractical for post-test examination of tension coupons. Nevertheless, there is potential to study and learn more about phenomena associated with necking, post-necking, and fracture of ductile metals in tension using these techniques. In particular, SEM has provided visual confirmation of micro-structural phenomena like void nucleation, growth, and coalescence, discussed in Section 2.9.4.2, and permitted the ability to measure and quantify imperfections and extremely fine details found within the fracture surface.

2.9.3.3 X-Ray Diffraction

X-ray diffraction is a technique used to study and track the movement of the grain structure within specially produced ductile metal samples during a tension test. The basic experimental test setup using X-ray diffraction is illustrated in Figure 2-42. In addition, the ability to define the microstructure of materials using X-ray diffraction has allowed for the development of microstructure-level FEA models that explicitly reproduce the observed material microstructure. An example image and corresponding microstructural FEA model are illustrated in Figure 2-43.

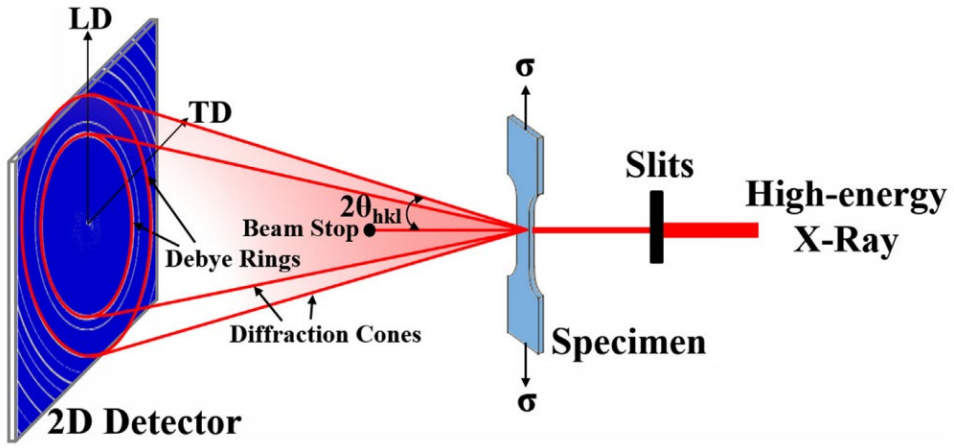

Figure 2-42: Experimental Setup using X-ray Diffraction (Li, et al., 2018)

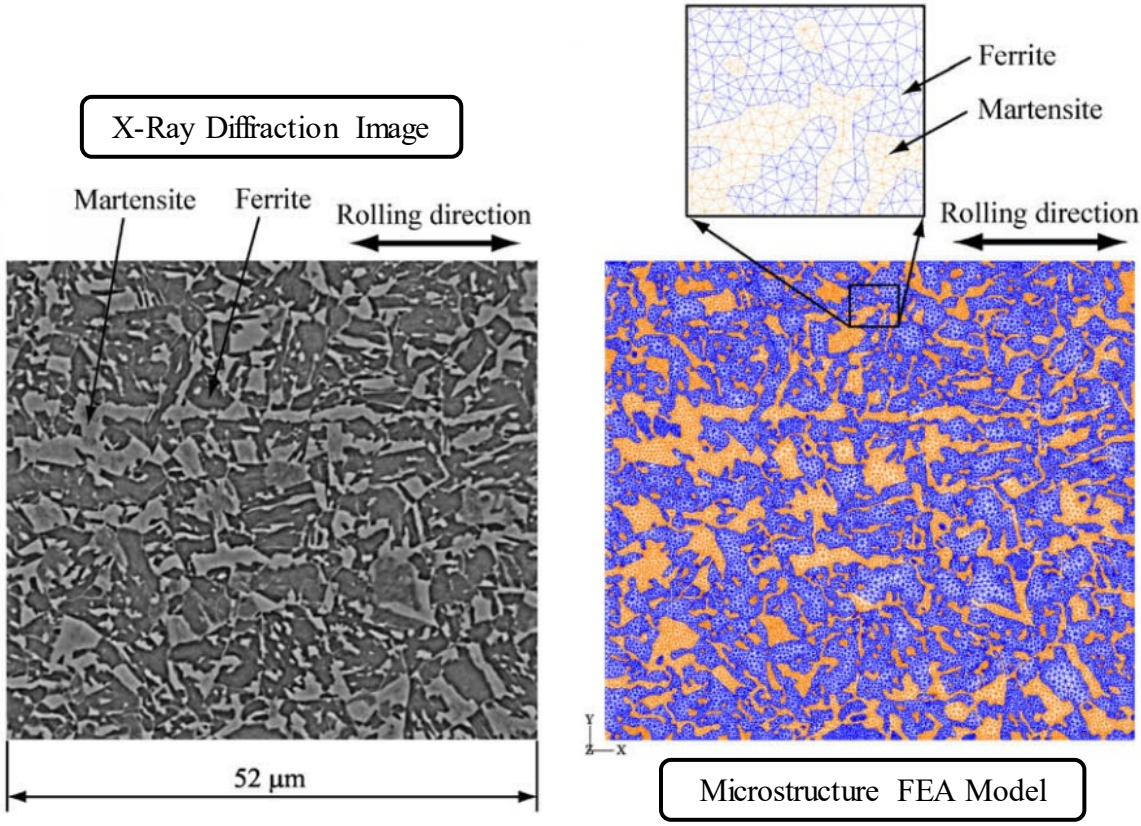

Figure 2-43: Image using X-Ray Diffraction and Accompanying Microstructural Finite Element Analysis Model (Sun, Choi, Liu, & Khaleel, 2009)

X-ray diffraction has been used by several recent researchers to study the post-necking response of ductile metals including Wang and Ren (Wang & Ren, 2007), Sun et al. (Sun, Choi, Liu, & Khaleel, 2009), Jia et al. (Jia, et al., 2009), and Li et al. (Li, et al., 2018), among many others. Like SEM, it requires special equipment and sample processing techniques that are not commonly found in labs performing tension coupon testing. As a result, there is limited practicality to its broad use to develop the true stress-strain relationship for computational analysis. However, it provides another potential opportunity to study and learn more about phenomena associated with necking, post-necking, and fracture of ductile metals in tension. The resulting conclusions of these experimental

studies can then be used to improve and refine the approach to developing the true stress-strain relationship for ductile metals in tension.

2.9.4 Microstructural Post-Necking Phenomena

Another recent evolution in research of post-necking response of ductile metals has been the study of material level phenomena. In most analytical and computational techniques, it is generally assumed that the material is homogeneous and uniform. In recent decades, the effects of non-uniformities and material-level phenomena on post-necking response have become a topic of considerable research. The following sections introduce two of the most prevalent areas of current research in material level effects on post-necking behavior. The potential to incorporate observations and conclusions derived from these material level phenomena into the recommendations presented in this dissertation is suggested as a topic for future research in Section 6.3.1.

2.9.4.1 Diffuse and Local Necking

Diffuse and local necking refers to necking phenomena commonly associated with the behavior of thin sheet metal tension coupon specimens. Diffuse necking refers to the inward deformation of the sides of a coupon specimen; much like the typical necking observed in thick plate, rectangular, and cylindrical ductile metal tension coupons. Localized necking refers to a rapid through thickness reduction at the neck that is exhibited in thin sheet metal coupon specimens just prior to failure. Local and diffuse necking are illustrated for a sheet metal coupon in Figure 2-44.

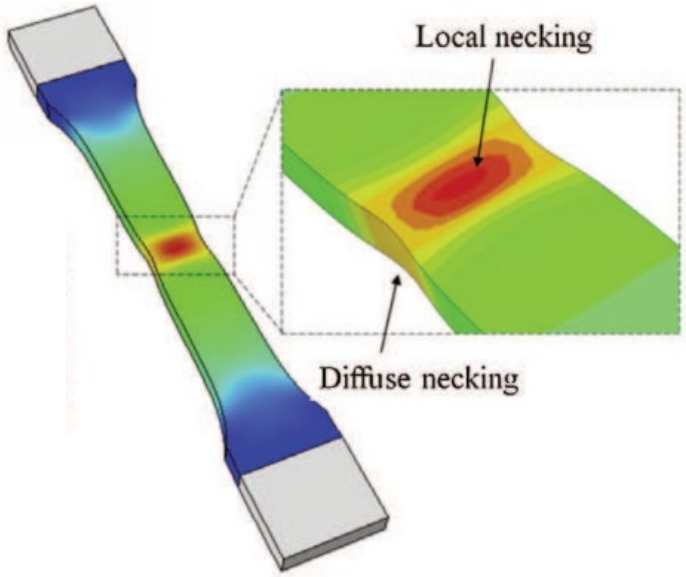

Figure 2-44: Diffuse and Local Necking (Abbassi, Mistou, & Zghal, 2013)

It is generally accepted that diffuse necking is the first indicator of failure in a tension specimen. Diffuse necking defines the onset of necking, beginning at the point of maximum load, or peak engineering stress. Diffuse necking is said to govern the early portion of the post-necking response of sheet metal tension coupons and is characterized by a reduction in the width (larger dimension) of thin metal coupons (e.g., sheet metal). Local necking is assumed to occur later, between diffuse necking and fracture. Local necking is identified as the mechanism precipitating final failure along an inclined band that runs across the width of the specimen and is characterized by a rapid reduction in thickness (smaller dimension) of thin metal coupons just prior to failure. The general relationship between diffuse and local necking with respect to a tension test load-deformation curve is exhibited in Figure 2-45, along with an illustration of the typical deformed shape within the necked region during both diffuse and local necking phases of response.

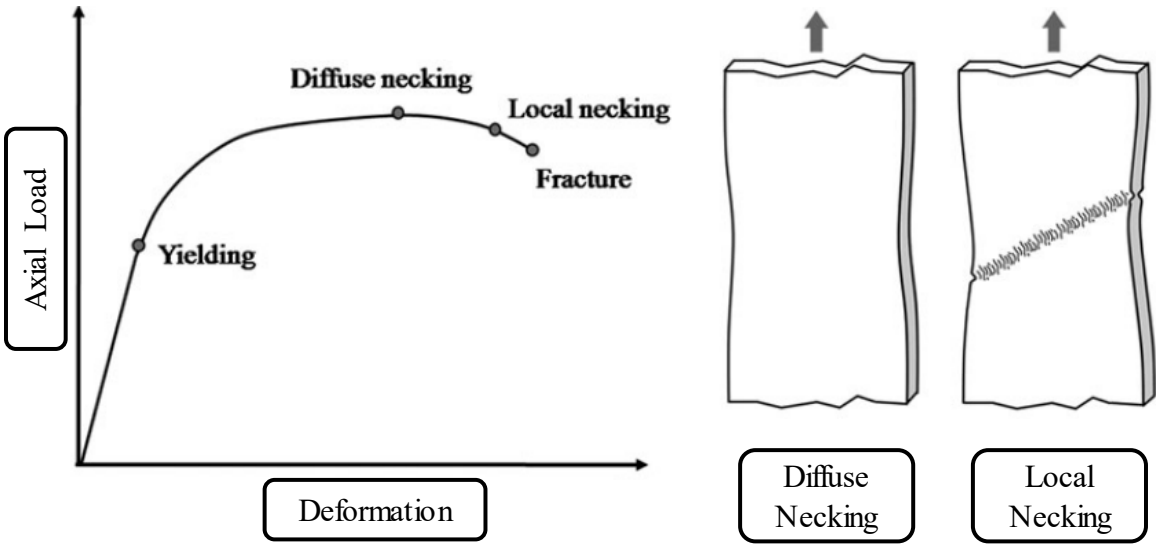

Figure 2-45: Diffuse and Local Necking on Tension Load-Deformation Curve (Hyun, Kim, Bang, & Lee, 2014)

Research on diffuse and localized necking appears to trace back to early analytical work on plastic instability published by Swift (Swift, 1952) and Hill (Hill R. , 1952). Their work, along with the work of other early researchers of local and diffuse necking, including Rice (Rice, 1976), Needleman and Rice (Needleman & Rice, 1978), and Tvergaard et al. (Tvergaard, Needleman, & Lo, 1981), focused on analytical studies that require initial geometric or material imperfections to initiate necking. Later research by Lian and Zhu (Lian & Zhou, 1989), Cabezas and Celentano (Cabezas & Calentano, 2004), and Hyun et al. (Hyun, Kim, Bang, & Lee, 2014) refined these early analytical relationships, incorporating the Bridgman correction, as well as its various modifications, discussed previously in Section 2.9.1. More recently, these researchers have leveraged iterative finite element analysis techniques discussed in Section 2.9.2 to study diffuse and local necking in greater detail.

The topic of local and diffuse necking was not a major consideration in the context of this dissertation because it is still unclear whether it is, in fact, a unique and separate set

of phenomena occurring only in sheet metal specimens, or whether it is the standard necking process manifesting somewhat unique behavior in these specimens due to their large cross-sectional aspect ratio. Thus, because it is possible that further investigation and application of lessons learned from research on local and diffuse necking phenomena could improve the conclusions developed in this dissertation, particularly capturing the behavior just prior to fracture, this is a topic recommended for future work in Section 6.3.1.

2.9.4.2 Void Nucleation, Growth, and Coalescence

Ductile metals are crystalline solids, as summarized in Section 2.5. They are made up from many crystals with different orientations, boundaries, flaws, and other non-uniformities. Void nucleation, growth, and coalescence in the context of ductile deformation and fracture in tension refers to the process by which microscopic voids form within a ductile metal during loading, growing with additional stress and deformation, and coalescing as they grow larger. This process can ultimately result in complete failure of the coupon specimen.

During void nucleation, applied stresses cause voids to form, typically along boundaries between crystalline grains within the metal, as illustrated in Figure 2-46. This process is assumed to significantly affect response once considerable plastic deformation has already occurred. With continued application of stress and deformation, the voids begin to grow and eventually coalesce to form larger voids and microcracks within the material, as illustrated in Figure 2-47 (McEvily, 2013).

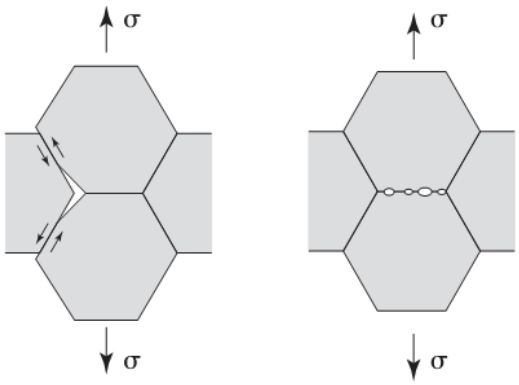

Figure 2-46: Void Nucleation along Granular Boundaries (McEvily, 2013)

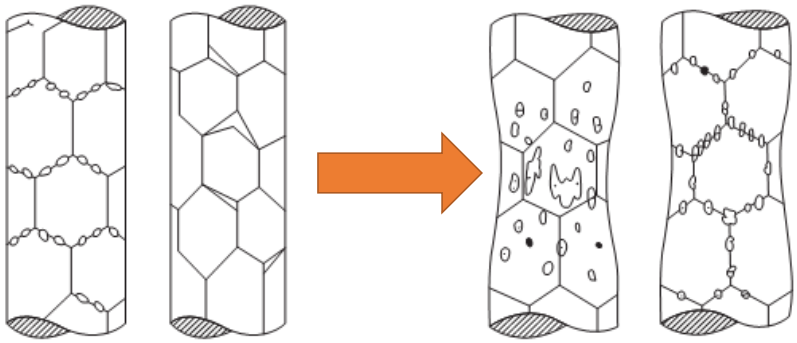

Figure 2-47: Void Growth and Coalescence (McEvily, 2013)

As the voids grow and coalesce, their effect on the behavior becomes increasingly significant. Ultimately, fracture is assumed to occur by brittle failure of the intact material between voids. Void nucleation, growth, and coalescence phenomena are supported by inspection of the failure surfaces of ductile metal coupons, which often exhibit a dimpled surface (McEvily, 2013), as shown in Figure 2-48 for ductile tension fracture and ductile shear fracture. The study of the fracture surface is called fractography and is discussed in Section 2.9.3.2. Note the relatively circular shape of the dimples for the ductile tension fracture in comparison to the elongated oval-shaped dimples exhibited in the ductile shear fracture. Features like this can be used to indicate the state of stress just prior to failure.

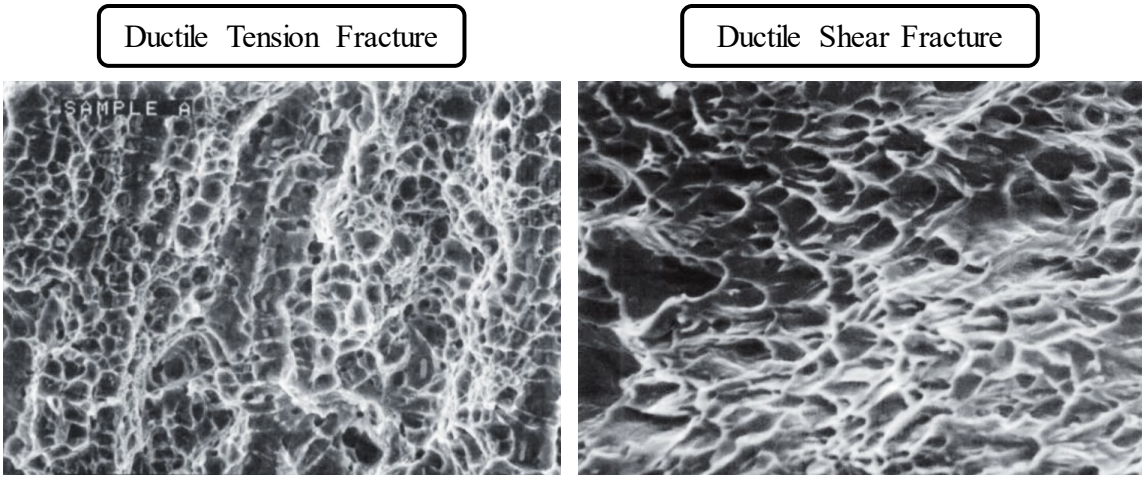

Figure 2-48: Dimpled Surfaces for Ductile Tension and Ductile Shear Fractures (McEvily, 2013)

Void nucleation, growth and coalescence was first identified in by Tipper (Tipper, 1949) and later investigated by a variety of researchers including Rice (Rice, 1976), Needleman and Rice (Needleman & Rice, 1978), LeRoy et al. (LeRoy, Embur, Edwards, & Ashby, 1981), Tvergaard (Tvergaard V. , 1981) (Tvergaard V. , 1982), Thomson (Thomson, 1985), Sun et al. (Sun, Choi, Liu, & Khaleel, 2009), and Scheyvaerts and Pardoen (Scheyvaerts & Pardoen, 2010), among many others. Due to the extremely finite nature of voids, also referred to as cavities in some publications, they are often not considered explicitly in analytical and computational studies. Rather, equivalent properties are used to capture the overall effect of these microstructural anomalies on the behavior of ductile metal materials.

Several methods have been developed to capture and approximate the effects of void nucleation, growth, and coalescence on material behavior. These range from directly representing voids in microstructural analysis models to simple modification factors applied to standard material properties, much like the previously discussed Bridgman correction (see Section 2.9.1.1) (Bridgman, 1952). Though, the most common way the

effects of void nucleation, growth, and coalescence are captured is through damage evolution models.

Damage evolution modelling was developed to quantify the effects of void nucleation, growth, and coalescence, within an FEA model. This approach considers aggregation of damage as a driver of post-necking response. Research by Needleman and Rice (Needleman & Rice, 1978), Gurson (Gurson, 1972), Tvergaard and Needleman (Tvergaard & Needleman, 1984), Chen and Dong (Chen & Dong, 2009), and Abbassi et al. (Abbassi, Mistou, & Zghal, 2013), among others, apply this approach to approximate the effects of the evolution of these microstructural damages within a typical solid continuum element. Damage evolution constitutive equations were not incorporated into the simple material models used in this research work. However, based on the observed trend of strength overestimation near the point of failure that occurs when applying the approach recommended in this dissertation (see Chapter 4), it is likely that these damage evolution models provide a means for further improvement. Thus, this is a topic suggested for future research in Section 6.3.1.

2.10 Research on Necking and Post-Necking True Stress and Strain Relationships for Other Materials

While generally beyond the scope of this dissertation, a brief investigation of research related to the true stress-strain response of other materials in tension was performed. Specifically, the tension behaviors of certain polymers were researched; particularly those that exhibit stabilized neck drawing, also referred to as cold-drawing. The main findings of this investigation provide useful insights into concepts explored in Chapter 3 and are presented in the following subsection.

2.10.1 Cold-Drawing Polymers

Certain polymers exhibit a unique behavior not observed in ductile metals; neck stabilization and drawing. Stabilized necking and drawing, commonly referred to as cold-drawing, is observed in common polymers, such as polyethylene and nylon, when tested in tension at temperatures approximately 50°C below the glass transition temperature, T_G (Ashby & Jones, 2006). Cold-drawing polymers loaded in tension elongate uniformly until a localized neck forms. This behavior is similar to that observed in standard tension coupon tests of ductile metals. Although, rather than precipitating failure as would be the case for a ductile metal, the neck in cold-drawing polymers eventually stabilizes, drawing out over the entire length of the reduced section of the tension specimen. After the neck has drawn out, the load carrying capacity of the specimen generally increases until failure. Images of stabilized necking during tension testing are provided in Figure 2-49. The typical cold-drawing stress-strain response for polymeric materials is illustrated in Figure 2-50.

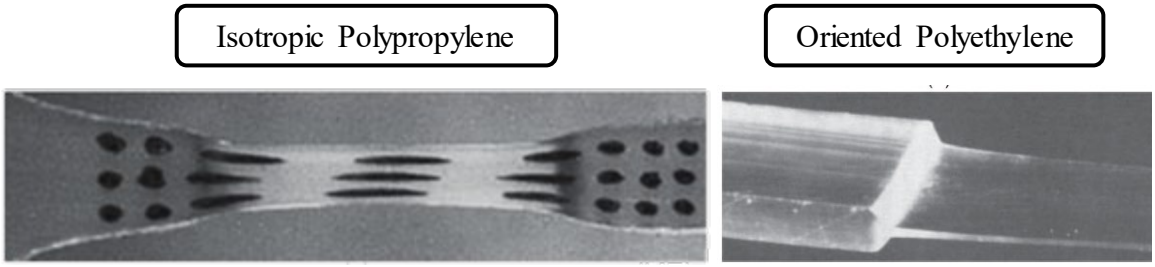

Figure 2-49: Photographs of Neck Cold-Drawing in Tension (Ward & Sweeney, 2013)

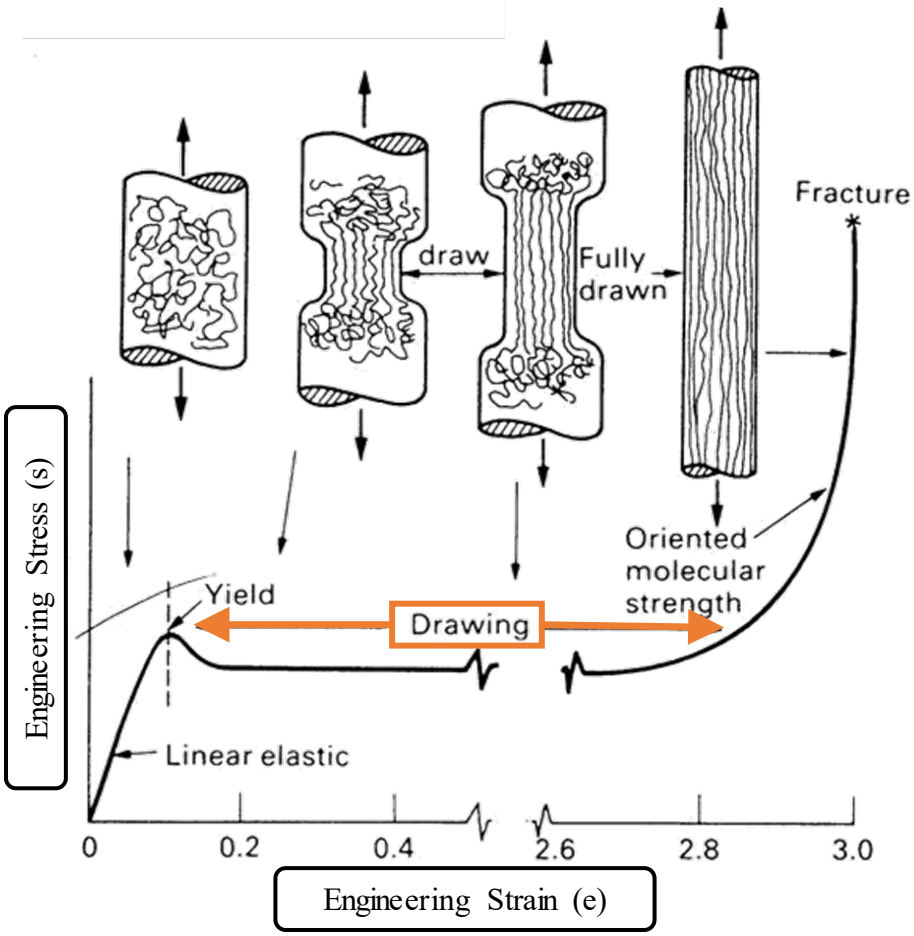

Figure 2-50: Stress-Strain Curve for Cold-Drawing Polymers in Tension (Ashby & Jones, 2006)

The true stress-strain relationship for cold-drawing polymeric materials has been studied by several researchers including Tuğcu and Neale (Tuğcu & Neale, 1987), Kontou and Farasoglou (Kontou & Farasoglou, 1998), and Masud and Chudnovsky (Masud & Chudnovsky, 1999), among many others. To maintain the focus of this dissertation, detailed study of this phenomena was not performed. Rather, cold-drawing was investigated and understood in the context of the major driver of the response; specifically, the reversal in curvature that allows the neck to stabilize and draw. In Section 3.4, the cold-

drawing phenomena is discussed in greater detail and contrasted with the material behavior exhibited in non-cold-drawing materials like ductile metals.

2.11 CONCLUSIONS

The true stress-strain relationship for ductile metals has been studied at great length by a wide variety of researchers over nearly a century and a half, with substantial focus on the onset of necking and post-necking behavior. Research efforts have included a wide variety of analytical, computational, and experimental methods, with a recent observed trend involving combining these approaches. The breadth and depth of research available makes it difficult to capture and present it all in adequate depth. Thus, the goal of this chapter was to convey the means and methods used across a range of these studies, along with the significant conclusions and lessons learned.

In addition, this chapter is intended to provide a starting point for investigation of the many topics discussed and a basis for the research work, observations, and conclusions presented in the following chapters. Thus, for brevity, certain areas of related research have been omitted. The approach taken is not meant to diminish or discount these prior works. Rather, it is a consequence of the fundamental nature of the topic of discussion; necking and post-necking response of ductile metals, coupled with the extremely broad existing body of related research.

In Chapter 3, the works of Considère (Considère, 1885), Drucker (Drucker, 1959), and Hill (Hill R. , 1958), are explored in greater detail to distill the first two recommended "rules" for developing the true stress-strain relationship for ductile metals, particularly structural steels. This is followed by a brief review of cold-drawing polymer behavior, discussed previously in Section 2.10.1, which reveals the third and final "rule." These rules are then incorporated in the recommended step-by-step process for determining the true

stress-strain relationship for structural steels from tension coupon test data in Chapter 4. Finally, the step-by-step process from Chapter 4 is illustrated by example in Chapter 5 where the load-deformation data developed from a uniaxial tension test of a structural steel coupon is used to determine a representative true stress-strain relationship. Then, that relationship is used in a FEA model to computationally match the experimental data illustrating the relative utility and accuracy of the proposed approach.

3 DERIVATIVE RULES FOR DEVELOPING THE TRUE STRESS-STRAIN RELATIONSHIP

3.1 INTRODUCTION

Three basic rules for determining the true stress-strain relationship for structural steel materials were developed through review and analysis of existing research, and application of a variety of the available recommended approaches developed for ductile metals. Determining the true stress-strain relationship only requires the application of these three rules and the data produced in a simple uniaxial tension test. These rules, discussed in detail in the following sections, outline basic criteria for developing the true stress-strain relationship for use in finite element analysis (FEA) models that use three-dimensional (3D) solid elements. Application of these rules to the process of developing the true stress-strain relationship for structural steels from tensile test data are intended to support the following objectives: (1) necking will be accurately predicted, (2) the model will remain numerically stable, and (3) that the general shape of the true stress-strain relationship will obey the physical laws governing the plastic response of ductile metals.

The first two rules, summarized in Sections 3.2 and 3.3, are founded on observations cited in research published in the late nineteenth century and middle twentieth century. The third rule, summarized in Section 3.4, was developed by investigating the behavior of polymeric materials that exhibit post-necking cold-drawing response, a phenomenon that is not observed in ductile metals. The following sections summarize the main research related to each of the proposed derivative rules followed by a mathematical presentation of each rule. Chapter 4 provides guidance on application of these rules to the process of developing of the true stress-strain relationship for FEA from standard coupon tensile test data.

3.2 CONSIDÈRE'S CONSTRUCTION

As introduced in Section 2.8.2, Armand Considère published an accurate analytical means for predicting necking. The following sections describe Considère's Construction, the most important finding of this analytical study relative to this dissertation and discuss its application to predicting the onset of necking. Section 3.2.1 provides a derivation of Considère's Construction. The following sections, 3.2.2 and 3.2.3, describe the graphical application of Considère's Construction and its application to power-law material models, followed by a brief summary of research citing this work in Section 3.2.4. Finally, the first derivative rule is presented in Section 3.2.5.

3.2.1 Derivation of Considère's Construction

Due to the fundamental and critical nature of accurate application of Considère's Construction to the overall process of analytically and computationally predicting the onset of necking, a step-by-step derivation is provided in this section. It is built upon the observation, presented in Section 2.8.1 and Figure 2-25, that necking occurs at the point of maximum measured load in a standard tension test. At this point, the change in force, as well as the change in engineering stress, is equal to zero. By investigating this relationship and manipulating it mathematically by considering conservation of volume and uniform strain within the gauge length prior to necking, Considère's Construction can be derived.

To begin, the relationship between true stress, σ, and applied force, P is given in Equation 3-1. Next, by definition, the slope at any point of the load-deformation curve is equal to the first derivative of the load function at that point. Thus, the relationship shown in Equation 3-2 can be established by taking the derivative with respect to true strain, ε. Note that the derivative could be taken with respect to deformation, engineering strain, e, or true strain, ε, and the relationship would remain valid. However, for the purposes of this derivation, it is simplest to use true strain, ε. Finally, as previously mentioned, at the onset

of necking the load function reaches a local maximum and, thus, the slope of the load function (i.e. the first derivative of the load function)– is equal to zero, as shown in Equation 3-3.

$$P = \sigma A \qquad \text{Equation 3-1}$$

$$\frac{dP}{d\varepsilon} = \sigma\left(\frac{dA}{d\varepsilon}\right) + A\left(\frac{d\sigma}{d\varepsilon}\right) \qquad \text{Equation 3-2}$$

$$\frac{dP}{d\varepsilon} = 0 \;\; \textit{at the onset of necking} \qquad \text{Equation 3-3}$$

Considering Equation 3-2, the right-hand side is composed of two terms that can be viewed critically in the context of previous discussions of necking in Section 2.8.1. The first term is the true stress, σ, multiplied by the incremental change in area, $dA/d\varepsilon$, which represents the rate of geometric softening due to reduction in current cross-sectional area, A. The second term is the current cross-sectional area including deformation effects, A, multiplied by the incremental change in stress, $d\sigma/d\varepsilon$, which represents the rate of material strain hardening. As shown in Equation 3-3, at the onset of necking, the change in force equals zero.

Next, Equation 3-4 is established by combining Equation 3-2 and Equation 3-3. This equation reveals that the true stress multiplied by the rate of geometric softening, a negative quantity for increasing values of tension strain, is equal to the negative of the area multiplied by the rate of material strain hardening, a positive quantity for real materials subject to increasing tension strain. Thus, at the precise onset of necking these two quantities must be equal.

$$\sigma\left(\frac{dA}{d\varepsilon}\right) = -A\left(\frac{d\sigma}{d\varepsilon}\right)$$ Equation 3-4

Next, for simplicity, the derivatives can be expressed by dropping the $d\varepsilon$, as shown in Equation 3-5 and rearranged to group like variables, as shown in Equation 3-6.

$$\sigma(dA) = -A(d\sigma)$$ Equation 3-5

$$\frac{d\sigma}{\sigma} = -\frac{dA}{A}$$ Equation 3-6

It can be shown that incremental true strain, $d\varepsilon$, is equal to the change in length with respect to the current length and, by conservation of volume, is also equal to the negative value of the change in area with respect to the current area, A, as shown in Equation 3-7. Note that the assumption of conservation of volume is founded upon assumptions of conservation of mass and constant of density at the onset of necking, along with an assumption of elastic strains being negligible relative to plastic strains. In addition, by assuming constant density and conservation of mass, it is inferred that local variations in density caused by things like void nucleation, growth and coalescence (see Section 2.9.4.2) are negligible as well.

$$d\varepsilon = \frac{dL}{L} = -\frac{dA}{A}$$ Equation 3-7

Combining Equation 3-6 with the relationship developed in Equation 3-7, the relationship shown in Equation 3-8 emerges. Finally, rearranging the terms reveals the common form of Considère's Construction, illustrating the basic relationship between true stress and its first derivative at the onset of necking, as shown in Equation 3-9. As noted,

this relationship is only valid at the onset of necking, thus at a true stress and strain of σ_{max} and ε_{max}, respectively as restated, for clarity, in Equation 3-10.

$$\frac{d\sigma}{\sigma} = d\varepsilon \qquad \text{Equation 3-8}$$

$$\sigma = \frac{d\sigma}{d\varepsilon} \qquad \text{Equation 3-9}$$

$$\sigma_{max} = \frac{d}{d\varepsilon}\left(\sigma(\varepsilon_{max})\right) \qquad \text{Equation 3-10}$$

The relationship between the true stress-strain function and its first derivative can be observed graphically by plotting the true stress-strain function, $\sigma(\varepsilon)$, and its first derivative, $d\sigma/d\varepsilon$, together. As shown in Figure 3-1, and in accordance with Equation 3-10, necking occurs at the precise point when these two functions intersect.

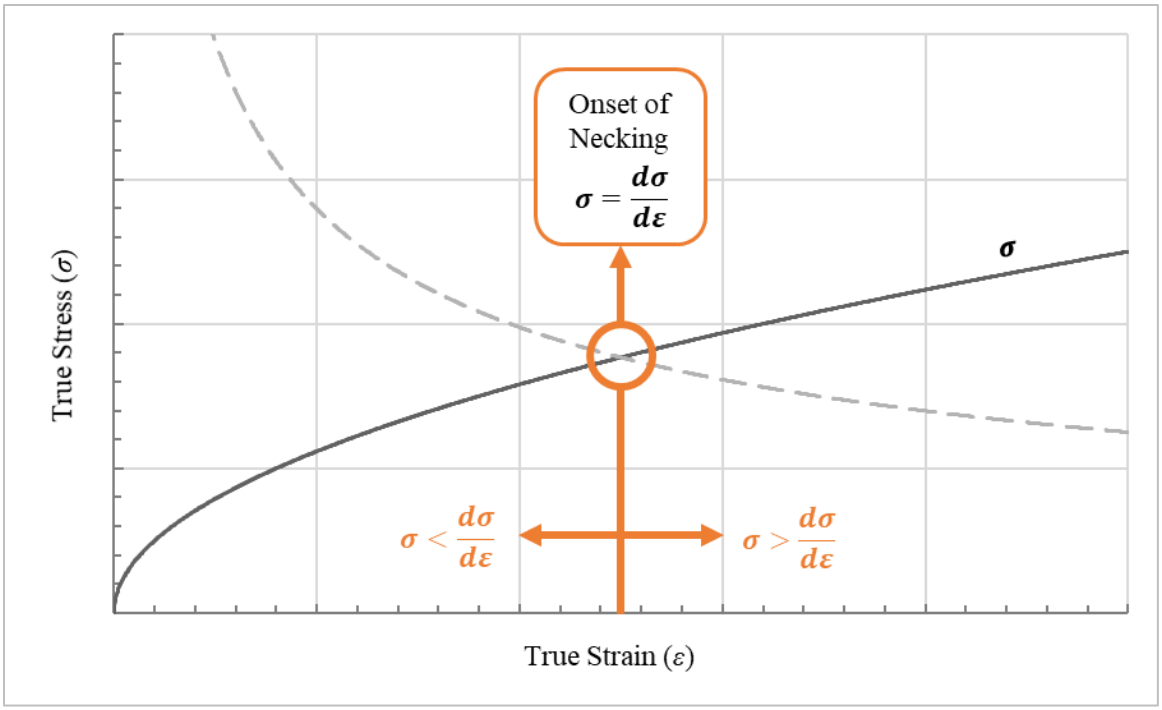

Figure 3-1: Summary of Relationships at the Onset of Necking

Thus, under the assumption of conservation of volume, true stress, σ, is equal to its first derivative at the onset of necking. In essence, prior to necking, the effect of material strain hardening is capable of balancing the effect of cross-section reduction, or geometric softening. However, these competing factors reach a critical bifurcation point at the onset of necking. As a result, after necking, the material cannot strain harden enough to balance the effect of geometric softening, causing a local reduction in cross-section; necking.

Stated differently, there are two competing properties that must be considered when evaluating whether a section will begin to neck in uniaxial tension. The first, material strain hardening, is the rate at which the material hardens for a given increment of stress (or strain). The rate of material hardening for ductile metals like structural steel decreases with increasing strain, as discussed in Section 3.4. The second, the rate of geometric softening, represents the rate at which the cross-sectional area changes with increasing strain. As a

result of conservation of volume, the rate of geometric softening increases with increasing strain. Prior to necking the rate at which the material hardens is greater than the relative softening for a given increment of strain. As a result, the section remains stable as it can support additional load with the associated reduction in cross-sectional area. However, after necking, the relationship reverses, and the effect material hardening can no longer balance the effect of geometric softening. The result is a decrease in load-carrying capacity, rapid section reduction (necking), and eventually fracture. This relationship, initially illustrated in Equation 3-6, is summarized in Figure 3-2.

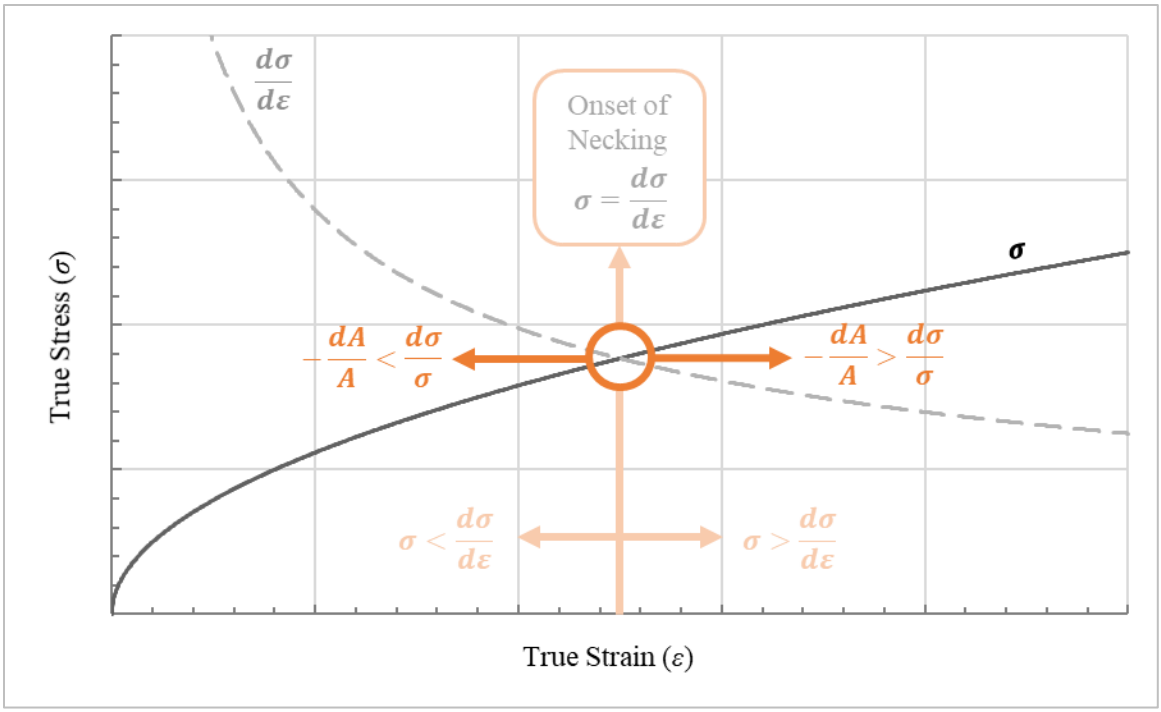

Figure 3-2: Summary of Relationships at the Onset of Necking

This relationship can be manipulated further and expressed graphically, providing additional insight into its usefulness and broad application to understanding ductile metal material response to uniaxial tension as described in Section 3.2.2.

3.2.2 Graphical Application of Considère's Construction

In certain applications it is useful to describe Considère's Construction in a graphical form. By taking the expression derived from conservation of volume expressed in Equation 3-7, and dividing all terms by the initial length, L_o, the relationship in Equation 3-11 emerges. By combining this equation with Equation 3-10, the fundamental relationship that defines Considère's Construction, the relationship in Equation 3-12 is established, which applies at the onset of necking. Finally, by evaluating the relationship between true and engineering stresses from Equation 2-3 at the onset of necking, this expression can be rearranged as shown in Equation 3-13.

$$d\varepsilon = \frac{dL}{L}\left(\frac{L_o}{L_o}\right) = \frac{de}{1+e} \qquad \text{Equation 3-11}$$

$$\frac{d\sigma}{e_{max}} = \frac{\sigma_{max}}{1+e_{max}} \qquad \text{Equation 3-12}$$

$$s_{max} = \frac{\sigma_{max}}{1+e_{max}} \qquad \text{Equation 3-13}$$

Therefore, based on the relationships in Equation 3-12 and Equation 3-13, the slope of the true stress-engineering strain function, $d\sigma/de$, is equal to the engineering stress, s, at the onset of necking. This relationship can be demonstrated graphically by plotting true stress, σ, on the ordinate axis against engineering strain, e, along the abscissa, as shown in Figure 3-3. In this figure, as demonstrated by the relationship between similar triangles, a straight line can be drawn through the points (0, -1.0) and (0, s_{max}). This line will then be tangent to the true stress versus engineering strain curve at the point (e_{max}, σ_{max}).

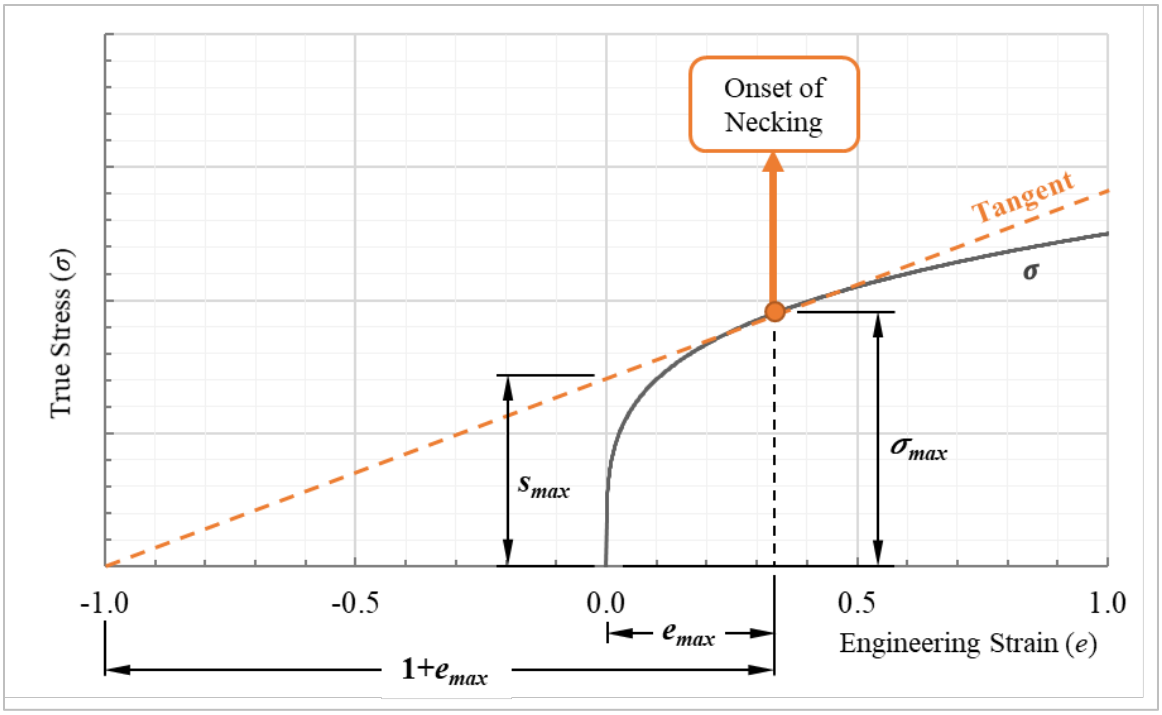

Figure 3-3: Graphical Expression of Considère's Construction for Ductile Metals

While this relationship has little practical application for metals beyond providing a simple way to graphically determine the stress and strain at necking, as explored in Section 3.4.3, the graphical expression of Considère's Construction provides unique insight into the response of other materials, such as polymers, that exhibit necking behaviors that differ from those exhibited by ductile metals.

3.2.3 Considère's Construction for Power Law Fits

Due to the limited need to capture post-necking response in most engineering applications, and their simplicity and accuracy, simple power law expressions are often used to approximate the true stress-strain relationship for engineering materials like steel, iron, aluminum, and copper. Most often, the form given in Equation 3-14 is used, where C_1 and C_2 are constants determined for best fit.

$$\sigma = C_1 \varepsilon^{C_2}$$ Equation 3-14

Commonly, Considère's Construction has been used to establish the exponent for a power law functions used to approximate the true stress-strain relationship. As shown in Equation 3-15 through Equation 3-19, the power law expression in Equation 3-14 can be manipulated algebraically and combined with observations from Considère's Construction to produce a power-law relationship that will accurately capture the strain at the onset necking. The resulting relationship then includes only a single constant, C_1, as shown in Equation 3-20.

$$\frac{d\sigma}{d\varepsilon} = C_1 C_2 \varepsilon^{C_2 - 1}$$ Equation 3-15

$$\frac{d\sigma}{d\varepsilon} = \sigma \quad at\ \varepsilon_{max}\ \textit{(onset of necking)}$$ Equation 3-16

$$C_1 {\varepsilon_{max}}^{C_2} = C_1 C_2 {\varepsilon_{max}}^{C_2 - 1}$$ Equation 3-17

$${\varepsilon_{max}}^{C_2} = C_2 {\varepsilon_{max}}^{C_2 - 1}$$ Equation 3-18

$$C_2 = \varepsilon_{max}$$ Equation 3-19

$$\sigma = C_1 \varepsilon^{\varepsilon_{max}}$$ Equation 3-20

While the power law expression shown in Equation 3-20 is developed through the application of Considère's Construction, it is often used without mention or reference to the underlying principles of Considère's Construction. As a result, the importance of

Considère's Construction is often obscured in engineering literature and its application to other curve fitting approaches is often missed. Further, the derived relationship in Equation 3-20 is developed only to precisely capture strain at necking. Taking this one step further, the relationship can be further defined to precisely capture both the stress and strain at the onset of necking. This is achieved by solving for C_1 at the onset of necking where the true stress and strain are equal to σ_{max} and ε_{max}, respectively. The resulting relationship for constant C_1 is shown in Equation 3-21. Thus, there is a single power law relationship that will precisely capture both the stress and strain at the onset of necking, as illustrated in Equation 3-22.

$$C_1 = {\sigma_{max}}/{(\varepsilon_{max})^{\varepsilon_{max}}} \qquad \text{Equation 3-21}$$

$$\sigma = \left({\sigma_{max}}/{(\varepsilon_{max})^{\varepsilon_{max}}}\right)\varepsilon^{\varepsilon_{max}} \qquad \text{Equation 3-22}$$

It is clear that the use of Considère's Construction is quite limited if applied only to developing power law fits. However, it is critical to accurate prediction of the onset of necking and, thus, a necessary consideration when determining the true stress-strain relationship for computational analysis of structural steel materials. Section 3.2.4 provides a summary of recent research related to necking and post-necking response of ductile metals citing, applying, and refuting Considère's Construction. As illustrated, despite its long existence, or possibly because of it, researchers often fail to recognize or appropriately acknowledge this important relationship when publishing related research.

3.2.4 Considère's Construction in Recent Research

Considère's work is observed across much of the available ductile metal necking and post-necking related research. Many cite his 1885 publication directly, while others

indirectly apply Considère's Construction to their work, particularly in simplified power law approximations of the true stress-strain relationship. In addition, some researchers either claim that there is no evidence to support his theory (i.e., Considère's Construction) or do not apply it when developing the true stress-strain relationship for ductile metals. In these cases, the result is often an inability to precisely and consistently capture necking and predict post-necking behavior.

The following sections provide a brief summary of the appearance, or lack thereof, of Considère's Construction in recent research. Due to the breadth of related research, the following sections merely summarize a representative cross section of the related work and are not intended to thoroughly document the full range of researchers referencing Considère's work.

3.2.4.1 Full Citation and Application of Considère's Construction

Of all groups discussed in this section, current researchers that in some way acknowledge the utility of Considère's Construction in capturing necking of ductile metals is the largest. The majority do so plainly citing Considère's work and presenting one or more of the relationships outlined in Sections 3.2.1 and 3.2.2. These researchers include published works by Zhang et al. (Zhang, Hauge, Ødegard, & Thaulow, 1999), Joun et al. (Joun, Choi, Eom, & Lee, 2007) (Joun, Eom, & Lee, 2008), and Choung and Cho (Choung & Cho, 2008). In addition, the works of these researchers, particularly Zhang et al. and Joun et al., are cited across many subsequently published and related research papers on necking of ductile metals in tension. Thus, to some extent, their acknowledgement and incorporation of the work by Considère has proliferated into work by many others.

3.2.4.2 Application of Considère's Construction to Power Law Approximations

The next largest group apply Considère's Construction to determine the exponent constant (C_2 in Equation 3-14) for use in the power law approximation of the true stress-strain relationship. In most cases, the resulting power law definition takes the form shown in Equation 3-20 where only the necking strain is precisely captured. While it is unclear due to the lack of explicit citation of Considère's work, the similar approach taken in determining the exponent constant in power law approximation of the true stress-strain relationship by these researchers implies that there is a shared understanding of Considère's Construction across these research efforts.

Interestingly, across all of the published research reviewed during the development of this dissertation, there were no observed instances of a researcher applying Considère's Construction to capture both the stress and strain at necking, as shown in Equation 3-22. However, this is likely because such a function tends to provide a poor fit to the experimental data in other areas, particularly in the elastic and early inelastic regime.

3.2.4.3 Omission of Considère's Construction

While the majority of researchers investigating necking of ductile metals cite Considère's work or apply its general relationships while citing other canonical works that themselves reference Considère, a minority of researchers do not. For example, Needleman (Needleman, 1972), Tvergaard et al. (Tvergaard, Needleman, & Lo, 1981), Majzoobi et al. (Majzoobi, Fariba, Pipelzadeh, & Hardy, 2015), and Coppieters et al. (Coppieters, Cooreman, Sol, Van Houtte, & Debruyne, 2011) do not adopt Considère's Construction when developing the true stress-strain relationship in the cited research publications. Often, these researchers did not clearly present their predictive model against the experimental data, so it is unclear how accurate their necking predictions were, particularly with respect to capturing the onset of necking.

Others, such as Ling (Ling, 1996), Arasaratnam et al. (Arasaratnam, Sivakumaran, & Tait, 2011), and Wang et al. (Wang, Xu, Ren, & Wang, 2016), do not incorporate Considère's Construction when developing their true stress-strain relationships, but capture necking and post-necking behavior fairly accurately through careful error minimization, iterative procedures. Their ability to capture necking and post-necking response with reasonable accuracy and without directly applying Considère's Construction demonstrates the potential and power of such approaches.

Finally, some others , including Zhang and Li (Zhang & Li, 1994), Cabezas and Celentano (Cabezas & Calentano, 2004), and Tao et al. (Tao, Zhang, & Tong, 2009), do not incorporate and apply Considère's Construction. As a result, their models typically provide less accurate prediction of the onset of necking and post-necking response. These examples in particular illustrate the importance of considering Considère's Construction explicitly. It should be noted, however, that for many of these researchers their focus was not solely the necking phenomenon. Therefore, they may not have placed particular emphasis on these aspects of the true stress-strain relationship.

3.2.4.4 Disagreement with Considère's Construction

While there may be additional researchers who explicitly disagree with the observations published by Considère and cited by so many others, only one was found in reviewing existing research to develop this dissertation. In their paper on developing the uniaxial true stress-strain relationship for ductile metals, Shen and Jones state "*there is no definite relation between dF/dL=0 and the onset of necking*," (Shen & Jones, 1993), where $dF/dL=0$ refers to the point of peak load during a standard uniaxial tension test. Rather, necking is attributed to structural plastic instability, where necking originates from an initial non-uniformity due to a local difference in thickness, the presence of microscopic voids, or the effect of imposed boundary constraints. While the observation that necking

can be initiated at a specific location due to differences in thickness, the presence of voids, or imposed boundary constraints, is technically correct, it does not actually preclude Considère's Construction from being valid. Thus, based on the work of many other researchers and the recommendations presented herein, there appears to be ample support for the validity of Considère's Construction, as well as numerous demonstrations of its utility in capturing necking in computational models. Therefore, it forms the basis of Derivative Rule #1, as summarized in Section 3.2.5.

3.2.5 Derivative Rule #1: $\sigma(\varepsilon) = d\sigma(\varepsilon)/d\varepsilon$ at Necking

The first derivative rule is a simple restatement of Considère's Construction. As shown in Equation 3-23, the rule states that, for accurate prediction of necking, the true stress-strain relationship must be defined such that the first derivative at the onset of necking is equal to the value of the function at necking. This rule can also be presented in terms of measurable engineering stress and strain parameters as shown in Equation 3-24.

$$\sigma(\varepsilon_{max}) = \frac{d\sigma(\varepsilon_{max})}{d\varepsilon} = \sigma_{max} \qquad \text{Equation 3-23}$$

$$\sigma(\varepsilon_{max}) = \frac{d\sigma(\varepsilon_{max})}{d\varepsilon} = s_{max}(1 + e_{max}) \qquad \text{Equation 3-24}$$

3.3 DRUCKER-HILL STABILITY CRITERIA

For a computational model to be useful, it must produce consistent stable results including predicted stresses, strains, displacements, and other outputs. To achieve this objective, there must be a singular unique solution for any given imposed displacements, stresses, strains, forces, or other inputs. Such a model is considered "stable" as it produces repeatable and predictable results. The issue of numerical stability of materials was

investigated and published in detail by Drucker (Drucker, 1959) and Hill (Hill R. , 1958) and is concisely summarized by two simple criteria, often referred to as Drucker's Stability Criteria. Materials that obey these criteria are considered numerically stable.

The first criterion, originally proposed by Hill and later confirmed and published by Drucker, states that incremental internal energy of a material can only increase. This relationship is referred to in the research literature as both Hill's Stability Criterion and Drucker's First Stability Criterion. This criterion is illustrated in Equation 3-25, where $d\boldsymbol{\sigma}$ refers to the stress increment tensor associated with strain increment tensor $d\boldsymbol{\varepsilon}$ through the material constitutive relationship. As derived by Hill and Drucker, obeying this relationship produces unique, repeatable solutions and stability of computational and numerical models. In addition, Drucker and Hill's First Stability criterion is illustrated in Figure 3-4 for elastic materials and Figure 3-5 for elastic-plastic materials. Note that σ and ε in these figures refer to true stress and strain, respectively.

$$d\boldsymbol{\sigma}: d\boldsymbol{\varepsilon} \geq 0 \qquad \text{Equation 3-25}$$

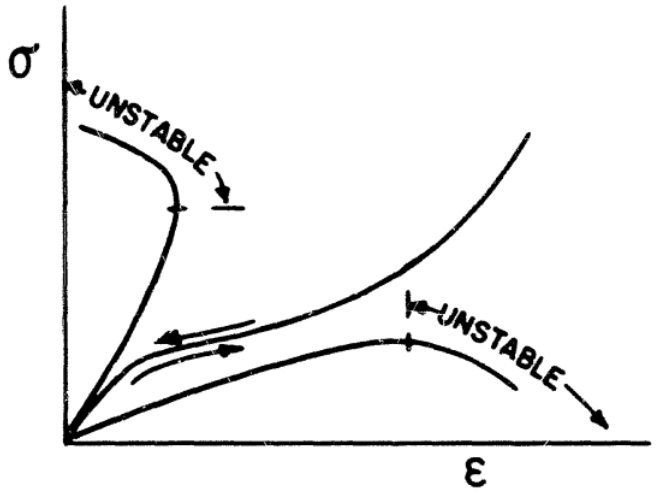

Figure 3-4: Drucker's First Stability Criterion for Elastic Materials (Drucker, 1959)

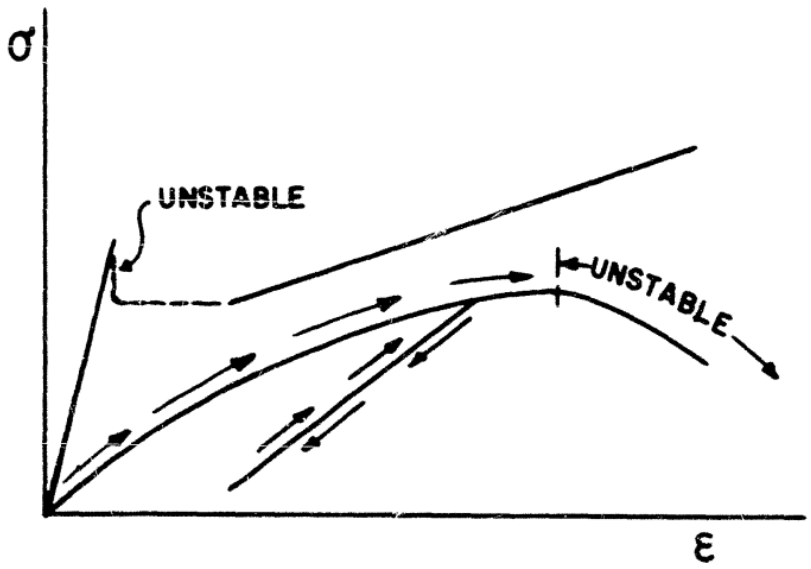

Figure 3-5: Drucker's First Stability Criterion for Elastic-Plastic Materials (Drucker, 1959)

The second criterion, published by Drucker, often referred to as Drucker's Second Stability Criterion, states that work is done during the cyclic plastic deformation of elastic-plastic materials. In essence, this means that materials cannot do work or create energy when deforming plastically. Rather, they absorb energy through plastic deformation. Stated differently, energy is required to deform a stable material elastically. This criterion is illustrated in Equation 3-26 where $d\boldsymbol{\varepsilon_p}$ is the incremental plastic strain tensor. Drucker's second stability criterion is illustrated in Figure 3-6.

$$d\boldsymbol{\sigma}: d\boldsymbol{\varepsilon}_p \geq 0 \qquad \text{Equation 3-26}$$

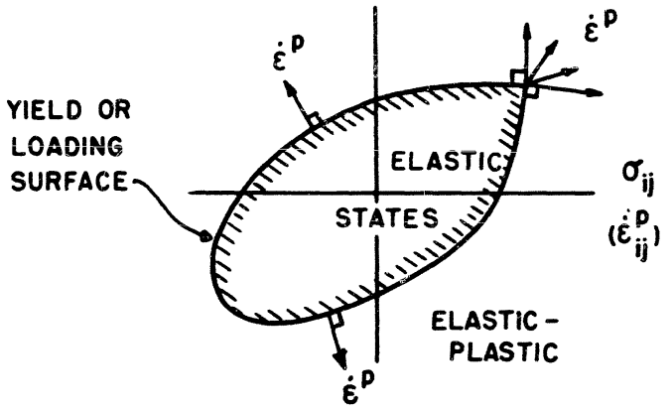

Figure 3-6: Drucker's Second Stability Criterion (Drucker, 1959)

Materials that do not obey these criteria are computationally unstable and cannot be modeled using nonlinear finite element analysis due to non-uniqueness of possible solutions. Research citing the importance and application of these stability criteria is discussed in Section 3.3.1, followed by a brief discussion of additional observations of application of these stability criteria in research in Section 3.3.2. Finally, Section 3.3.3 provides a restatement of these stability criteria in the context of uniaxial tension for use when developing the material true stress-strain relationship for FEA.

3.3.1 Hill's Stability Criterion in Recent Research

The stability criterion developed by Drucker and Hill has been cited in early research related to necking and post-necking behavior of ductile metals. For example, the foundational analytical study in necking of circular bars by Needleman (Needleman, 1972), discussed in Section 2.9.1.2, cites Hill's Stability Criterion as well as his observations on necking as a bifurcation between uniform and non-uniform stress (Hill R. , 1961), along with the canonical work by Bridgman (Bridgman, 1952), discussed in Section 2.9.1.1. Later works by Tvergaard et al. (Tvergaard, Needleman, & Lo, 1981), building on the work of Bridgman and Needleman, also cite Hill's Stability Criterion.

More recent published research by Lian and Zhou (Lian & Zhou, 1989), Shen and Jones (Shen & Jones, 1993), Ling (Ling, 1996), Garcia-Garino at al. (Garcia-Garino, Gabaldon, & Goicolea, 2006), Tao et al. (Tao, Zhang, & Tong, 2009), Coppieters et al. (Coppieters, Cooreman, Sol, Van Houtte, & Debruyne, 2011) (Coppieters & Kuwabara, 2014), and Hyun et al. (Hyun, Kim, Bang, & Lee, 2014) also cite Hill's work. However, they each reference his published research in yield criteria and general plasticity, rather than his published research related to stability. It seems that this more recent body of research has not directly cited or explicitly incorporated the stability criterion developed by Hill and Drucker when investigating necking and post-necking behavior, and the true stress-strain relationship for ductile metals. For example, research by Hyun et al. failed to apply this stability criteria because the researchers defined a material model with zero slope beyond the fracture strain, ε_f, as shown in Figure 3-7. This is just one of many examples of such an assumption. Whether intentionally or not, it is generally done to force failure at a certain strain, the strain at which the hardening ceases and the slope of the true stress-strain relationship is equal to zero. This can produce accurate prediction of failure in the numerical model of the uniaxial tension test; however, it can produce inaccurate predictions of behavior where stable strains beyond the tension rupture strain are predicted.

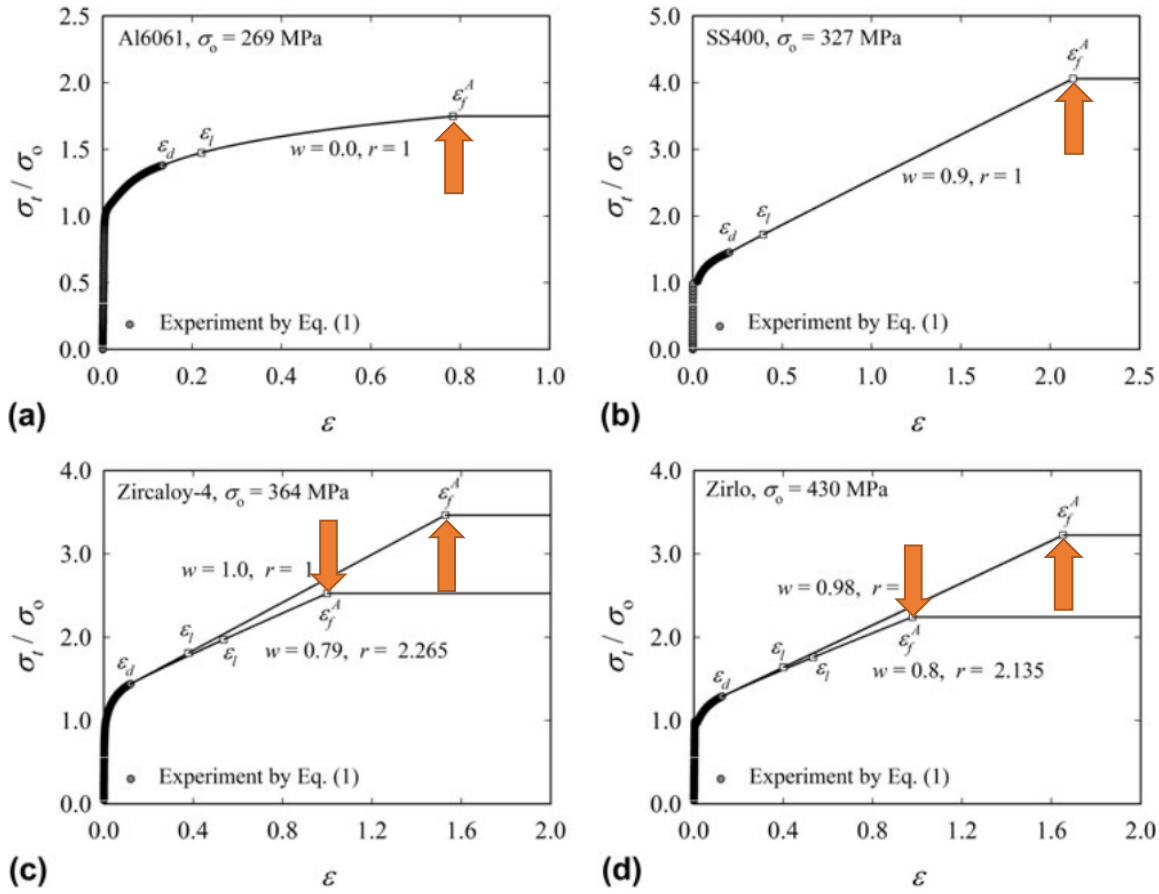

Figure 3-7: True Stress-Strain Relationship with Zero Slope Condition (Hyun, Kim, Bang, & Lee, 2014)

3.3.2 Additional Observation of Hill's Stability Criterion

Despite the lack of citation in recent research, most true stress-strain relationships and constitutive material models developed with the goal of accurately simulating necking and post-necking response have, whether intentionally or not, incorporated Hill's Stability Criterion. In addition, various reference materials for non-linear analysis of ductile metals, have also ensured that their reported true stress-strain relationships maintain a positive slope at all times. For example, advanced modeling work by NIST related to the collapse of the World Trade Center (WTC) (Luecke, et al., 2005) employed steel material models

with positive slope throughout the defined true stress-strain relationship, as shown in Figure 3-8. Similarly, guidance related to FEA of steel materials subjected to blast loading conditions reported by Crawford et al. (Crawford, Magallanes, & Lan, 2006) provides similar recommendations, where material models are defined with only positive slope as shown in Figure 3-9. However, as is the case for most technical guidance and published research neither explicitly state this behavior as a requirement or rule.

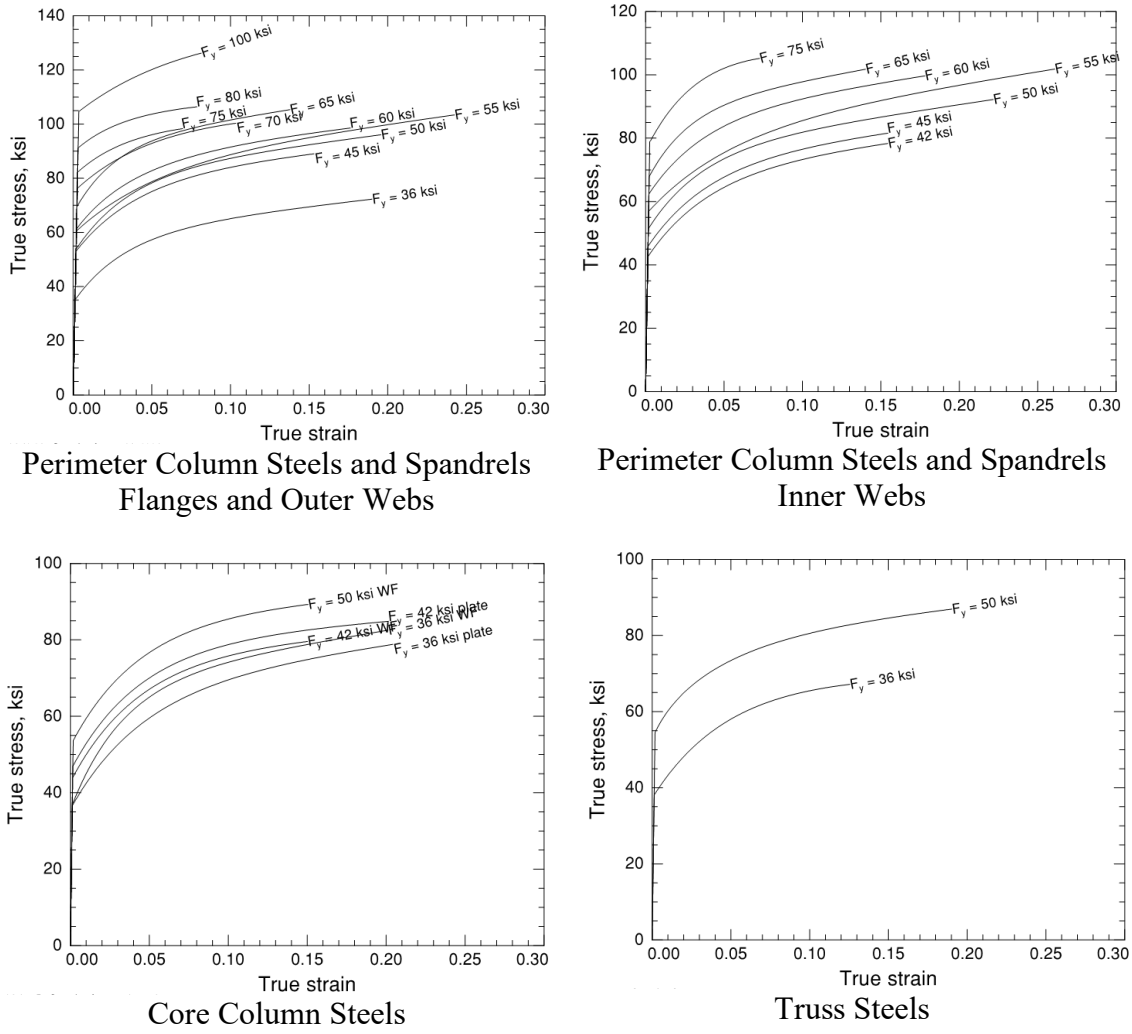

Figure 3-8: True Stress-Strain Relationships used in WTC Analyses by NIST (Luecke, et al., 2005)

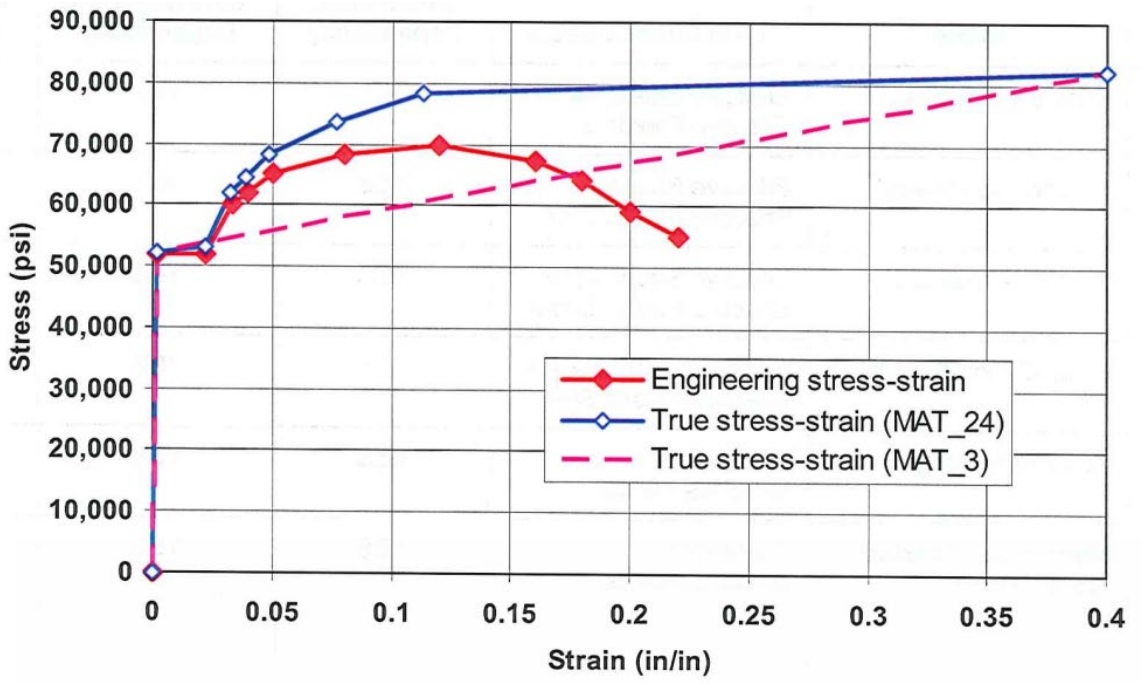

Figure 3-9: True Stress-Strain Relationships for Blast Analysis of Steel (Crawford, Magallanes, & Lan, 2006)

3.3.3 Derivative Rule #2: $d\sigma(\varepsilon)/d\varepsilon \geq 0$ after Necking

The second derivative rule is a simplified uniaxial restatement of Drucker's first stability criterion for materials, originally proposed by Hill, as shown in Equation 3-27. By obeying this relationship, incremental internal energy can only increase, which results in a numerically stable material definition that produces singular, unique predictions of behavior. Thus, the true stress-strain relationship must be defined such that the first derivative is positive at all points. Failure to obey this relationship could result in numerical instability, including scenarios with multiple possible equilibrium solutions for a given state of stress, strain, load, and/or deformation.

$$\frac{d\sigma}{d\varepsilon} \geq 0 \qquad \text{Equation 3-27}$$

3.4 DRAWING MATERIAL RESPONSE

When discussing metals, drawing is often envisioned as the process of stretching materials by pulling them through a die, into sheets, wires, bars, and tubes. This process is illustrated in Figure 3-10 as a point of clarification. This drawing process is a result of mechanical work and does not provide insight into the true stress-strain relationship for structural steels and other ductile metals considered context of this dissertation. However, review of the cold-drawing behavior exhibited by polymeric materials under uniaxial tension loading provides interesting insight into material response in tension as discussed later in this section.

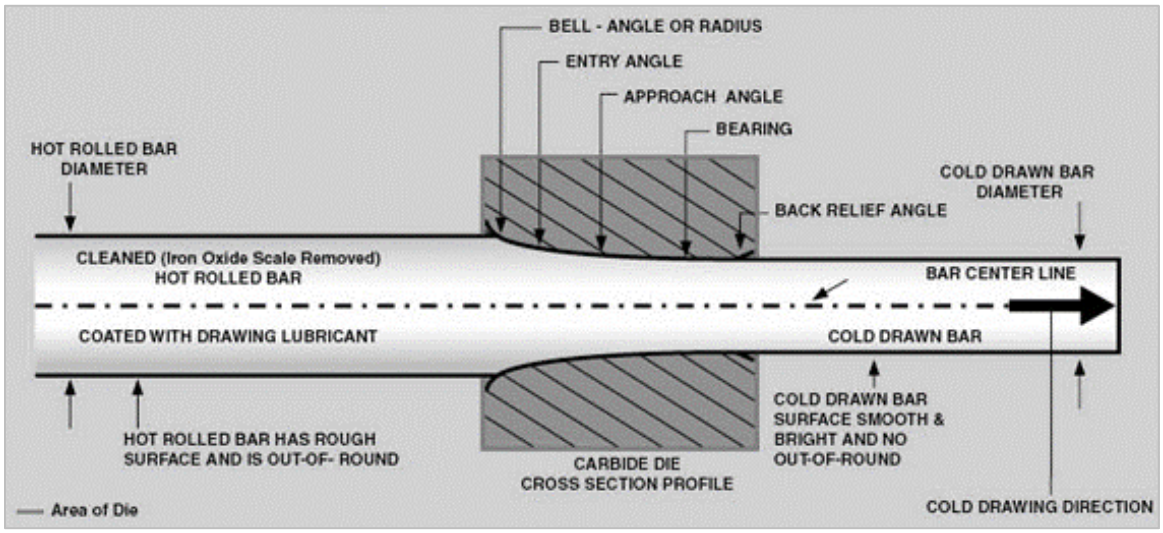

Figure 3-10: Cold-Drawing Process for Metal Bars and Wires (Precision Kidd Steel Company, Inc., 2010)

Drawing in the context of this discussion, also called neck drawing or cold-drawing, refers to the formation of a neck which stabilizes and draws stably over the length of a tension coupon specimen. This phenomenon can be observed in certain polymers, such as polyethylene and nylon, at temperatures approximately 50°C below the glass transition

temperature, T_G (Ashby & Jones, 2006). The drawing process for polymers is illustrated in Figure 3-11.

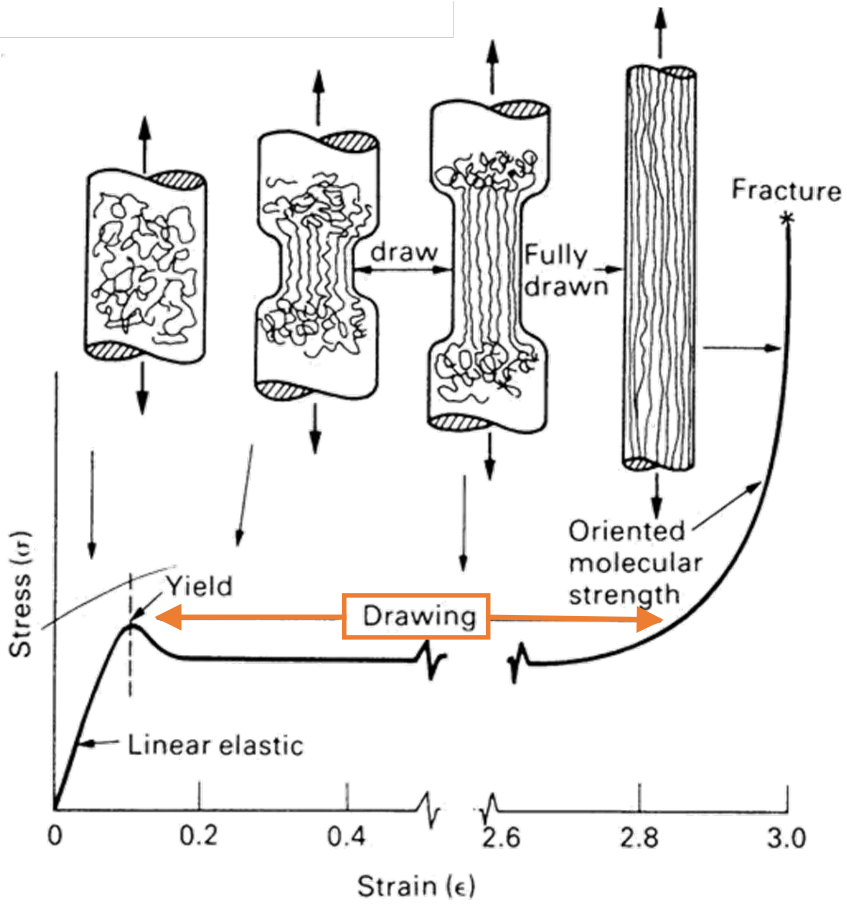

Figure 3-11: Cold-Drawing Process for Polymeric Materials (Ashby & Jones, 2006)

The drawing response of polymers is actually quite similar to the yield plateau exhibited by certain low carbon steels in uniaxial tension. In both cases, the material reaches a certain yield point, after which it elongates at a near constant load. In polymers, this process of elongation is much more pronounced; however, in both cases the material draws out over the entire (reduced section) length of the specimen (Davis, 2004). For reference, the analogous yielding process in low carbon steel is illustrated in Figure 3-12.

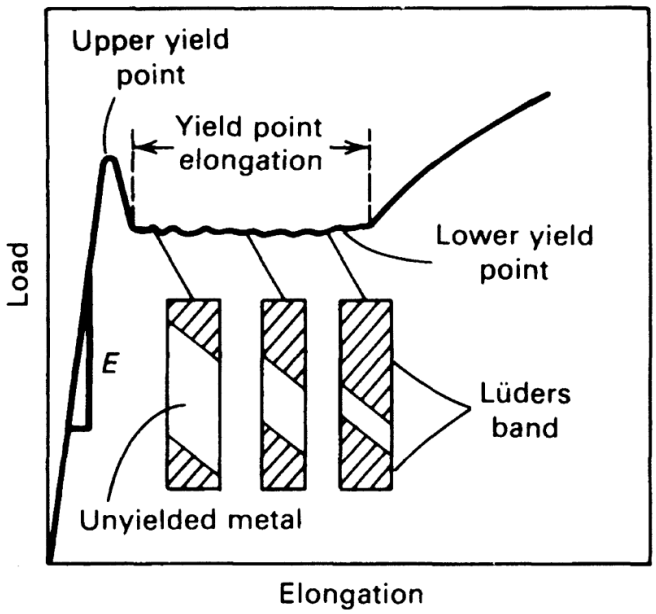

Figure 3-12: Yielding Process in Low Carbon Steels (Davis, 2004)

To better understand the process of cold-drawing, Section 3.4.1 provides a brief description of solid polymers, particularly those that exhibit the subject cold-drawing behavior. Next, Section 3.4.2 discusses the engineering stress-strain response of cold-drawing polymers, and Section 3.4.3 describes the true stress-strain relationship that must be satisfied for cold-drawing to occur. Finally, Section 3.4.4 presents the third derivative rule which, if applied, ensures that cold-drawing behavior will not be predicted.

3.4.1 General Description of Solid Polymers

Polymer molecules make up many common materials observed throughout daily life including plastics, fabrics such as nylon, coatings such as Teflon, epoxies, and rubber. They are formed through chemically linking a series of smaller molecules, called monomers, into networks creating larger, more complex molecules. These monomers building blocks can be simple molecules made from one or a few atoms, or complex ring-shaped structures with a dozen or more atoms. In simple polymers like polyethylene and

nylon, the structure of the polymer molecules is a chain. For example, Figure 3-13 illustrates the general structure of a polyethylene molecule.

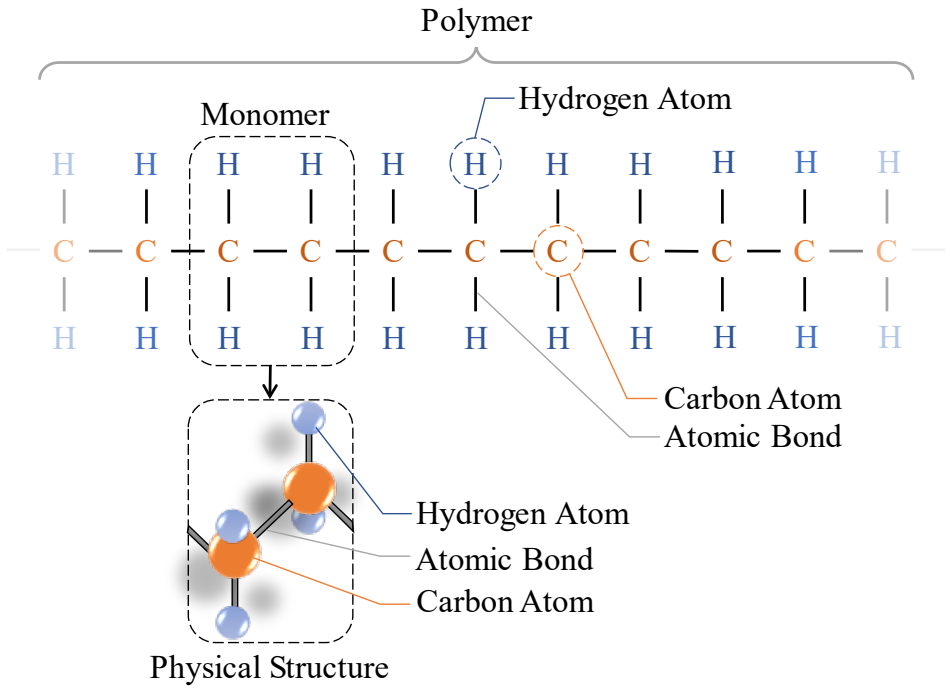

Figure 3-13: Polyethylene Molecule

Polymers and polymeric materials can exhibit a broad range of properties. The constitutive polymer chains can be arranged in organized crystalline structures, amorphous structures, or, most commonly, a combination of the two. The relative order of polymers and interconnectivity between molecules, called cross-linking, can greatly affect their physical properties. While a detailed discussion of the properties of polymers is beyond the scope of this discussion, of interest in this dissertation is the group of polymeric materials that exhibit cold-drawing response. These materials and the general features of the material true stress-strain relationship for cold-drawing polymers are discussed later in this section.

Cold-drawing polymers exhibit a unique behavior when tested in tension, as shown in Figure 3-11. Their initial response, like many other materials including ductile metals,

is typically linear elastic. During the elastic range of response of a typical coupon tested in uniaxial tension, the entire reduced section deforms uniformly. At the end of the elastic response, the material yields, typically resulting in the formation of a necked region where the cross-sectional area reduces locally. As a result, the stresses and strains localize and concentrate within the neck. After yielding, there is typically a reduction in load carrying capacity, much like the necking response observed in ductile metals like structural steel.

However, at this point, cold-drawing polymer behavior begins to diverge from that of a typical ductile metal. Specifically, shortly after necking, the neck stabilizes, becoming stronger than the neighboring un-necked material. As a result, with continued elongation, additional material is drawn into the neck until the entire reduced section has effectively necked. This process, called cold-drawing, occurs at a near constant stress. Once the full length of the reduced section of the coupon has drawn into the necked region, the material strain-hardens, resisting additional load, typically until rupture, as shown previously in Figure 3-11. The full tension response of cold-drawing polymers is described in additional detail in the following sections.

3.4.2 Engineering Stress-Strain Response of Cold-Drawing Polymers

The following paragraphs describe the load-elongation and engineering stress-strain response of cold-drawing of polymeric materials in the context of a standard coupon tension test. The full idealized engineering stress-strain curve is provided in Figure 3-14 where engineering stress, s, and engineering strain, e, are determined using the standard analytical relationships presented previously in Equation 2-1 and Equation 2-2, respectively. Schematic coupon figures are provided along the bottom to illustrate the typical deformed shape during testing. As previously noted, this cold-drawing behavior can be observed in polyethylene and nylon polymers at temperatures approximately 50^{o}C below the glass transition temperature, T_G (Ashby & Jones, 2006).

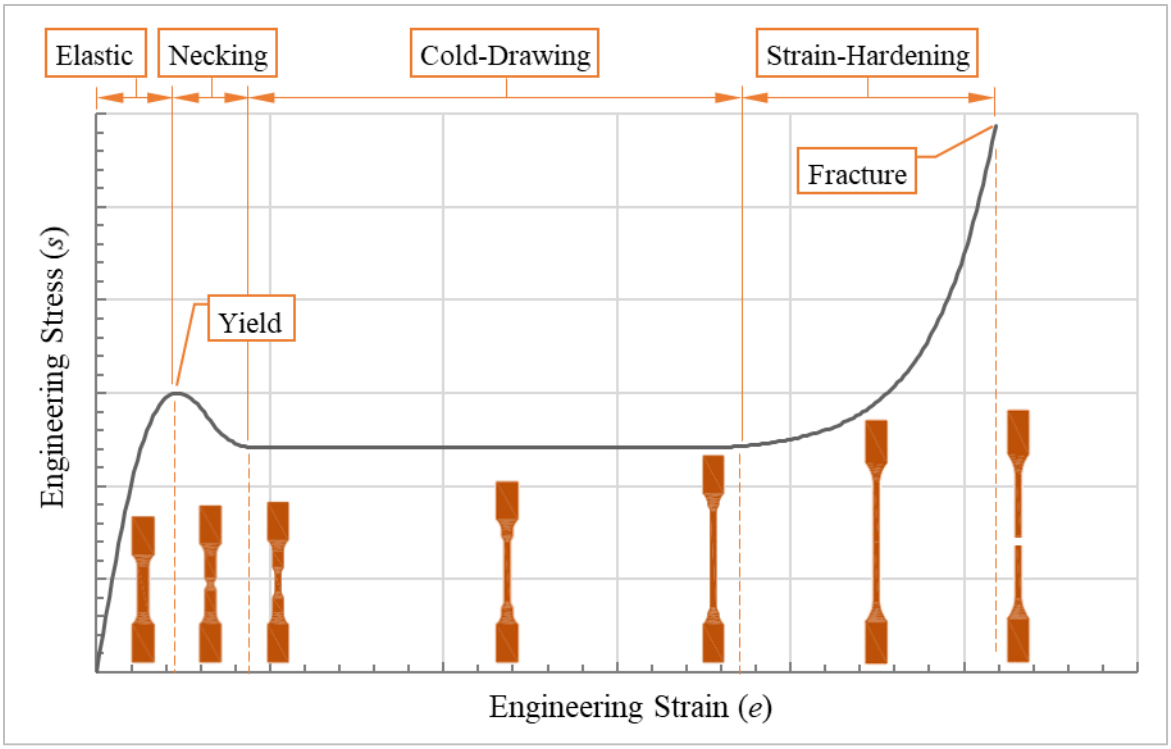

Figure 3-14: Engineering Stress-Strain Relationship for Cold-Drawing Polymers

When testing is initiated, during the elastic range of response, the polymer coupon initially stretches uniformly over the reduced section of the tension coupon. This initial elastic response typically begins as linear, though it can become non-linear, particularly as it approaches the yield point. During elastic deformation, the chains making up the polymer maintain their general form, whether amorphous or crystalline, elastically stretching the bonds within and between them. This portion of the response is generally recoverable upon unloading.

At the yield point, the engineering stress-strain curve reaches a local maximum and, much like necking in ductile metals, a localized reduction in section occurs within the reduced section of the coupon. Within the neck, polymer chains begin to align in the direction of the applied load. As the polymer chains align, either by unfolding the organized crystalline structured chains, or by drawing out amorphous tangles, the material becomes

stronger and, at a critical point, due to the more efficient load-bearing alignment of molecules within the neck, the necked region becomes stronger than the neighboring un-necked material despite its smaller cross-sectional area. At this critical point, the tension coupon begins to cold-draw.

During cold-drawing, material outside the neck deforms, reducing in cross-sectional area to match the dimension of the neck. The cold-drawing process continues until the neck expands and encompasses the entire reduced section of the coupon specimen. Through this process, the molecular chains continue to align in the direction of stress along the length of the specimen. Once the entire reduced section has necked, cold-drawing ends and the strain hardening process begins.

During strain hardening, with the polymer chains generally aligned in the direction of loading, the coupon becomes stiffer and stronger. At this point, the material is stronger in the draw direction and the stress-strain curve rises rapidly. Stress increases until the eventual tension fracture of the coupon due to rupture of the material.

3.4.3 True Stress-Strain Relationship for Cold-Drawing Polymers

The true stress-strain relationship of cold-drawing polymers is uniquely different from the relationship observed in ductile metals like structural steel. Where ductile metals continue to soften with increasing strain beyond the point of necking, the ability of polymer molecules to align in the direction of loading allows the material to stiffen and strengthen as it deforms. The result is a reversal in curvature of the true stress-strain relationship. Figure 3-15 qualitatively illustrates the true stress-strain relationship for polymers, including this reversal in curvature at higher strains. The reversal in curvature is the feature of the true stress-strain relationship that allows post-neck hardening and cold-drawing, as described later in this section.

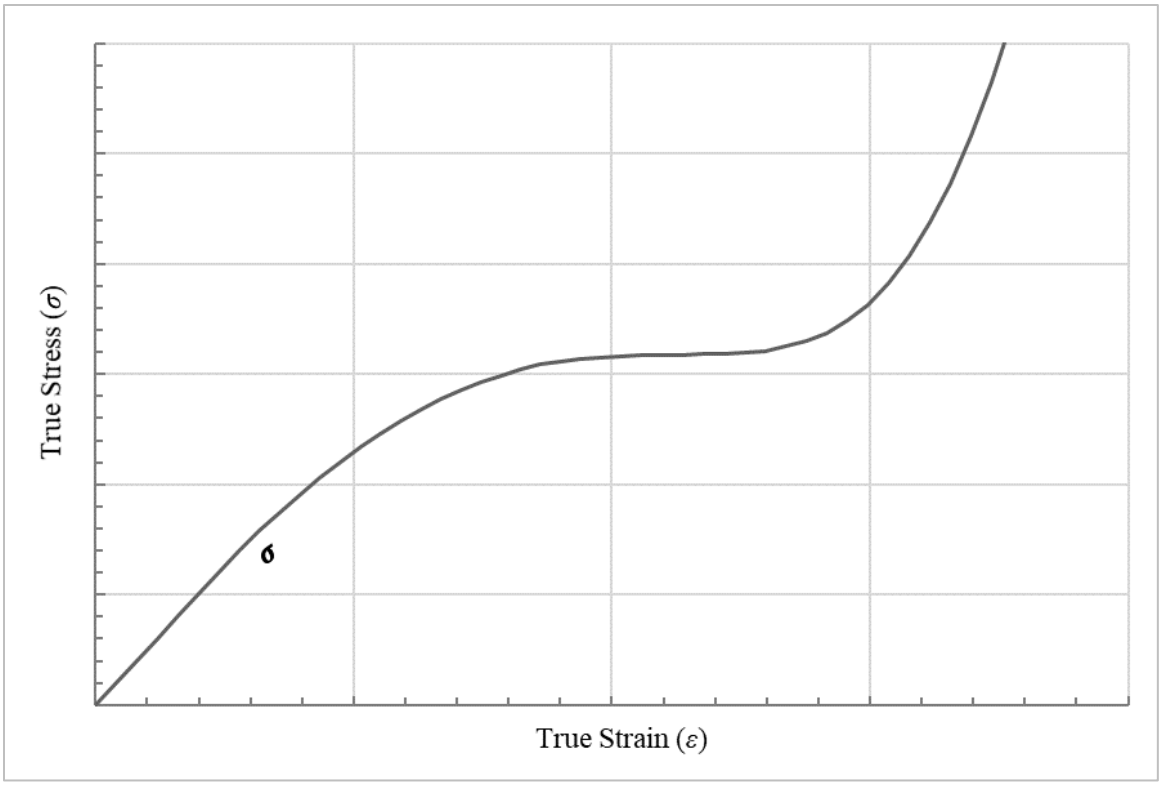

Figure 3-15: True Stress-Strain Curve for Cold-Drawing Polymers

While the polymer true stress-strain relationship is quite different from that of ductile metals, it is important to recognize that it still obeys the first and second derivative rules presented in Sections 3.2 and 3.3, respectively. Specifically, the slope remains positive throughout the entire range of the true stress-strain relationship, obeying Hill's Stability Criterion and Drucker's First Stability Criterion (Derivative Rule #2), as is clear from Figure 3-15. In addition, as illustrated in Figure 3-16, Considère's Construction (Derivative Rule #1) can be used to predict the point at which necking occurs. However, unlike for ductile metals, the first derivative is not decreasing at all points after the onset of necking. Rather, at a certain point after necking, the first derivative reaches a local minimum and begins increasing again. However, due to the localized effect of necking, the relative relationship between the material true stress-strain definition and its first derivative

shown in this figure loses meaning because one of the underlying assumptions of Considère's Construction, specifically uniform strain in the reduced section of the coupon, is invalidated. Thus, the observed second crossing of these functions that occurs at a higher strain has no physical meaning.

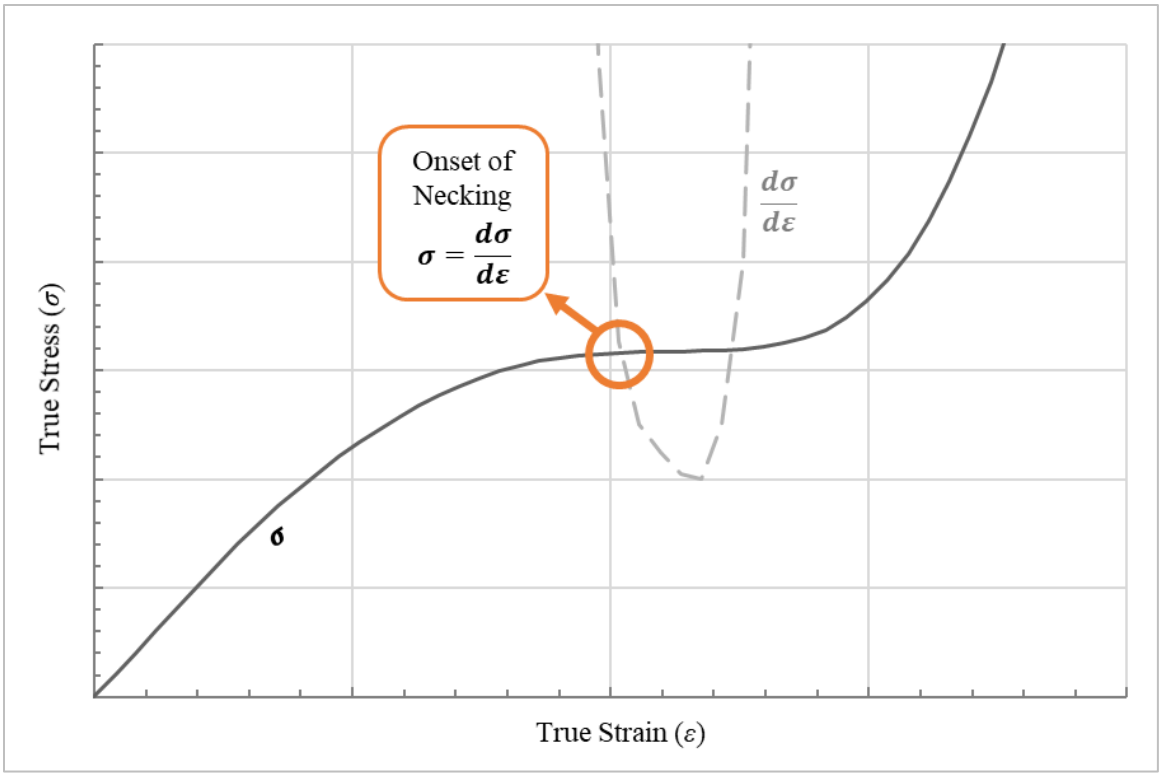

Figure 3-16: Considère's Construction for Cold-Drawing Polymers

Additional insight can be gleaned from reviewing the graphical application, discussed previously in Section 3.2.2 for ductile metals, for the idealized polymer true stress-strain relationship shown previously. Specifically, the graphical approach allows for the identification of true stress-strain relationships where cold-drawing behavior is possible. By plotting the true stress with respect to engineering strain, the relationship that emerges can be graphically interrogated to not only determine the onset of necking, as done previously for ductile metals, but also the onset of cold-drawing. As shown in Figure 3-17,

a second tangent line can be drawn through the point (0, -1.0). This second line is tangent at the point where the neck will stabilize, and cold-drawing will begin. Thus, any true stress-strain relationship with a reversal in curvature will permit a second instance where a tangent can be drawn through the plot of true stress versus engineering strain, a condition that is indicative of cold-drawing response.

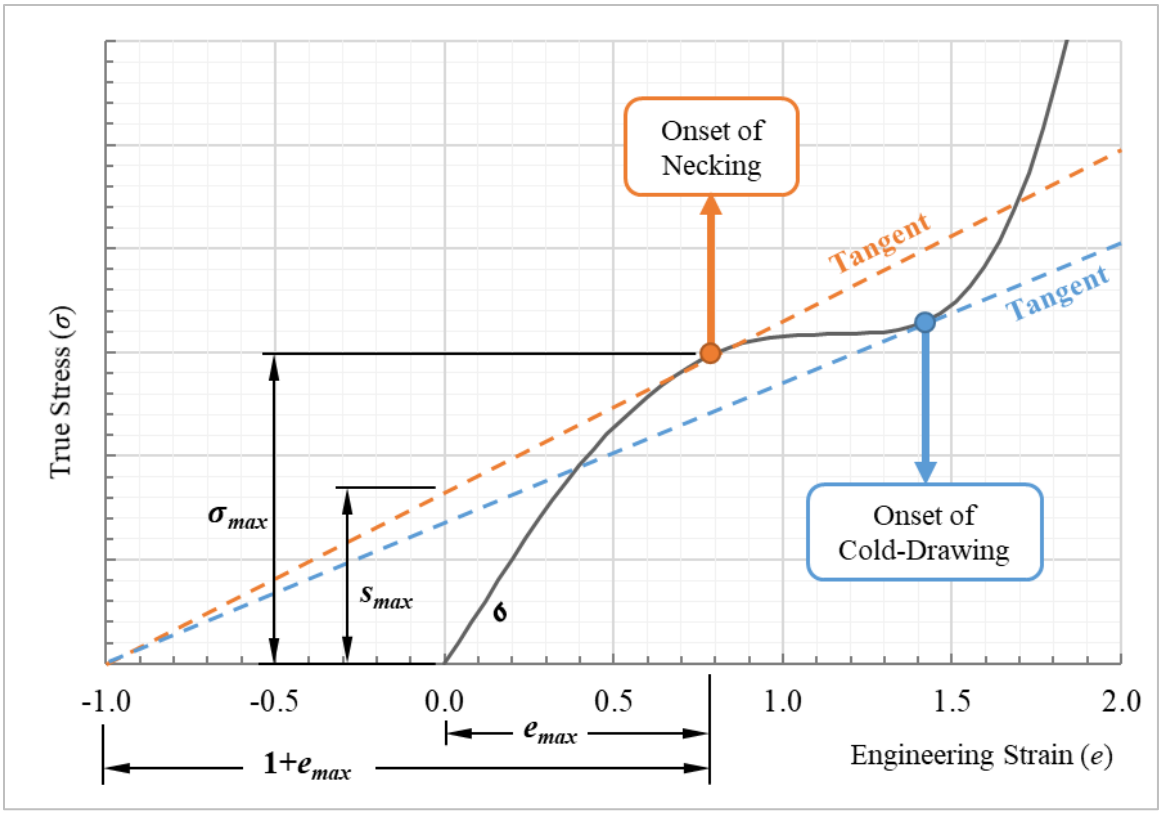

Figure 3-17: Graphical Expression of Considère's Construction for Cold-Drawing Polymers

By shifting the plot in Figure 3-17 along the abscissa by adding one, an important parameter for cold-drawing materials can be observed, the draw ratio. The draw ratio reflects the potential for strain within the stabilized neck. Because the entire reduced section of a cold-drawing polymeric tension coupon draws to this strain, the draw ratio is

also equal to the ratio of the length of the fully drawn section to the original undeformed length. This is illustrated for the idealized cold-drawing stress-strain relationship in Figure 3-18, where the draw ratio is approximately equal to 2.4 indicating that, at the end of cold-drawing, the reduced section will be approximately 2.4 times longer than the undeformed specimen.

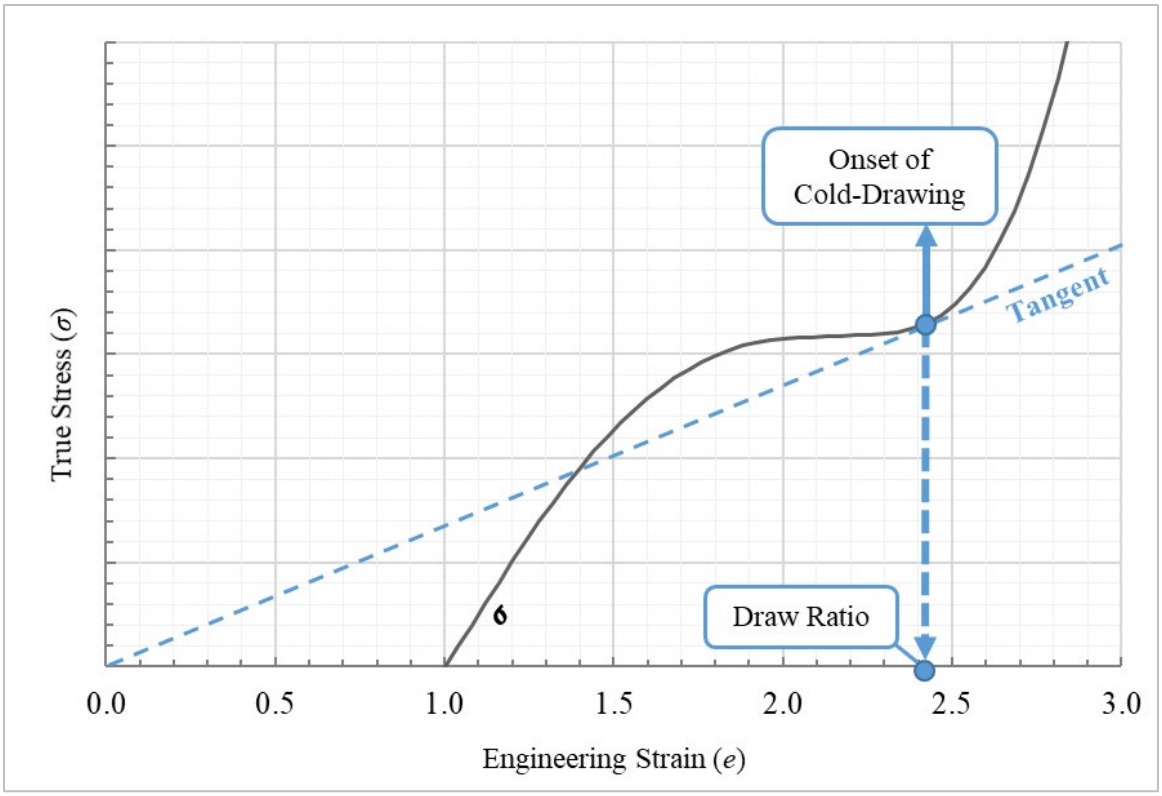

Figure 3-18: Draw Ratio for Cold-Drawing Polymers

Because cold-drawing is not a behavior observed in ductile metals, and prediction of cold-drawing requires a reversal in curvature of the true stress-strain relationship, there should be no reversal in curvature in the post-necking branch for any ductile metal material. This observation is the basis for the third and final derivative rule, presented in Section 3.4.4.

3.4.4 Derivative Rule #3: $d^2\sigma(\varepsilon)/d\varepsilon^2 \leq 0$ after the Onset of Necking

The third and final derivative rule was developed based on observations of drawing materials. After neck formation, ductile metals like structural steel do not reach a point when the neck stabilizes and draws; therefore, there cannot be a reversal in curvature in the post-necking regime. It is suspected that this rule applies through the entire plastic regime except for within the yield plateau, if present, as summarized in Section 3.4. However, this has not been explicitly proven in this research.

Mathematically, curvature is captured by the second derivative of a function. Thus, as shown in Equation 3-28, the second derivative of the true stress-strain relationship for ductile metals, a normally negative quantity as the general relationship is concave down, must never become positive. Obeying this rule when developing the material true stress-strain relationship will ensure post-necking cold-drawing response will not be predicted.

$$\frac{d^2\sigma}{d\varepsilon^2} \leq 0 \qquad \text{Equation 3-28}$$

3.5 SUMMARY

The previous sections provided a detailed description of the three derivative rules. These rules can be used to guide the process of developing the true stress-strain relationship for structural steels for FEA using 3D solid elements from standard coupon tension test data. The three derivative rules are restated together in Equation 3-29, Equation 3-30, and Equation 3-31. By obeying these simple rules when developing the true stress-strain relationship, necking will be accurately predicted, the material model will be numerically stable, and prediction of cold-drawing behavior will be avoided.

$$\sigma(\varepsilon_{max}) = \frac{d\sigma(\varepsilon_{max})}{d\varepsilon} \qquad \text{Equation 3-29}$$

$$\frac{d\sigma}{d\varepsilon} \geq 0 \qquad \text{Equation 3-30}$$

$$\frac{d^2\sigma}{d\varepsilon^2} \leq 0 \qquad \text{Equation 3-31}$$

While these rules are quite simple, their application and the larger process of developing the true stress-strain relationship for FEA of structural steels, presented in Chapter 4, is much more complex. However, by incorporating these rules into the process, several common errors can be easily avoided, expediting the development of this relationship and, often, improving the quality of the final result.

3.6 CONCLUSIONS

While each of the presented derivative rules is neither new nor novel on its own, their collective application to the process of defining the true stress-strain relationship for use in FEA of ductile metals, particularly structural steels, provides great value. Following these rules when developing a constitutive material model will result in accurate prediction of necking (Derivative Rule #1), numerically stable behavior (Derivative Rule #2), and no prediction of stable drawing (Derivative Rule #3). In addition, while beyond the scope of this research, these simple rules can be used to improve the speed and accuracy of iterative techniques used to determine the material true stress-strain relationship from test data, a recommended topic for future work discussed in Section 6.3.6.

4 DEVELOPING THE TRUE STRESS-STRAIN RELATIONSHIP

4.1 INTRODUCTION

This chapter presents a detailed step-by-step summary of the recommended process for determining the true stress-strain relationship for structural steel materials using experimental tension coupon load-deformation data from a standard coupon tension test. This relationship is valuable when using finite element analysis (FEA) with three dimensional (3D) solid elements. The process incorporates the three derivative rules, summarized in Chapter 3, along with some basic guidelines for defining material constitutive relationships used in FEA models, derived from a variety of published sources, as well as personal experience.

To simplify and clarify the process, the engineering stress-strain curve calculated from coupon test data using Equation 2-1 and Equation 2-2 is subdivided into five zones, as described in Section 4.2. Section 4.3 summarizes the recommended approach to fitting each of the five zones: (1) the linear-elastic range, (2) the proportionality limit and yield plateau, (3) the strain-hardening branch, (4) the onset of necking, and (5) post-necking. Note that consideration of fracture, which lies at the end of the fifth zone, is beyond the scope of this dissertation; however, basic guidance for simply including fracture in typical FEA tension coupon models is provided in Section 4.3.5.3.

4.2 ZONES OF THE ENGINEERING STRESS-STRAIN CURVE

Several researchers have used a zonal approach to dissect and analyze the engineering stress-strain relationship for use in determining the corresponding true stress-strain relationship. For example, Choung and Cho (Choung & Cho, 2008) divided the curve into three "blocks": (1) elastic response up to yield, (2) post-yield response up to necking, and (3) post-necking response to fracture, as illustrated in Figure 4-1. Similarly,

Arasaratnam et al. (Arasaratnam, Sivakumaran, & Tait, 2011) divided the engineering stress-strain curve into five "regions": (I) linear elastic range, (II) nonlinear elastic range, (III) yield plateau, (IV) strain-hardening, and (V) strain softening, as shown in Figure 4-2. Still others, such as Wang et al. (Wang, Xu, Ren, & Wang, 2016), recommend division of the engineering stress-strain curve into an undefined number of smaller segments to facilitate development of the true stress-strain relationship for use in numerical analysis.

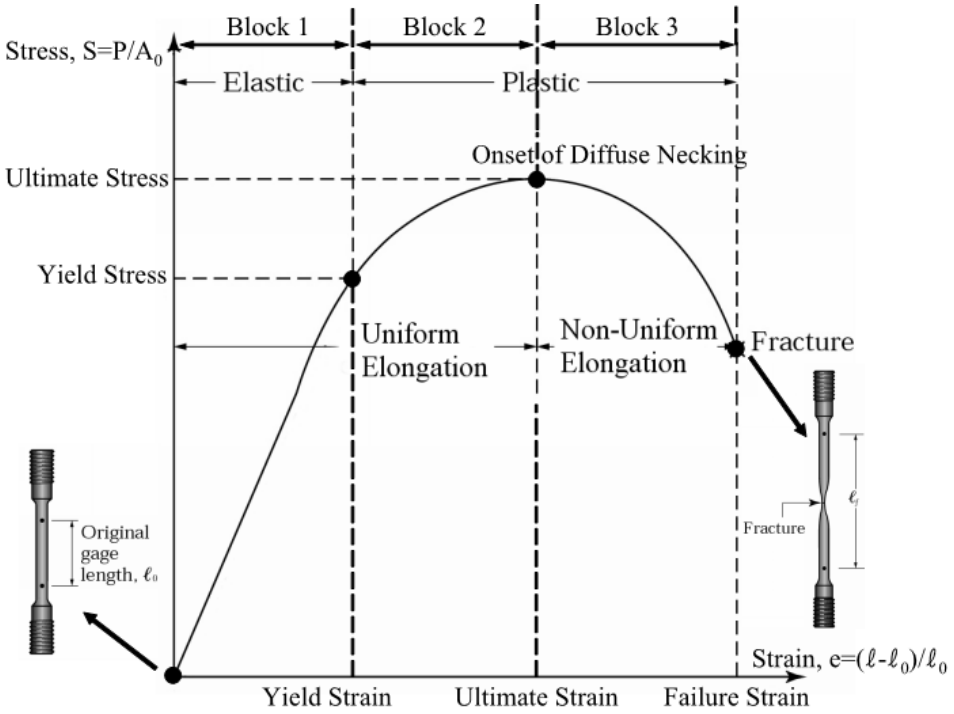

Figure 4-1: Engineering stress-strain "blocks" defined by Choung and Cho (Choung & Cho, 2008)

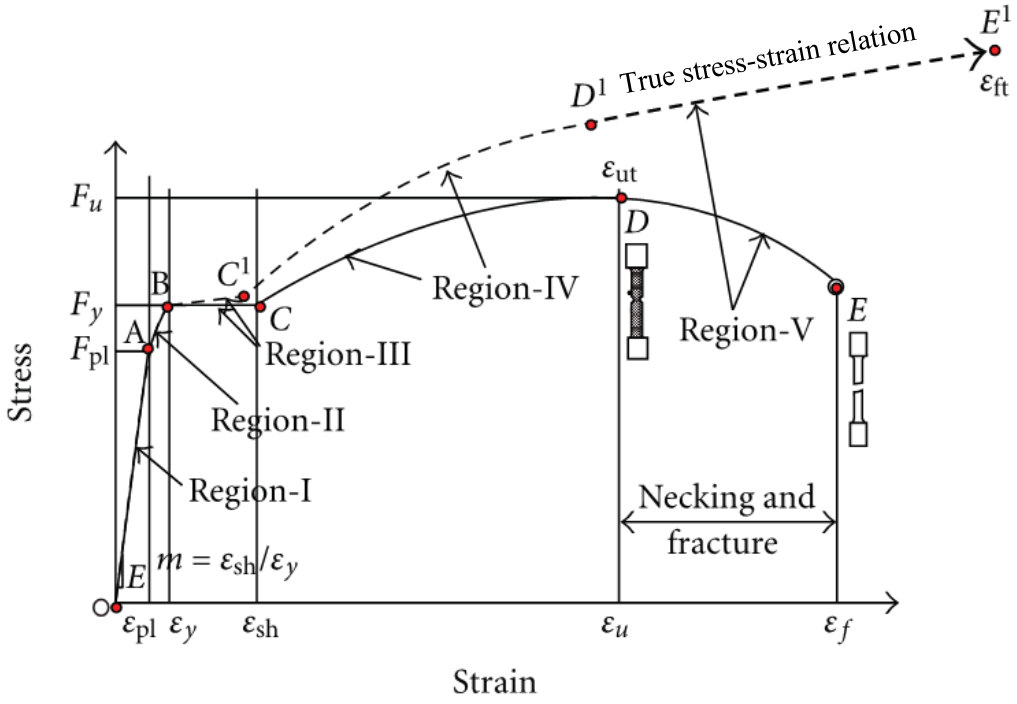

Figure 4-2: Engineering stress-strain "regions" defined by Arasaratnam et al. (Arasaratnam, Sivakumaran, & Tait, 2011)

In light of the practicality, flexibility, and precision allowed by the five-zone dissection developed by Arasaratnam et al. (Arasaratnam, Sivakumaran, & Tait, 2011), a similar approach is adopted in this dissertation. As shown in Figure 4-3, five zones are defined for an idealized ductile metal engineering stress-strain curve for uniaxial tension response. For the purposes of this discussion, the idealized stress-strain curve is most like that expected for a lower strength steel material (i.e., steel with a yield strength less than approximately 50 ksi), though the behaviors observed are generally analogous to those exhibited by other ductile metals.

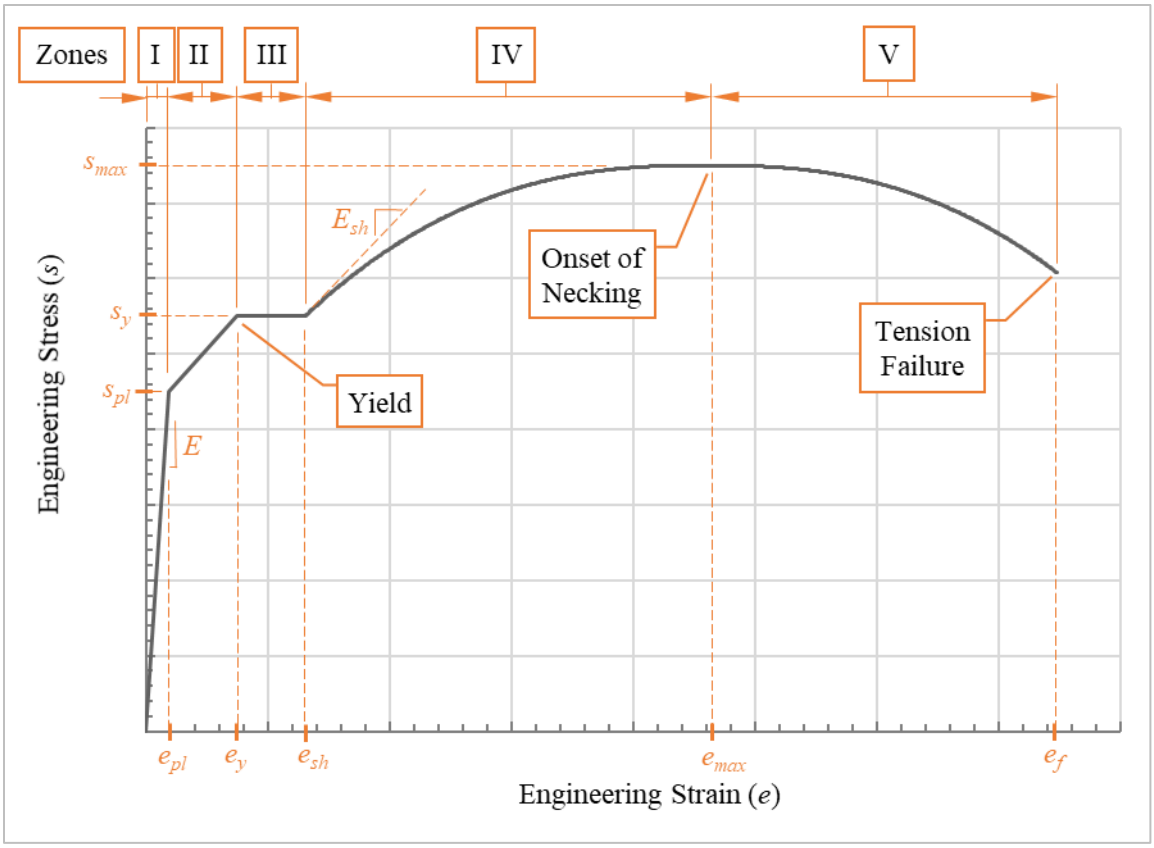

Figure 4-3: Engineering Stress-Strain Relationship Zones

The following sections summarize the basic observed behaviors in each of the five regions, along with recommendations for developing the true stress-strain relationship from engineering stress-strain data within each zone. Additional guidance is provided for the transitions between zones to ensure numerical stability is maintained. It is important to note that the relationship in the zones should be determined sequentially, beginning with Zone I and finishing with Zone V. Sequential development is important because the relationships defined in successive zones generally use information determined by the relationship in the prior zone as a constraint on possible solutions in that zone.

4.3 TRUE STRESS-STRAIN RELATIONSHIP FOR NUMERICAL ANALYSIS

Due to differences in response, both in terms of general shape of the stress-strain relationship and uniformity of deformations over the gauge length, the recommended process for developing the true stress-strain relationship for use in FEA analysis with 3D elements has been dissected into five regions, described in detail in the following sections. Each section includes relevant information related to the physical coupon response, the engineering stress-strain relationship, and the true stress-strain relationship within each zone, or at key transitions between zones, as appropriate.

The presented approach was developed considering several simplifying assumptions including idealized material behavior (e.g., isotropy) and neglecting certain behaviors as noted in Section 2.4. The proposed approach focuses on directly interrogating and matching a known engineering stress-strain relationship, with an emphasis on capturing post-necking response. Care should be taken when using book values of material properties to define a material model for FEA, as the method used may change how it should be incorporated into the development of the true stress-strain relationship.

To avoid mistakes that can manifest in the common approach of fitting by arbitrarily selecting points that capture key features of the true stress-strain relationship, functional relationships are recommended when developing the true stress-strain relationship. These functions may be linear, quadratic, or, more complex such as logarithmic, exponential, or some combination of these. Leveraging functional relationships allows for a simple means to ensure that the derivative rules in Chapter 3 are maintained across the entire domain, and provides a means to constrain transitions between zones, guaranteeing continuity where required. To aide in the process, it is recommended that a spreadsheet be used to develop the true stress-strain data that will eventually be used to define the material model for FEA.

Finally, use of the simple relationships is generally recommended for selecting functional fits to test data within each zone. In most cases, there are two to four constraints to consider in defining a functional fit, along with the general shape of the data within a given zone. Therefore, linear, quadratic, exponential, and logarithmic functions are recommended, as well as combinations of these simple relationships, as appropriate. By following this approach excessive complexity, such as overfitting (i.e., fitting noise within the data, discussed briefly in Section 5.3.2) and similar issues can typically be avoided.

4.3.1 Zone I: Linear-Elastic Range

The initial portion of the engineering stress-strain response for structural steels in tension, highlighted in Figure 4-4, is linear with a slope equal to the elastic modulus, E. It begins at the point of zero stress and strain and ends at the proportional limit. This early response is the typical range within which standard elastic design is conducted in accordance with model building codes like the *International Building Code* (IBC) (International Code Council, 2018), general design standards like *ASCE7 Minimum Design Loads and Associated Criteria for Buildings and Other Structures* (American Society of Civil Engineers, 2016), and material-specific standards for metals such as the AISC Steel Design Manual (American Institute of Steel Construction, 2017), the AISI Cold-Formed Steel Design Manual (American Iron and Steel Institute, 2017), and the Aluminum Design Manual (Aluminum Association, 2015).

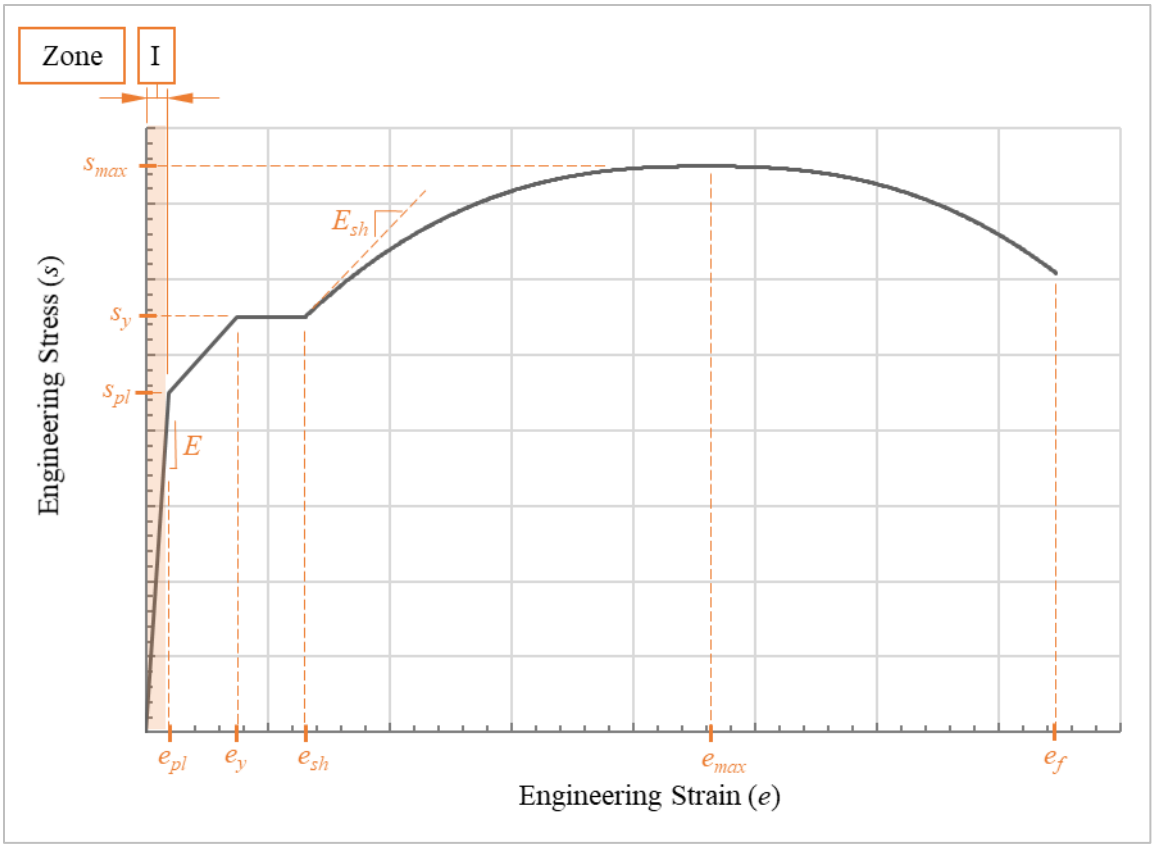

Figure 4-4: Engineering Stress-Strain Relationship – Zone I

Many material models used in FEA will adopt standard elastic engineering material properties, such as the modulus of elasticity, E, and internally determine the true stress-strain properties for elastic analysis. Where explicit calculation of elastic true stress-strain properties is required, the standard analytical conversions presented in Equation 2-3 and Equation 2-4 can be used. These relationships are repeated in Equation 4-1 and Equation 4-2, for later reference within this chapter. Conversion from engineering to true stress and strain using these relationships is possible in Zone I because the underlying assumption that stresses and strains are uniform throughout the reduced section of the tension coupon is valid. Because this assumption remains valid through elastic and plastic response up to necking, as discussed in the following sections of this dissertation, these same conversions

will apply to those areas as well. Thus, the relationship applies through Zone IV, at which point necking occurs at the transition to Zone V, violating the assumption of uniform stress and strain, as discussed in Sections 4.3.4.2 and 4.3.5.

$$\sigma = \frac{P}{A} = s(1 + e) \qquad \text{Equation 4-1}$$

$$\varepsilon = \frac{L - L_o}{L} = \ln(1 + e) \qquad \text{Equation 4-2}$$

The linear elastic range of response ends at the proportionality limit where the engineering stress-strain curve deviates from early linear-elastic response. This deviation occurs at a proportional limit engineering stress and strain, s_{pl}, and e_{pl}, respectively. Once converted using the equations presented previously, the proportional limit true stress and strain are referred to as σ_{pl}, and ε_{pl}, respectively.

Using the conversion relationships provided in Equation 4-1 and Equation 4-2, a relationship for the true elastic modulus, E_{true}, can be developed assuming the true behavior, like the engineering behavior, is linear, as shown in Equation 4-3. Overlaying this Zone I conversion onto the idealized engineering stress-strain curve from Figure 4-3 and constraining the extents to view only this portion of the curve, as shown in Figure 4-5, it is apparent that the true elastic modulus, E_{true}, is greater than the corresponding engineering elastic modulus, E. In addition, the true proportional limit stress, σ_{pl}, is greater than its the engineering counterpart, s_{pl}, and the true proportional limit strain, ε_{pl}, is less than the engineering proportional limit strain, e_{pl}. These observations about the relative comparison between true and engineering stress-strain relationships hold true for all zones when considering uniaxial tension behavior. Specifically, the true stress is always greater than the engineering stress for a given value of strain. Similarly, the true strain is always

less than the engineering strain at a given value of stress. The difference becomes more apparent with increasing strain. The preceding comments apply to tension response only, as discussed in detail in Section 2.7.1.1. For materials that do not exhibit nonlinear elastic behavior, the plastic limit is equal to the yield point. Thus, s_{pl} can be replaced by s_y, and e_{pl} can be replaced by e_y in Equation 4-3.

$$E_{true} = \frac{s_{pl}(1 + e_{pl})}{\ln(1 + e_{pl})} \qquad \text{Equation 4-3}$$

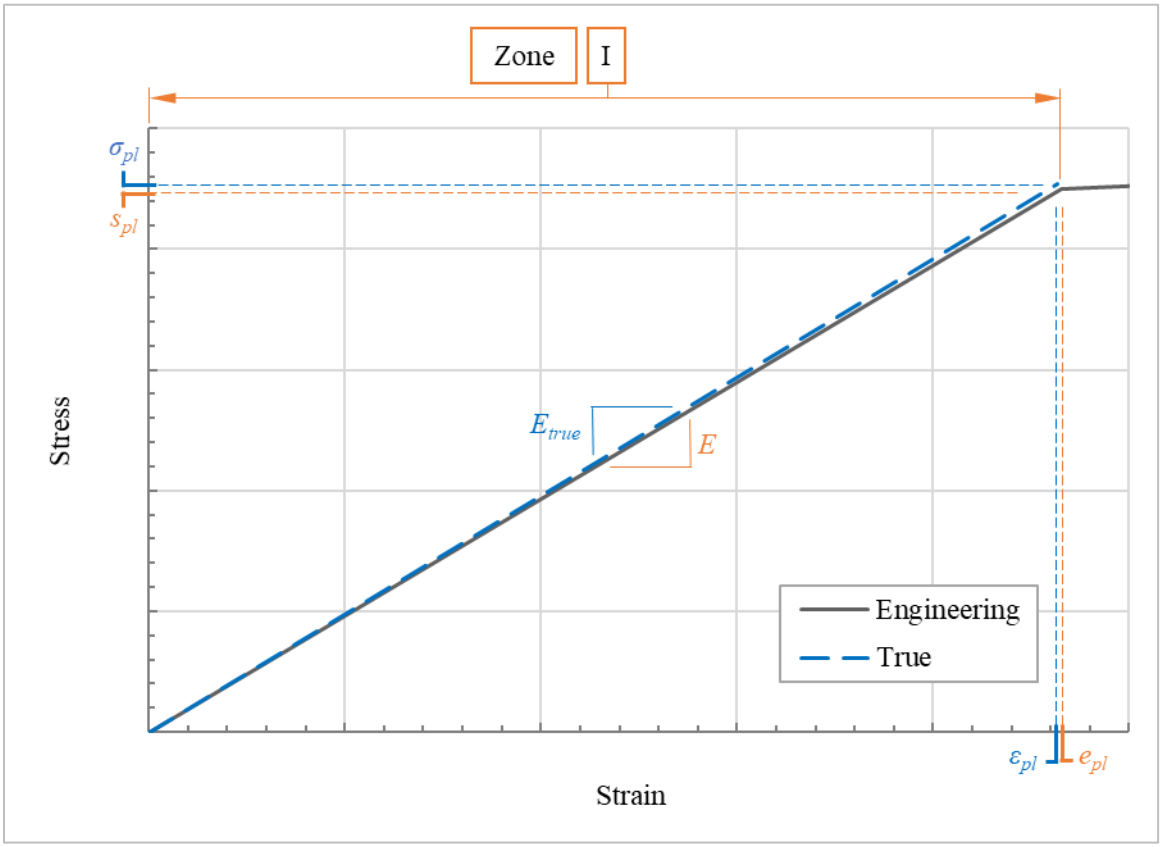

Figure 4-5: True Stress-Strain Relationship – Zone I

4.3.1.1 Commentary on Experimentally Measured Elastic Modulus

As summarized in the previous section, the elastic stiffness of a material, or elastic modulus, can theoretically be measured directly through tension testing. However, elastic moduli are generally not determined through tensile testing (Davis, 2004). There are several reasons for this. First, the assumption that a coupon is in pure tension can be made inaccurate by any slight misalignment of the specimen, which induces bending in the coupon during testing, as illustrated in Figure 4-6. Misalignment-induced bending causing a distribution of stresses across the section that deviates from the assumed uniaxial tension stress condition, thus introducing error into the measured tensile response of the coupon. While this effect can be minimized through careful alignment or other means (e.g., using pinned grips), it is likely to contribute to some extent in most typical test data.

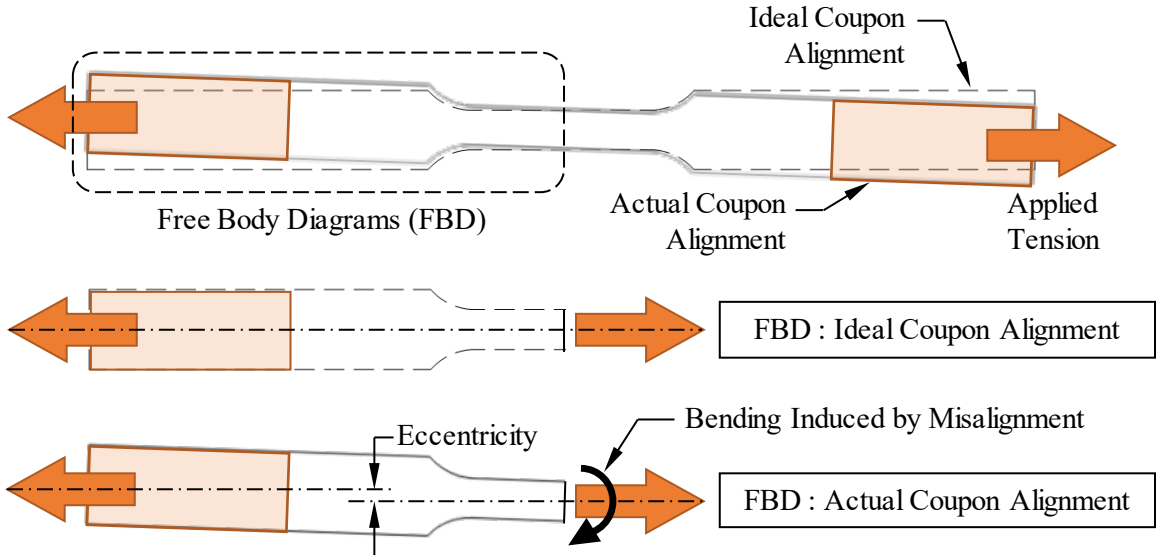

Figure 4-6: Bending Induced by Grip Misalignment

Second, the grips that hold the ends of a tension coupon come in a variety of types including screw-action grips, wedge-type grips, pneumatic-action grips, buttonhead grips, and pinned grips (Davis, 2004). In addition, a variety of surface materials (e.g., rubber or

metal) and surface finishes (e.g., smooth or textured) are employed to transfer load from the testing machine to the tension coupon. In reality, this load transfer is imperfect, particularly during initial load application when the grips "seat" and, often, slip slightly in the process. As a result, the initially measured loads appear to gradually transfer because of seating, slipping, and other imperfect load transfer issues in between the grips and the tension coupon. Figure 4-7 illustrates an example of seating effects on the early measured engineering stress-strain response of a tension coupon. Refer to Appendix A for additional information on the sources of experimental data used in this dissertation.

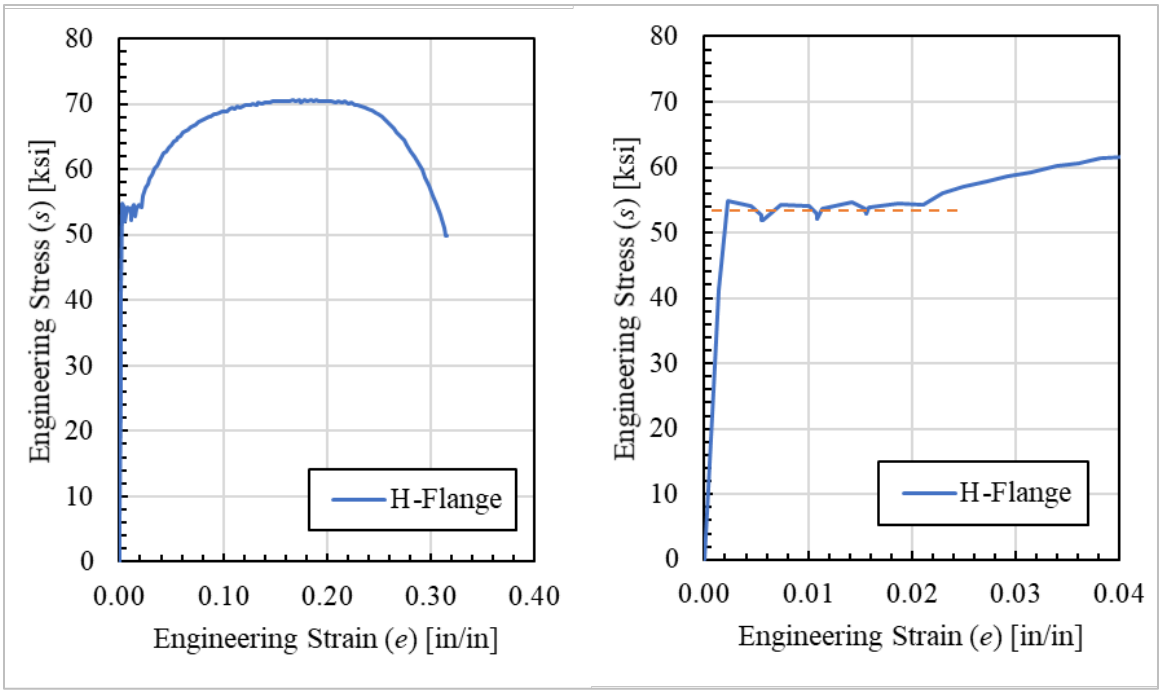

Figure 4-7: Example of Grip Seating in Tension Test Data

Third, the rate at which loads are applied during a standard tension test can affect the measured stiffness and strength of the specimen. This load-rate-dependent material response is referred to as the *strain rate effect*, where strain rate refers to the rate of change

in strain with respect to time, *t*, as defined in Equation 4-4 and Equation 4-5 for engineering and true strains, respectively.

$$\dot{e} = \frac{de}{\mathrm{dt}} \qquad \text{Equation 4-4}$$

$$\dot{\varepsilon} = \frac{d\varepsilon}{dt} \qquad \text{Equation 4-5}$$

Strain rates particularly affect the early portions of the stress-strain relationship developed from experimental testing, and thus affect quantities like elastic modulus, *E*, and yield stress, s_y, more than properties that occur at higher plastic strains such as the ultimate tensile stress, s_{max} (Davis, 2004). In addition, the strain-rate dependence of typical ductile metals like structural steel increases with increasing temperature. If cross-head velocity of the testing machine, v_{xh}, is recorded, strain-rates can be estimated in terms of conventional engineering strain, e, using Equation 4-6. Similarly, the true strain rate can be determined as shown in Equation 4-7. These true and engineering strain rates are related, as shown in Equation 4-8, which can be used to relate one to the other. Note that for true strain rate, $\dot{\varepsilon}$, a constant cross-head velocity, v_{xh}, will result in a decreasing strain rate throughout the test, because the length, *L*, is increasing. Therefore, a constant engineering strain rate is not indicative of a constant true strain rate.

$$\dot{e} = \frac{de}{\mathrm{dt}} = \frac{d(L - L_o)/L_o}{dt} = \frac{1}{L_o}\left(\frac{dL}{dt}\right) = \frac{v_{xh}}{L_o} \qquad \text{Equation 4-6}$$

$$\dot{\varepsilon} = \frac{d\varepsilon}{dt} = \frac{d[\ln(L - L_o)]}{dt} = \frac{1}{L}\left(\frac{dL}{dt}\right) = \frac{v_{xh}}{L} \qquad \text{Equation 4-7}$$

$$\dot{\varepsilon} = \frac{v_{xh}}{L} = \frac{L_o}{L}\left(\frac{de}{dt}\right) = \frac{1}{1+e}\left(\frac{de}{dt}\right) = \frac{\dot{e}}{1+e} \qquad \text{Equation 4-8}$$

Once the strain-rates are estimated, relative strain rate effects can be estimated using a variety of sources (Luecke, et al., 2005) (Crawford, Magallanes, & Lan, 2006) (Sierakowski, 1997) (Rajendran, 1992). Due to the complex interaction between strain rates, temperature, and tensile behavior of ductile metals, however, this dissertation neglects them (see Section 2.4) to avoid complicating these discussions. Nevertheless, for accuracy of analysis and computational models, they should be considered and included when they are expected to affect the computed results.

Thus, for most cases, the measured elastic modulus should not be used when developing the true stress-strain relationship. Rather, standard book values should be chosen instead. Book values for several typical ductile metals are provide in Table 4-1, adapted from values reported by Davis (Davis, 2004). Similar values are reported by Dieter (Dieter, Jr., 1961), and others.

Table 4-1: Engineering Elastic Modulus for Typical Ductile Metals

Material	**Engineering Elastic Modulus, *E* [ksi]**
Carbon Steel	30,000
Stainless Steel	28,000
Aluminum	10,000
Copper	17,000
Brass	16,000

Once the appropriate book value for engineering elastic modulus, E, is chosen, and the engineering stress at the proportionality limit, s_{pl}, is measured, the approximate engineering strain at the proportionality limit, e_{pl}, can be determined using Equation 4-9.

Similarly, the true elastic modulus, E_{true}, can be determined using Equation 4-3, presented earlier. As previously noted, for materials that do not exhibit nonlinear elastic behavior, the plastic limit is equal to the yield point. Thus, s_{pl} can be replaced by s_y, and e_{pl} can be replaced by e_y in Equation 4-9.

$$e_{pl} = \frac{s_{pl}}{E} \qquad \text{Equation 4-9}$$

4.3.1.2 True Stress-Strain Data for Numerical Analysis – Zone I

Where direct conversion is not already handled within the chosen computational software or material model, the true stress-strain relationship for structural steels should be defined as a linear function using the measured engineering stress at the proportional limit, s_{pl}, and a book value for elastic modulus, E, as summarized in Section 4.3.1.1. For steels, a value between 28,000 ksi and 30,000 ksi is commonly chosen. Depending on the analysis software, analytical approach, and/or material model chosen, the inputs for material properties may vary. However, a linear relationship should be defined for Zone I, beginning at zero true stress and strain and ending at the true stress and strain at the proportional limit, σ_{pl} and ε_{pl}, respectively. Thus, the resulting linear function relationship should have a slope equal to the true elastic modulus, E_{true}. The resulting general linear functional relationship that should be used to define the true stress-strain relationship in Zone I is presented in Equation 4-10.

$$\boxed{\text{I}}\ 0 < \varepsilon < \varepsilon_{pl} \qquad \sigma(\varepsilon) = \mathrm{E}_{true}\,\varepsilon \qquad \text{Equation 4-10}$$

4.3.1.3 Transition Constraints between Zones I - II: Proportionality Limit

For continuity, the relationship defined for Zone II must coincide with the one used to define Zone I at the point of transition between the two zones. Put simply, the initial

point in Zone II must equal the final point in Zone I. Doing so ensures continuity in the transition between zones and numerical stability because it permits a single stress value for a given material strain, provided the derivative rules of Chapter 3 have been followed. In addition to general continuity, slope continuity may be necessary at certain key points as well, as discussed in later sections. These continuity constraints can be captured most efficiently by leveraging functional relationships, as noted previously, though it is not explicitly required.

For the transition between Zone I and Zone II, there are two typical transition types that occur at the proportional limit: (1) gradual smooth deviation, referred herein as tangential deviation, and (2) abrupt deviation, exemplified by a distinct change in stiffness or "kink" in the stress-strain response. These behaviors are also referred to as continuous yielding and discontinuous yielding, respectively (ASM International, 2002).

Where no nonlinear elastic range, defined herein as Zone II, exists for given material, the proportionality limit is equal to the yield point, and the transition requirements discussed in this section between Zones I and II must be followed in transitioning directly from Zone I to Zone III. Thus, the transition would typically take the form of an abrupt transition from the linear elastic behavior in Zone I to the yield plateau in Zone III, discussed in Section 4.3.3. These idealized transitions are illustrated in Figure 4-8. In addition, Figure 4-9 illustrates a real example of each of these transitions observed in data from actual steel coupon tensions. Refer to Appendix A for additional information on the sources of experimental data used in these examples.

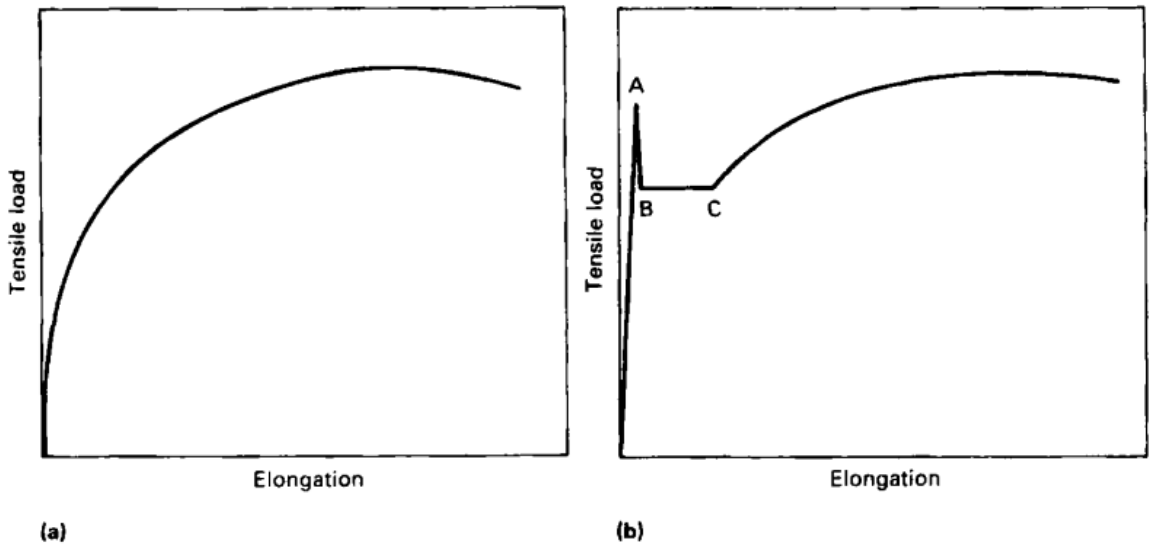

Figure 4-8: Idealized Plots of (a) Tangential (Continuous) and (b)Abrupt (Discontinuous) Yielding (ASM International, 2002)

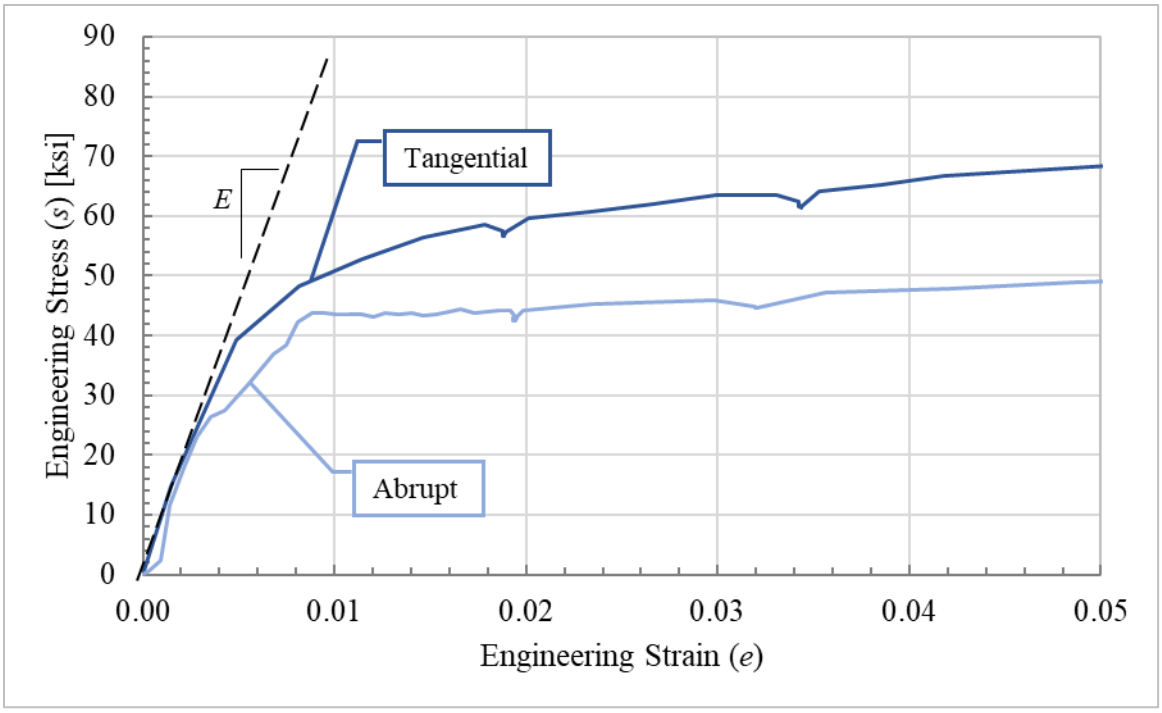

Figure 4-9: Transition Zone I - II – Tangential and Abrupt Deviation

Care should be taken when capturing this transition, especially where it may be important to the results of the numerical analysis model. For abrupt transition, no consideration of the Zone I relationship beyond the value of the stress and strain at the transition point is required. Accordingly, the functional constraint on the definition of Zone II response is the initial proportional limit stress and strain. Where a gradual and tangential deviation from the linear elastic response of Zone I to the nonlinear elastic response in Zone II occurs, slope continuity should also be preserved. This constraint can be achieved by using the elastic slope from Zone I to define the initial slope of the relationship in Zone II. Expressed a different way, for the case of tangential deviation, the functional relationship for Zone II must maintain first derivative continuity with Zone I.

4.3.2 Zone II: Nonlinear Elastic Range

Zone II of the engineering stress-strain response for structural steels in tension, highlighted in Figure 4-10, is characterized by elastic deviation from the initial linear elastic slope, E. It begins at the proportional limit and ends at the yield point. Because stresses and strains remain uniform in the reduced section, the standard relationships for conversion from engineering to true stress and strain provided in Equation 4-1 and Equation 4-2 still apply. As discussed previously, transition to Zone II can be abrupt or tangential. In some specimens, this range of response, Zone II, can be small or non-existent.

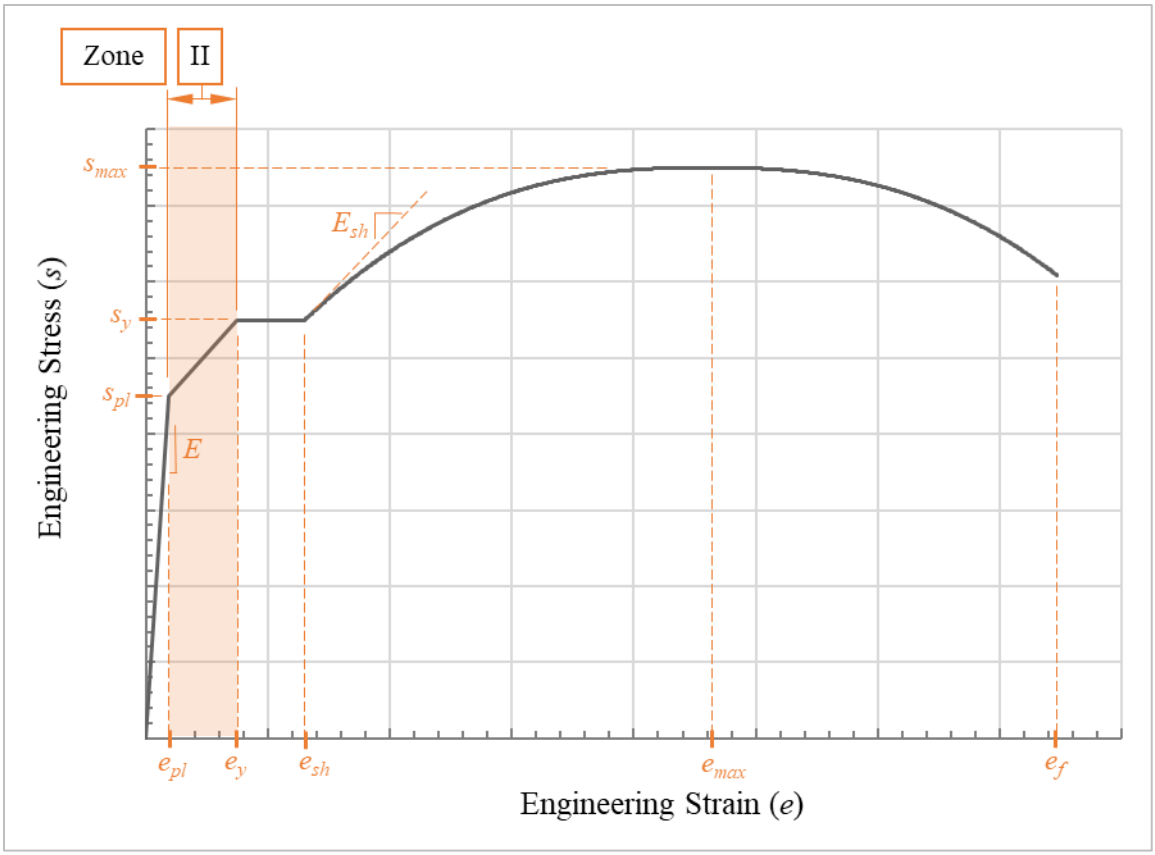

Figure 4-10: Engineering Stress-Strain Relationship – Zone II

This nonlinear elastic range is common in high strength steels such as ASTM A852, ASTM A514, and other high-yield strength steels, as illustrated in Figure 4-11. It is also common for ductile metals like aluminum and copper to exhibit nonlinear elastic response, as shown in Figure 4-12 and Figure 4-13, respectively.

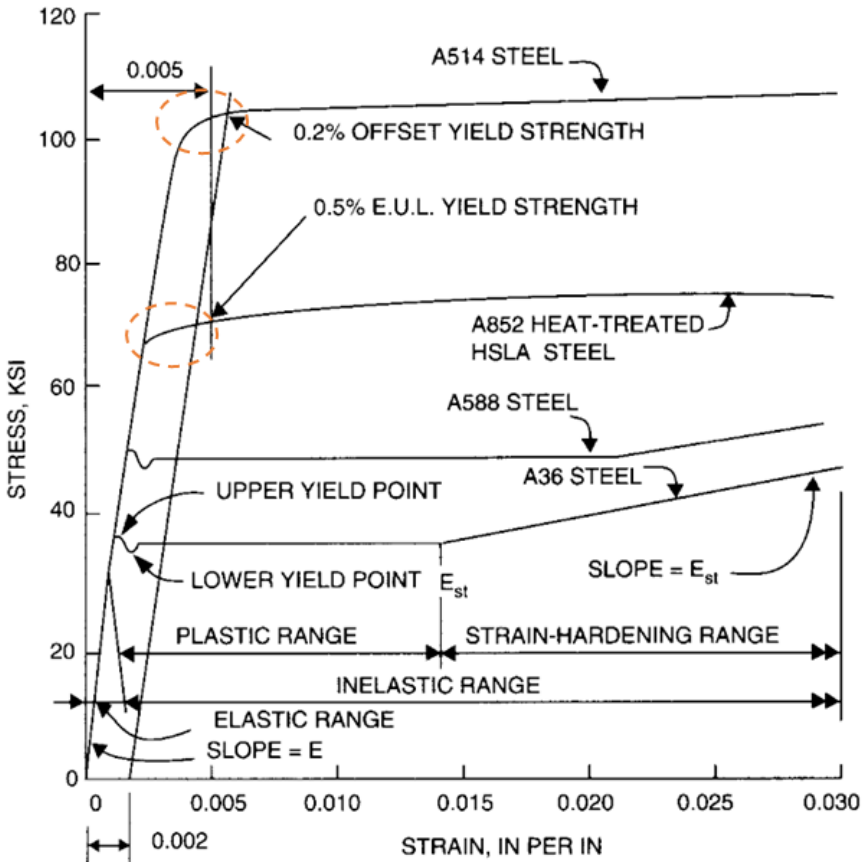

Figure 4-11: Examples of Nonlinear Elastic Response of Steel (Brockenbrough & Merritt, 1972)

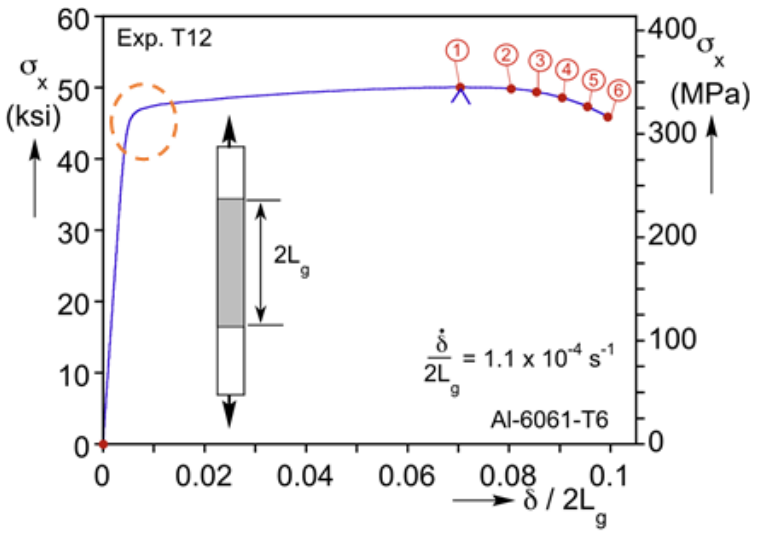

Figure 4-12: Example of Nonlinear Elastic Response of Aluminum (Tardif & Kyriakides, 2012)

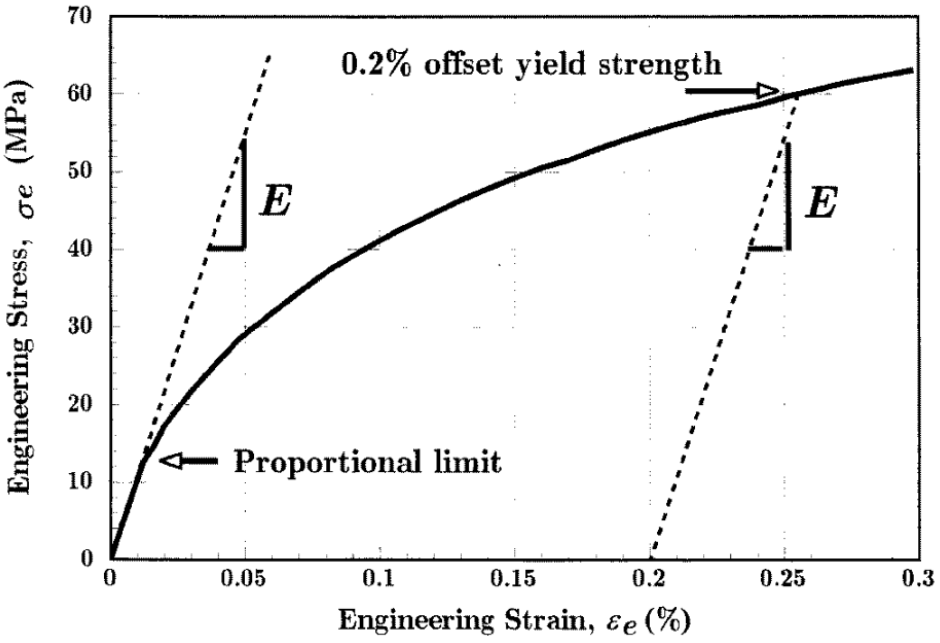

Figure 4-13: Example of Nonlinear Elastic Response of Copper (Roylance, 2001)

For materials that do not exhibit this nonlinear elastic response, such as lower-strength steels (i.e., steel with a yield strength less than approximately 50 ksi) (see Figure

4-11), the transition can be made directly from Zone I to Zone III, discussed in Section 4.3.3. Similarly, if both nonlinear elastic response and a yield plateau are not exhibited, as is the case for the aluminum and copper examples in Figure 4-12 and Figure 4-13, respectively, direct transition from Zone I to Zone IV, discussed in Section 4.3.4, may be appropriate.

4.3.2.1 True Stress-Strain Data for Numerical Analysis – Zone II

For an abrupt transition and a Zone II response that is mostly linear, a linear functional relationship can be defined for Zone II, much like Zone I, that takes the forms shown in Equation 4-11, where the characteristic linear slope of the true stress-strain relationship in Zone II is equal to E_{II}. A similar approach can be used to capture the Zone II response using quadratic, exponential, or other functional relationships, provided the function passes through the proportional limit stress and strain, σ_{pl} and ε_{pl}, that defines the final point in Zone I and provides appropriate slope continuity, as required. These functions are not derived here, however, due to the breadth of possible functions that could be used to fit Zone II data. Finally, E_{II} can be determined by calculating the change in true stress and dividing by the change in true strain over the extents of Zone II, as shown in Equation 4-12 and Equation 4-13.

$\boxed{\text{II}}\ \varepsilon_{pl} < \varepsilon < \varepsilon_y$ $$\sigma(\varepsilon) = E_{II}\left(\varepsilon - \varepsilon_{pl}\right) + \sigma_{pl}$$ Equation 4-11

$$E_{II} = \frac{\Delta\sigma}{\Delta\varepsilon} = \frac{\sigma_y - \sigma_{pl}}{\varepsilon_y - \varepsilon_{pl}}$$ Equation 4-12

$$E_{II} = \frac{s_y\left(1 + e_y\right) - s_{pl}\left(1 + e_{pl}\right)}{\ln\left(1 + e_y\right) - \ln\left(1 + e_{pl}\right)} = \frac{s_y\left(1 + e_y\right) - s_{pl}\left(1 + e_{pl}\right)}{\ln\left(\frac{1 + e_y}{1 + e_{pl}}\right)}$$ Equation 4-13

Alternatively, for a tangential transition where the initial slope of Zone II is also constrained and must be equal to the final slope in Zone I, or the true elastic modulus, E_{true}, the relationship in Equation 4-14 can be used, as an example, if a natural log relationship captures the true stress-strain relationship in Zone II. A similar approach can be used to capture the Zone II response using other functional relationships, provided the function passes through the proportional limit stress and strain, σ_{pl} and ε_{pl}, that define the final point in Zone I, and has an initial slope equal to the true elastic modulus, E_{true}.

$$\boxed{\text{II}}\ \varepsilon_{pl} < \varepsilon < \varepsilon_y \qquad \sigma(\varepsilon) = \sigma_{pl}\left(1 + \ln\left(\frac{\varepsilon}{\varepsilon_{pl}}\right)\right) \qquad \text{Equation 4-14}$$

Once a function is chosen to define Zone II, the proposed fit should be verified to determine whether the constraints are, in fact, met. As shown in Equation 4-15, the relationship developed in Equation 4-14 guarantees that the computed stress at a strain equal to the plastic limit strain, ε_{pl}, is equal to the plastic limit stress, σ_{pl}, ensuring functional continuity. In addition, the derivative of the natural log relationship in Equation 4-14, shown in general form in Equation 4-16, should be checked at the plastic limit strain, ε_{pl}, to verify that it is equal to the true elastic modulus, E_{true}, as illustrated in Equation 4-17. Thus, the sample Zone II functional fit presented in Equation 4-14 meets the functional (value) and first derivative continuity requirements for tangential deviation from Zone I to Zone II. Finally, as mentioned previously (see Section 4.3), simple functions such as linear, quadratic, exponential, logarithm should be used to avoid overfitting the data.

$$\boxed{\text{II}}\ \varepsilon_{pl} < \varepsilon < \varepsilon_y \qquad \sigma(\varepsilon_{pl}) = \sigma_{pl}\left(1 + ln\left(\frac{\varepsilon_{pl}}{\varepsilon_{pl}}\right)\right) = \sigma_{pl} \qquad \text{Equation 4-15}$$

II $\varepsilon_{pl} < \varepsilon < \varepsilon_y$ $$\frac{d\sigma(\varepsilon)}{d\varepsilon} = \frac{\sigma_{pl}}{\varepsilon}$$ Equation 4-16

II $\varepsilon_{pl} < \varepsilon < \varepsilon_y$ $$\frac{d\sigma(\varepsilon_{pl})}{d\varepsilon} = \frac{\sigma_{pl}}{\varepsilon_{pl}} = E_{true}$$ Equation 4-17

Similar relationships can be derived for other mathematical functions, as required to approximate the data. As noted previously, the reason for a functional relationship is to ensure that derivative rules established in Chapter 3, particularly those described in Sections 3.3 and 3.4, and transition constraints are met for each zone. For the natural log relationship defined in Equation 4-14, it has already been demonstrated that there is functional continuity and first derivative continuity; accordingly, transition constraints have been obeyed. However, this relationship should also be checked against the derivative rules.

Derivative Rule #2, described in Section 3.3, requires that the first derivative be always positive for numerical stability. As shown in Equation 4-16, for all values of ε, between ε_{pl} and ε_y, both the true stress and the true strain are positive. Therefore, the first derivative will always be positive within Zone II, ensuring that energy is always increasing, and the stability requirements of Derivative Rule #2 have been met. Examining the second derivative, shown in Equation 4-18, reveals that the second derivative must always be negative within Zone II because the strain squared is always positive. Therefore, the relationship obeys Derivative Rule #3, ensuring the material is always softening with increasing strain and will not predict cold drawing behavior, as described in Section 3.4.

II $\varepsilon_{pl} < \varepsilon < \varepsilon_y$ $$\frac{d^2\sigma(\varepsilon)}{d\varepsilon^2} = -\frac{1}{\varepsilon^2}$$ Equation 4-18

4.3.2.2 Transition Constraints between Zones II - III: Yield

Unlike the transition between Zones I and II presented in Section 4.3.1.3, the transition between Zones II and III almost always occurs in an abrupt manner for materials that exhibit a yield plateau. Thus, the relationship defined for Zone III will typically have a single constraint — the values of true stress and strain at the yield point, σ_y and ε_y — which will ensure functional continuity, neglecting continuity of the first derivative. For materials that do not have a distinct yield plateau, the elastic and strain hardening branches are directly connected. Consequently, Zone III can be eliminated and the prior zone, Zone I or Zone II as appropriate, can be directly linked to Zone IV with any necessary constraints.

4.3.2.3 Commentary on Upper Yield Point

One phenomenon that should be carefully considered when developing the true stress-strain relationship for FEA is the upper yield point. It is important to understand that yielding, and other plastic deformations of ductile metals such as structural steel, occurs due to physical movement of dislocations within the atomic crystalline structure of the material, as discussed in Section 2.5.3. For this reason, these strains are non-recoverable when load is removed. The upper yield point is often attributed to one or both of the following distinct phenomena: (1) strain rate effects, and (2) the difference between the stress required for initiation of atomic crystalline dislocation movement and the stress required for continued propagation of those dislocations. These issues are addressed in greater detail in the following paragraphs.

Regarding strain rate effects, several studies of the topic clearly demonstrate that, with increasing strain rate, the appearance and relative magnitude of the upper yield becomes much more apparent as strain rate increases. This phenomenon is demonstrated by Wang et. al (Wang, et al., 2018) for high specific strength steels, as illustrated in Figure

4-14, and Cadoni and Forni (Cadoni & Forni, 2015) for reinforcing bar steel, as illustrated in Figure 4-15, among others.

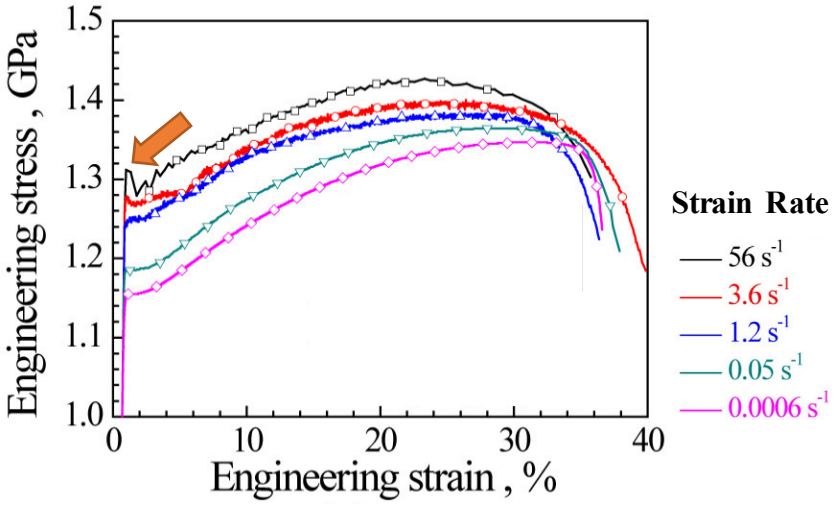

Figure 4-14: Influence of Strain-rate on Upper Yield Point in High-Strength Steels (Wang, et al., 2018)

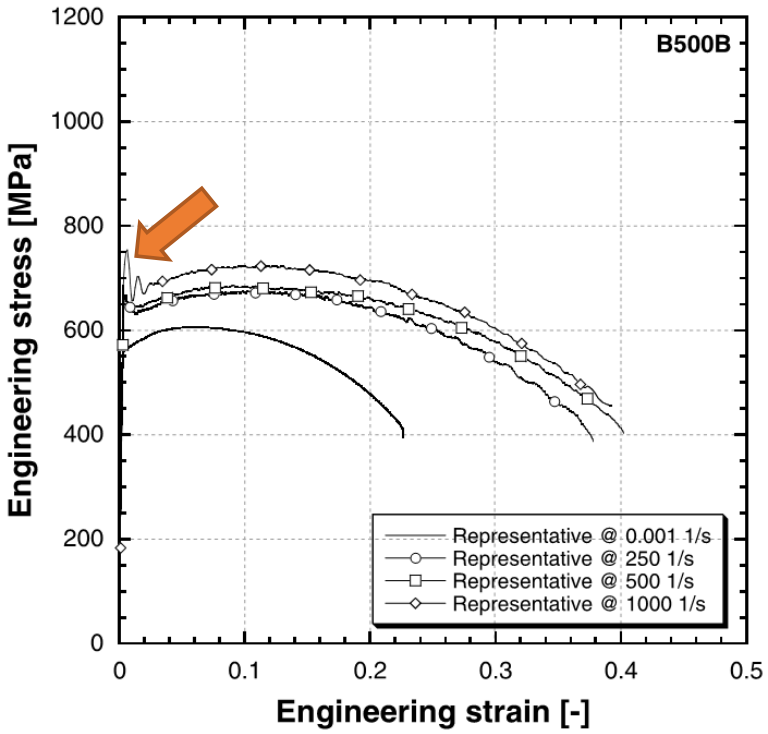

Figure 4-15: Influence of Strain-rate on Upper Yield Point in Reinforcing Steels (Cadoni & Forni, 2015)

Regarding the difference between initiation and propagation of dislocations, Dieter (Dieter, Jr., 1961) describes the upper yield point as a phenomenon where a discrete band of material creates a localized stress concentration in the coupon, which then propagates over the length of the specimen. The initial formation of this band of yielding material is characterized by the upper yield point. The propagation of the yielding band over the coupon is characterized by the lower yield point and yield plateau. A theoretical representation of the typical yield-point behavior of carbon steels is shown in Figure 4-16. In addition, test results from a low-carbon steel tension specimen demonstrating this upper yield point behavior are provided in Figure 4-17 for further illustration.

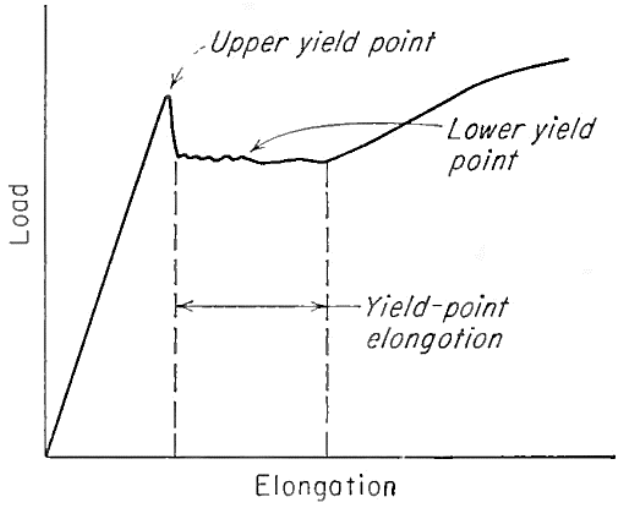

Figure 4-16: Upper and Lower Yield Point Defined (Dieter, Jr., 1961)

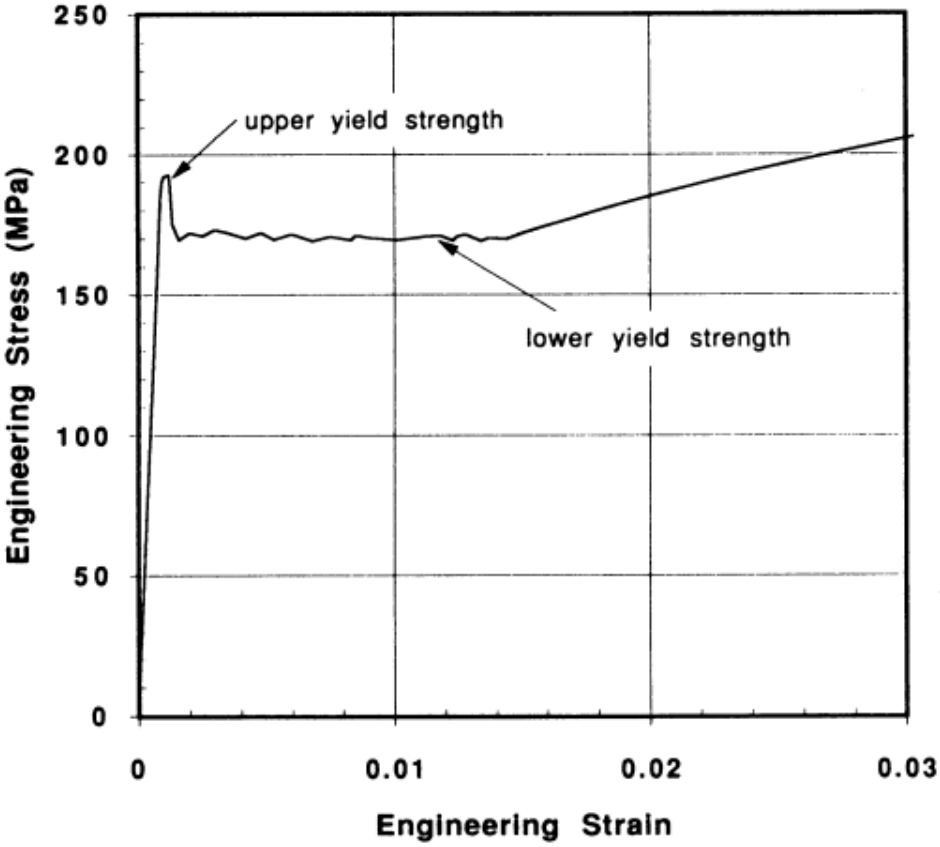

Figure 4-17: Steel Tension Test Data Illustrating Upper Yield Point (Davis, 2004)

Due to the tendency of the upper yield phenomena to manifest from strain rate effects, and the typical lack of knowledge of the precise strain rate and other similar circumstances and conditions under which a tension test is performed, care should be taken when deciding whether it is appropriate to capture this effect in the material true stress-strain relationship. Generally, unless it will have a significant bearing on the results of the model, it is recommended that any upper yield be neglected and that the lower yield point be used to define the yield strength of the material for numerical analysis. If there is a desire to capture this effect, it should be included by appropriately accounting for strain rate effects in the FEA model.

4.3.3 Zone III: Yield Plateau

Zone III, highlighted in Figure 4-18, is referred to herein as the yield plateau. The yield plateau, also referred to as the lower yield point or lower yield strength, is a region of approximately constant stress that may occur during the early plastic deformation of a tension coupon. Zone III begins at first yield and ends at the onset of strain hardening. While the deformations in the tension coupon are no longer elastic in this zone, they are assumed to occur uniformly over the reduced section of the coupon. Consequently, the use of the standard analytical relationships for conversion from engineering to true stress and strain presented in Equation 4-1 and Equation 4-2 remains valid.

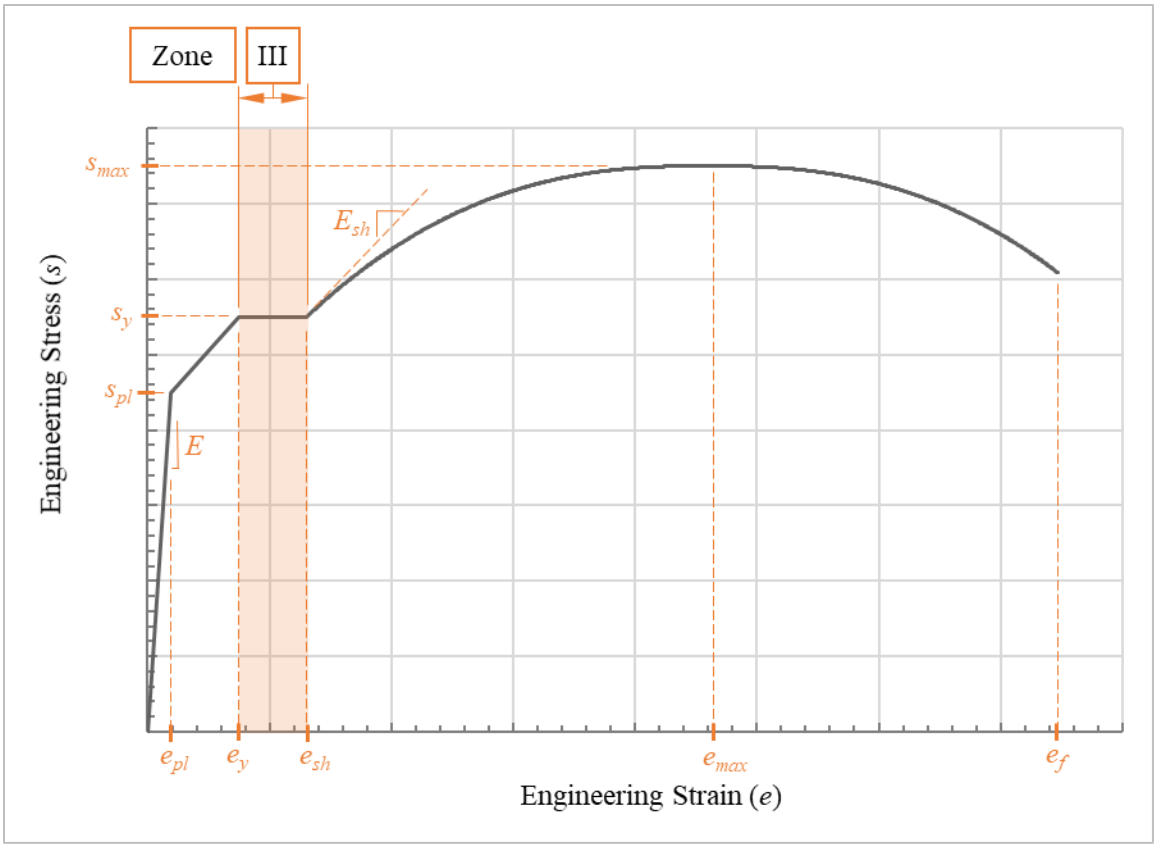

Figure 4-18: Engineering Stress-Strain Relationship – Zone III

It is common to observe a distinct yield plateau in lower-strength structural steels (i.e., steel with a yield strength less than approximately 50 ksi); however, this behavior is often absent from the response of high-strength steel, iron, aluminum, copper, and other ductile metals. For materials without a yield plateau, the prior zone should be directly transitioned to Zone IV response, as discussed in detail in Section 4.3.3.2. Otherwise, given the constant level of engineering stress that occurs over the yield plateau, it is typically sufficient to fit the data in this zone with a linear function defined using the values of stress and strain at the ends, as discussed in Section 4.3.3.1.

4.3.3.1 True Stress-Strain Data for Numerical Analysis – Zone III

While the slope of the engineering stress-strain relationship in Zone III is approximately equal to zero due to the nearly constant value of engineering stress, the corresponding true stress-strain relationship has a slight positive slope. This slope occurs because the true stress is calculated based on the actual area, which becomes smaller as strains increase due to conservation of volume. The slope of the true stress-strain relationship in Zone III, E_{III}, can be derived by simply determining the change in true stress and dividing by the change in true strain as summarized illustrated in Equation 4-19 and Equation 4-20 in terms of engineering stresses and strains.

$$E_{III} = \frac{\Delta\sigma}{\Delta\varepsilon} = \frac{\sigma_{sh} - \sigma_y}{\varepsilon_{sh} - \varepsilon_y} \qquad \text{Equation 4-19}$$

$$E_{III} = \frac{s_y(1 + e_{sh}) - s_y(1 + e_y)}{\ln(1 + e_{sh}) - \ln(1 + e_y)} = \frac{s_y(e_{sh} - e_y)}{\ln\left(\frac{1 + e_{sh}}{1 + e_y}\right)} \qquad \text{Equation 4-20}$$

Because functional continuity is required, the first point in Zone III must be coincident with the last point in Zone II. Therefore, the line with slope E_{III} must be defined such that at a strain equal to the true yield strain, ε_y, the calculated stress is equal to the true yield stress, σ_y. The linear function that obeys the necessary boundary conditions and captures the yield plateau response is illustrated in Equation 4-21.

III $\varepsilon_y < \varepsilon < \varepsilon_{ysh}$ $\qquad \sigma(\varepsilon) = E_{III}(\varepsilon - \varepsilon_y) + \sigma_y$ $\qquad$ Equation 4-21

Although the engineering stress-strain relationship within the yield plateau is typically assumed to have a constant value of stress, or zero slope, the true stress-strain will always maintain a positive slope. This positive slope ensures numerical stability is maintained, per Derivative Rule #2 (see Section 3.3).

4.3.3.2 Transition Constraints between Zones III - IV: Onset of Strain-Hardening

The transition between Zones III and IV is typically observed as an abrupt increase in stiffness from near zero within the yield plateau (if present) to a positive value in the range of approximately 10% of the elastic modulus. Lower-strength steels (i.e., steel with a yield strength less than approximately 50 ksi) are the most common ductile metal to exhibit a yield plateau and onset of strain hardening. Examples of stress-strain curves that exhibit this behavior are provided in Figure 4-19.

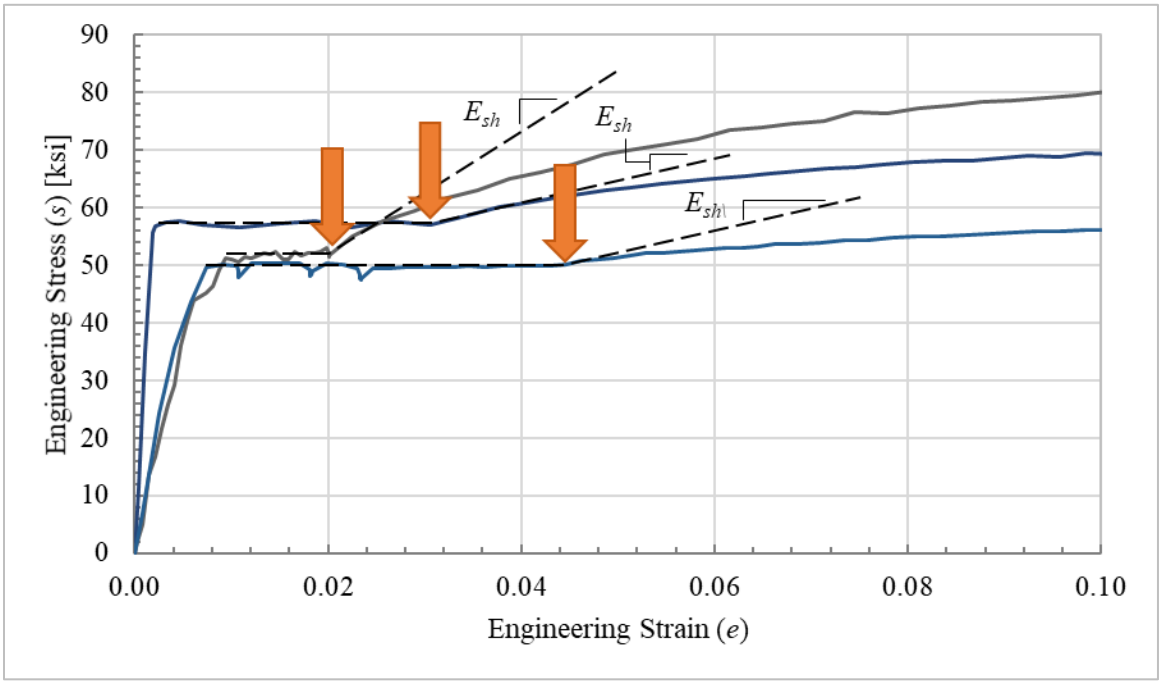

Figure 4-19: Examples of Strain-Hardening Transition

Therefore, the only constraint dictated by the Zone III relationship is that initial stress and strain at the beginning of Zone IV be equal to those at the end of Zone III, specifically the values of true stress and strain at the onset of strain hardening, σ_{sh} and ε_{sh}. In addition, the initial conditions of the relationship in Zone IV will be constrained by the initial slope of the strain hardening branch, E_{sh}, as discussed in Section 4.3.4.1.

4.3.3.3 Materials without Distinct Yield Plateau

For materials without a distinct yield plateau, there is typically a gradual change from linear-elastic response to strain hardening, which can occur with or without nonlinear elastic response in between. Examples of ductile metal materials that exhibit this type of behavior are high-strength steels, aluminum, and copper as previously shown in Figure 4-11, Figure 4-12, and Figure 4-13, respectively. For these materials, because there is no yield plateau, there is no Zone III for these materials. As a result, the transition to Zone IV occurs directly from Zone I for materials that do not exhibit nonlinear elastic response, or from Zone II for those that do. Depending on the stress-strain relationship, this transition can be abrupt or tangential. Therefore, the transition should be handled in a manner similarly to that described in Section 4.3.1.3.

4.3.3.4 Comparison of Yielding to Cold-Drawing of Polymers

Despite the fact that the derivative rules described in Chapter 3 are critical to ensuring accurate post-necking response, they may not be met for all instances in early response, particularly for materials that exhibit a distinct yield plateau followed by strain hardening, as shown in Figure 4-20. This is a unique instance where there is a natural reversal in curvature that must be captured to accurately develop a material model for numerical analysis. While not often considered in this context, the yield plateau observed in some lower-strength steels (i.e., steel with a yield strength less than approximately 50 ksi) is analogous to the cold-drawing behavior observed in polymers. As mentioned in Section 4.3.2.3, Dieter (Dieter, Jr., 1961) describes the upper yield point as a phenomenon where a discrete band of material creates a localized stress concentration in the coupon which then propagates over the length of the specimen. Thus, the yield process is much like the cold-drawing process for polymers, discussed in Section 2.10.1, in that it locally occurs and spreads over the section. Consequently, the stress-strain relationship produced

when testing these materials exhibits a similar reversal in curvature between the yield plateau and the onset of strain hardening.

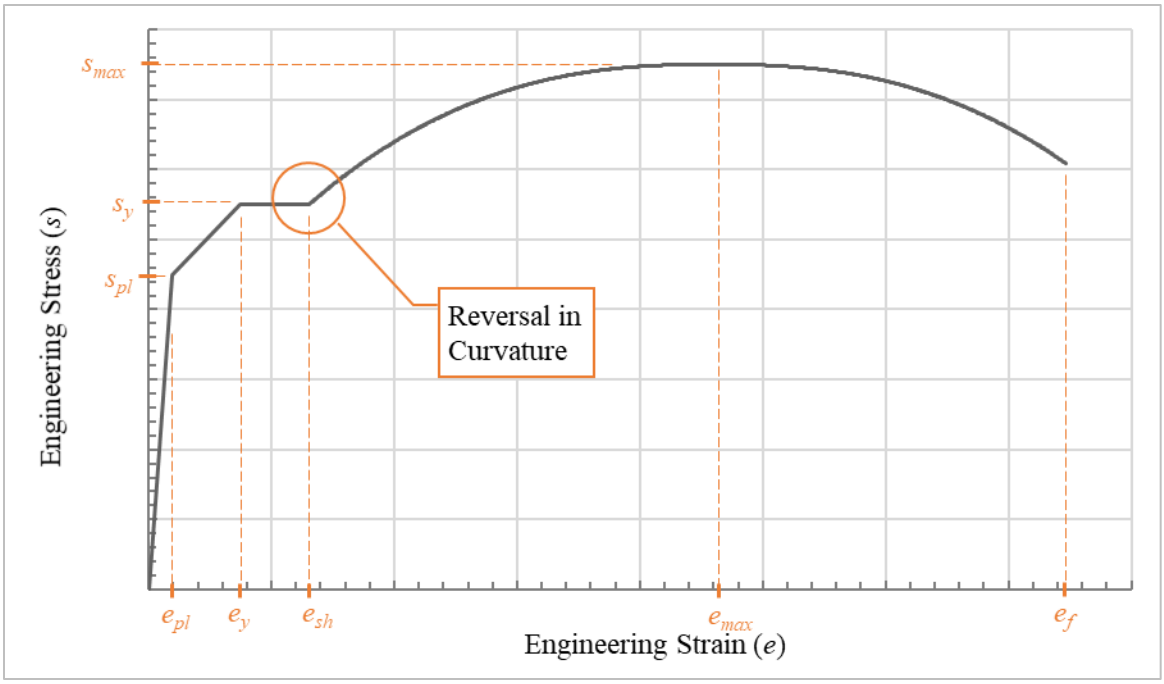

Figure 4-20: Reversal in Curvature at the Onset of Strain Hardening

4.3.4 Zone IV: Strain-Hardening Branch

Zone IV of the engineering stress-strain response for structural steels in tension, highlighted in Figure 4-21, is commonly referred to as the strain-hardening branch. The onset of strain hardening, which constitutes the initial portion of this zone, is characterized by a state of post-elastic deformation with increasing engineering stress. The initial slope within this zone is equal to the strain-hardening modulus, E_{sh}. This initial slope is a constraint that must be considered in the functional relationship defining this zone, as discussed in Section 4.3.4.1. In addition, within this zone the rate at which stress increases, or the slope of the engineering stress-strain relationship, decreases with increasing strain until the stress reaches a local maximum, resulting in a point of zero slope. This point of zero slope is referred to as the onset of necking and defines the end of Zone IV. Because

Zone IV encompasses the regime of response just prior to necking, stresses and strains in the reduced section of the coupon can still be assumed to be uniform, permitting the continued use of the standard analytical relationships for converting engineering stress and strain to true stress and strain provided (Equation 4-1 and Equation 4-2, respectively).

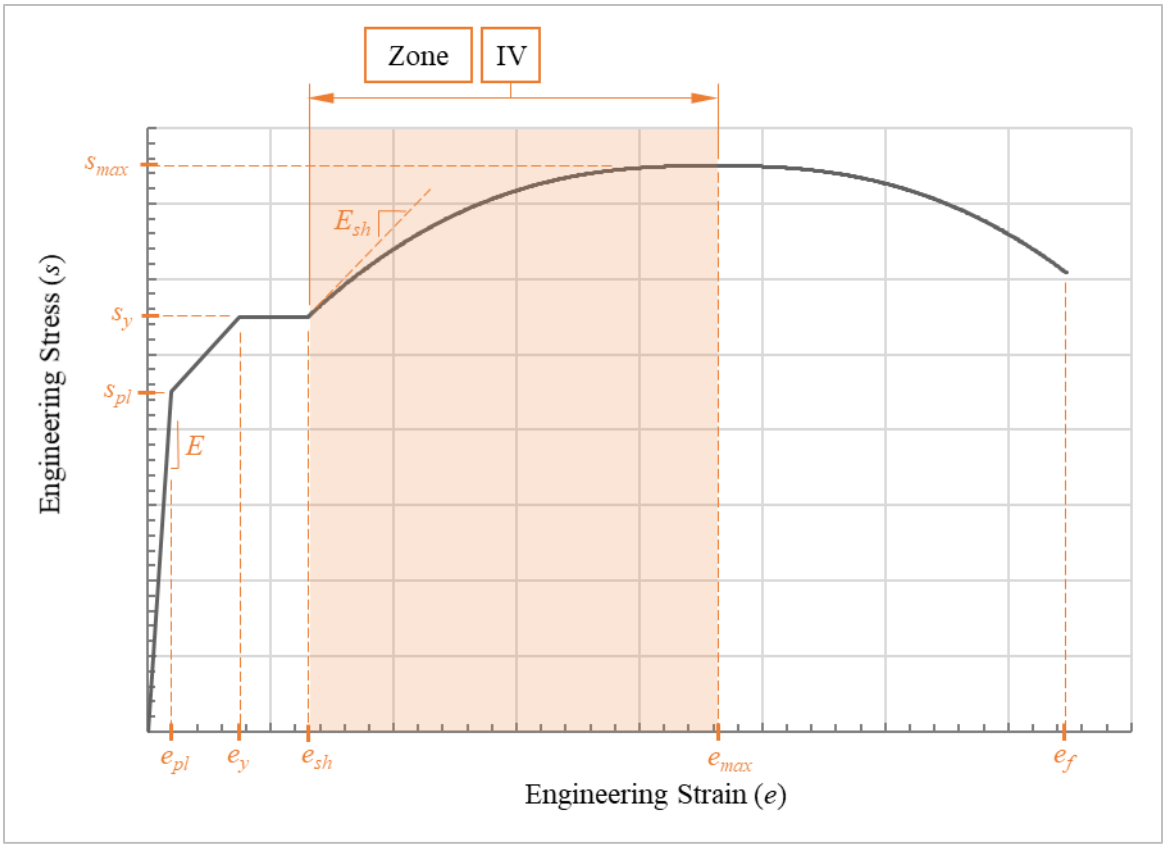

Figure 4-21: Engineering Stress-Strain Relationship – Zone IV

As described in Section 3.2, the onset of necking is characterized by zero slope in the engineering stress-strain relationship. This point is also defined by a true stress-strain function that is equal in value to its first derivative at the onset of necking, a relationship often referred to as Considère's Construction, discussed in Sections 2.8.2 and 3.2. Therefore, unlike previous zones, Zone IV is constrained in both the value of stress and strain, and the slope at both its beginning and end, making it functional fitting more

challenging than for previous zones. In addition, the derivative rules must also be followed to accurately predict necking (already guaranteed by slope constraint), maintain numerical stability, and avoid prediction of cold-drawing behavior. Thus, the first derivative of the function chosen to fit Zone IV should be positive, and the second derivative should always be negative over the range of this zone. Given the different constraints on this function, it is generally the hardest of the pre-necking zones to accurately fit with common linear, quadratic, exponential and/or logarithm functions. The constraints on this zone are discussed in additional detail in Sections 4.3.4.1 and 4.3.4.2.

4.3.4.1 Initial Slope Constraint for Zone IV

The stiffening response that occurs at the onset of strain-hardening represents the beginning of Zone IV, the strain-hardening branch, discussed in Section 4.3.4. For materials that exhibit Zone III behavior, or a yield plateau, this transition typically occurs in an abrupt manner where the stress-strain relationship transitions from zero slope within the yield plateau to the strain hardening modulus of elasticity, E_{sh}. Therefore, the relationship defined for Zone IV will be constrained by the values of true stress and strain at the onset of strain hardening, σ_{sh} and ε_{sh}, ensuring functional continuity. Because the slope changes abruptly, continuity of the first derivative is not required. However, an attempt should be made to capture the initial strain hardening modulus accurately, creating an additional constraint on the initial conditions of the functional relationship used in Zone IV. Materials that do not exhibit a distinct yield plateau are discussed in Section 4.3.3.3.

To capture the initial slope in Zone IV, a relationship for the true strain hardening modulus, herein referred to as $E_{sh\text{-}true}$, must be established based on the measurable engineering strain hardening modulus, E_{sh}. To develop this relationship, consider the simple definition of E_{sh} presented in Equation 4-22, where δs and δe are used to define an arbitrary small change in engineering stress and strain occurring at the onset of strain

hardening, where the stress-strain relationship is essentially linear with slope equal to E_{sh}. The relationship for $E_{sh\text{-}true}$ can be defined using these terms as shown in Equation 4-23.

$$E_{sh} = \frac{\delta s}{\delta e} = \frac{E_{sh}\delta e}{\delta e} \qquad \text{Equation 4-22}$$

$$E_{sh-true} = \frac{\delta \sigma}{\delta \varepsilon} = \frac{(\sigma_{sh} + \delta\sigma) - \sigma_{sh}}{(\varepsilon_{sh} + \delta\varepsilon) - \varepsilon_{sh}} \qquad \text{Equation 4-23}$$

Expanding the terms in the numerator and denominator, factoring, and simplifying yields Equation 4-24. Further simplification and elimination of the δs term by replacing it with $E_{sh}\delta e$, which is valid for small values of δe and inherent in the original definition of δs and δe, yields Equation 4-25.

$$E_{sh-true} = \frac{\delta s(1 + e_{sh}) + \delta e(s_{sh} + \delta s)}{\ln\left(1 + \frac{\delta e}{1 + e_{sh}}\right)} \qquad \text{Equation 4-24}$$

$$E_{sh-true} = \frac{\delta e(E_{sh} + E_{sh}e_{sh} + s_{sh}) + E_{sh}\delta e^2}{\ln\left(1 + \frac{\delta e}{1 + e_{sh}}\right)} \qquad \text{Equation 4-25}$$

Finally, to determine the true strain hardening modulus, $E_{sh\text{-}true}$, an instantaneous representation of the slope of the true stress-strain relationship at the onset of strain-hardening, consider the case where the strain increment used to define these terms, δe, approaches zero. This can be captured by taking the limit, as shown in Equation 4-26.

$$E_{sh-true} = \lim_{\delta e \to 0} \frac{\delta e(E_{sh} + E_{sh}e_{sh} + s_{sh}) + E_{sh}\delta e^2}{\ln\left(1 + \frac{\delta e}{1 + e_{sh}}\right)} \qquad \text{Equation 4-26}$$

By inspection, the numerator and denominator of this limit each approach zero as δe approaches zero. Thus, the limit cannot be taken directly. To address this issue, consider the application of L'Hôpital's rule and restate the limit as shown in Equation 4-27, the general form used to represent L'Hôpital's rule. In this case, the numerator is replaced by function $f(x)$, and the denominator by function $g(x)$. Similarly, strain incremented δe is replaced by x, and the constant, zero, that this strain increment approaches is replaced by general constant, C_1.

$$\lim_{\delta e \to 0} \frac{\delta e(E_{sh} + E_{sh} e_{sh} + s_{sh}) + E_{sh} \delta e^2}{\ln\left(1 + \frac{\delta e}{1 + e_{sh}}\right)} = \lim_{x \to C_1} \frac{f(x)}{g(x)} \qquad \text{Equation 4-27}$$

For this case, L'Hôpital's rule requires three conditions to be met. The first and second conditions are shown in Equation 4-28 and Equation 4-29, respectively, where the numerator and denominator functions, $f(x)$ and $g(x)$, respectively, must each approach zero as x approaches constant, C_1. The final condition requires that both functions, $f(x)$ and $g(x)$, are differentiable and the limit of their ratio equal to some non-infinite, non-zero constant, here C_2, as shown in Equation 4-30. If each of these conditions is satisfied, L'Hôpital's rule states that the limit of the ratio of the functions is equal to the limit of the ratio of their first derivatives, as shown in Equation 4-31.

$$\lim_{x \to C_1} f(x) = 0 \qquad \text{Equation 4-28}$$

$$\lim_{x \to C_1} g(x) = 0 \qquad \text{Equation 4-29}$$

$$\lim_{x \to C_1} \frac{f'(x)}{g'(x)} = C_2 \qquad \text{Equation 4-30}$$

$$\lim_{x \to C_1} \frac{f(x)}{g(x)} = \lim_{x \to C_1} \frac{f'(x)}{g'(x)} \qquad \text{Equation 4-31}$$

The derivatives of the numerator functions are provided in Equation 4-32 and Equation 4-33. Similarly, Equation 4-34 and Equation 4-35 provide the derivative of the denominator. The limit as the engineering strain increment, δe, approaches zero is shown in Equation 4-36. Note that the limits of these derivatives are finite; therefore, all conditions for application of L'Hôpital's rule are met. Thus, the slope of the true stress-strain relationship at the onset of strain-hardening, $E_{sh\text{-}true}$, can be determined as shown in Equation 4-37.

$$f'(x) = \frac{d}{d(\delta e)}(\delta e(E_{sh} + E_{sh}e_{sh} + s_{sh}) + E_{sh}\delta e^2) \qquad \text{Equation 4-32}$$

$$f'(x) = E_{sh} + E_{sh}e_{sh} + s_{sh} + 2E_{sh}\delta e \qquad \text{Equation 4-33}$$

$$g'(x) = \frac{d}{d(\delta e)}\left(\ln\left(1 + \frac{\delta e}{1 + e_{sh}}\right)\right) \qquad \text{Equation 4-34}$$

$$g'(x) = \frac{1}{1 + e_{sh} + \delta e} \qquad \text{Equation 4-35}$$

$$E_{sh-true} = \lim_{x \to C_1} \frac{f'(x)}{g'(x)} = \lim_{\delta e \to 0} \frac{E_{sh} + E_{sh}e_{sh} + s_{sh} + 2E_{sh}\delta e}{1/(1 + e_{sh} + \delta e)} \qquad \text{Equation 4-36}$$

$$E_{sh-true} = (E_{sh} + E_{sh}e_{sh} + s_{sh})(1 + e_{sh}) \qquad \text{Equation 4-37}$$

Thus, when defining the constraints for the functional fit to Zone IV, the true strain hardening modulus, $E_{sh\text{-}true}$, can be defined directly from known properties of the engineering stress-strain relationship determined from testing.

To verify the derived relationship in Equation 4-37, consider it in the generalized form shown in Equation 4-38, where the "*x*" subscript denotes any generalized location on the engineering stress-strain relationship. Given the assumptions made when determining this relationship, it should remain valid for any point on the true stress-strain relationship prior to necking where the standard analytical relationship between engineering and true stress and strain (see Equation 4-1 and Equation 4-2) holds true. Therefore, this generalized relationship can be evaluated to confirm that it is appropriate and accurate.

$$E_{x-true} = (E_x + E_x e_x + s_x)(1 + e_x) \qquad \text{Equation 4-38}$$

To illustrate, consider the case at the onset of necking. The assumptions of uniform stress and strain in the reduced section of the tension coupon remain valid, so the same derivation could be applied to develop the relationship shown in Equation 4-39. Simplifying, recall that at the onset of necking the slope of the engineering stress-strain relationship is equal to zero. Replacing E_{max} with zero and simplifying yields Equation 4-40, which, as shown and per the standard analytical conversion shown in Equation 4-1, reconfirms that at the onset of necking the slope of the true stress-strain relationship, $E_{max\text{-}true}$, is equal to the true stress at the onset of necking, σ_{max}. This observation, often referred to as Considère's Construction, is introduced in Sections 2.8.2 and discussed in detail in Section 3.2.

$$E_{max\ -true} = (E_{max} + E_{max}\, e_{max} + s_{max})(1 + e_{max}) \qquad \text{Equation 4-39}$$

$$E_{max\,-true} = s_{max}\,(1 + e_{max}) = \sigma_{max} \qquad \text{Equation 4-40}$$

4.3.4.2 Transition Constraints between Zones IV - V: Onset of Necking

The transition between Zones IV and V occurs at the onset of necking, which is defined as the point of maximum stress in the engineering stress-strain relationship. Per Considère's Construction and the first derivative rule, the true stress-strain function must be equal to its first derivative at the onset of necking, as detailed in Section 3.2. Therefore, the functional relationship used to capture the true stress-strain response in Zone IV will be constrained at the end of the zone.

Therefore, as described in Sections 4.3.3.2, 4.3.4, and 4.3.4.2, the functional relationship for the true stress and strain relationship in Zone IV is constrained in four ways: (1) the stress and strain at the beginning must be equal to the final stress and strain from the previous Zone, σ_{sh} and ε_{sh}, (2) the initial slope of the true stress-strain function must be equal to the true strain hardening modulus, $E_{sh\text{-}true}$, (3) the final stress and strain must be equal to the values determined using the standard conversions at the onset of necking, σ_{max} and ε_{max}, and (4) the final slope must be equal to the true stress at necking, σ_{max}, in accordance with Considère's construction. In addition, the derivative rules, particularly Derivative Rules #2 and #3 must also be met. With these constraints, a closed-formed functional solution that adequately captures the behavior in this zone is oftentimes difficult to develop, as discussed in Section 4.3.4.3.

4.3.4.3 True Stress-Strain Data for Numerical Analysis – Zone IV

Realistically, addressing the six constraints required to define a functional fit in Zone IV can be challenging, particularly as simple functional forms such as quadratic, power and natural logarithm, often fail to precisely match the data. Higher order

polynomials (third order and higher) are not recommended as they tend to reverse curvature one or more times, violating Derivative Rule #3. Additionally, while they may fit the boundaries, they generally do a poor job of approximating the relationship between these end points due to one or more reversals in curvature

Typically, the simplest way of defining the true stress-strain relationship for Zone IV is to define the relationship as a multi-point piece-wise linear dataset where the standard conversions in Equation 4-1 and Equation 4-2 are used to directly convert the engineering stress-strain data to true stress-strain data at regular intervals. Next, the piece-wise linear data developed using the standard conversions can be modified to ensure the initial and final points satisfy the necessary constraints on stress, strain, and slope. Modification should generally be minimal because the standard conversion remains valid within Zone IV. Finally, the dataset should be checked and adjusted, as appropriate, to ensure the derivative rules of Chapter 3 have been met. Thus, as was the case for Zones I, II, and III, the true stress-strain relationship in Zone IV can be fully defined through careful application of the standard analytical engineering to true conversions, as shown in Figure 4-22.

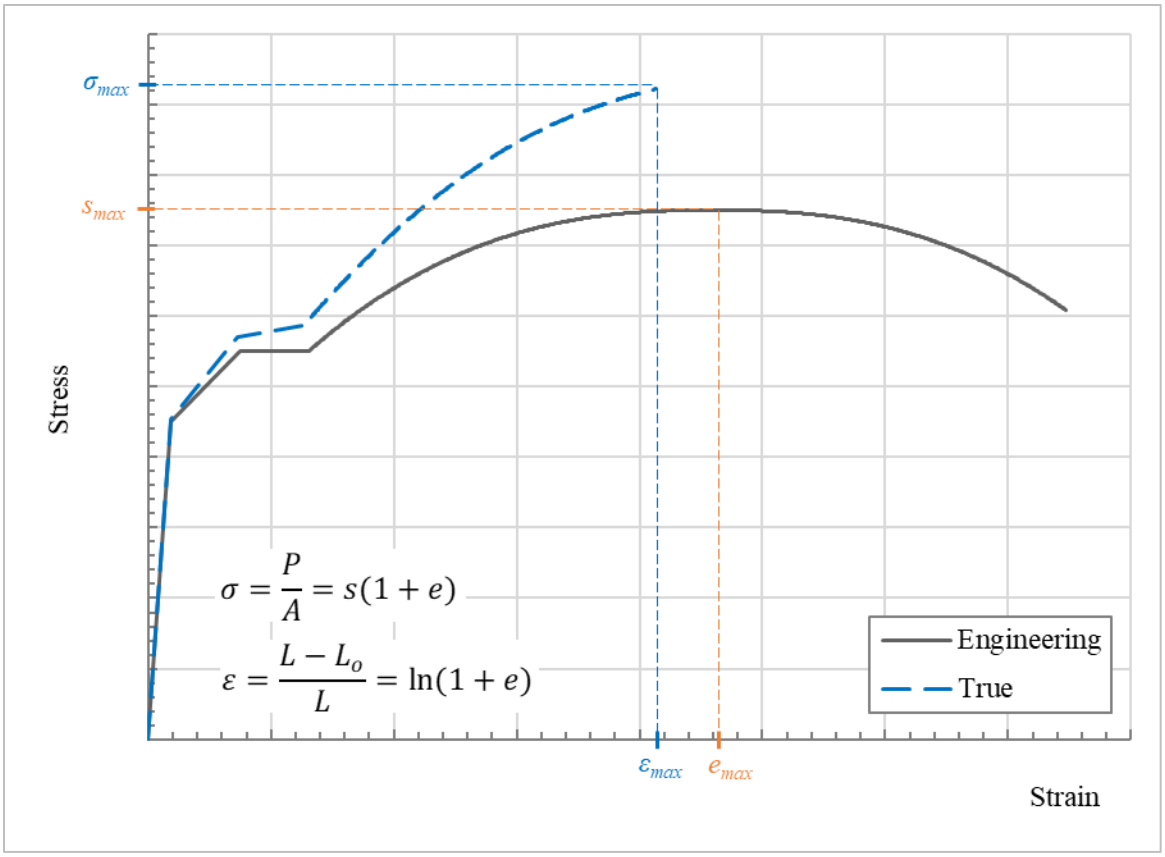

Figure 4-22: Standard Analytical Conversion to True Stress-Strain up to Necking

While often impractical, functional fits can be used in Zone IV. For example, a cubic curve taking the form shown in Equation 4-41 having four constants, C_i, can be used to meet all necessary end constraints. As shown in Equation 4-42 through Equation 4-45, the constants for the cubic function in Equation 4-41 can be determined such that the stress, strain, and slope constraints at the beginning and end of Zone IV are met. Note, however, that the function must still be evaluated with respect to the derivative rules. The first derivative, shown in Equation 4-46, is not guaranteed by the end constraints to be to be greater than zero throughout Zone IV. Similarly, the second derivative, shown in Equation 4-47, is not guaranteed by the end constraints to be to be less than or equal to zero throughout Zone IV. Therefore, care should be taken when applying this functional

relationship to verify that the derivative rules, particularly Derivative Rules #2 and #3 (because Rule #1 is captured by the end constraints), are obeyed through the entire domain of Zone IV, especially when third order (i.e., cubic) and higher order polynomials are used, as mentioned previously.

$\boxed{\text{IV}}\ \varepsilon_{sh} < \varepsilon < \varepsilon_{max}$

$$\sigma(\varepsilon) = C_1(\varepsilon - \varepsilon_{sh})^3 + C_2(\varepsilon - \varepsilon_{sh})^2 + C_3(\varepsilon - \varepsilon_{sh}) + C_4 \quad \text{Equation 4-41}$$

$$C_1 = -\frac{E_{sh-true} - \sigma_{max} + 2C_2(\varepsilon_{max} - \varepsilon_{sh})}{3(\varepsilon_{max} - \varepsilon_{sh})^2} \quad \text{Equation 4-42}$$

$$C_2 = \frac{3(\sigma_{max} - \sigma_{sh})}{(\varepsilon_{max} - \varepsilon_{sh})^2} - \frac{2E_{sh-true} + \sigma_{max}}{\varepsilon_{max} - \varepsilon_{sh}} \quad \text{Equation 4-43}$$

$$C_3 = E_{sh-true} \quad \text{Equation 4-44}$$

$$C_4 = \sigma_{sh} \quad \text{Equation 4-45}$$

$$\sigma'(\varepsilon) = 3C_1(\varepsilon - \varepsilon_{sh})^2 + 2C_2(\varepsilon - \varepsilon_{sh}) + C_3 \quad \text{Equation 4-46}$$

$$\sigma''(\varepsilon) = 6C_1(\varepsilon - \varepsilon_{sh}) + 2C_2 \quad \text{Equation 4-47}$$

Instead of evaluating the first and second derivatives directly, the piece-wise data can be plotted for rapid visual examination to identify possible points where the slope is zero or negative or the curvature reverses. An example plot is provided in Figure 4-23 using true stress-strain data developed using the standard analytical conversions from engineering stress-strain data derived from a standard steel coupon tension test. Note the

poor fit, as well as the possible flat or negative slope and reversal in curvature toward the end of Zone IV. This example reinforces the value of visualizing dataset to ensure it accurately captures the desired trends, as an accurate fit is not guaranteed by precise fit of the end constraints.

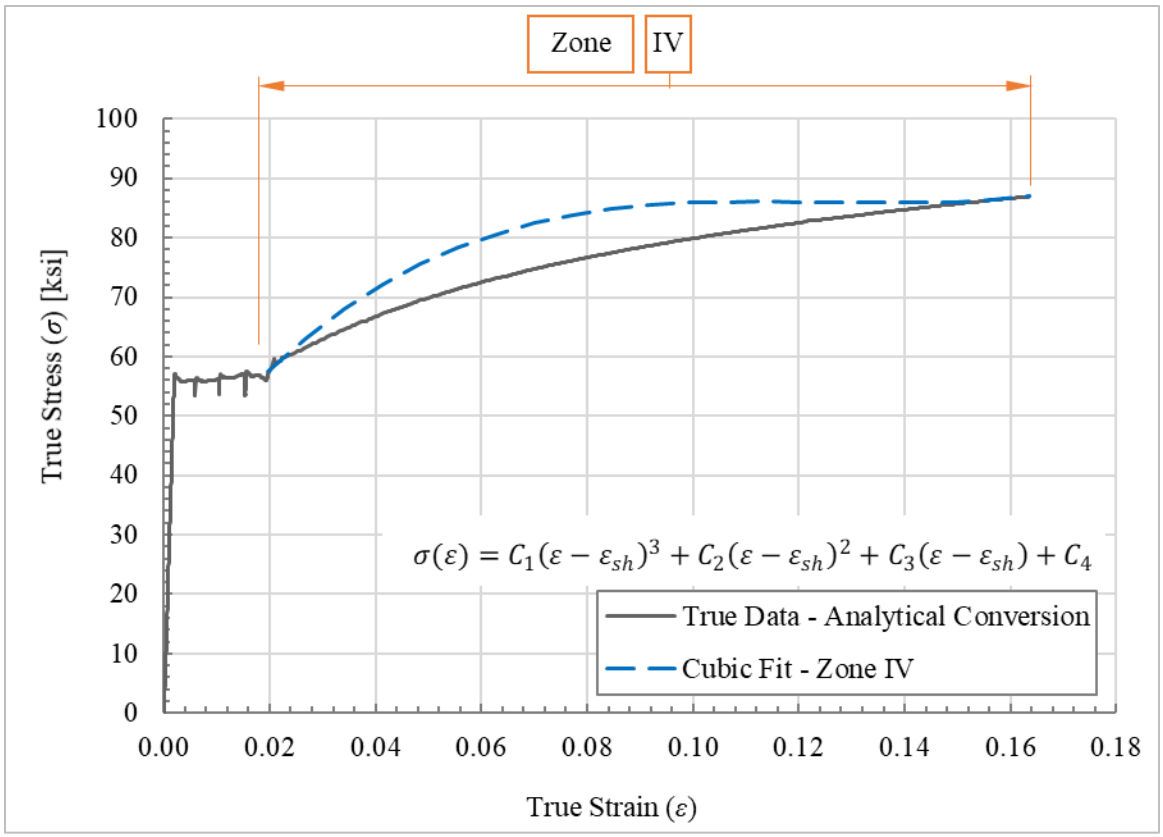

Figure 4-23: Example Cubic Fit to True Stress-Strain Data in Zone IV

After visual examination, the piece-wise data should be more rigorously reviewed by performing the following two checks. First, the data should be checked to ensure that true stresses increase with increasing strain, as summarized in Equation 4-48. This will ensure Derivative Rule #2 is obeyed. Second, the data should be checked to ensure that rate at which stress changes is either constant or decreasing, as summarized in Equation

4-49. This will ensure that Derivative Rule #3 is obeyed. These derivative rule checks can be applied to piece-wise defined data used in other zones, as well.

$$\sigma_{i+1} > \sigma_i \qquad \text{Equation 4-48}$$

$$\frac{\sigma_{i+1} - \sigma_i}{\varepsilon_{i+1} - \varepsilon_i} \leq \frac{\sigma_{i+2} - \sigma_{i+1}}{\varepsilon_{i+2} - \varepsilon_2} \qquad \text{Equation 4-49}$$

The data in Zone IV can also be approximated using a combined linear and exponential fit, taking the form shown in Equation 4-50. Exponential fits are often used to approximate true stress-strain response of ductile metals like structural steel, and the addition of a linear term provides the necessary number of constants to capture the initial and final value and slopes constraints in Zone IV (i.e., the zone boundary constraints). Thus, like the cubic fit, there are four constants, C_i. These constants were determined for the known end constraints and are reported in Equation 4-51 through Equation 4-54. The first and second derivatives are presented in Equation 4-55 and Equation 4-56, respectively. These can be initially checked visually, and then more rigorously through evaluation of the first and second derivative functions or through using Equation 4-48 and Equation 4-49 where piece-wise data are used. . An example plot of the calculated fit to the same data shown in Figure 4-23 is provided in Figure 4-24. Note the fit is considerably improved; however, this improvement should not be assumed to be the case for all datasets.

IV $\varepsilon_{sh} < \varepsilon < \varepsilon_{max}$ $\qquad \sigma(\varepsilon) = C_1(\varepsilon - \varepsilon_{sh})^{C_2} + C_3(\varepsilon - \varepsilon_{sh}) + C_4$ Equation 4-50

$$C_1 = \frac{\sigma_{max} - E_{sh-true}}{C_2(\varepsilon_{max} - \varepsilon_{sh})^{C_2 - 1}} \qquad \text{Equation 4-51}$$

$$C_2 = \frac{\sigma_{max} - E_{sh-true}}{\frac{\sigma_{max} - \sigma_{sh}}{\varepsilon_{max} - \varepsilon_{sh}} - E_{sh-true}} \quad \text{Equation 4-52}$$

$$C_3 = E_{sh-true} \quad \text{Equation 4-53}$$

$$C_4 = \sigma_{sh} \quad \text{Equation 4-54}$$

$$\sigma'(\varepsilon) = C_1 C_2 (\varepsilon - \varepsilon_{sh})^{C_2 - 1} + C_3 \quad \text{Equation 4-55}$$

$$\sigma''(\varepsilon) = C_1 C_2 (C_2 - 1)(\varepsilon - \varepsilon_{sh})^{C_2 - 2} \quad \text{Equation 4-56}$$

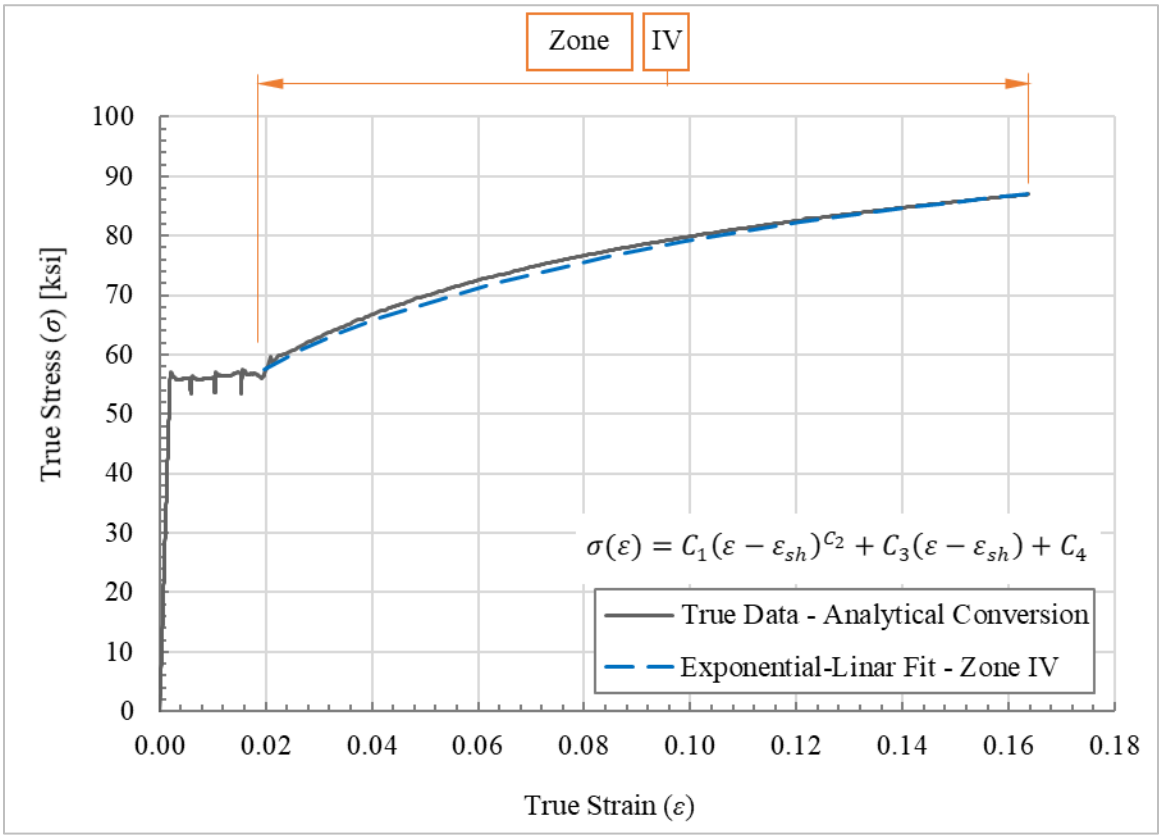

Figure 4-24: Example Exponential-Linear Fit to True Stress-Strain Data in Zone IV

Depending on the application, the approximation of Zone IV data shown in Figure 4-24 may or may not be adequate. Another alternative functional approach is to use a computer software generated fit. For example, Microsoft Excel can be used to generate curve fits to the data in Zone IV. However, this method requires consideration of the boundary values, slopes, and derivative rules to ensure that everything is adequately captured. Thus, an automated curve fit can be used to generate data that can be then manipulated to ensure the necessary constraints are captured. This process is illustrated in the example in Section 5.3. Refer to this section for additional information and discussion of computer-generated data fits for the strain-hardening material true stress-strain relationship in Zone IV.

4.3.5 Zone V: Strain Softening Branch

Zone V, highlighted in Figure 4-25, is the final portion of the engineering stress-strain response for structural steels in tension, and is commonly referred to as the strain-softening branch. The onset of necking, which constitutes the initial portion of this zone, is the bifurcation point separating the stable and uniform deformations observed at strains prior to necking from the non-uniform behavior where subsequent deformations are concentrated within the neck at strains beyond this point. Zone V ends with tension failure (i.e., tension rupture) of the coupon.

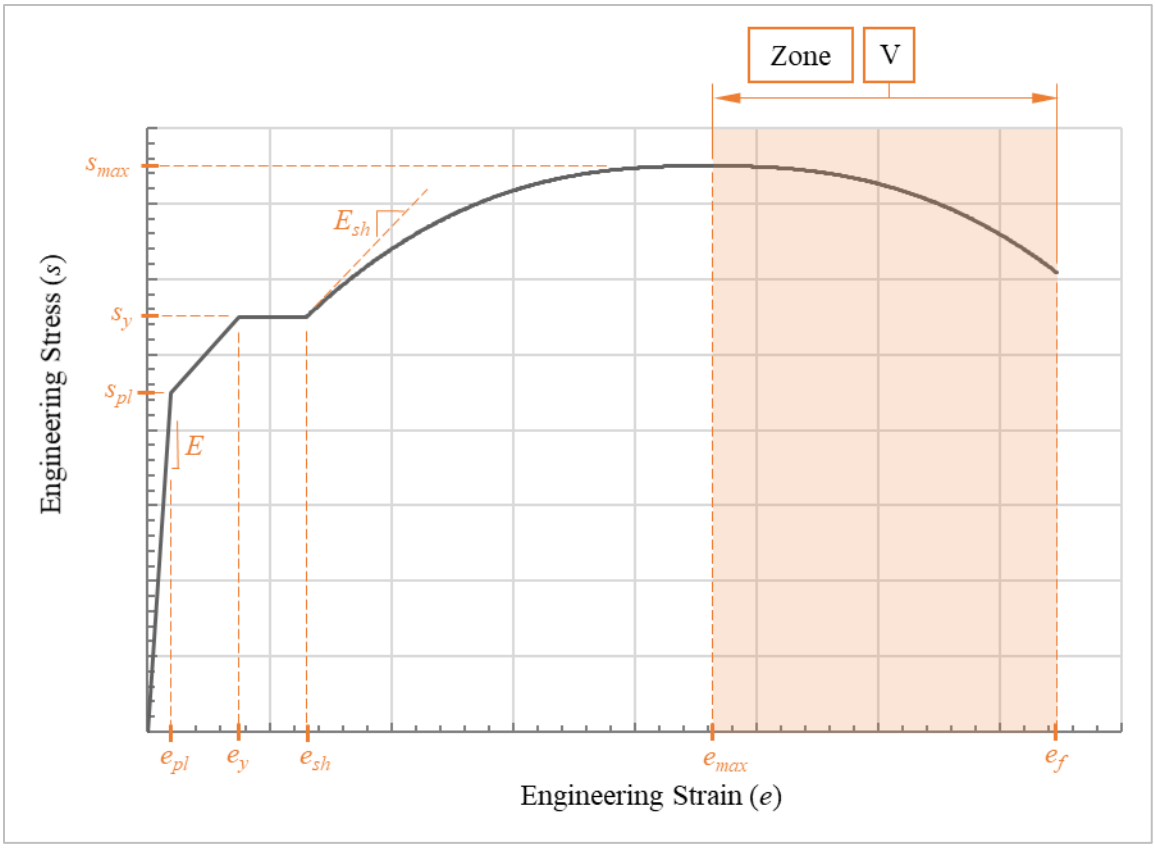

Figure 4-25: Engineering Stress-Strain Relationship – Zone V

Prior to the onset of necking, stresses and strains in the reduced section of the coupon are essentially uniform, permitting the use of the standard analytical conversion of engineering to true stress and strain using Equation 4-1 and Equation 4-2. Beyond this point, these conversions no longer apply due to the localized stresses, strains, and deformation within the neck. Therefore, the standard analytical conversions cannot be used in Zone V. With the onset of necking comes a decrease in engineering stress. This process continues, with additional localized deformation in the neck, and reduced strength and stiffness of the coupon until the coupon ultimately fails in tension. Failure typically occurs through a relatively rapid rupture through the smallest cross-section at the center of the neck. Because the standard analytical conversion equations for engineering to true stress

and strain no longer apply, a different approach must be taken to determine the true stress-strain relationship in this zone.

4.3.5.1 Constraints in Zone V

Like previous zones, functional continuity is required in transitioning to Zone V. This means the stress and strain at the beginning of Zone V must be equal to the stress and strain at the end of Zone IV; specifically, σ_{max} and ε_{max}. In addition, at the beginning of Zone V, per Considère's Construction (Derivative Rule #1), the first derivative, should be equal to the $E_{max\text{-}true}$ or σ_{max}. Although, a slope less than this value is also acceptable given that the constraints in Zone IV will ensure Derivative Rule #1 is met so long as the slope of the true stress-strain relationship does not increase (violating Derivative Rule #3), as would be a common occurrence when using piece-wise data to define the relationship. As before, Derivative Rules #2 and #3 must also be considered and obeyed throughout Zone V. As such, care should be taken to ensure that extrapolation of the material stress-strain relationship performed by a given computational analysis software (e.g., for strains beyond those explicitly defined by the user in the material model) continues to obey the derivative rules.

Because the analytical relationships for conversion of engineering stress and strain to true values shown in Equation 4-1 and Equation 4-2 can no longer be applied, an alternate method must be used to determine the relationship in Zone V, as described in the following sections. To provide additional background, the following sections also provide a discussion of research. Section 4.3.5.2 discusses approaches recommended for determining the post-necking true stress-strain relationship for computational analysis. Section 4.3.5.3, summarizes proposed upper and lower bounds for the post-necking true stress-strain relationship. Section 4.3.5.4 summarizes an iterative technique for rapidly determining the post-necking true stress-strain relationship. Finally, Section 4.3.5.5

provides additional guidance and discussion related to refinement of the post-necking true stress-strain relationship, presenting a final example of the possible level of precision and accuracy that can be achieved using this approach.

4.3.5.2 Research Related to Determining the Post-Necking True Stress-Strain Relationship

Current published research includes several different approaches to determining the post-necking true stress-strain relationship for ductile metals in tension. While there have been a wide range and variety of approaches, they generally fall into two general categories: (1) analytically developed correction to the standard conversion (i.e., Equation 4-1 and Equation 4-2), and (2) error minimizing iterative techniques. This section includes a brief summary of research relevant to each of these general topics, including discussions of relevant findings and observations.

Because the assumption of uniform stress and strain in the reduced section of the tension coupon no longer applies, the post-necking stress-strain relationship becomes increasingly complex. Attempts have been made by several researchers to develop a close-formed analytical post-necking relationship including Bridgman (Bridgman, 1952), Needleman (Needleman, 1972), Tvergaard (Tvergaard, Needleman, & Lo, 1981), and Ling (Ling, 1996), among others. These post-necking analytical relationships often rely on difficult to measure properties of the coupon specimen (e.g., radius of the neck) and are impractical to apply for most cases due to such complex experimental measurement requirements. Finally, where only standard test data or book values are available, they cannot be used without assuming values for these missing measurements, introducing additional variability and uncertainty. For additional information on these correction factor approaches, refer to the discussion in Section 2.9.1.

More recently, with advances in computational methods, computing speed, and computer power, research has shifted toward the use of iterative techniques to determine the post-necking true stress-train relationship. These studies can be divided generally into two basic approaches: (1) bounded iterative fitting, and (2) iterative fitting through error minimizing. In bounded iterative fitting, upper and lower bounds are defined for the post-necking true stress-strain relationship, and these bounds are combined using a weighting function to approximate the Zone V relationship. Fitting through error minimization refers to the use of iterative techniques, often using FEA models that seek to minimize error between a model and test data. Recent research using these techniques to determine the post-necking true stress-strain relationship is discussed in the following paragraphs.

Bounded iterative fitting leverages and manipulates defined boundaries to develop possible fits. These techniques are often iterative, in that either multiple solutions are analyzed together or sequentially to develop a best fit to the post-necking data. Bounds to post-necking behavior are rarely referenced in existing research; however, Ling (Ling, 1996), Joun et al. (Joun, Choi, Eom, & Lee, 2007), and Arasaratnam et al. (Arasaratnam, Sivakumaran, & Tait, 2011) each recommend a lower bound as the power law fit defined to capture the strain at necking, as shown in Equation 4-57, and derived previously in Section 3.2.3. A limitation of this work is that these researchers do not provide any analytical, theoretical, or other physics-based justification for the choice of this lower bound. However, Ling attributes it to the observation that in log-space, the power law function tends to underestimate the relationship, (see Figure 4-26), Joun attributes it to general observation, and Arasaratnam cites work by Ling for this proposed lower bound. In effect, each of these justifications is based essentially in observation, lending little weight to their wide use.

$$\sigma = C_1 \varepsilon^{\varepsilon_{max}}$$ Equation 4-57

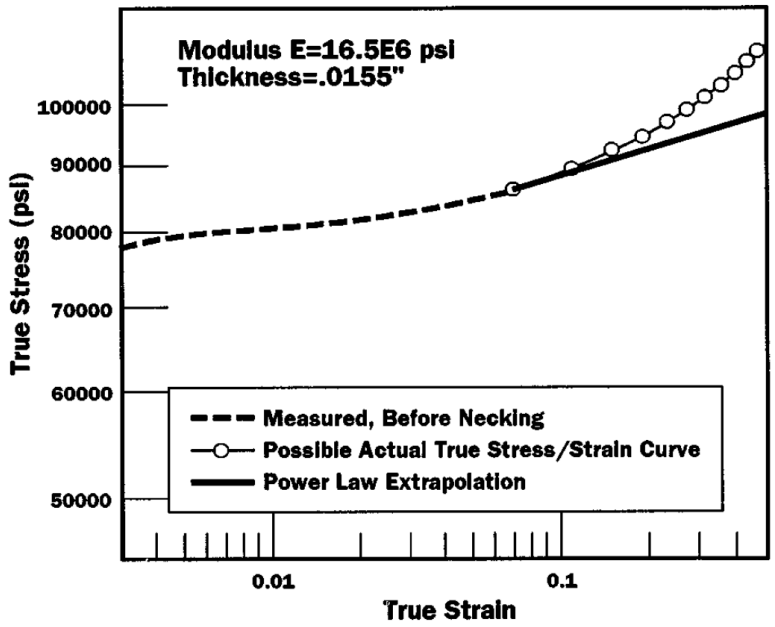

Figure 4-26: Log-log Plot of True Stress-Strain Relationship showing Underestimation of Actual Relationship using Power Law Fit (Ling, 1996)

In addition, Ling (Ling, 1996), Joun (Joun, Choi, Eom, & Lee, 2007), and Arasaratnam (Arasaratnam, Sivakumaran, & Tait, 2011) each cite a linear relationship with slope defined using Considère's Construction (Derivative Rule #1) as the upper bound to the post-necking true stress-strain relationship. As before, this proposed upper bound is generally attributed to observation. However, there is, in fact, a theoretical basis for this linear upper bound to the true stress-strain relationship; the derivative rules of Chapter 3. Specifically, given the known slope at the beginning of the post-necking regime (Zone V) dictated by Derivative Rule #1 and Considère's Construction, considered with the stability and drawing requirements of Derivative Rules #2 and #3, the only possible behavior in Zone V is a decreasing positive slope. Thus, an unchanging positive slope, defined by a

line with slope equal to $E_{max\text{-}true}$ or σ_{max} is a natural upper bound to the behavior in Zone V. In fact, after the onset of strain hardening (i.e., within Zone IV and V) per the derivative rules, any line tangent at a given point could be viewed as the upper bound for a behavior occurring at strains beyond that point. This linear upper bound is discussed in additional detail in in Section 4.3.5.3.

Ultimately, once bounds are defined by these researchers, the typical approach to determine the post-necking true stress-strain relationship is to begin by defining a generalized function that uses weighted averages and a weighting term to combine the upper- and lower-bound functions. An example of a generalized boundary weighting function is provided in Equation 4-58, where $\sigma_{UB}(\varepsilon)$ and $\sigma_{LB}(\varepsilon)$ are arbitrary upper and lower-bound functions, respectively. By appropriately weighting these bounds, in this example, choosing a weighting factor between zero and one, one or more relationships can be created that will lie somewhere between these bounds. Finally, either series or parallel iteration can be done to determine a best fit using this approach.

$\boxed{\text{V}}\ \varepsilon_{max} < \varepsilon$ $\qquad \sigma(\varepsilon) = (w)\sigma_{UB}(\varepsilon) + (1-w)\sigma_{LB}(\varepsilon)$ Equation 4-58

An alternate approach has developed recently, in large part due to increasing availability and speed of computational FEA software and the ability to use programming languages to control the pre-processing, executing, and post-processing of FEA models. This approach uses iterative error minimizing techniques applied to detailed FEA models to develop the post-necking true stress-strain relationship. As used by Zhang and Li (Zhang & Li, 1994), Joun et al. (Joun, Eom, & Lee, 2008), and Tao et al. (Tao, Zhang, & Tong, 2009), among others, the technique involves piece-wise fitting technique where the stress-strain relationship is divided incrementally by strain. Then, an arbitrary prediction is developed for each strain increment, and then the model is analyzed. If the predicted result

matches the measured relationship within a defined error range, it is accepted, and the process is repeated for the next increment of strain. This process is described in detail in Section 2.9.2. As the procedure advances, and the analytical relationship is adjusted until the entire engineering stress-strain response predicated by the FEA model matches the measured engineering data within a defined error tolerance.

For reference, data developed using this error minimizing approach presented in current published research are presented later in this section. The earliest observed use, by Zhang and Li (Zhang & Li, 1994), is shown in Figure 4-27 and Figure 4-28. Note that, even in these early efforts, the method produces a reasonably accurate approximation of the experimental data, though not without some visible error, particularly later in the post-necking response.

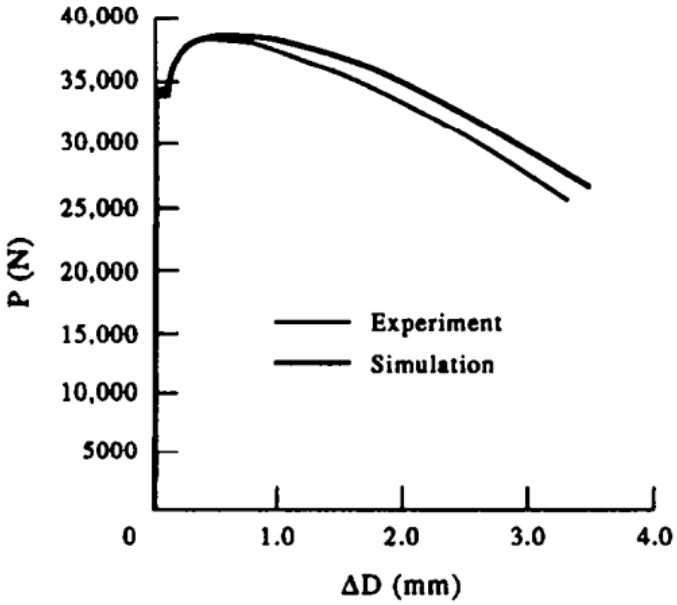

Figure 4-27: Early Results of Iterative Numerical Fitting of Post-Necking True Stress-Strain (Zhang & Li, 1994)

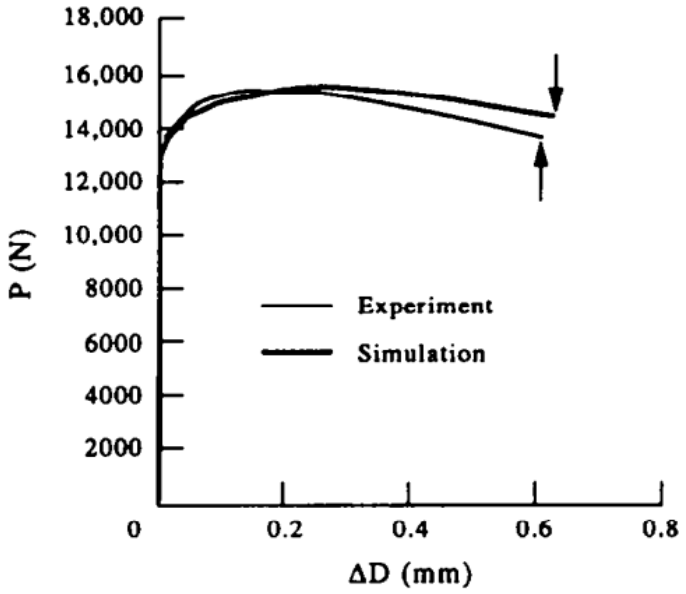

Figure 4-28: Early Results of Iterative Numerical Fitting of Post-Necking True Stress-Strain (Zhang & Li, 1994)

In contrast, later work by Joun et al. (Joun, Eom, & Lee, 2008) illustrated in Figure 4-29 and Figure 4-30 shows improvement, particularly in the later post-necking response. The progressive iteration and refinement process used to develop these final approximations is illustrated in Figure 4-31 and Figure 4-32.

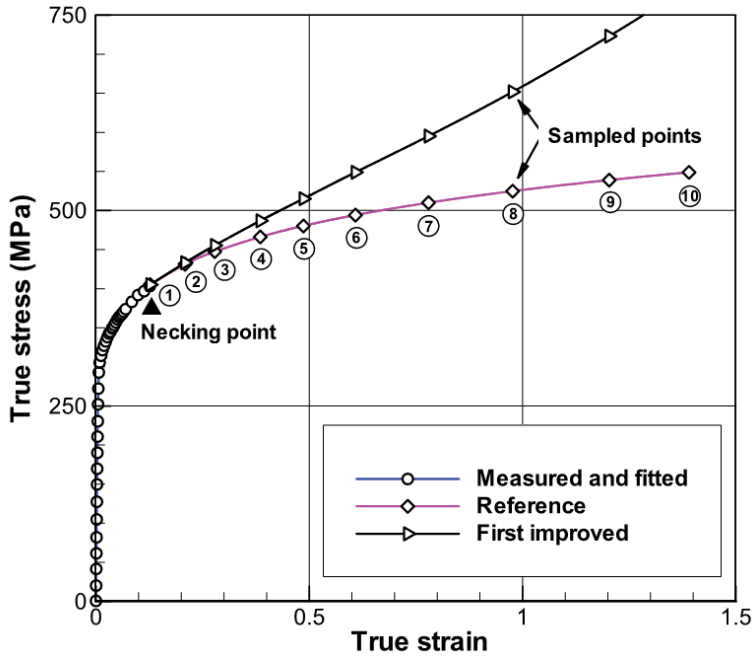

Figure 4-29: Later Results of Iterative Numerical Fitting of Post-Necking True Stress-Strain Relationship – True Stress-Strain (Joun, Eom, & Lee, 2008)

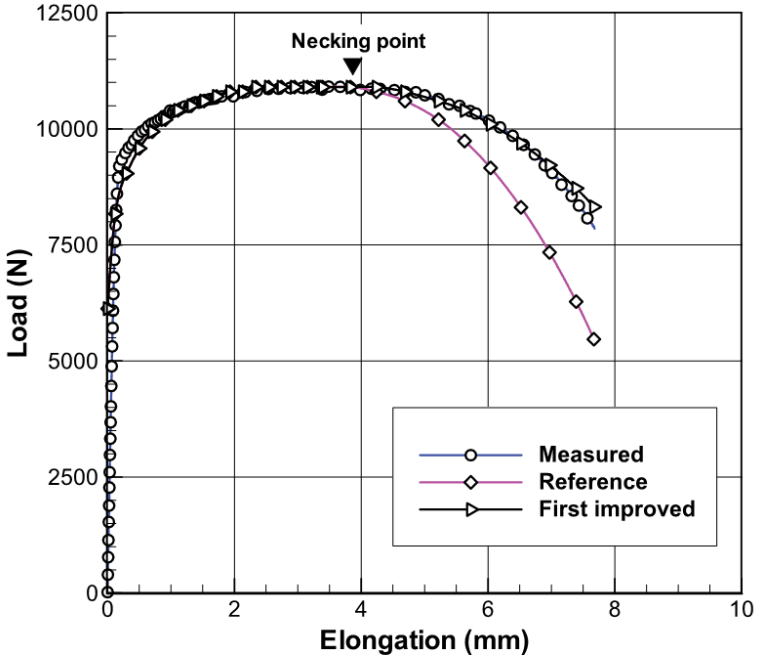

Figure 4-30: Later Results of Iterative Numerical Fitting of Post-Necking True Stress-Strain Relationship – Engineering Stress-Strain (Joun, Eom, & Lee, 2008)

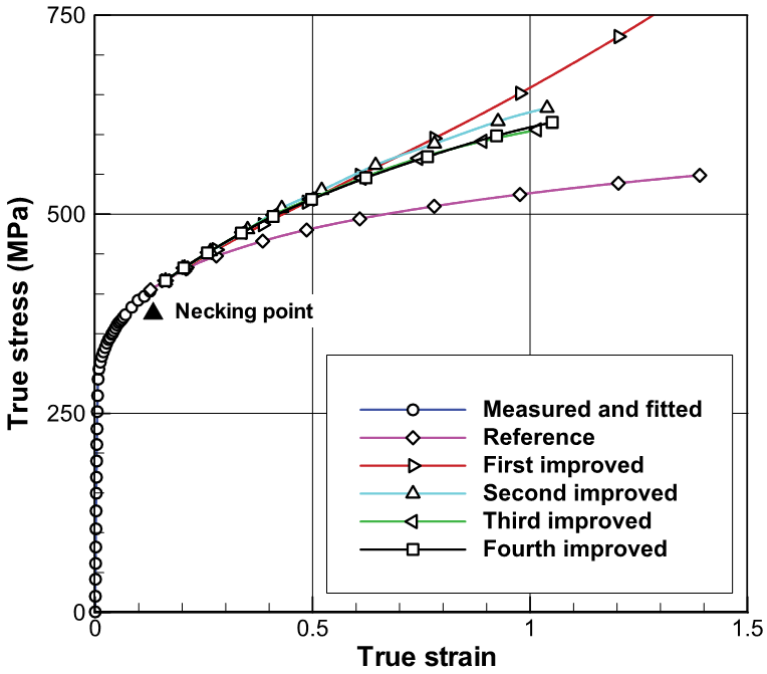

Figure 4-31: Process for Iterative Numerical Fitting of Post-Necking True Stress-Strain Relationship – True Stress-Strain (Joun, Eom, & Lee, 2008)

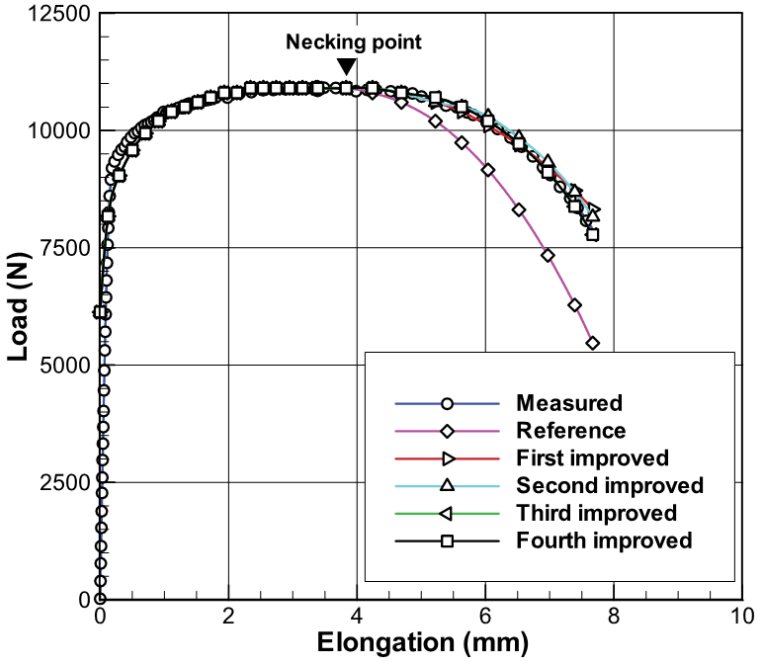

Figure 4-32: Process for Iterative Numerical Fitting of Post-Necking True Stress-Strain Relationship – Engineering Stress-Strain (Joun, Eom, & Lee, 2008)

Figure 4-33 and Figure 4-34 provide additional recent examples of iterative numerical fitting, developed by Tao et al. (Tao, Zhang, & Tong, 2009). These particular examples illustrate the relatively poor quality of fit, especially for the post-necking behavior, that can be result from using this method. While the developed fits may be reasonable for certain types of analysis, it is clear there is considerable error starting as early as the yield point and continuing through much of the post-elastic range of response. The contrast between these examples and those presented previously by Joun et al. (Joun, Eom, & Lee, 2008) demonstrates the variability in accuracy that can result from applying such an approach. As discussed later in this section, it appears Tao et al. take a relatively "brute force" automated approach to iteration, resulting in significant variation between studies.

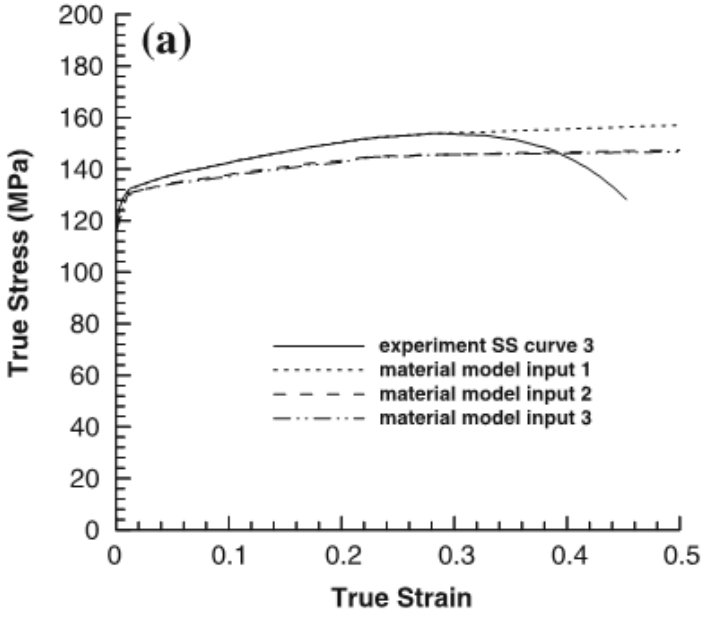

Figure 4-33: Example of Poor Iterative Numerical Fitting of Post-Necking True Stress-Strain Relationship (Tao, Zhang, & Tong, 2009)

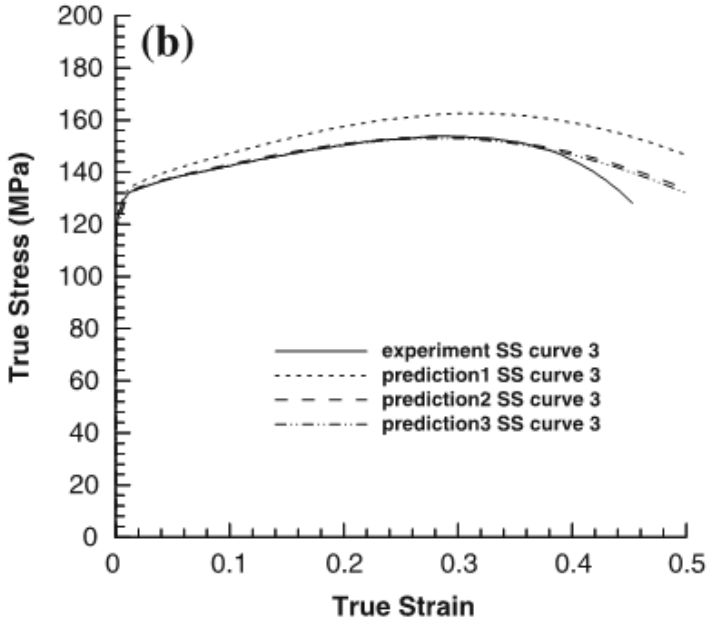

Figure 4-34: Example of Poor Iterative Numerical Fitting of Post-Necking True Stress-Strain Relationship (Tao, Zhang, & Tong, 2009)

A review of currently available and published research on iterative error minimizing to develop the post-necking true stress-strain relationship suggests this approach is typically applied in an automated "black box" manner, where few, if any, rules beyond error tolerances appear to be used to guide the iterative approach. Consequently, it is likely the process is computationally inefficient and could be improved through application of physics-based rules to the iterative technique. For example, a model may have unobserved issues including fitting noise in the data or violating some other physical law of the material considered (e.g., violating one or more of the derivative rules in Chapter 3). In addition, such a blind approach to iteration could produce a fit to the experimental data that appears visually accurate but may result in incorrect predictions or prediction of spurious behaviors when applied to other cases, particularly where stresses and strains beyond those in a uniaxial tension test are expected, requiring extrapolation of the model results. Therefore, this approach, as it is currently used in research, is not recommend.

Thus, this dissertation does not pursue this approach for several reasons, but primarily due to the unnecessary complexity it would add to the discussion and recommendations included in this research. However, the observations and rules developed herein could be applied to such an approach to more carefully guide the iterative numerical analysis fitting process, potentially improving the overall derived fit and economizing the fitting process, reducing the required number of iterations for each incremental step (or permitting the use of larger steps) by providing boundaries to potential fits. In addition, by overlaying these physical rules, there would be reduced opportunity for errors like overfitting. Therefore, integration of the findings of this research into these automated iterative error minimizing approaches is a topic for recommended future research, as discussed in Section 6.3.6.

4.3.5.3 Upper and Lower Bounds for True Stress-Strain Data in Zone V

Like Ling (Ling, 1996), Joun et al. (Joun, Choi, Eom, & Lee, 2007), and Arasaratnam et al. (Arasaratnam, Sivakumaran, & Tait, 2011), a bounded functional fit is recommended for developing the post-necking true stress-strain relationship in Zone V. As described in the following paragraphs, however, the approach to determining this relationship is slightly different than that recommended by these researchers. While arguably not ideal, especially when considering the relative ease of use and power of the error minimizing approaches, this more straight-forward boundary weighting approach was chosen primarily for its simplicity and broad applicability. It is intended to serve as a transparent and clear framework for presenting the general approach that will, ideally, allow it to be easily understood and simple to adapt to more sophisticated methods of developing the post-necking relationship (e.g., iterative error minimizing approaches).

As noted in Section 4.3.5.2, the derivative rules of Chapter 3 can be used to aid in defining the absolute upper and lower bounds for this zone. Based on these rules, the upper

bound of the post-necking response must be a linear function with slope equal to the true stress at necking. This line must be the overall upper limit because any function lying above this line would violate Derivative Rule #3, described in Section 3.4. Similarly, the absolute lower bound is captured by a horizontal line with zero slope. This limit is necessitated by Derivative Rule #2, described in Section 3.3, because any continuous function producing values below this absolute lower bound would violate the numerical stability requirements derived by Drucker (Drucker, 1959) and Hill (Hill R. , 1958). These absolute upper and lower bounds on Zone V response are provided in Equation 4-59 and Equation 4-60, respectively, and illustrated graphically in Figure 4-35. Note that the exponential pre-necking fit recommended as a lower bound by others (see Section 4.3.5.2) lies between these bounds recommended in this research.

$\boxed{\text{V}}\ \varepsilon_{max} < \varepsilon$ $\qquad \sigma_{UB}(\varepsilon) = \sigma_{max}\,(\varepsilon - \varepsilon_{max}\,)$ Equation 4-59

$\boxed{\text{V}}\ \varepsilon_{max} < \varepsilon$ $\qquad \sigma_{LB}(\varepsilon) = \sigma_{max}$ Equation 4-60

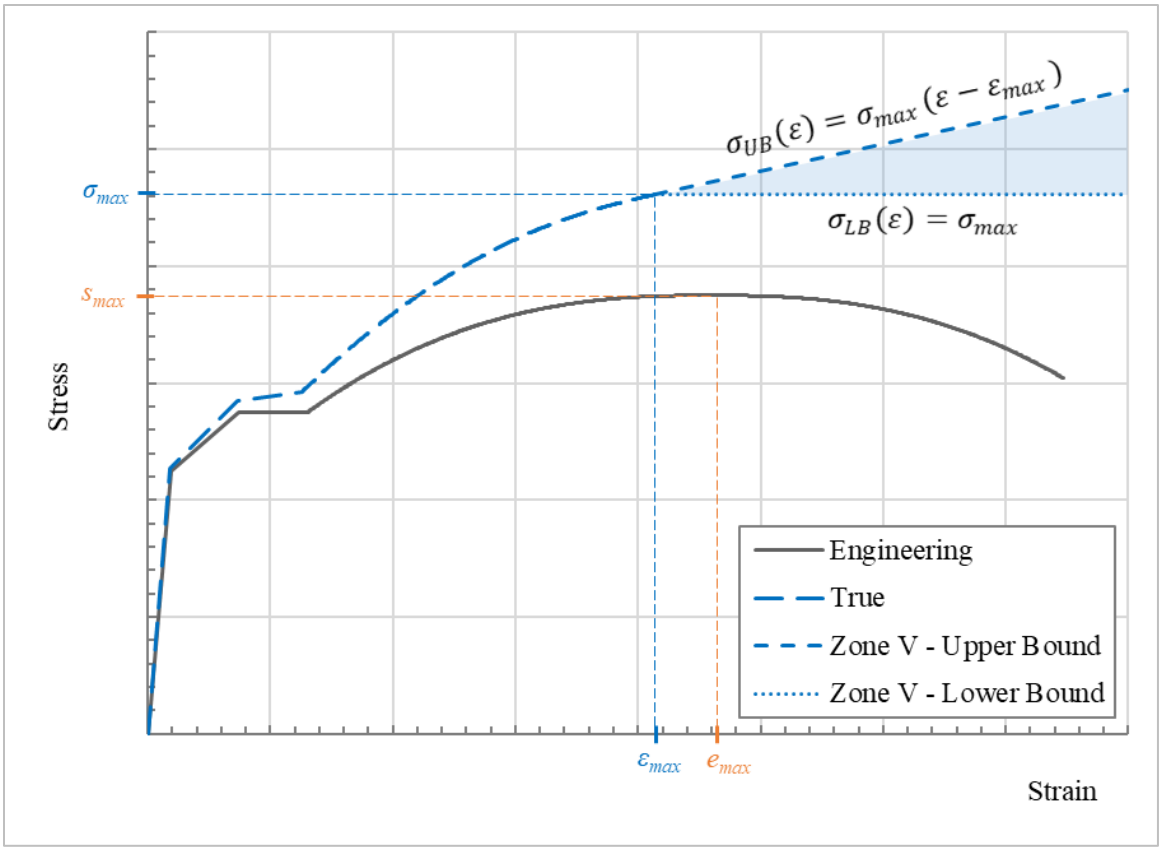

Figure 4-35: Bounds on True Stress-Strain Relationship – Zone V

This approach is similar to that described by Wang et al. (Wang, Xu, Ren, & Wang, 2016) for use in their proposed experimental-numerical combined method for determining the true constitutive relation (i.e., the true stress-strain relationship) of tensile specimens after necking. While Wang uses the power law as the lower bound in his examples, his general figure demonstrating the (ENM) process, previously presented as Figure 2-34 in Section 2.9.2, shows the lower bound is a horizontal line, as generally recommended herein.

To further refine and restrict the bounds for the true stress-strain behavior in Zone V, an initial exploratory analysis is recommended where the functional relationship (if used) developed for Zone IV is extrapolated and used to develop preliminary Zone V true

stress-strain relationship. The caveat of this approach is that the extrapolated fit for Zone V must be checked to ensure it obeys the derivative rules from Chapter 3. Once run, there are three possible outcomes that can result from this analysis. First, and most commonly, is that the model using the computational model will under-predict the tested post-necking response; meaning the FEA results will lie below the experimental data. In this case, the extrapolated relationship can be used as the lower bound in Zone V, rather than using the lower bound in Equation 4-60. Second, the model may over-predict the post-necking response, where the FEA results lie above the experimental data. In this case, the extrapolated relationship can replace the previously recommended upper bound in Equation 4-59. Third, while unlikely based on experience, the model may both under- and over-predict the response in different portions of Zone V. In this case, the extrapolated relationship cannot be used to adjust either upper or lower bounds; although it may provide a reasonable approximation to the post-necking behavior, thereby eliminating the need for additional iteration. In this case, the upper and lower bounds illustrated in Equation 4-59 and Equation 4-60, respectively, should be used as-is.

After revising the bounding functions, as appropriate, a series of analyses can be performed to efficiently determine the post-necking true stress-strain relationship using the weighted iterative technique developed by Ling (Ling, 1996) and further refined and implemented by Arasaratnam et al. (Arasaratnam, Sivakumaran, & Tait, 2011) (see Equation 4-58). An example illustrating the process of iteratively fitting Zone V post-necking test data is provided in Section 4.3.5.4. Section 4.3.5.5 discusses and demonstrates a viable approach for further refinement of the post-necking fit presented in Section 4.3.5.4.

4.3.5.4 True Stress-Strain Data for Computational Analysis – Zone V

Consider the case where the extrapolated Zone IV fit obeys the common trend observed by Ling (Ling, 1996), Joun et al. (Joun, Choi, Eom, & Lee, 2007), and

Arasaratnam et al. (Arasaratnam, Sivakumaran, & Tait, 2011), under-predicting the post-necking response. In this scenario, this extrapolated curve can serve as the lower bound for Zone V, replacing the general lower bound σ_{LB}, presented in Equation 4-60. Additionally, for this example, the upper bound to the behavior in Zone V should be a linear function with slope equal to the true stress at necking, σ_{max}, as shown in Equation 4-59 and discussed in Section 4.3.5.3.

Knowing these bounds, the simple weighting approach summarized by Equation 4-58 can be applied to develop a family of possible true stress-strain relationships that can be quickly analyzed, post-processed, and reviewed to determine the appropriate post-necking true stress-strain relationship. By considering a range of values for the weighting factor, *w*, between zero and one, several reasonable relationships can be developed simultaneously and analyzed in parallel to rapidly determine which best captures the post-necking response. For most cases, the best fit can be determined through visual inspection of the results. Though, as desired, more rigorous mathematical techniques (e.g., regression analysis) can also be applied to evaluate and compare the accuracy of different true stress-strain relationships. An example of such a family of relationships is provided in Figure 4-36, where *w* was varied between a minimum of zero and a maximum of one by consistent increments of 0.2, resulting in six potential solutions. The post-processed predictions produced by FEA models using these relationships are shown in Figure 4-37, overlaid on the experimental data. In addition, for reference, the deformed shape of the coupon model used to produce these results is provided for qualitative review in Figure 4-38. Note that this process can be repeated as necessary to further adjust the value of weighting factor, *w*, for best fit of the experimental data. Note that where a constant value of weighting factor, *w*, does not produce satisfactory results, additional steps can be taken to further refine the fit as discussed in Section 4.3.5.5.

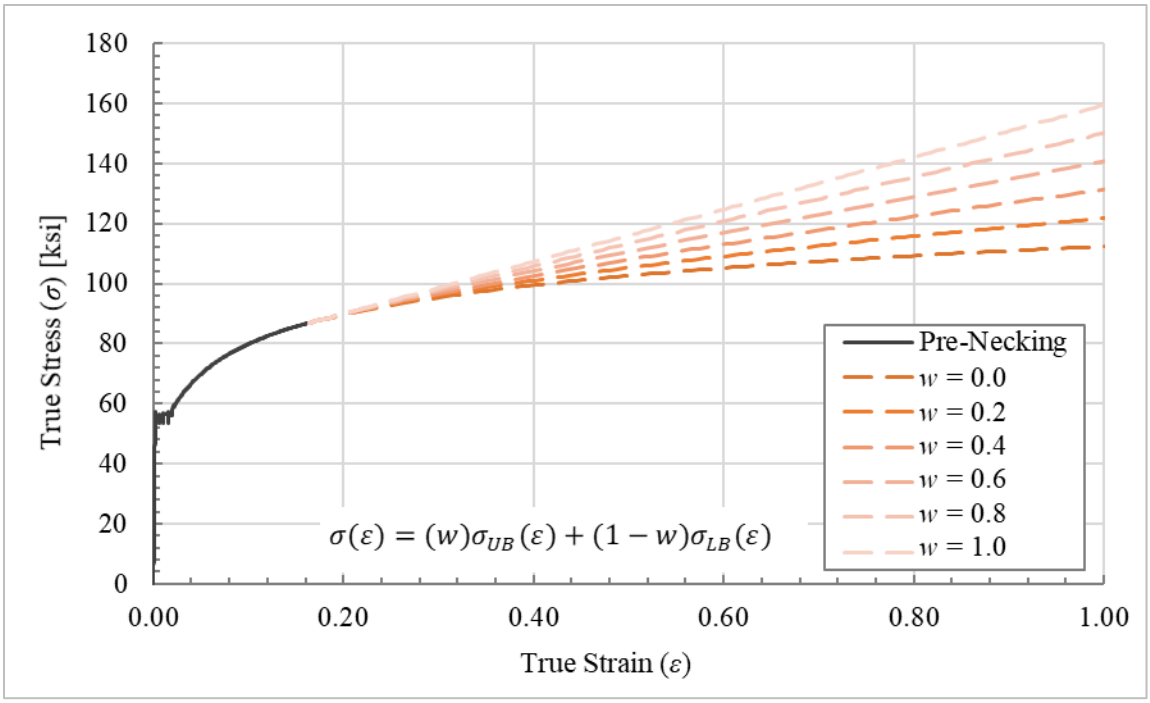

Figure 4-36: Family of Possible Post-Necking True Stress-Strain Relationships

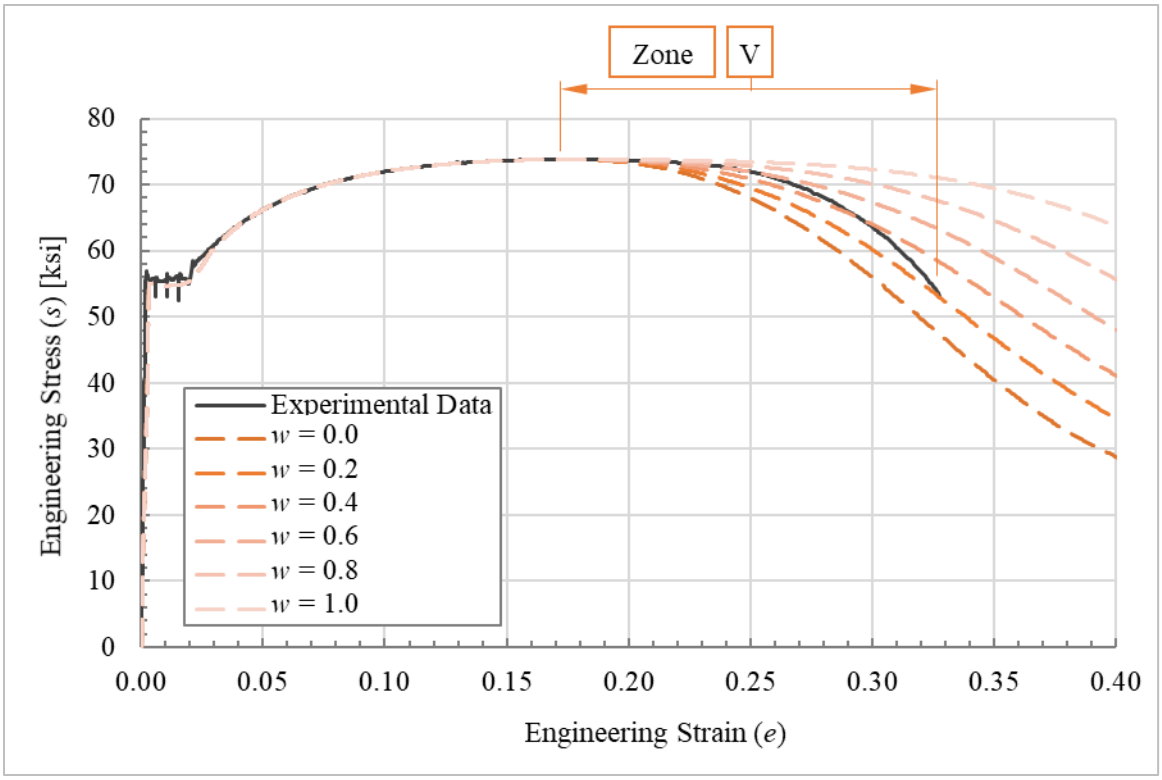

Figure 4-37: FEA Model Results for Family of Possible Post-Necking Relationships

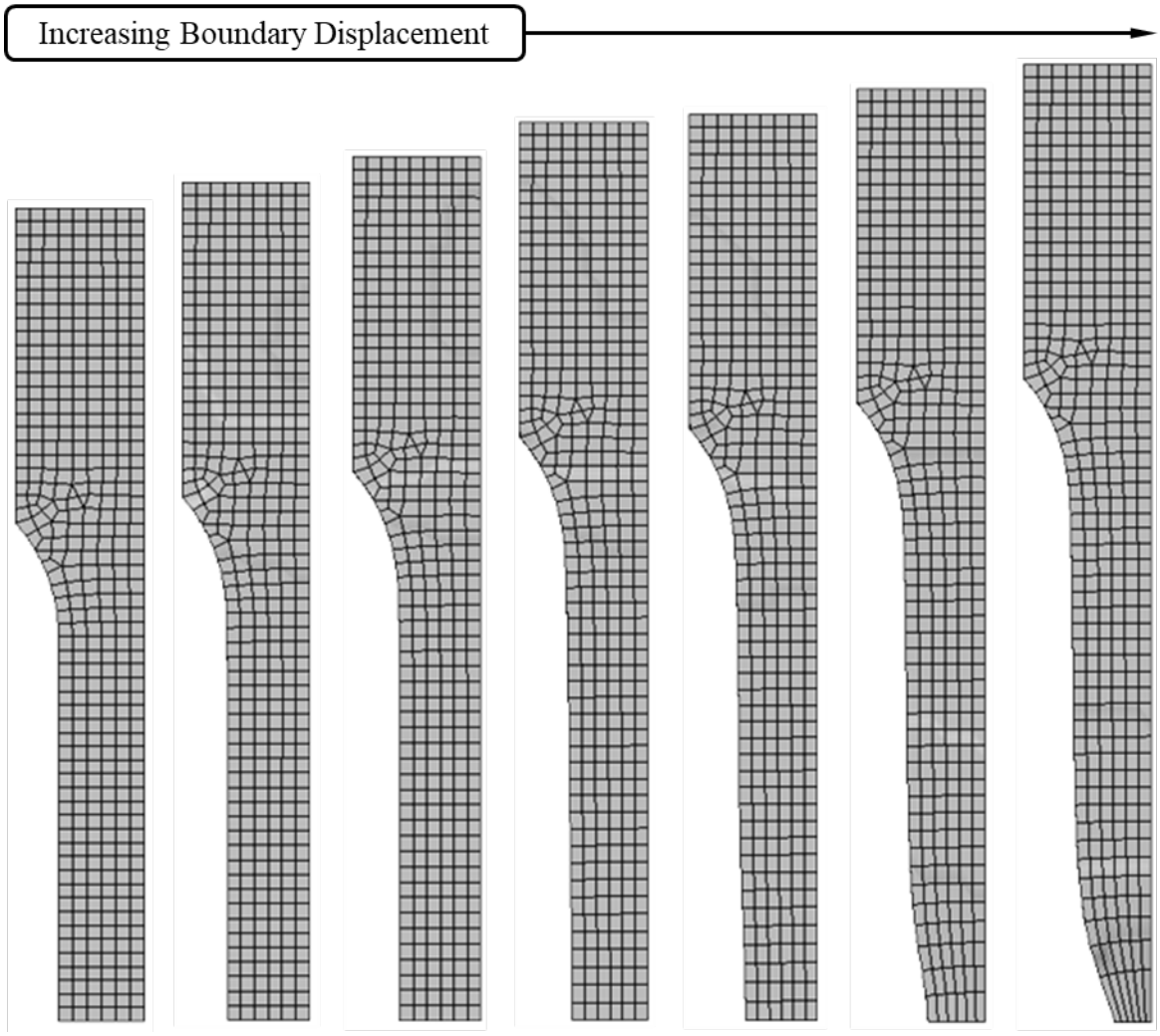

Figure 4-38: Deformed Shape of Coupon Model with Increasing Boundary Displacement

4.3.5.5 Further Refinement of Weighting Factor Approach

As illustrated in Figure 4-37, the proposed weighting process does not provide a particularly precise approximation of the post-necking experimental data over the entire range of Zone V for this example. This lack of fit occurs as a result of the limitations and simplicity of the bounding functions and weighting factor, *w*. To improve results, additional complexity can be introduced. For example, a variable weighting factor can be used in the material true stress-strain relationship to provide a better computational prediction of the test data from Section 4.3.5.4. Specifically, the factor *w* can be defined as

a function of strain, $w(\varepsilon)$, as shown in Equation 4-61. After multiple iterations and visual comparison against the test data, the final weighting function, $w(\varepsilon)$, was defined as a multi-linear function, equal to 0.65 at the onset of necking, reducing (linearly) to 0.1 at a strain of approximately 0.9, and remaining constant at 0.1 thereafter. The resulting fit is shown in Figure 4-39. Note that the model prediction is nearly indistinguishable from the test data.

$\boxed{\text{V}}\ \varepsilon_{max} < \varepsilon$ $\qquad \sigma(\varepsilon) = (w(\varepsilon))\sigma_{UB}(\varepsilon) + (1 - w(\varepsilon))(\sigma_{LB}(\varepsilon))$ Equation 4-61

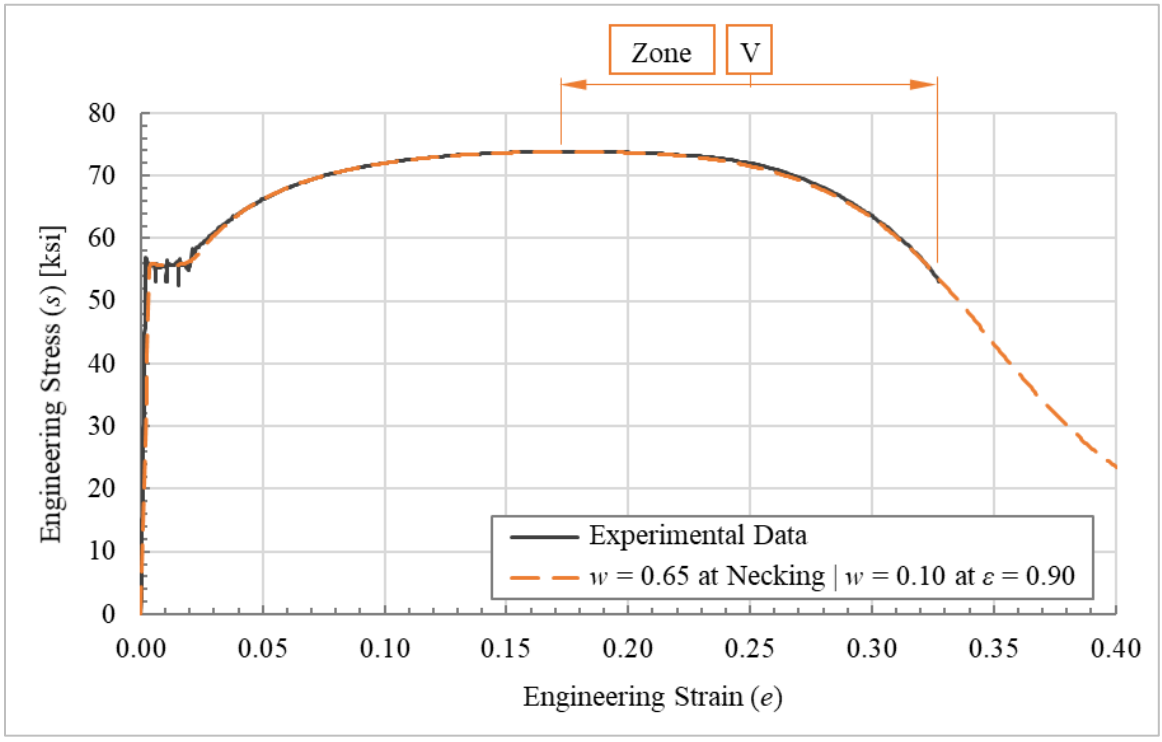

Figure 4-39: Example of Refined Fit of True Stress-Strain Relationship

Figure 4-39 illustrates a single example of the potential of this approach. A rigorous means of manipulation, iteration, and evaluation of post-necking fits, however, has not been developed as part of this research and is suggested as a topic for further study in Section 6.3.

Thus, a weighting factor, w, or weighting function, $w(\varepsilon)$, can be applied to appropriate bounding functions, $\sigma_{UB}(\varepsilon)$ and $\sigma_{LB}(\varepsilon)$, to obtain extremely precise predictions. When applying this approach, care should be taken to verify that the derivative rules from Chapter 3 are met across the full range of the post-elastic true stress-strain relationship definition once a final relationship selected. Also, while not a focal point in this dissertation, it is likely that the true stress-strain relationship developed using the recommended approach will be used to define a material constitutive relationship that may be applied to a different model (i.e., a model other than a duplicate of the coupon tension test). For these cases, care should be taken to identify instances where stress and/or strains beyond those observed in the tension test will be predicted in the new model, as further discussed in Section 4.3.5.6.

4.3.5.6 Commentary on Extrapolation

While extrapolation should generally be avoided, certain situations can necessitate it. For example, extrapolation of the true stress-strain relationship may occur when a true stress-strain relationship developed to match standard coupon tension test data is applied in a new model that predicts stresses and/or strains beyond those measured in the coupon test. A similar situation can arise in the absence of test data, or where only standard "book values" of select material properties are available (e.g., elastic modulus, yield strength, and ultimate strength). In these instances, care must be taken to properly develop a true stress-strain relationship that accurately reproduces necking, maintains computational stability, and does not predict spurious behaviors like cold-drawing. Each of these objectives can be achieved by following the recommendations in this dissertation for development of the material true stress-strain relationship, particularly the three derivative rules (see Chapter 3).

Furthermore, the value of the rules and recommendations presented in this dissertation is greatest in the post-necking region (i.e., Zone V) where standard relationships between engineering stress-strain and true stress-strain (see Equation 4-1 and Equation 4-2) no longer apply. In these cases, the zone-to-zone continuity recommendations and derivative rules ensure the true stress-strain relationship developed will, at the least, provide physically plausible results and predict key points (e.g., yield, onset of strain-hardening, and onset of necking) precisely.

4.3.6 Tension Failure

Detailed consideration of tension failure is beyond the scope of this dissertation. However, it is a topic worthy of basic discussion and consideration. In particular, recognizing the stress and strain gradients within the coupon both prior to and after necking allows for improved understanding of the onset of necking, post-necking behavior, and tension failure. In addition, if peak strains can be identified, they can be used to rapidly determine an appropriate failure strain for application of simplified plastic-strain-based erosion and failure criteria in FEA models (see discussion in Appendix Section B.9).

This section provides a qualitative exploration of the observed stress distribution in a perfect uniaxial tension coupon prior to necking. It is assumed the coupon is made from uniform, continuous, and homogeneous material. This information can be used to predict the point at which necking will occur in such a perfect specimen. After necking, a similar qualitative review of stress distribution is presented to illustrate the relative changes in stress and strain distribution that occur as a result of necking. Finally, the post-necking stress distribution is investigated to determine, from a material level, the point exhibiting maximum stress and strain; thus, the point where material failure should initiate. To illustrate these points, results from the FEA model used in the example problem presented

in Chapter 5 are provided. Additional information on this model and the general FEA approach are provided in Appendix B.

4.3.6.1 Stress and Strain Distribution Prior to Necking

Many researchers have studied pre- and post-necking stress and strain distribution in uniaxial tension coupons in great detail, as discussed in Chapter 2. For the purposes of this dissertation, the discussion will remain quite simple, focusing on a qualitative presentation and review of the stress and strain distributions predicted to occur within a typical coupon model with homogenous uniform material and generic geometry of a thick-plate specimen (i.e., rectangular cross-section within the center reduced section).

Prior to necking, the stress distribution can be investigated to determine where necking should occur. Using a one-eighth symmetry model (see discussion in Appendix Section B.3.3) with three orthogonal symmetry planes intersecting at the center of the coupon, a plot of the distribution of stresses and strains predicted just prior to necking was developed, as shown in Figure 4-40. As illustrated, the stresses and strains are highest near the center of the coupon. This observation is expected, as the wider gripped ends provide restraint to the coupon, forcing stresses to concentrate at the center, away from this geometric restraint, as discussed previously in Section 2.8.3.

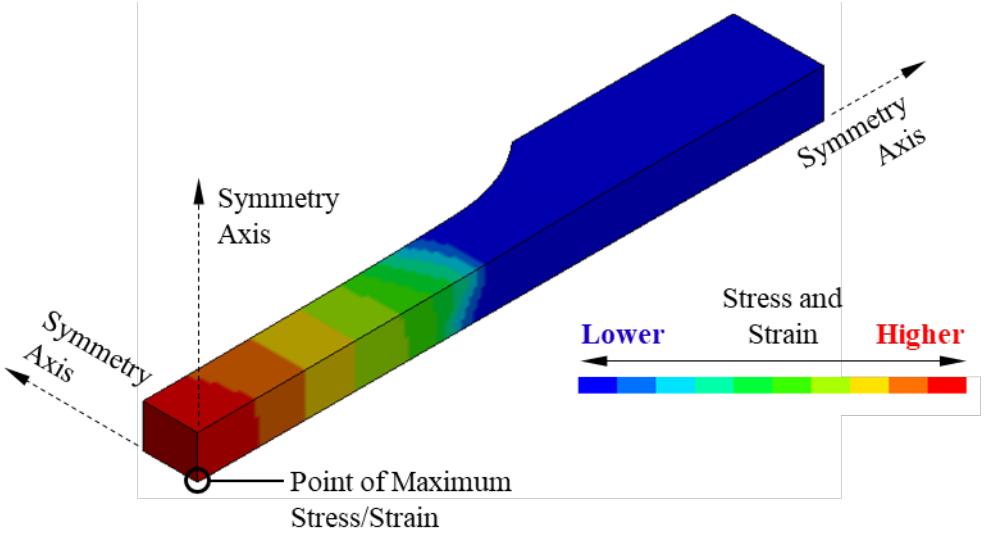

Figure 4-40: Longitudinal Stress and Strain Gradient Prior to Necking

Investigating further, the cross-section at the center of the reduced section clearly exhibits the most extreme stresses and strains. Therefore, the stresses and strains in this critical cross-section can be reviewed to understand their distribution, as shown in Figure 4-41. Review of this figure reveals that the stresses and strains are maximum at the precise center of the coupon, which corresponds to the point of intersection of the three symmetry planes. This result matches the analytical prediction of the point of peak stress developed by Bridgman (Bridgman, 1952), Chen (Chen W. H., 1971), and many others. Further review reveals slight irregularity in the computed stress gradient; this is the combined result of mesh discretization and the fine gradient of stresses, which differ by approximately 0.5% over the illustrated section. Additional mesh refinement would reduce the exhibited irregularity.

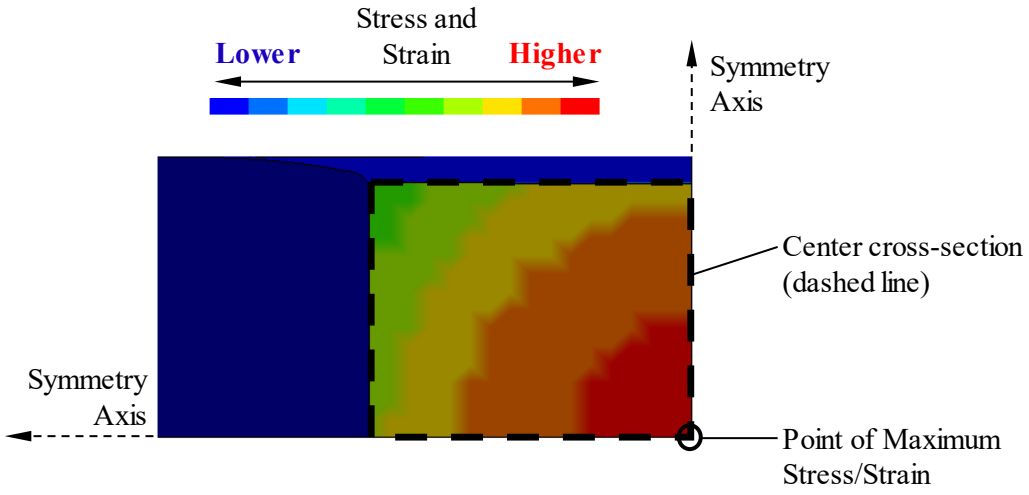

Figure 4-41: Cross-Sectional Stress and Strain Gradient Prior to Necking

Because the peak stresses and strains occur at the center, necking should also initiate there, as that will be the first point to satisfy Considère's Construction and Derivative Rule #1. Once this critical section reaches the bifurcation in cross-sectional stability that initiates necking (i.e., the strain beyond which geometric softening occurs at a faster rate than material strain hardening), the section will reduce in area. As a result, the load-bearing capacity of the necking section will decrease and the adjacent material will elastically unload to maintain equilibrium. The combined effect of reduced load-bearing capacity of the necking section and the elastic unloading of the adjacent material is concentration of further deformations at the neck (see Figure 2-1, for example). Further study of the stress and strain distribution in this critical (necked) section at strains beyond the onset of necking provides insight into the approximate location where fracture will initiate, as discussed in the following section.

4.3.6.2 Stress and Strain Distribution After Necking

As illustrated in Figure 4-42 and Figure 4-43, the stress and strain distribution in the post-necking coupon are qualitatively quite similar to those predicted prior to necking,

except that the longitudinal gradients. These stress and strain gradients along the long axis of the coupon are generally more extreme and complex due to the cross-sectional changes occurring as a result of necking. Of note, while peak stresses and strains occur at the centerline of the neck (see Figure 4-43), surface stresses and strains are higher away from the neck (see Figure 4-42). While this effect was not evaluated in detail as part of this research, it would appear that it results from the need for the material adjacent to the neck to accommodate deformation of the necked section. In particular, away from the neck, the centerline of the coupon experiences only longitudinal (long-direction) deformations, while the surface elements away from the neck experience similar longitudinal deformations as well as through-width and through-thickness deformations due to the adjacent necking. Finally, it is also of note that the predicted shape of the necked cross-section (see Figure 4-43) matches quite closely with that predicted by Scheider (Scheider, Brocks, & Cornec, 2004) for a rectangular coupon cross-section ("bow-tie" shape), illustrated previously in Figure 2-37.

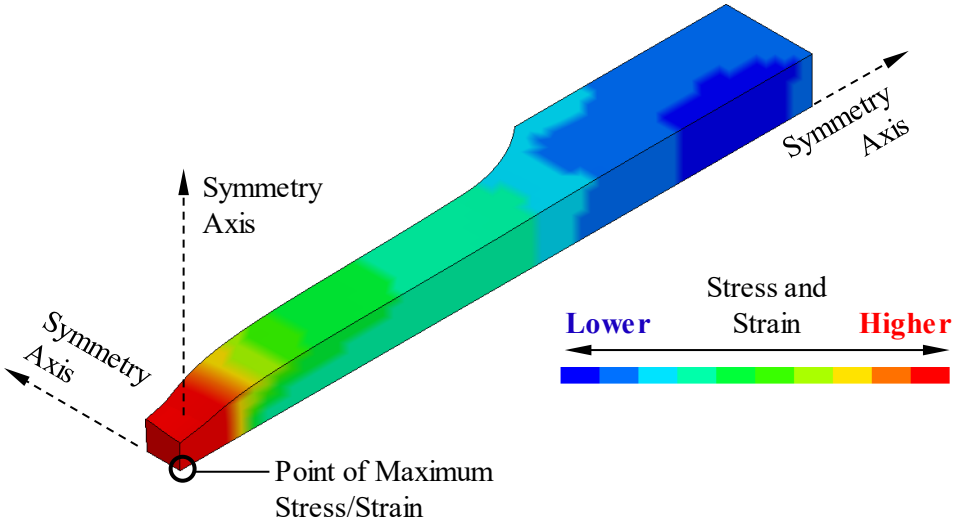

Figure 4-42: Longitudinal Stress and Strain Gradient After Necking

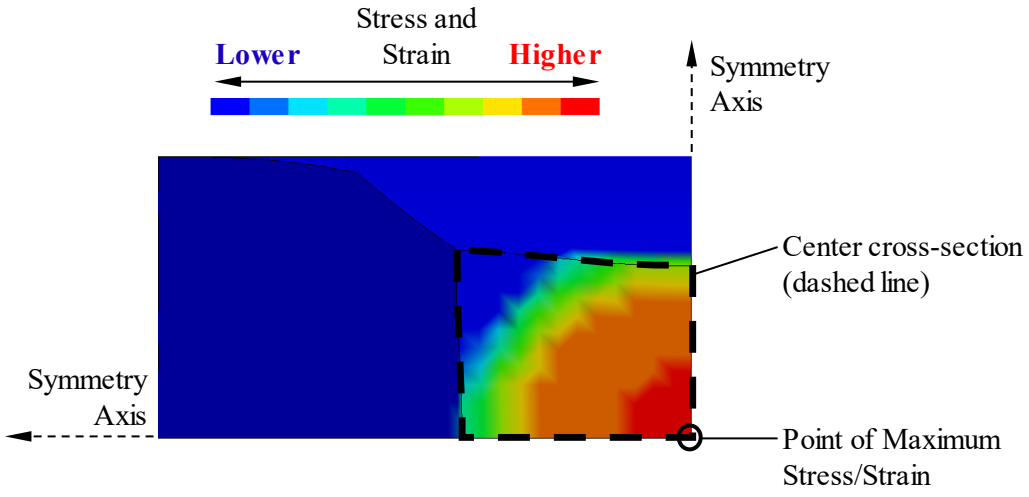

Figure 4-43: Cross-Sectional Stress and Strain Gradient After Necking

Therefore, as before, much like at the onset of necking, the maximum stresses and strains occur at the precise center of the specimen, mirroring the analytical prediction by Bridgman (Bridgman, 1952), Chen (Chen W. H., 1971), and many others. As a result, fracture in a perfect, homogeneous, continuous uniaxial tension coupon should initiate from the precise center. After failure of the center, stresses redistribute to adjacent material resulting in local overstress and failure of that material and outward propagation of the fracture across the necked cross-section. This process continues until the specimen is completely fractured. Thus, fracture propagates outward from this central initiating point of material failure until the entire section fails and separates. This general outward failure propagation has been implied by the stress distributions reported by Bridgman (Bridgman, 1952) and Chen (Chen W. H., 1971), concluded by a several researchers (Jia & Kuwamura, 2014) (Zhu, 2017) (Kõrgesaar, 2015), reported in general technical references (Davis, 2004) (Campbell, 2012) (Dieter, Jr., 1961), and supported by fractographic inspection of the failure surface of ductile metal tension coupons (Askeland & Fulay, 2004) (Davis, 2004) (McEvily, 2013), as discussed previously in Section 2.9.3.2.

4.4 SUMMARY AND CONCLUSIONS

By following the steps outlined in this chapter, the load-deformation data captured in a standard coupon test can be used to develop a true stress-strain relationship for use in numerical modeling of structural steel materials. Up until the onset of necking, the standard analytical conversion shown in Equation 4-1 and Equation 4-2 can be used to determine the true stress-strain relationship because the assumptions of uniform stress and strain in the reduced section remain valid. After the onset of necking, an iterative approach can be used to determine a best fit for post-necking response.

When developing true stress-strain relationships for structural steels, it is often helpful to use functional best fits to the various zones of response to ensure the derivative rules presented in Chapter 3 are met. By following these rules, the numerical material model will precisely capture the onset of necking, will remain computationally stable, and will not predict spurious cold-drawing response. Furthermore, because these rules are founded in the physical material response observed during testing, computational models can be readily used in a predictive manner for other material geometries and states of stress.

Finally, while not a topic of focus in this dissertation, application of the proposed approach within a properly defined FEA model (see Appendix B) will result in prediction of peak stresses and strains at the precise center of the specimen during both pre- and post-necking response. Thus, necking should be predicted at the longitudinal centerline of a specimen, as supported by analytical studies from several researchers. Further, fracture should initiate at the precise center point of the tension coupon, propagating outward as supported by a range of researchers, technical references, and experimental fractography.

In the following chapter (Chapter 5), an example is provided the methods described in this chapter (Chapter 4) for developing the true stress-strain relationship for structural steels from the date produced in a standard tension test. Alongside, commentary is provided

to further describe the process, including discussions of potential issues that may arise during application of the proposed approach.

5 EXAMPLE TRUE STRESS-STRAIN RELATIONSHIP DERIVATION FOR FINITE ELEMENT ANALYSIS

5.1 INTRODUCTION

To illustrate the recommendations provided in Chapter 4 for defining the uniaxial tension true stress-strain relationship for structural steels, a simple example demonstrating the process is provided in this chapter. Commentary is included to provide additional insight. The experimentally measured engineering stress-strain curve used to develop this example is illustrated in Figure 5-1. Dimensions of the tested tension coupon are summarized in Figure 5-2 and Table 5-1. The coupon is made from ASTM A992 steel cut from the flange of a W10×19 beam. The test was run using the procedure recommended in Structural Stability Research Council (SSRC) Technical Memorandum No. 7: Tension Testing (Structural Stability Research Council, 2010), with a machine cross-head rate of 0.02 inches per minute.

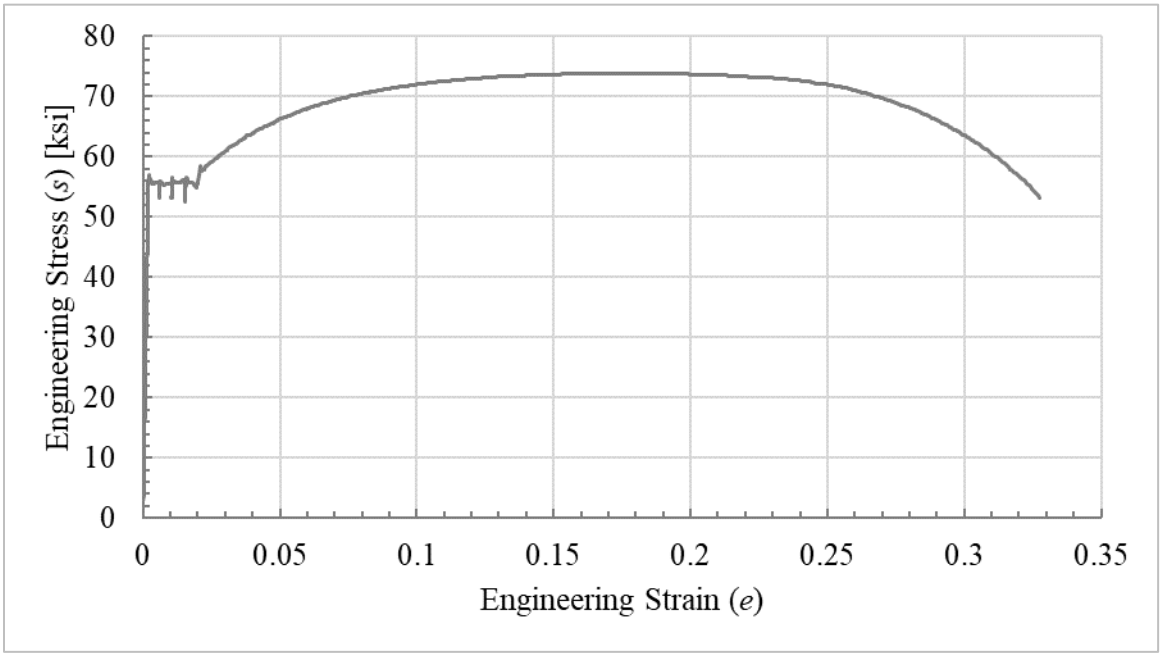

Figure 5-1: Experimentally Derived Engineering Stress-Strain Data

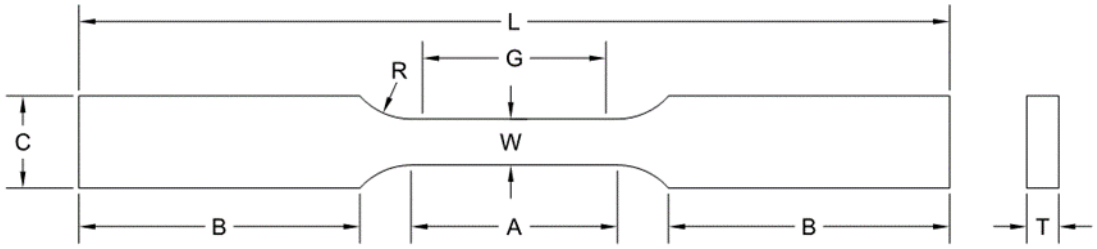

Figure 5-2: Tension Coupon Geometry

Table 5-1: Tension Coupon Dimensions

Coupon Dimensions [in]							
A	**B***	**C**	**G**	**L***	**R**	**T**	**W**
2.25	0.92	0.75	2.00	4.75	0.50	0.395	0.50

*Modeled length (ends truncated to reflect approximate grip location)

The engineering stress-strain curve was developed from measured load-deformation data using the standard conversions presented previously in Equation 2-1 and Equation 2-2. Sections 5.2 and 5.3 summarize the process of developing the true stress-strain relationship from the engineering stress-strain data, using an eighth-symmetry finite element analysis (FEA) model of the tension coupon. The final result is presented at the end of Section 5.3 followed by a short discussion of underpredicting the post-necking behavior in Section 5.3.1 and overfitting post-necking behavior in Section 5.3.2. Finally, fracture and failure is briefly discussed in Section 5.4 (additional guidance in Appendix Section B.9) followed by concluding remarks in Section 5.5. LS-DYNA was used to develop this approach and LS-DYNA **MAT_24* was used for the material model definition. Refer to Appendix B for additional information on the modeling methodology.

5.2 FITTING THE PRE-NECKING RESPONSE

While the pre-necking response is discussed at great length in Chapter 4, the process of fitting the pre-necking response can be done using simple spreadsheet tools without any need for iteration or model development. This is because the standard

analytical relationships previously shown in Equation 4-1 and Equation 4-2 apply throughout the entire pre-necking range of response allowing for direct conversion of measured engineering stress-strain data to true stress-strain data. Using these conversion equations up to the onset of necking, or the point of maximum engineering stress, the true stress-strain relationship can be approximated and subsequently fit up to that point. The direct converted data determined using the standard conversions up to the onset of necking is shown in Figure 5-3.

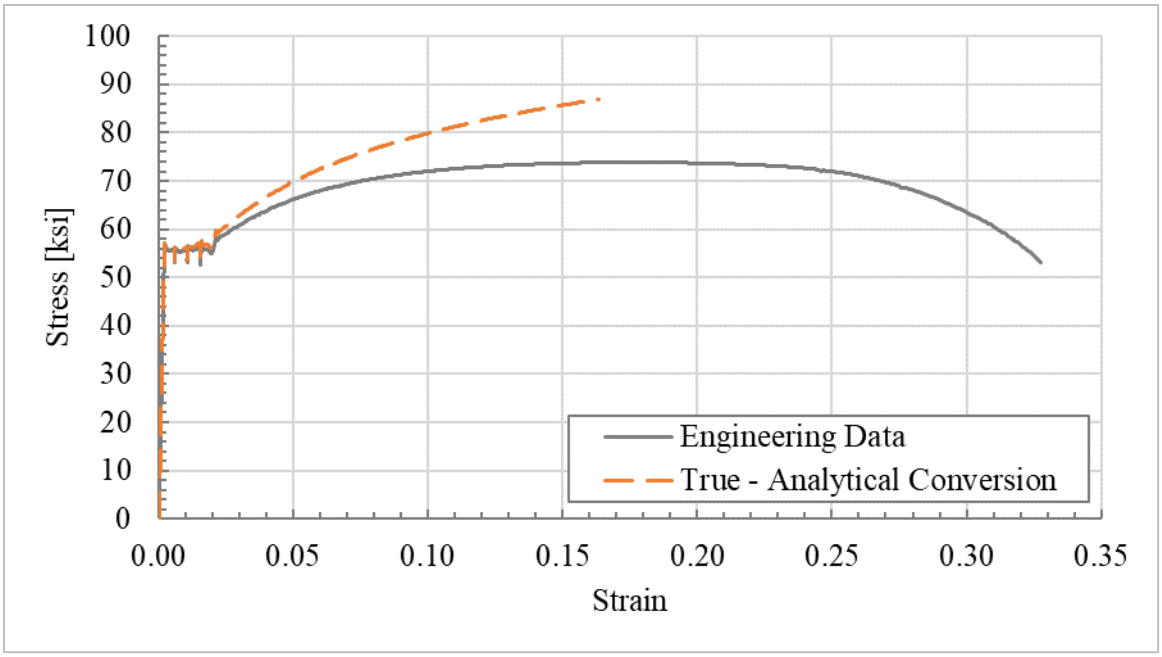

Figure 5-3: True Stress-Strain Relationship to Onset of Necking

Per the approach and equations outlined in Sections 4.3.1 through 4.3.4.3, many of the key quantities defining the true stress strain up to the onset of necking can be determined a priori, as summarized in Table 5-2. Figure 5-4 illustrates the fit through the analytically converted key quantities of the true stress-strain relationship. Because there is no observed non-linear elastic range, the proportional limit is equal to the onset of yield and for accuracy of fit, the measured elastic modulus was used in the material definition

rather than the standard book value as recommended in Section 4.3.1.1. In addition, despite the ability to directly convert the measured engineering stress-strain curve to a true stress-strain relationship up to the onset of necking, the strain hardening branch was excluded from this fit to allow a mathematical function to be used to defined the relationship between these points as described later in this section. By using a mathematical function, the potential for inadvertently incorporating noise and/or variability inherent in the experimentally derived data is reduced significantly.

Table 5-2: Key Quantities for True Stress-Strain Relationship to Onset of Necking

Variable	Value [2]	Units	Equation
s_y	55,000	psi	---[1]
σ_y	55,110	psi	Equation 4-1
e_y	0.002	---	---[1]
ε_y	0.001998	---	Equation 4-2
s_{sh}	55,000	psi	---[1]
σ_{sh}	56,105	psi	Equation 4-1
e_{sh}	0.0201	---	---[1]
ε_{sh}	0.0199	---	Equation 4-2
s_{max}	73,830	psi	---[1]
σ_{max}	86,955	psi	Equation 4-1
e_{max}	0.178	---	---[1]
ε_{max}	0.1636	---	Equation 4-2
E	27,500,000	psi	---
E_{true}	27,582,550	psi	Equation 4-3
E_{II}	N/A	---	Equation 4-13
E_{III}	55,600	psi	Equation 4-20
E_{sh}	726,600	psi	---[1]
$E_{sh\text{-}true}$	811,900	psi	Equation 4-37
$E_{max\text{-}true}$	73,830	psi	Equation 4-40

[1] Observed directly from test data in Figure 5-1

[2] Values truncated and rounded where appropriate

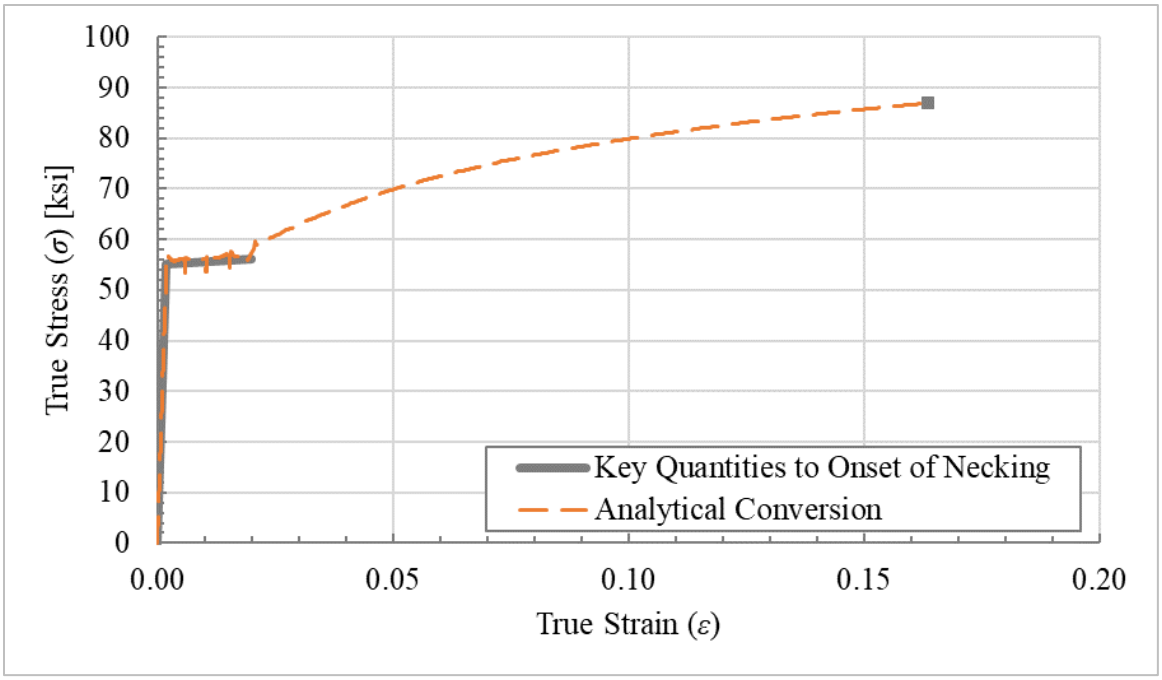

Figure 5-4: True Stress-Strain Relationship Comparison to Onset of Necking

With these key quantities defined, the relationship in Zones I through III, described in Section 4.3, is established. Next, the strain hardening branch up to necking can be approximated using the recommended mathematical function fitting approach for Zone IV, described in Section 4.3.4.3, can be applied. Table 5-3 provides a summary of the constants for the cubic relationship described by Equation 4-41. Similarly, the constants for the exponential-linear relationship described in Equation 4-50 are presented in Table 5-4. These approximate fits are plotted against the analytical conversion of the true stress-strain relationship in Figure 5-5.

Table 5-3: Constants for Cubic Relationship (Equation 4-41)

Constant	Value [1]	Units	Equation
C_1	22,746,821	psi	Equation 4-42
C_2	-7,426,950	psi	Equation 4-43
C_3	811,900	psi	Equation 4-44
C_4	56,105	psi	Equation 4-45

[1] Values truncated and rounded where appropriate

Table 5-4: Constants for Exponential-Linear Relationship (Equation 4-50)

Constant	Value [1]	Units	Equation
C_1	-904,507	psi	Equation 4-51
C_2	1.2137	psi	Equation 4-52
C_3	811,900	psi	Equation 4-53
C_4	56,105	psi	Equation 4-54

[1] Values truncated and rounded where appropriate

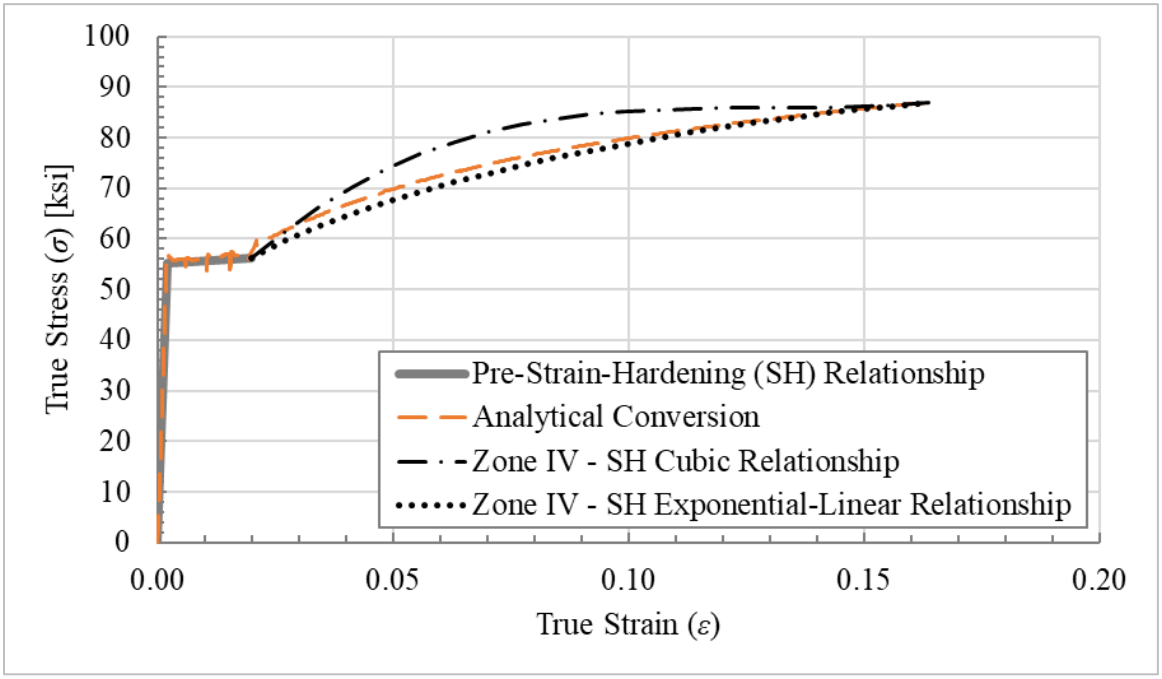

Figure 5-5: Strain-Hardening Fit Comparisons for Equation 4-41 and Equation 4-50

Review of the fits to the data in the strain-hardening branch (Zone IV) in Figure 5-5 reveals that neither provides an accurate fit to the experimental data. Specifically, the exponential-linear relationship generally under predicts the relationship and the cubic relationship generally over predicts the relationship. In addition, the cubic approximation reverses in curvature as it approaches the onset of necking, violating Derivative Rule #3. Therefore, with neither approximation producing an ideal fit, alternate fitting approaches will be considered, as discussed later in this section.

For rapid curve fitting, Microsoft Excel or other similar automated curve fitting software can be used to generate a precise curve fit over a specific range of data. For this example, two curve fits, a power law fit and a natural logarithm (log) fit, were developed that visually approximate the analytically converted true stress-strain data quite precisely, as shown in Figure 5-6 and Figure 5-7, respectively. The best-fit equations and coefficient of determination, R^2, for each of these automated curve fits are included in the plots for reference. Note that the equations are presented in standard format where the abscissa value, strain, is referred to as "x", and the ordinate variable, stress, is referred to as "y".

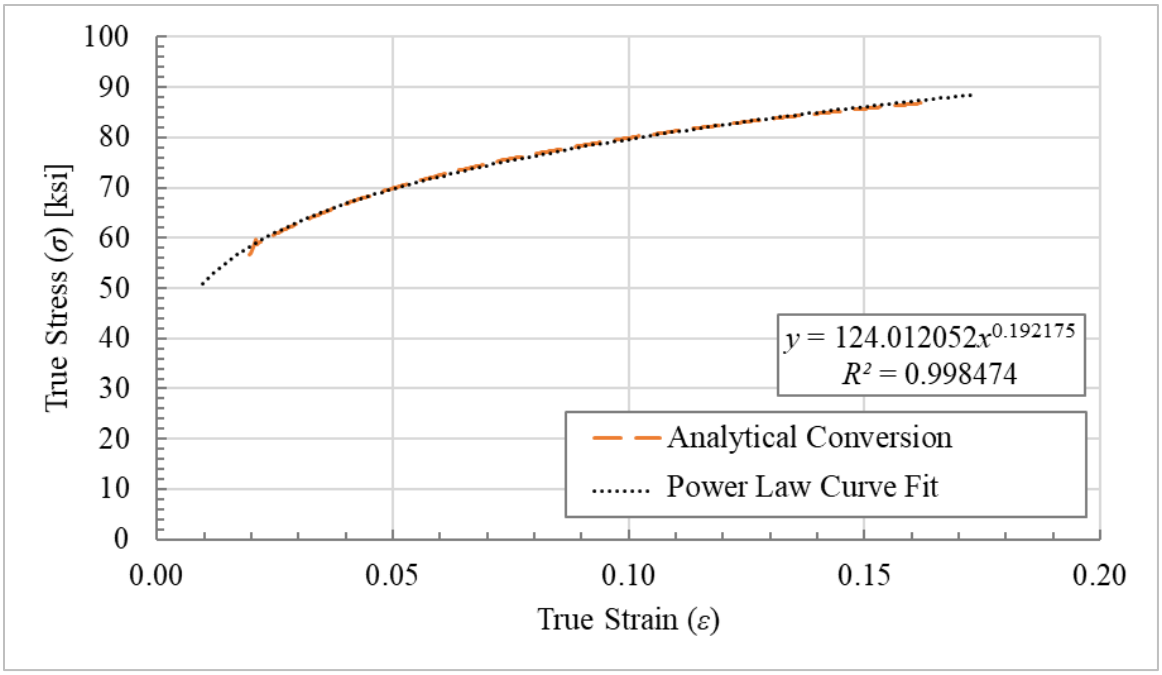

Figure 5-6: Strain-Hardening Comparison for Microsoft Excel Power Law Curve Fit

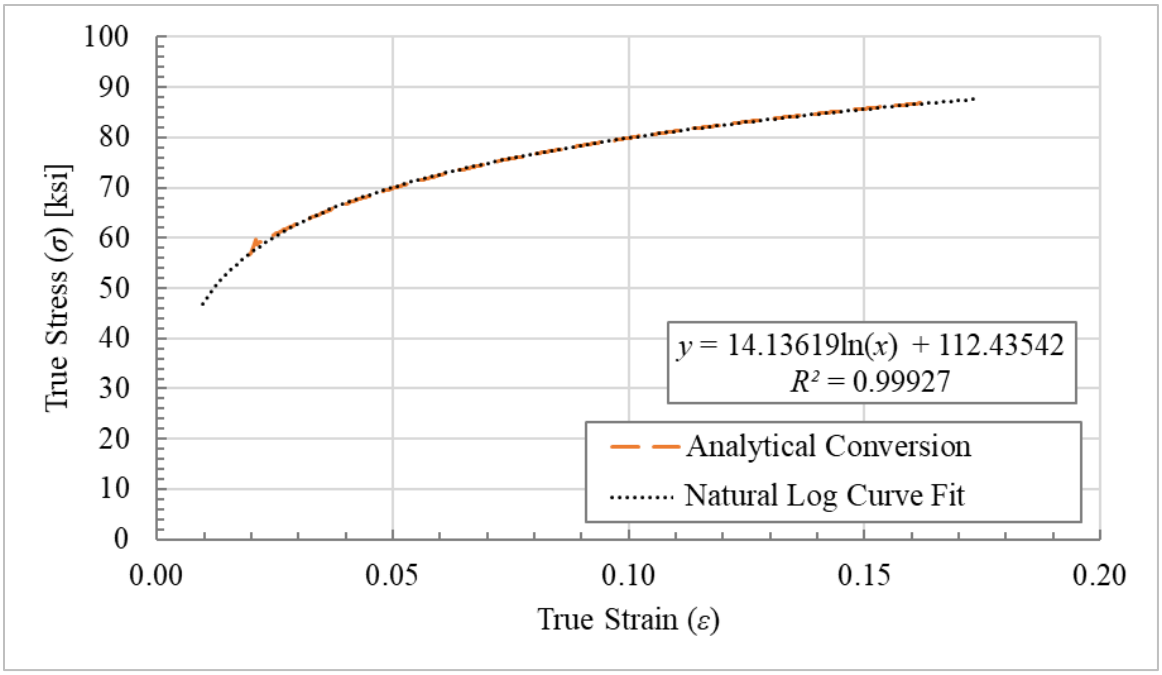

Figure 5-7: Strain-Hardening Comparison for Microsoft Excel Natural Log Curve Fit

Review of the preceding figures reveals that these computer-generated fits capture the strain hardening branch much more accurately than the previous analytically derived relationships presented in Figure 5-5. Both approximations capture the data nearly perfectly with R^2 values nearly equal to 1.0. Therefore, further interrogation is required to determine and verify whether they are viable fits for use in the constitutive true stress-strain relationship, and/or which of them is the best fit for this purpose.

By inspection, each fit obeys Derivative Rule #2, maintaining a positive slope over the full strain-hardening branch. In addition, by inspection it appears that each also follows Derivative Rule #3, as there is no apparent reversal in curvature, though this should be verified prior to use. However, because a built-in curve fit function was used, it is unclear whether either, neither, or both satisfy Derivative Rule #1 which is required for accurate prediction of the onset of necking. Therefore, additional investigation is required to evaluate these approximations of the Zone IV data with respect to these requirements beginning with verification of Derivative Rule #1, Considère's Construction, as discussed in Section 5.2.1.

5.2.1 Verifying Derivative Rule #1 (Considère's Construction)

As discussed in detail in Chapters 3 and 4, to provide a viable fit to the data and accurately predict the onset of necking, the true stress-strain relationship must obey Derivative Rule #1; Considère's Construction. To determine whether either fit satisfies this requirement, each automatically generated curve fit and its first derivative can be plotted together to visually confirm. As summarized in Sections 2.8.2 and 3.2, a viable fit will be one where these two functions cross at the onset of necking; in this example, a strain equal to 0.1636. Figure 5-8 and Figure 5-9 provide the graphs of the Zone IV strain-hardening fits plotted along with their first derivative for the computer-generated power and logarithm fits, respectively.

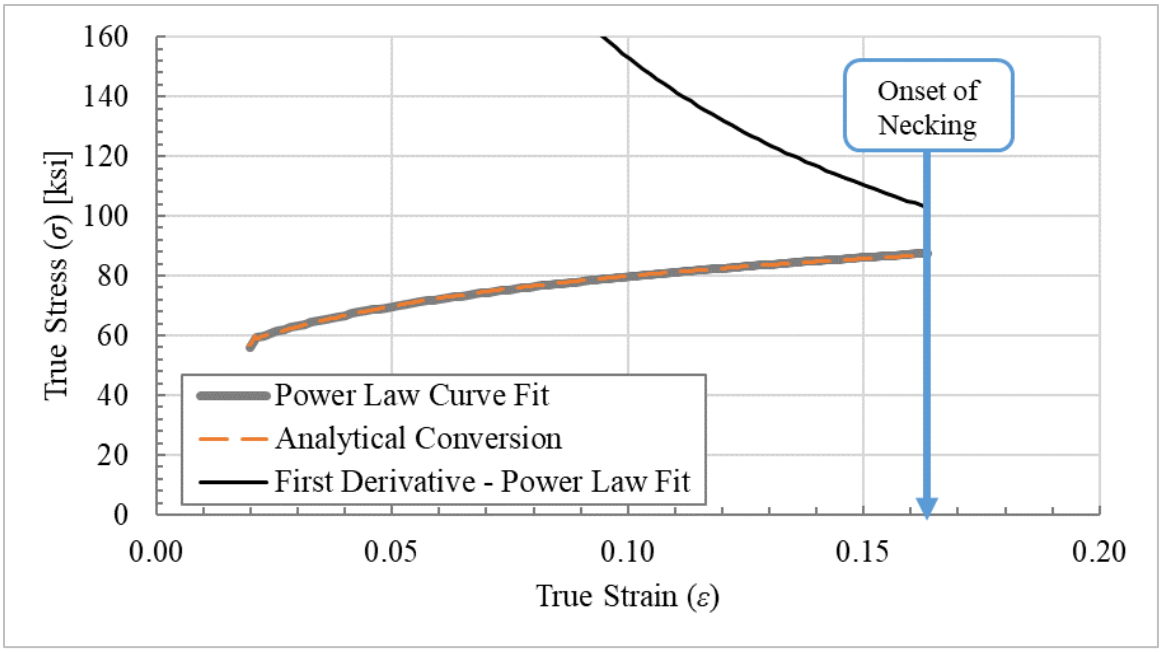

Figure 5-8: Derivative Rule #1 Check for Microsoft Excel Power Law Curve Fit

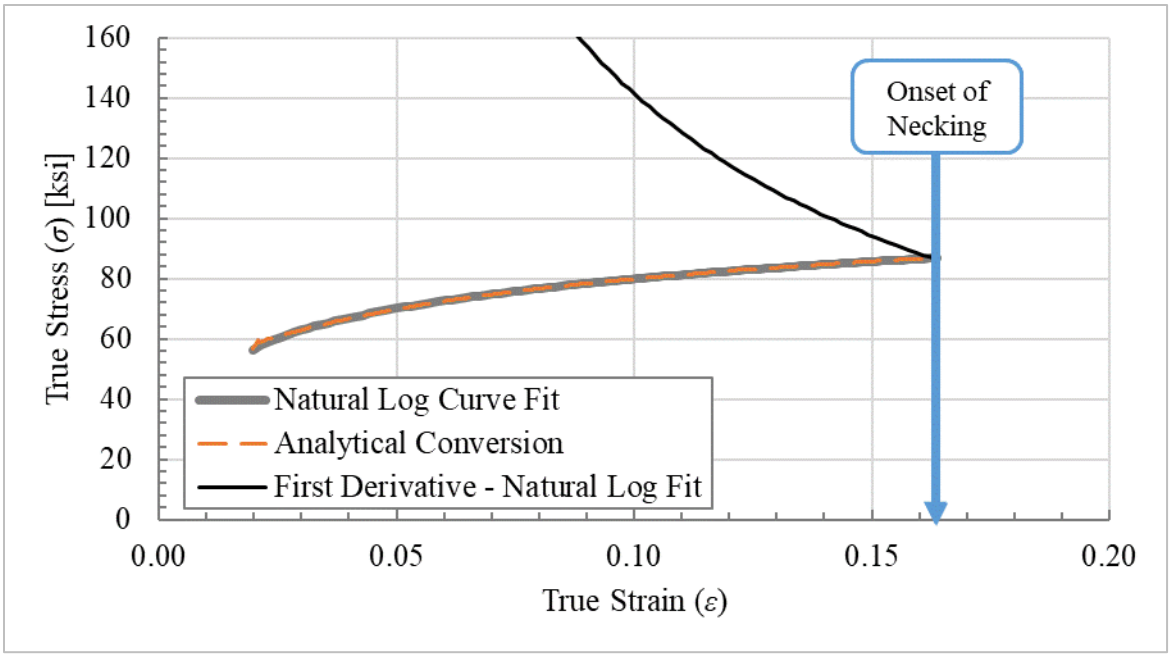

Figure 5-9: Derivative Rule #1 Check for Microsoft Excel Natural Log Curve Fit

Based on a review of Figure 5-8 and Figure 5-9, it is clear that only the natural log fit will predict the onset of necking accurately and that use of the power law fit would result

in inaccurate prediction of the onset of necking. Therefore, the power law fit is not a viable solution for the Zone IV strain-hardening relationship despite its nearly perfect visual fit to the data and the natural log fit will be used to define the true stress-strain relationship in Zone IV. Figure 5-10 illustrates the combined fit of Zone I through Zone IV to the onset of necking. While the derived true stress-strain relationship should produce an accurate prediction of behavior up to the onset of necking, this assumption should typically be verified. Therefore, prior to determining the post-necking relationship in Zone V, a FEA model using this proposed fit should be developed and executed to verify that the model produces an acceptably accurate prediction of pre-necking response; this verification process is summarized in Section 5.2.2.

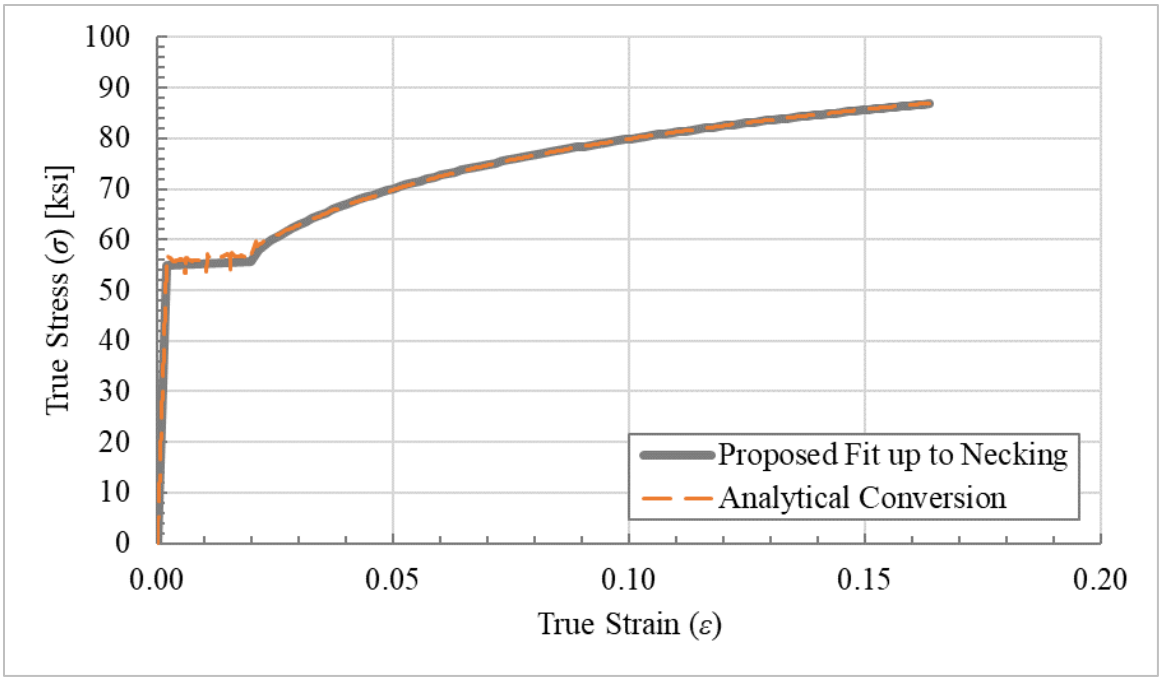

Figure 5-10: True Stress-Strain Relationship for Zone I through Zone IV

5.2.2 Verifying the Pre-Necking Response

While the pre-necking response can be determined entirely without execution of an FEA model, the final pre-necking true stress-strain relationship should typically be

analyzed to verify, prior to investigating the post-necking fit, that it is predicting and reproducing, adequately, the desired engineering stress-strain response. Therefore, a FEA model was developed to verify the response up to necking. The geometry was defined to match the actual coupon dimensions summarized in Table 5-1, and eighth-symmetry was used to reduce the size and runtime of the model. The final geometry and mesh discretization are illustrated in Figure 5-11 along with a diagram detailing the relationship between the eighth symmetry model and the full coupon specimen.

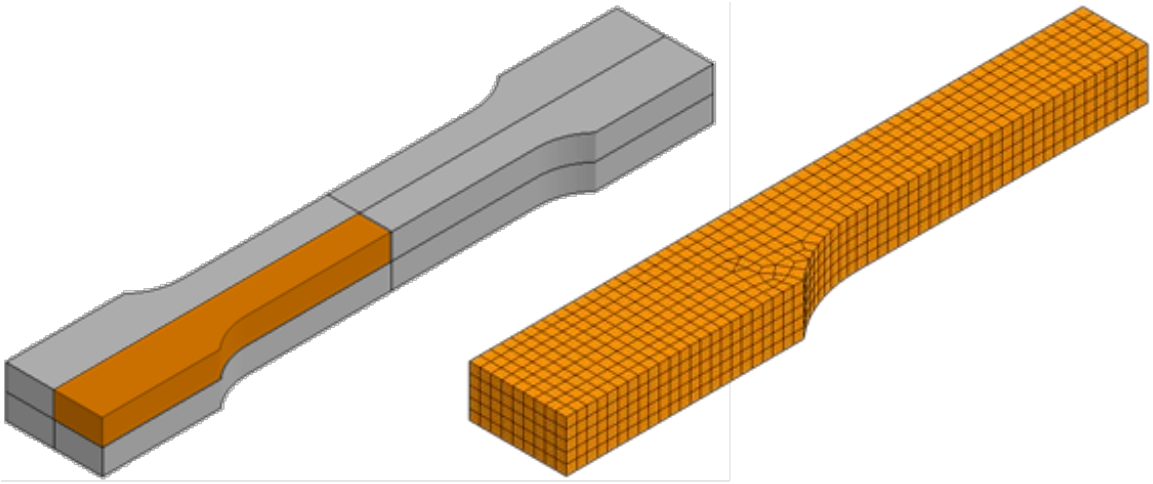

Figure 5-11: Eighth-symmetry Model and FEA Mesh Discretization

The model was analyzed using the proposed relationship illustrated in Figure 5-10 to define the material stress-strain response. The pre-necking relationship was extrapolated using the natural log relationship for the pre-necking response as an estimate of the post-necking response as shown in Figure 5-12. Then, the FEA model was analyzed using the implicit solver in LS-DYNA (see Appendix Section B.5).

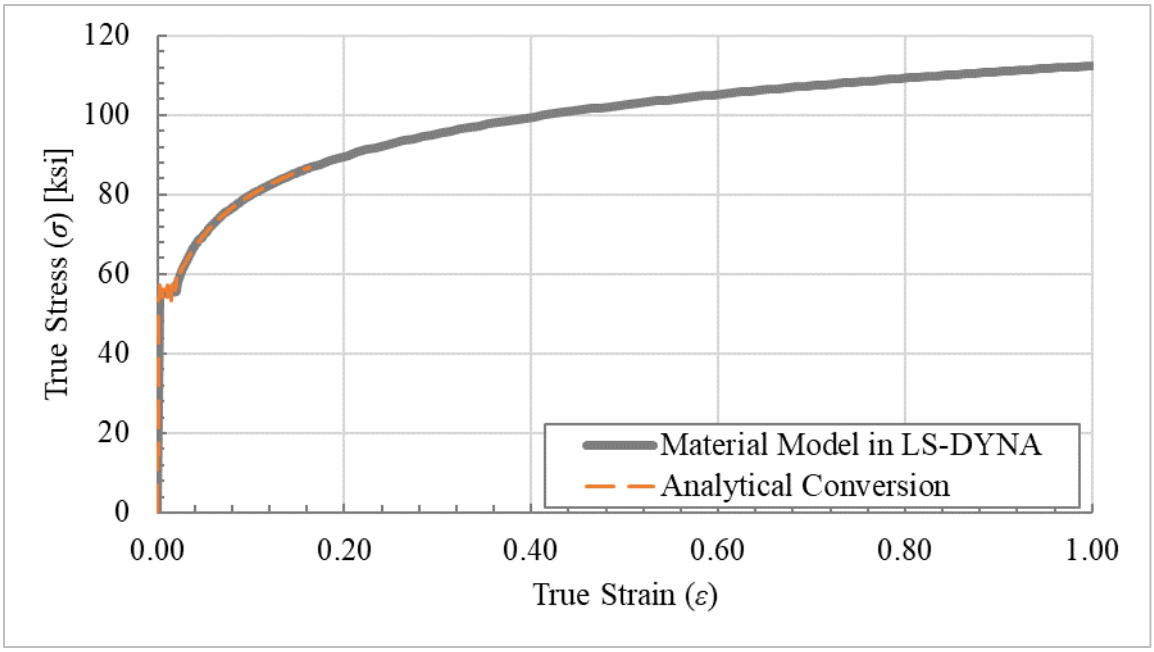

Figure 5-12: Pre-Necking Verification Model Material True Stress-Strain Relationship

The resulting predicted engineering stress-strain response of the coupon model using the FEA model is overlaid on the measured engineering stress-strain response from the physical coupon test in Figure 5-13. The engineering stress-strain response was calculated from the load-deformation data extracted from the FEA model (see Appendix Section B.8.3).

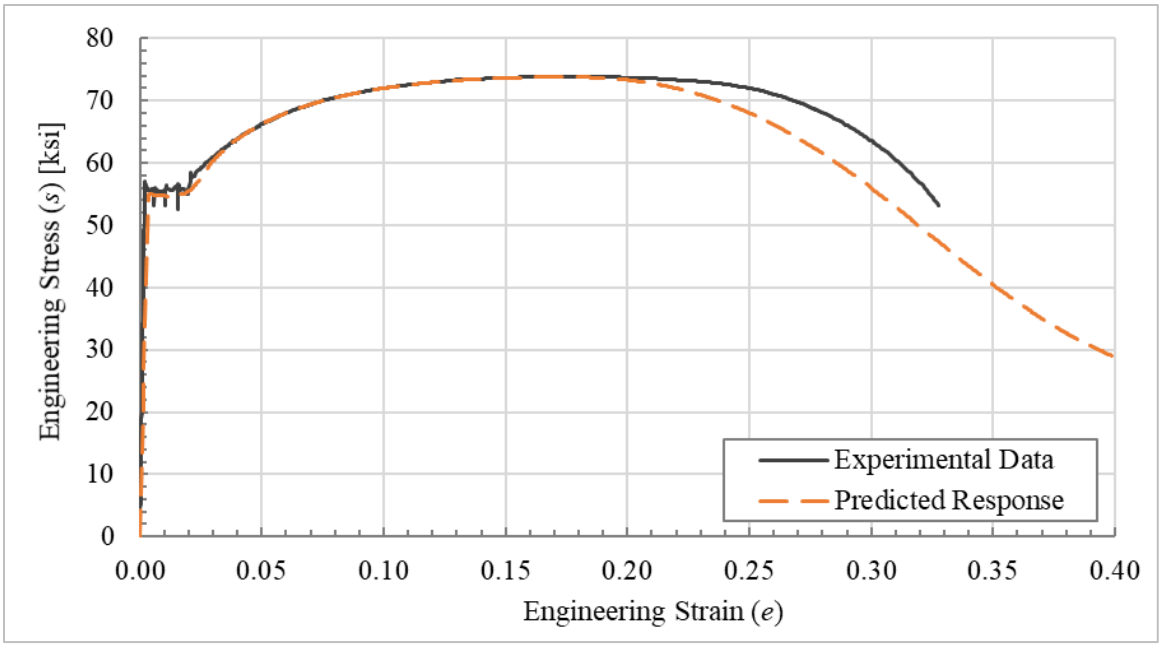

Figure 5-13: Comparison of Test Data and FEA Prediction

Based on review of this figure, it is clear that, up to necking, the engineering stress-strain relationship is captured accurately and precisely by the derived true stress-strain relationship and the FEA model. Beyond the onset of necking, the experimental data is underpredicted by the FEA model. Thus, the extrapolated pre-necking relationship can serve as the lower bound for the post-necking response narrowing the possible post-necking solutions versus the absolute lower bound of a function with zero slope, captured in Equation 4-60. Finally, with the pre-necking relationship fully defined and the onset of necking accurately captured, the iterative determination of the post necking relationship in Zone V can be performed, as described in detail in Section 4.3.5 and carried out for this example case in the following section.

5.3 Fitting the Post-Necking Response

As described in Section 4.3.5.3, the post-necking response can be rapidly fit by developing a family of viable true stress-strain relationships that lie between upper and

lower bounding solutions, similar to the approach recommended by Ling (Ling, 1996), Joun et al. (Joun, Choi, Eom, & Lee, 2007), and Arasaratnam et al. (Arasaratnam, Sivakumaran, & Tait, 2011). As noted, because the extrapolated pre-necking functional fit to the true stress-strain data underpredicted the experimental data, it will serve as the lower bound for this iterative procedure. The upper bound, per Section 4.3.5.3 and Equation 4-59, is then a linear function with slope equal to the stress at the onset of necking as any function with a steeper slope would result in a reversal in curvature, failing to obey Derivative Rule #3. Between these bounds lies a range of possible solutions for the post-necking true stress-strain relationship as illustrated in Figure 5-14.

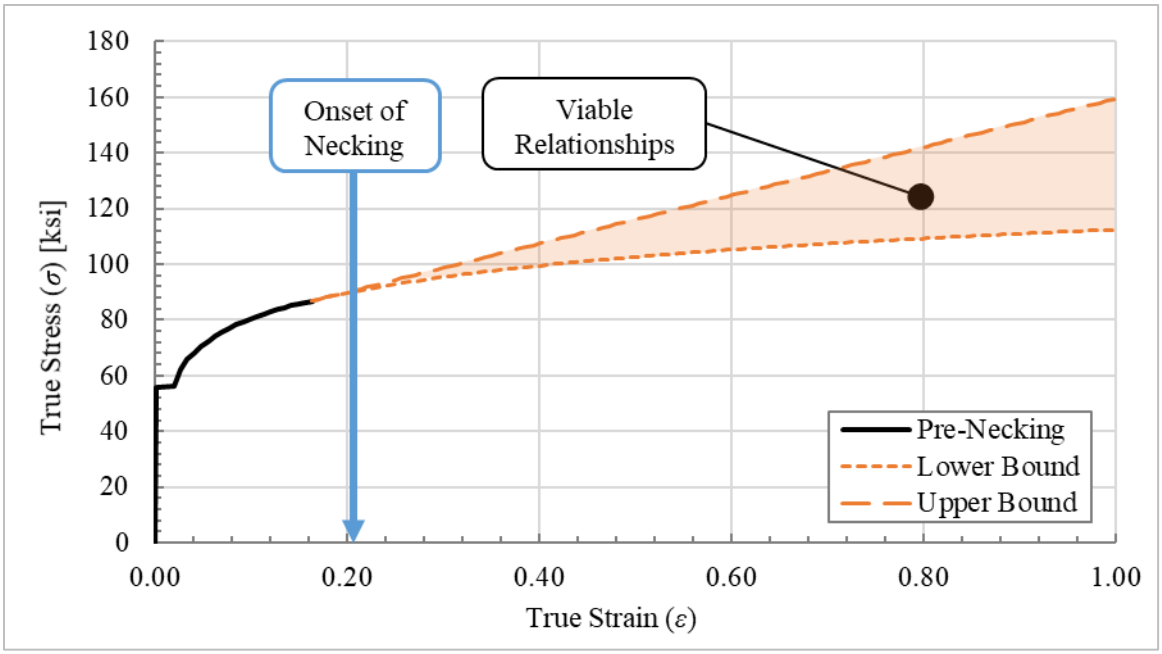

Figure 5-14: Bounding Post-Necking True Stress-Strain Relationships

With known bounding functions, a family of curves can be developed by applying Equation 4-58. For this example, viable relationships were developed by incrementing the weighting factor, *w*, by 0.2 over the range from zero to one. Thus, a family of six potential

true stress-strain relationships were defined for further investigation. These relationships are illustrated in Figure 5-15.

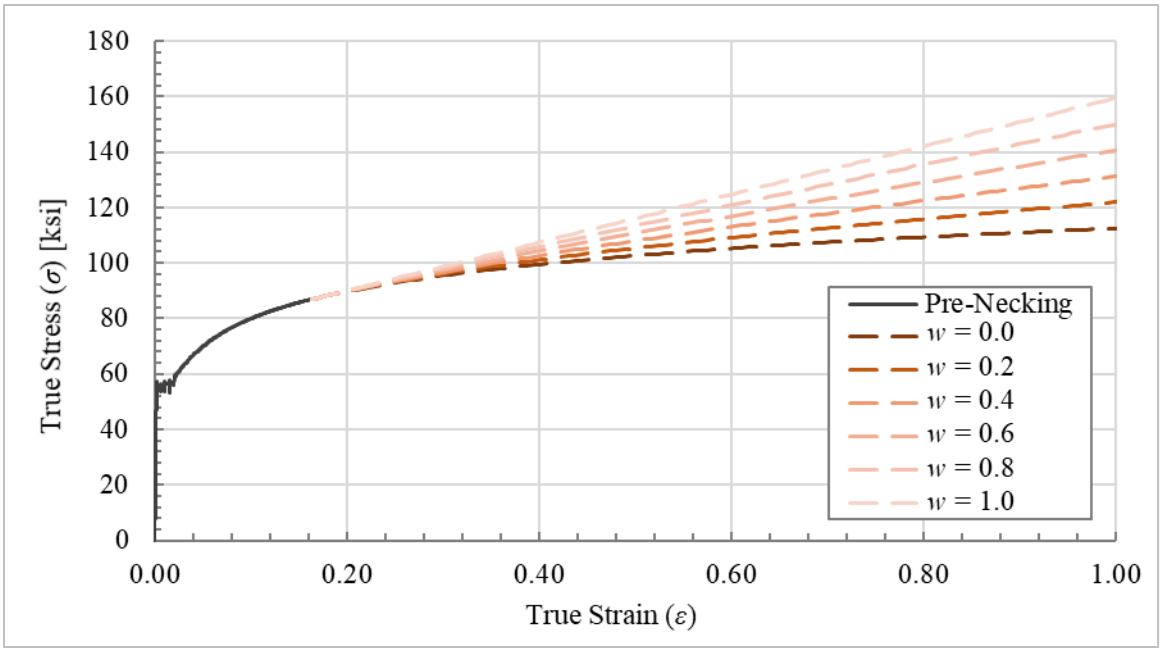

Figure 5-15: Post-Necking True Stress-Strain Relationships for Iterative Analysis

With these relationships defined, a FEA was performed using the previously discussed model for each of the six true stress-strain relationships to determine which provide the most accurate prediction of the experimental data and whether additional refinement would be required. As shown in Figure 5-16, the range of models accomplish the goal of both overpredicting the experimental data, in the case of the upper bound relationship, and underpredicting it, in the case of the lower bound relationship. In between, the relationships developed with weighting factors, w, equal to 0.4 and 0.6 provide the best fit to the data. These best fit relationships are extracted and plotted along with the experimental data in Figure 5-17.

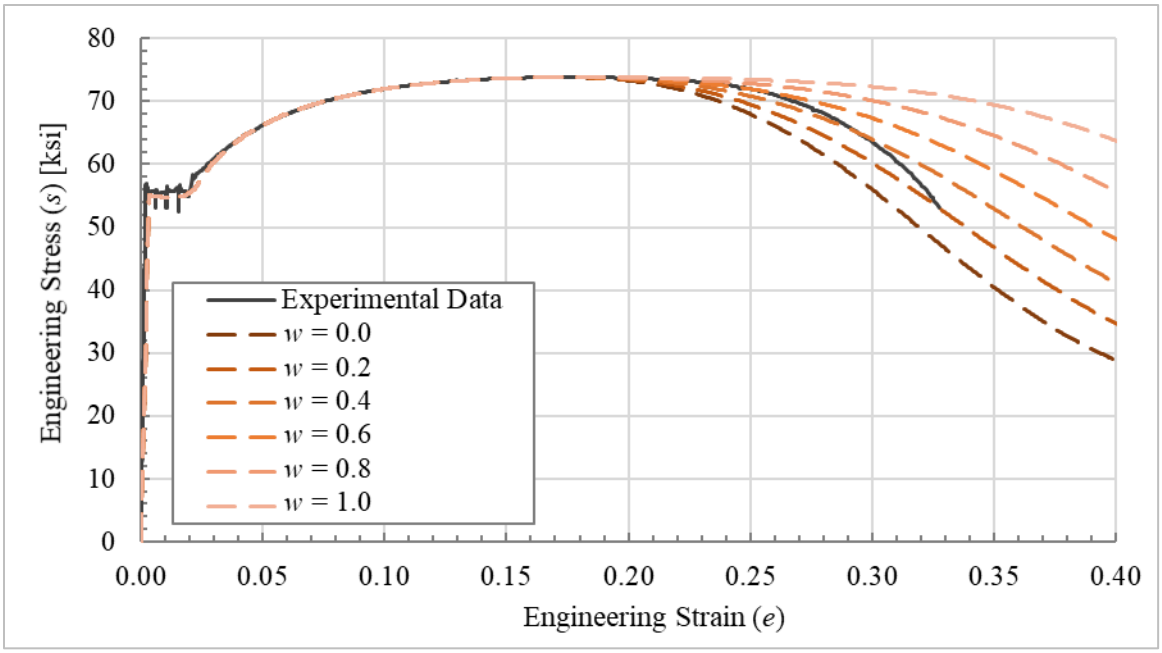

Figure 5-16: Iterative Analysis Model Results

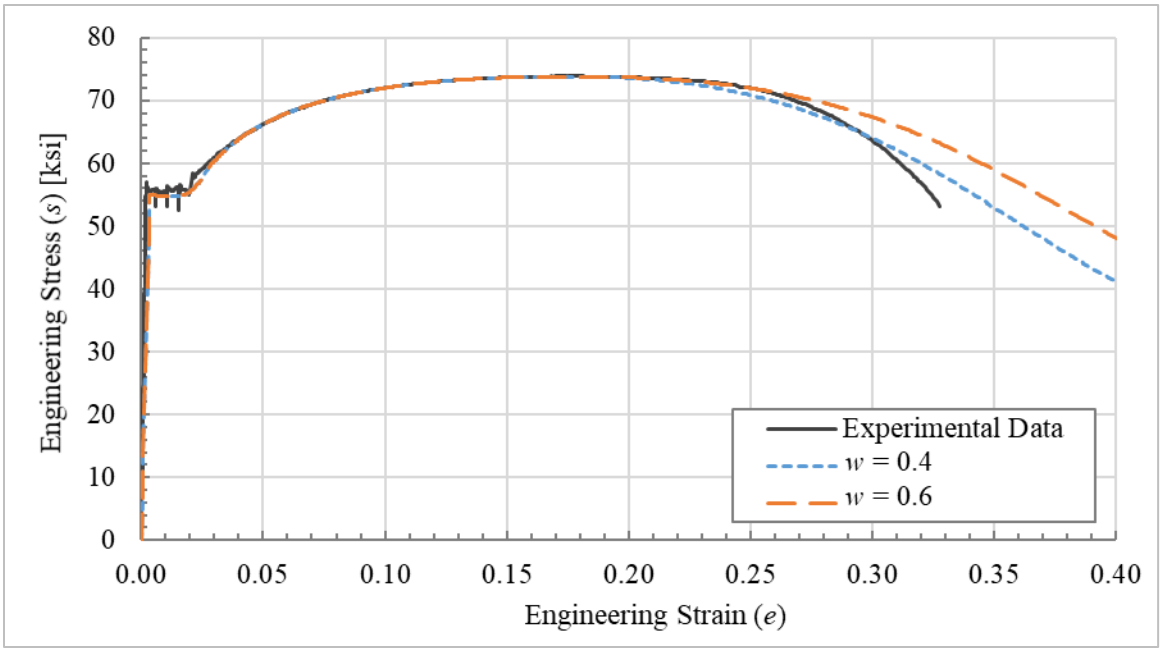

Figure 5-17: Best Fit to Experimental Data using Iterative Analysis

Depending on the potential application, either of these relationships may be adequate. However, additional refinement may be desired to provide a more precise fit. In

addition, it should be noted that no mesh refinement has been performed on this model, so the results may change with a smaller element size. While a detailed discussion of mesh refinement and convergence is beyond the scope of this dissertation, a simple example was developed to demonstrate the process and effect of mesh refinement for this example. Because mesh refinement generally softens the predicted behavior, the model with the weighting factor, *w*, equal to 0.6 was re-analyzed with a finer mesh, by dividing the mesh in half in all three directions resulting in eight times as many elements, as illustrated in Figure 5-18. The results of this refined model are presented along with the initial mesh and the experimental data in Figure 5-19. Note the softening of the post-necking response predicted with the refined mesh.

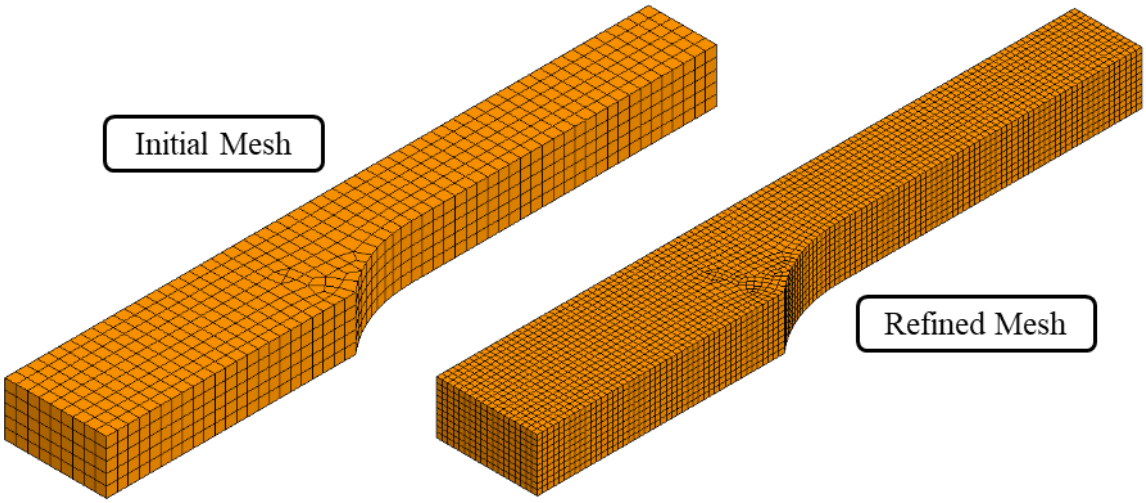

Figure 5-18: Refined Mesh in One-eighth Symmetry Model

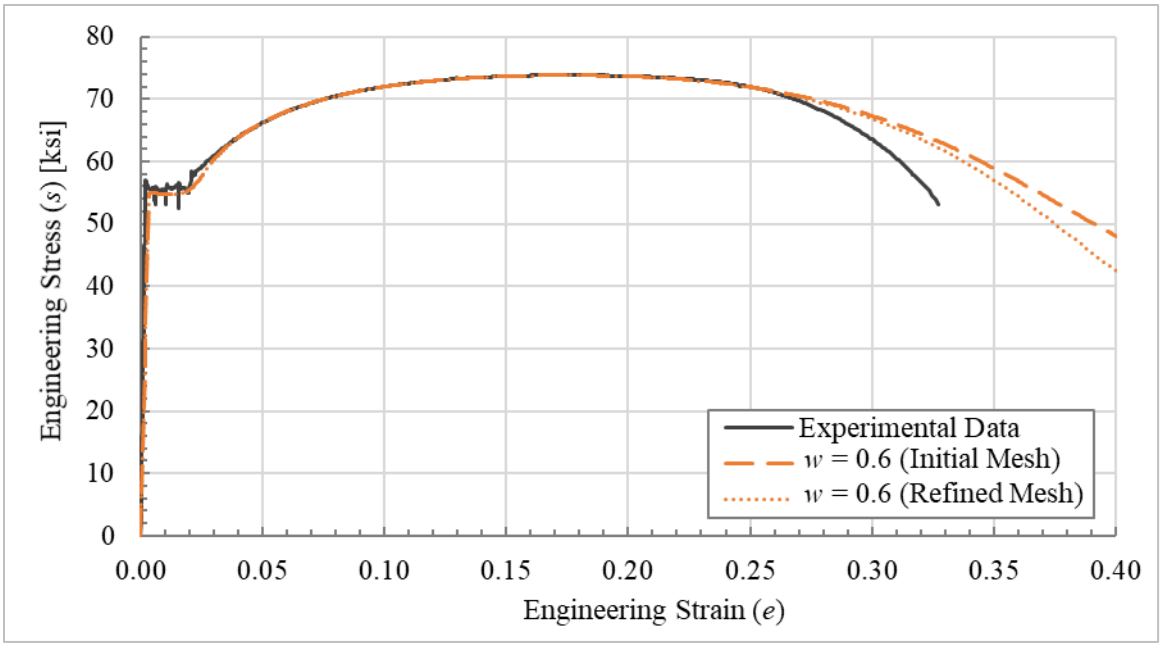

Figure 5-19: Mesh Refinement Results

Because the fit provided thus far still fails to accurately capture the late post-necking response up to fracture, additional refinement was performed. Specifically, to achieve a more precise fit, the weighting factor, w, was functionally varied as shown in Equation 4-61. Ultimately, a best fit to the experimental data was achieved by setting the weighting factor equal to an initial value of 0.65 at the onset of necking, and linearly reducing it to 0.1 at a strain of approximately 0.9 and holding it constant at 0.1 thereafter. As shown in Figure 5-20, the initial coarse mesh model just slightly overpredicts the experimental results. However, by repeating the mesh refinement discussed previously, halving the mesh in each orthogonal direction, the fit shown in Figure 5-21 was predicted.

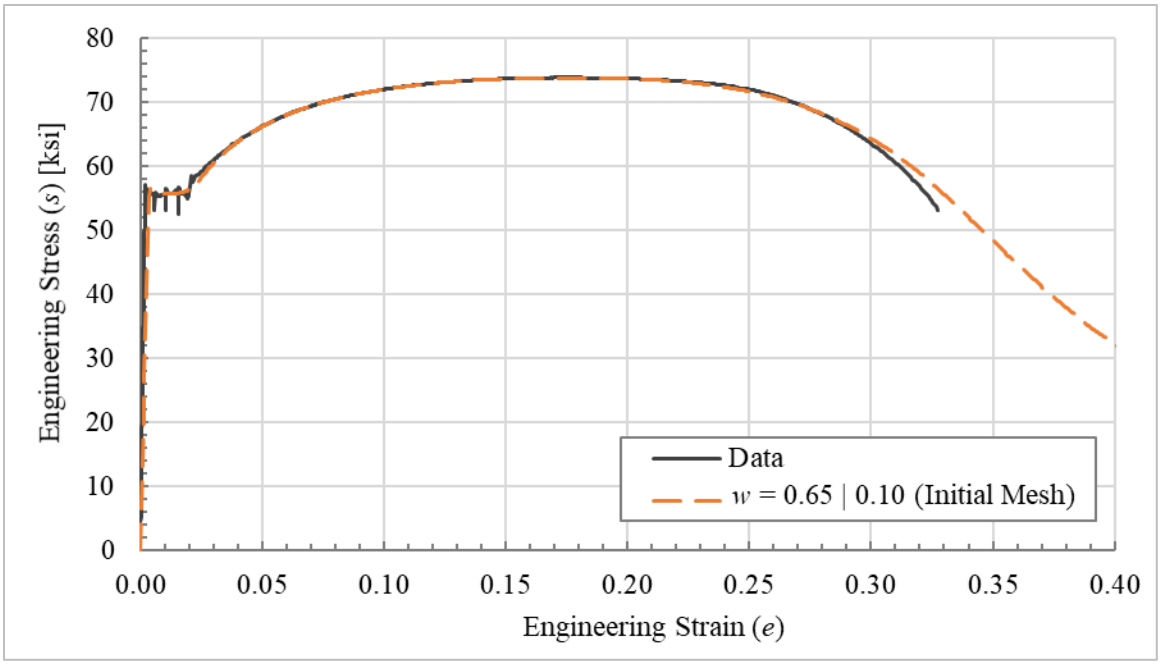

Figure 5-20: Functionally Defined Weighting Factor with Initial Coarse Mesh

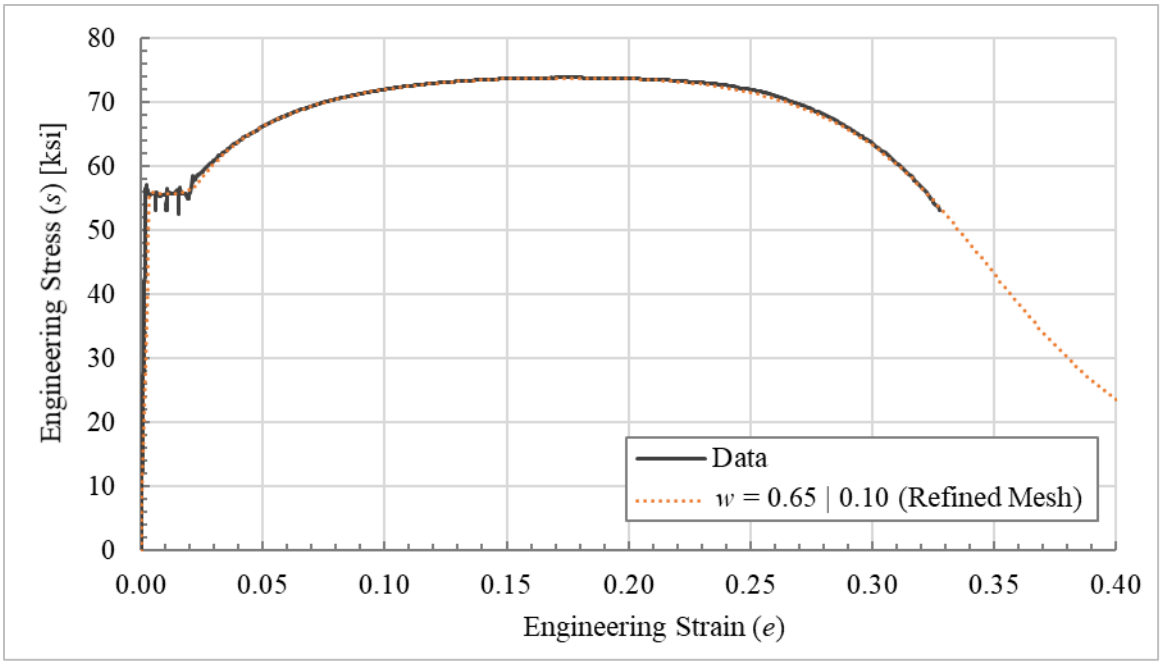

Figure 5-21: Functionally Defined Weighting Factor with Refined Mesh

Thus, with care, the true stress-strain relationship can be defined to precisely match a given set of experimental data from a standard coupon tension test provided the geometry of the coupon specimen is known. However, care should be taken to avoid significantly underpredicting the experimental data over any range of response, as discussed in Section 5.3.1. In addition, Section 5.3.2 provides a brief discussion of overfitting, using this example to illustrate that extreme precision may not be warranted given the inherent assumptions and limitations of continuum finite element analysis.

5.3.1 Underpredicting the Post-Necking Response

While beyond the scope of this dissertation, this section provides brief justification for avoiding underprediction of the post-necking response. For an example of underprediction, consider the family of viable solutions previously presented in Figure 5-17, specifically, the case with weighting factor, w, equal to 0.4. As shown in Figure 5-22, the post-necking response is underpredicted by this model just after the onset of necking.

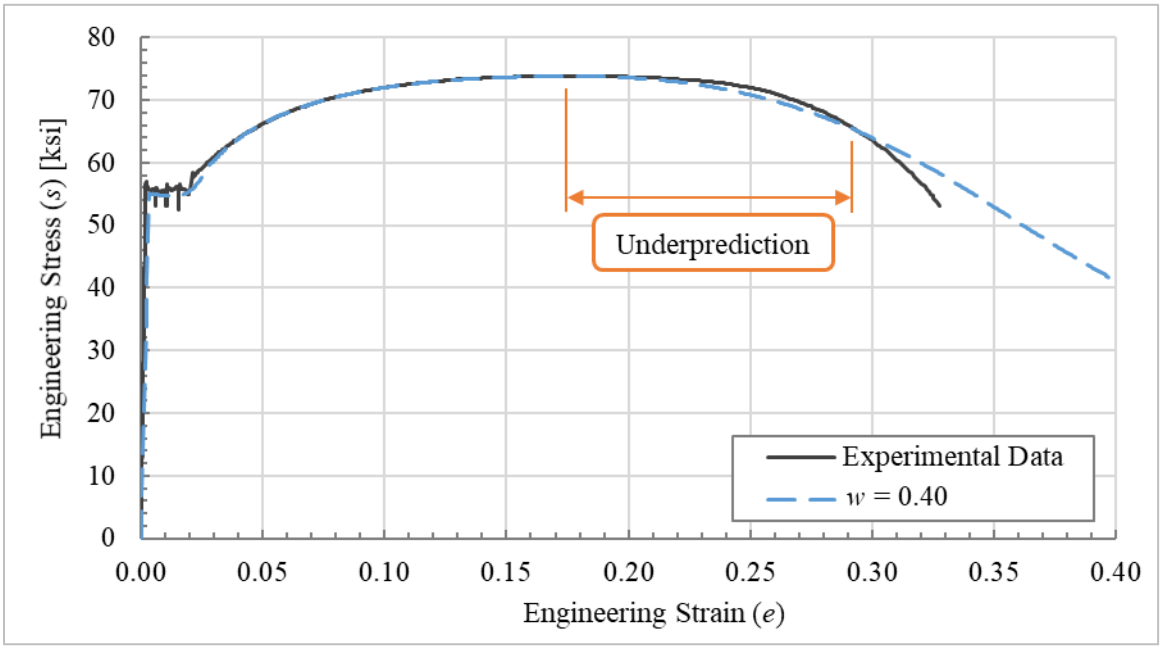

Figure 5-22: Underprediction of Post-Necking Response

Based on the experience gained in developing the recommendations in this dissertation, care should be taken to avoid using a true stress-strain relationship that significantly under predicts experimental results for two main reasons. First, through mesh refinement, the post-necking response tends to soften. As a result, when using a coarser mesh to determine the true stress-strain relationship, these underpredicting models will generally become worse through refinement, deviating further from the experimental data. Second, and most important, because the continuous material behavior assumed within an element is an approximation of the material response, it fails to capture true material-level phenomena in the post-necking branch; specifically, void nucleation, growth, and coalescence (see Section 2.9.4.2). While not in the scope of this dissertation, void nucleation, growth, and coalescence is a known contributor to material response at large strains in tension (Steinbrunner, Matlock, & Krauss, 1988) (Avramovic-Cingara, Saleh, Jain, & Wilkinson, 2009) (Scheyvaerts & Pardoen, 2010). This phenomenon, where microscopic voids within the material form, grow, and coalesce forming larger voids, cannot be captured directly by standard solid elements as the material is considered uniform and continuous. While, this mode of behavior is not captured in the model, its inclusion would result in additional observed softening of the predicted behavior. Therefore, underprediction should be avoided, as the application of the material true stress-strain relationship that under predicts tension response, particularly in the later post-necking response, to alternate states of stress, like compression, where voids are not a significant contributor to behavior will result in potentially significant inaccuracies.

5.3.2 Overfitting the Post-Necking Response

Overfitting is a problem that plagues many data driven areas of research, and material modeling is no exception. Overfitting refers to a modeling error where a function is too closely fit to a limited set of data, essentially fitting noise and variability within the

data and failing to accurately capture the underlying trend. In the context of material true stress-strain relationship development, the term overfitting is meant to capture the case where the relationship is developed to approximate the experimental data so precisely that it fits noise and experimental variability, and/or overcompensates for phenomena which cannot be directly captured, such as void formation, coalescence, and growth, as discussed in the previous example.

For example, the fit previously developed in this chapter and presented in Figure 5-21 is extremely accurate across the full range of response, including the full post-necking regime (Zone V) through fracture. This fit was purposely developed to predict a behavior that matches, as accurately and precisely as possible, the experimental data. However, such a fit would generally be non-ideal given the means and methods used in its development. Specifically, the use of continuum solid elements that are incapable of directly capturing material voids that occur prior to fracture. Thus, it is likely that such a precise fit will not extrapolate well to other states of stress where these material-level factors are minimal or non-contributors. To demonstrate, interrogation of the first derivative, shown in Figure 5-23, reveals that the slope of the true stress-strain relationship rapidly approaches zero after necking, at a strain of approximately 0.90.

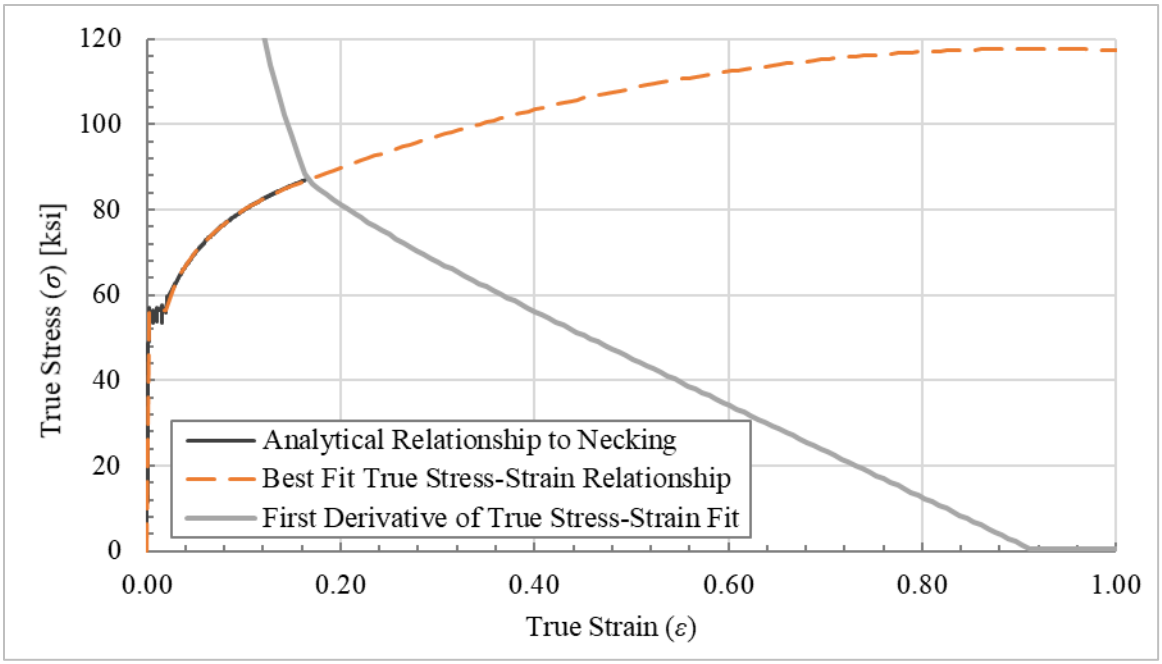

Figure 5-23: First Derivative for Best Fit Case presented in Figure 5-21

Examination of the FEA results revealed that true strains beyond this "kink" in the first derivative are predicted within the necked region of the model prior to the elongation associated with tension rupture. Thus, the presence of this feature has some level of influence on the results of the model that produced the best fit illustrated in Figure 5-21. Specifically, this near-zero slope condition likely softens the observed performance, especially just prior to the strain at fracture. While not confirmed in this research effort, it is suspected that this softening is not characteristic of the true material behavior and is required as a compensatory "overfitting" measure to capture the effect of material and microstructure level behaviors (e.g. void nucleation, growth and coalescence) that cannot be directly modeled using 3D continuum elements.

This theoretically inaccurate material true stress-strain relationship provides a more precise fit in this specific case; however, it is likely to produce inaccurate predictive results when applied to models with states of stress other than uniaxial tension and/or alternate

physical geometries and scales. Thus, because material true stress-strain relationships are often developed in this fashion and then applied to more complex models, care should be taken to avoid overfitting to match the results of the tension coupon test.

5.3.3 Additional Considerations for Capturing the Post-Necking Response

As described in Sections 5.3.1 and 5.3.2, material level phenomena like void nucleation, growth, and coalescence may not be well captured using standard FEA with solid continuum elements. Therefore, care should be taken to avoid underprediction and overfitting. In addition, other physical material behavior phenomena associated with post-necking response such as flow localization (Tvergaard, Needleman, & Lo, 1981), diffuse and localized necking (Lian & Zhou, 1989) (Ling, 1996) (Zhang, Hauge, Ødegard, & Thaulow, 1999) (Hyun, Kim, Bang, & Lee, 2014), plastic strain localization (Sun, Choi, Liu, & Khaleel, 2009), fracture initiation (Zhang & Li, 1994), and ductile fracture (T, 1998) (Hayden & Floreen, 1969), while beyond the scope of this dissertation, could also affect the process and approach to developing the true stress-strain relationship. These are all topics of ongoing research producing interesting results related to ductile metal behaviors and the stress-strain response of structural steels. Thus, they are worthy of further consideration and possible incorporation and combination with the rules and procedures proposed in this dissertation. However, additional research is required to determine whether and how to account for these effects when developing the material true stress-strain relationship, as discussed in Section 6.3.1.

5.4 FRACTURE AND FAILURE

Due to the breadth of interacting phenomena associated with fracture and failure of ductile metals like structural steel, accurately capturing these phenomena is a complex topic that is beyond the scope of this dissertation. However, a brief discussion of a simple

ultimate plastic strain approach for including fracture in the FEA model of a tension coupon is provided in Appendix Section B.9. In addition, because the ability to accurately predict fracture is important to understanding and predicting the post-necking response of ductile metals like structural steels, this topic is also a recommendation for additional work and future research, as discussed in Section 6.3.5.

5.5 CONCLUSIONS

As illustrated throughout this chapter, careful application of the derivative rules of Chapter 3 and the true stress-strain relationship development steps presented in Chapter 4 can produce a material true stress-strain relationship for FEA that is capable of capturing, extremely precisely, both the pre- and post-necking response of structural steels in tension. However, as discussed in Sections 5.3.1, 5.3.2, and 5.3.3, care must still be taken to ensure the material stress-strain relationship is able to be extrapolated to other states of stress, geometries, and model scales, and that the determined true stress-strain relationship is not somehow overfitting to compensate for an inability of the FEA methodology to capture material-level and microstructure-level behaviors such as void formation, growth, and coalescence, among others. Similarly, underprediction of the experimental data should generally be avoided, as most of the material behaviors that cannot be directly captured using three-dimensional (3D) solid continuum elements will result in additional softening. However, it is clear that prediction of the post-necking response of structural steels will surely benefit from a better understanding of these phenomena and their incorporation into the recommendations presented in this dissertation. Therefore, capturing these micro-level material phenomena is a topic for recommended future research, as discussed in Section 6.3.1.

In addition, while this methodology was developed for 3D solid elements, with careful modification it can be extended and adapted to alternate element formulations like two-dimensional (2D) shell elements or one-dimensional (1D) beam elements if the appropriate simplifications in these element formulations are properly accounted for when defining the material stress-strain relationship. Therefore, this is discussed as another potential topic for future research in Section 6.3.2. Similarly, material models other than the chosen **MAT_24*, or **MAT_PIECEWISE_LINEAR_PLASTICITY*, can be used when applying the methodology proposed in this dissertation without issue, provided the derivative rules and recommendations for functional continuity are obeyed. However, due to the breadth of available material models, detailed guidance on this process is beyond the scope of this dissertation.

Finally, while the focus of this dissertation is on fitting the post-necking response, discussion of capturing failure and fracture has been intentionally brief to maintain the narrow focus to this research. Failure in ductile metals is a complex issue encompassing many material level phenomena and interacting effects. However, accurate prediction of post-necking behavior includes accurate prediction of failure. Therefore, accounting for and capturing these interrelating phenomena across a range of states of stress is a topic that necessitates further investigation and consideration, particularly with respect to the methodologies and rules proposed in this dissertation. Thus, additional research into this topic is also recommended in Section 6.3.5.

6 SUMMARY, CONCLUSIONS, AND FUTURE WORK

6.1 INTRODUCTION

This dissertation begins with a detailed review of published literature related to ductile metal material behavior, focusing on necking and post-necking response. Next, three simple derivative rules are presented, which are intended to guide the process of developing the true stress-strain relationship for use in a finite element analysis (FEA) model with three-dimensional (3D) solid elements. Then, a step-by-step approach for determining the true stress-strain relationship for structural steel materials using standard tension coupon test data is presented, including reference to the three derivative rules. Finally, the recommended approach for developing the true stress-strain relationship is demonstrated for a real case to illustrate the process. While this approach could likely be directly applied or adapted to determine the true stress-strain relationship to other ductile metals, additional investigation and experimental validation is recommended prior to doing so.

The following sections present a summary of the most important findings of this research project. Section 6.2 provides a restatement of the three derivative rules followed by a concise summary of the basic steps recommended for quickly and efficiently developing the true stress-strain relationship for structural steel materials. Section 6.3 provides a summary of recommendations for future research work to address next steps, limitations, and issues encountered and identified during this research and the development of this dissertation.

6.2 SUMMARY

The primary contributions to new understanding developed through this research work are the three derivative rules and the step-by-step methodology for developing the

true stress-strain relationship for FEA of structural steels using 3D elements. The derivative rules, discussed in detail in Chapter 3, are summarized in Section 6.2.1. The step-by-step methodology, discussed in detail in Chapter 4, is summarized in Section 6.2.2.

6.2.1 Derivative Rules

As described in Chapter 3, there are three fundamental rules that must be followed to precisely predict necking, maintain numerical stability, and avoid prediction of neck stabilization and cold-drawing in a FEA model of a ductile metal (e.g., structural steel) coupon loaded in uniaxial tension. Each of these rules can be presented in the form of a simple relationship for the true stress-strain function and its first and second derivatives. These three "derivative rules" are presented in Equation 6-1, Equation 6-2, and Equation 6-3 for Derivative Rule #1, #2, and #3, respectively.

$$\sigma(\varepsilon_{max}) = \frac{d\sigma(\varepsilon_{max})}{d\varepsilon} \qquad \text{Equation 6-1}$$

$$\frac{d\sigma}{d\varepsilon} \geq 0 \qquad \text{Equation 6-2}$$

$$\frac{d^2\sigma}{d\varepsilon^2} \leq 0 \qquad \text{Equation 6-3}$$

Derivative Rule #1 is a restatement of Considère's Construction. It is best understood as the precise point where the relationship between the rates of material strain-hardening and of geometric softening are equal. This condition occurs at the precise onset of necking, as summarized in Section 3.2.1. Derivative Rule #2 is a uniaxial presentation of Drucker's first stability criterion for materials, originally proposed by Hill. Obeying this rule ensures the incremental internal energy can only increase with increasing strain and

assures that the material stress-strain relationship remains numerically and computationally stable. Derivative Rule #3 was developed based on observations of drawing materials, like certain polymers. For cold-drawing to occur, there must be a curvature reversal in the material true stress-strain relationship after necking. Thus, by obeying this rule, the model will not predict stabilized necking and cold-drawing behavior, a mode of response not exhibited by ductile metals. This rule is particularly important as this observation has not been applied to ductile metals like structural steel and is a new and unique contribution of this research.

By ensuring the true stress-strain definitions developed for computational analysis of ductile metals follow these simple rules, the resulting model will accurately predict necking (Rule #1), be numerically stable (Rule #2), and avoid prediction of neck stabilization and cold-drawing (Rule #3). By incorporating these rules into the process by which one develops a true stress-strain relationship for FEA using 3D solid elements, several common errors can be avoided, expediting the process of developing appropriate constitutive material models, often improving the quality of the final result.

6.2.2 Process to Develop the True Stress-Strain Relationship

The recommended procedure for developing the true stress-strain relationship for computational analysis of structural steel materials is described in detail in Chapter 4, including derivation of several key relationships that improve the accuracy and efficiency of the process. Table 6-1 provides a brief summary of the key steps. Note that, while many researchers have proposed similar piece-wise fitting approaches to developing the true stress-strain relationship for ductile metals, this particular approach provides additional focus on physics and behavior, through application of the derivative rules, and on maintaining continuity in the first derivative between zones and at critical points (e.g., the onset of necking).

Table 6-1: Proposed Steps to Develop True Stress-Strain Relationship

Step	Zone	Description
1	I	Fit the linear elastic response with a linear function matching the analytical conversion of the measured engineering stress-strain relationship, developed from the tested coupon's load-deformation data.
2	II	Where present, fit the non-linear elastic response by matching the analytical conversion of the measured engineering stress-strain relationship, developed from the tested coupon's load-deformation data. For cases where the non-linear elastic branch deviates tangentially, ensure the fit to this zone maintains slope continuity with Zone I.
3	III	Where present, fit the yield plateau with a linear function matching the analytical conversion of the measured engineering stress-strain relationship, developed from the tested coupon's load-deformation data.
4	IV	Fit the strain-hardening branch by matching the analytical conversion of the measured engineering stress-strain relationship. A functional relationship is recommended to ensure that the derivative rules are met over the full range of response, especially at the onset of necking. As required, ensure appropriate first-derivative values at each end of this zone of response (i.e., strain-hardening modulus, and onset of necking).
5	V	Determine the best fit for the post-necking strain-softening branch through an iterative approach where bounds are determined by examining the extrapolated pre-necking fit, as well as one or more other bounding relationships which include a linear function with zero slope (absolute lower bound) and a linear function with slope equal to the true stress at the onset of necking, σ_{max} (absolute upper bound). Avoid under-prediction of the post-necking response and overfitting of the data.

While the proposed approach may be improved and expedited through additional refinement and/or automation of some or all of the steps (discussed in Section 6.3.6), it provides step-by-step guidance for the critical steps required to determine the true stress-strain relationship for structural steels from only the typical data developed in a standard tension coupon test. In addition, despite the lengthy description and discussion of the process presented in Chapter 4, as demonstrated in Chapter 5, this process can be executed quite rapidly and is capable of producing highly accurate predictions of experimental results with a standard computational FEA model using 3D continuum elements.

6.3 RECOMMENDED FUTURE WORK

While conducting the research for this dissertation, several key areas for additional future work were identified. Further investigation of each of these recommended topics could potentially improve and refine the methods and rules presented in this dissertation. These topics, discussed in the following sections, are not intended to capture the full breadth of potential areas for additional research that can result in improvements to the rules and methodologies discussed herein. Rather, they represent clear next steps for improving and further formalizing the process of developing the true stress-strain relationship for computational analysis of structural steels.

6.3.1 Incorporating Material-Level Post-Necking Phenomena

FEA using 3D solid elements is founded upon several assumptions about material behaviors. Of relevance to this research is the assumption of material continuity within a given element. Due to this assumption, material-level phenomena like void formation, growth, and coalescence, are not directly captured. In addition, because material response is dependent on the state of stress (e.g., void formation being predicted in tension but not compression), more complex material true stress-strain relationships may be required to

accurately capture these effects. Additional research is therefore recommended to evaluate best practices for incorporating such material behaviors into an FEA model. Ultimately, through incorporation and inclusions of these material-level phenomena, predicted response at higher levels of plastic strain, including post-necking response in tension, could be further improved.

Similarly, other related post-necking phenomena observed in structural steels and other ductile metals, such as flow localization, diffuse and localized necking, plastic strain localization, fracture initiation, and ductile fracture, should be similarly incorporated, as appropriate. Additional investigation of these phenomenon is recommended, particularly with respect to fitting the final portion of the stress-strain curve where the methods recommended herein tend to over-predict strength just prior to fracture. By incorporating lessons learned from research into material behaviors that cannot be directly captured using standard 3D solid continuum elements in FEA models, it may be possible that some or all of this over-prediction could be remedied.

6.3.2 Application to Alternative Element Formulations

The derivative rules and step-by-step approach for developing the true stress-strain relationship presented in this dissertation were determined specifically for three-dimensional (3D) solid continuum elements. However, alternative element types such as one-dimensional (1D) beams, two-dimensional (2D) plates, and 2D shells, may be more appropriate for a given application. Due to the changes in the assumptions made in developing the element formulations for these other element types, the recommendations presented in this dissertation cannot be directly applied without modification. Therefore, application of the proposed rules and recommendations presented in this dissertation to other element formulations is recommended as an area of future research. This work could include a detailed vetting of the recommendations presented herein, modifications for 1D

and 2D elements as well as other element types (e.g., SPH, ALE, etc.), and additional modifications and limitations associated with the use of these other element formulations.

6.3.3 Application to Alternate Mesh Densities

The process described for developing the true stress-strain relationship for structural steels presented in this dissertation is often an early step in developing larger scale component (e.g., bolt), sub-system (e.g., connection), and system (e.g., frame) level FEA models. Frequently, these larger models utilize coarser meshes through some or all of the components. Thus, in addition to the recommended investigation of application of this approach to alternative element formulations presented in Section 6.3.2, it is recommended additional research time and effort are spent in understanding the process of taking a material model developed using a relatively fine mesh and capturing the impact of coarser meshes.

6.3.4 Application to Other Ductile Metals

As alluded to and mentioned several times in this dissertation, it is likely that much or all of the conclusions, rules, and procedures described in herein could be applied to other ductile metal materials like aluminum or copper. For example, the derivative rules from Chapter 3, which form much of the basis for the recommended procedure for determining the true stress-strain relationship in Chapter 4, were borne from review of the behavior of ductile metals in general, not steel alone. Therefore, it is likely that they could see direct application to other ductile metals. However, the necessary validation and verification of such an approach was not undertaken in this research. Therefore, additional research, critical review, and thoughtful consideration are required to determine if and how these rules procedures can be applied to other ductile metals.

6.3.5 Fracture and Failure

Fracture and material failure are complex phenomena with an extensive body of associated research. Due to the complexities associated with failure of ductile metals, the topic of fracture was not covered in the research conducted for this dissertation. Nonetheless, the recommendations presented herein could be greatly improved by accompanying guidance on phenomena associated with failure and fracture of ductile metals, and direction on defining appropriate failure criteria for use in FEA. While this guidance does exist, to some extent, across a range of research publications and technical guidance documents, adaptation and alignment with the methods presented in this dissertation would prove useful. Therefore, additional research, particularly consolidating and coordinating the existing body of research on the topic is recommended.

6.3.6 Automation and Integration with Error Minimizing Approaches

Given the level of detail and repetition in the presented step-by-step guidance for developing the true stress-strain relationship, particularly for the pre-necking response, there is excellent potential for automation and incorporation with existing iterative computational error minimizing approaches, such as those discussed in Section 2.9.2. Where these current approaches fall short is in their apparent focus purely on accurate data fitting, leaving them prone to overfitting errors and inefficiencies. Thus, these iterative error minimizing approaches could benefit greatly from an approach to fitting the pre-necking response that requires no iteration, along with the application of rules to guide the iteration process, ensuring that each iteratively chosen post-necking point does not violate criteria that govern material response and numerical stability.

For example, the derivative rules presented in Chapter 3 could be applied to guide the post-necking iterative error minimization process, thereby constraining the possible viable solutions at each iteration step. As a result, iteration time would likely be reduced

and improvements in the speed and accuracy of such approaches would likely result. In addition, through application of these rules, errors such as overfitting will be reduced because the act of overfitting often requires violation of these rules to fit the noise and variability often present in experimental data. An example of how these rules could be applied to the general iterative error minimizing process is illustrated in Figure 6-1.

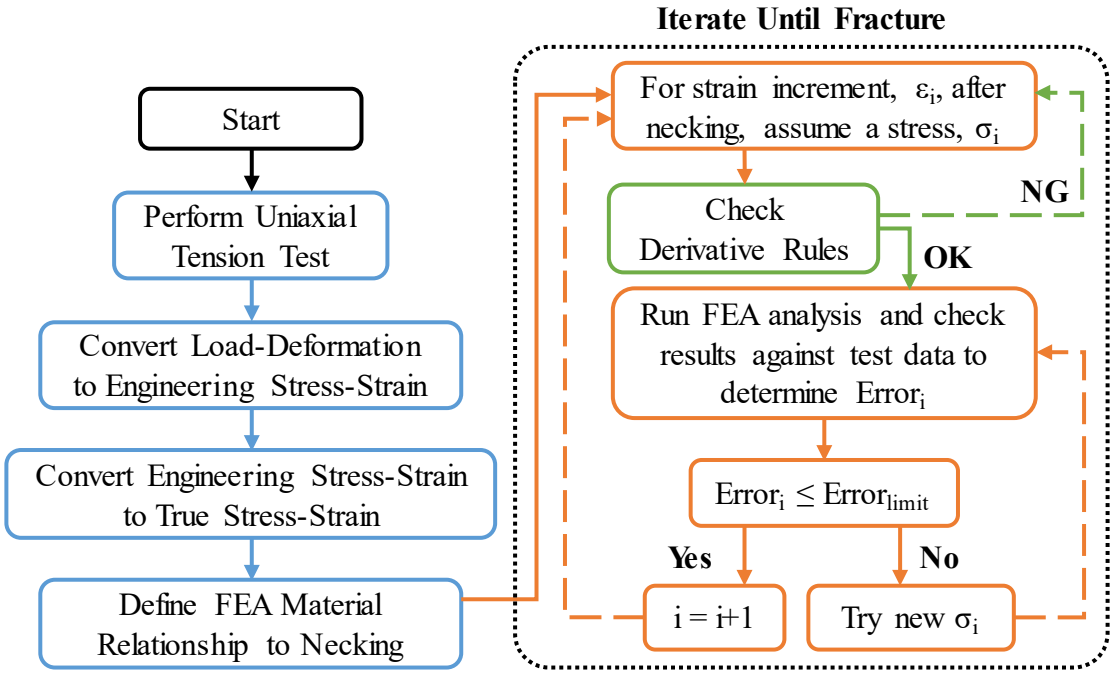

Figure 6-1: Application of Derivative Rules to Iterative Error Minimization Techniques

6.4 CONCLUSIONS

The guidance and recommendations for determining the true stress-strain relationship for structural steels presented in this dissertation was developed with two primary goals in mind: simplicity and broad applicability. Of particular importance are the three derivative rules. These rules, distilled from existing research, provide simple guidelines for capturing necking, maintaining computational stability and uniqueness, and prohibiting post-necking cold-drawing behavior. Moreover, to avoid excessive complexity,

elaborate experimental measurement techniques were avoided. Rather, the rules and the recommendations for determining the true stress-strain relationship presented in this dissertation require only the information that can be determined during a standard coupon tension test. By taking this approach, the recommendations lend themselves to broader use in a variety of industries and applications. Finally, as demonstrated through example (see Chapter 5), application of the recommendations presented in this dissertation can produce a material model that is capable of predicting both pre- and post-necking tension response of structural steels quite accurately. It is the hope of the author that the relative simplicity of the rules and recommendations, along with the limited requirements for experimental testing, encourage others to adopt, refine, and improve the presented means and methods through additional research.

There is still considerable room for additional research on this topic, however. As noted in Section 6.3, some simple additions and improvements could be made by reviewing the proposed rules and recommendations presented in this dissertation for additional element formulations. There also appears to be significant potential to incorporate material-level phenomena to improve how late post-necking response is captured. In addition, through incorporation and automation of the recommendations presented herein, speed and accuracy of iterative error minimizing techniques used to develop the true stress-strain relationship for structural steels in tension could be improved significantly. Thus, through additional research and application of lessons learned to the rules and recommendations in this dissertation, the process of developing the material true stress-strain relationship for use in FEA models has the potential to become quite fast and precise, allowing research focus to shift toward the investigation and prediction of more complex and nuanced material- and microstructure-level phenomena such as void formation, growth, and coalescence, diffuse and localized necking, and even dislocation motion. While this effort

has maintained a limited focus, it is the authors hope that it serves others as one more small step toward accurate prediction of the load-deformation behavior of ductile metals.

APPENDIX A: EXPERIMENTAL DATA

A.1 INTRODUCTION

The following sections summarize the test data used throughout this dissertation to illustrate various relationships, issues, and steps in the process of developing the true stress-strain relationship for use in finite element analysis (FEA) models using three-dimensional (3D) solid elements. Included within the following test data are a variety of coupon geometries and material grades to demonstrate a range of stress-strain relationships for structural steels. A summary of the specimen geometries, typical experimental test setup, measured load-deformation curves, and derived engineering stress-strain curves is provided in the following sections. All testing was performed at relatively low strain rates to produce quasi-static results, minimizing strain-rate effects on material response.

Tension coupon test data for specimens **A** through **P**, summarized in Section A.4, were developed as a part of progressive collapse research effort lead by Dr. Michalis Hadjioannou and published in the 2015 University of Texas at Austin Civil Engineering Department Doctoral Dissertation titled *Large-Scale Testing and Numerical Simulations of Composite Floor Slabs Under Progressive Collapse Scenarios* (Hadjioannou, 2015). Tension coupon **Q** was tested as a part of this research effort to incorporate an additional material and geometry type for additional calibration data.

A.2 COUPON GEOMETRY

The geometry of each of the four coupon types included in this chapter is summarized in Figure A-1 and Table A-1. The coupons represent a variety of geometries. Width and thickness of the center region – W and T, respectively – are reported as averages of multiple measurements. The remainder of the dimensions are nominal values.

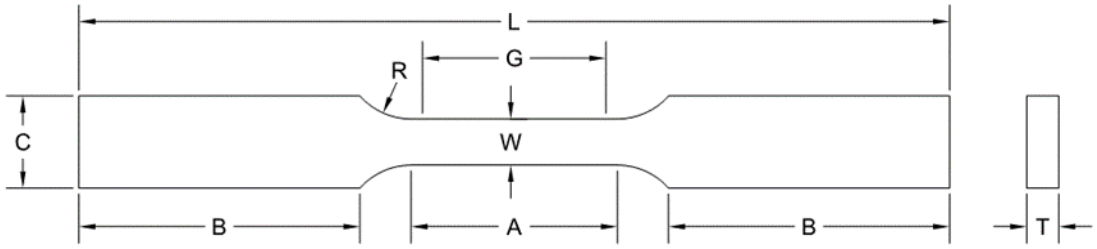

Figure A-1: Generalized Tension Coupon Geometry

Table A-1: Tension Coupon Dimensions

Coupon	**Coupon Dimensions [in]**							
ID	*A*	*B*	*C*	*G*	*L*	*R*	*T*	*W*
A	2.50	4.25	1.00	2.00	12.0	0.75	0.166	0.506
B	2.50	4.25	1.00	2.00	12.0	0.75	0.166	0.506
C	2.50	4.25	1.00	2.00	12.0	0.75	0.209	0.506
D	2.50	4.25	1.00	2.00	12.0	0.75	0.211	0.504
E	2.50	4.25	1.00	2.00	12.0	0.75	0.196	0.505
F	2.50	4.25	1.00	2.00	12.0	0.75	0.197	0.502
G	2.50	4.25	1.00	2.00	12.0	0.75	0.231	0.505
H	2.50	4.25	1.00	2.00	12.0	0.75	0.234	0.505
I	1.25	2.00	1.00	1.00	7.25	0.25	0.190	0.249
J	1.25	2.00	1.00	1.00	7.25	0.25	0.185	0.249
K	1.25	2.00	1.00	1.00	7.25	0.25	0.177	0.246
L	1.25	2.00	1.00	1.00	7.25	0.25	0.188	0.251
M	2.50	4.25	1.00	2.00	12.0	0.75	0.029	0.492
N	2.50	4.25	1.00	2.00	12.0	0.75	0.029	0.497
O	2.50	4.25	1.00	2.00	12.0	0.75	0.032	0.496
P	2.50	4.25	1.00	2.00	12.0	0.75	0.029	0.498
Q	11.00	2.50	1.94	8.00	18.5	1.25	0.901	1.510

A.3 COUPON SECTION AND MATERIAL TYPES

These coupons represent a variety of steel materials including two grades of standard structural steel used for hot-rolled sections, and cold-formed stainless steel used in structural metal decking. A summary of the materials and members from which each coupon was cut is provided in Table A-2.

Table A-2: Tension Coupon Materials and Members

Coupon ID	Member Type	Member Size	Coupon Location	Material Type
A	Wide Flange	W6×9	Web	A992 Gr. 50
B	Wide Flange	W6×9	Web	A992 Gr. 50
C	Wide Flange	W6×9	Flange	A992 Gr. 50
D	Wide Flange	W6×9	Flange	A992 Gr. 50
E	Wide Flange	W12×14	Web	A992 Gr. 50
F	Wide Flange	W12×14	Web	A992 Gr. 50
G	Wide Flange	W12×14	Flange	A992 Gr. 50
H	Wide Flange	W12×14	Flange	A992 Gr. 50
I	Angle	L2½×2×3/16	---	A36
J	Angle	L2½×2×3/16	---	A36
K	Plate	3/16-in. Thick	---	A36
L	Plate	3/16-in. Thick	---	A36
M	Cold-form Ribbed Deck	Vulcraft 2VLI22	---	A653 (SS) Gr. 50
N	Cold-form Ribbed Deck	Vulcraft 2VLI22	---	A653 (SS) Gr. 50
O	Cold-form Ribbed Deck	Vulcraft 2VLI22	---	A653 (SS) Gr. 50
P	Cold-form Ribbed Deck	Vulcraft 2VLI22	---	A653 (SS) Gr. 50
Q	Wide Flange	W12×96	Flange	A992 Gr. 50

A.4 DATA AND RESULTS

Applied load data for tension coupon tests were typically collected using the built-in load cell in the testing machine, and deformation data over a preset gauge length were collected using a clip-on extensometer capable of measuring large deformations and remaining attached up to and through coupon fracture. Data were measured at a high sample rate to ensure critical features like the onset of yielding, yield plateau, onset of strain hardening, and the failure branch were captured accurately. Tension coupon load-deformation curves were converted to engineering stress-strain curves using standard relationships. Load, P, was converted to engineering stress, s, using Equation A-1 and deformation was converted to engineering strain, e, using Equation A-2.

$$s = \frac{P}{A_o} \qquad \text{Equation A-1}$$

$$e = \frac{L - L_o}{L_o} = \frac{\Delta}{L_o} \qquad \text{Equation A-2}$$

where P = Applied load

A_o = Initial cross-sectional area of the specimen

L = Current length measured by the extensometer

L_o = Initial length measured by the extensometer

Δ = Deformation measured by the extensometer

Engineering stress-strain curves are summarized for each coupon and material type. Direct conversion of the raw measured load-deformation data from each tension test, grouped by material and coupon geometry, are illustrated in Figure A-2 for A992 Gr. 50 W-beam web coupons, Figure A-3 for A992 Gr. 50 W-beam flange coupons, Figure A-4

for A36 angle coupons, Figure A-5 for A36 plate coupons, and Figure A-6 for A653 Gr. 50 stainless steel cold-formed deck coupons.

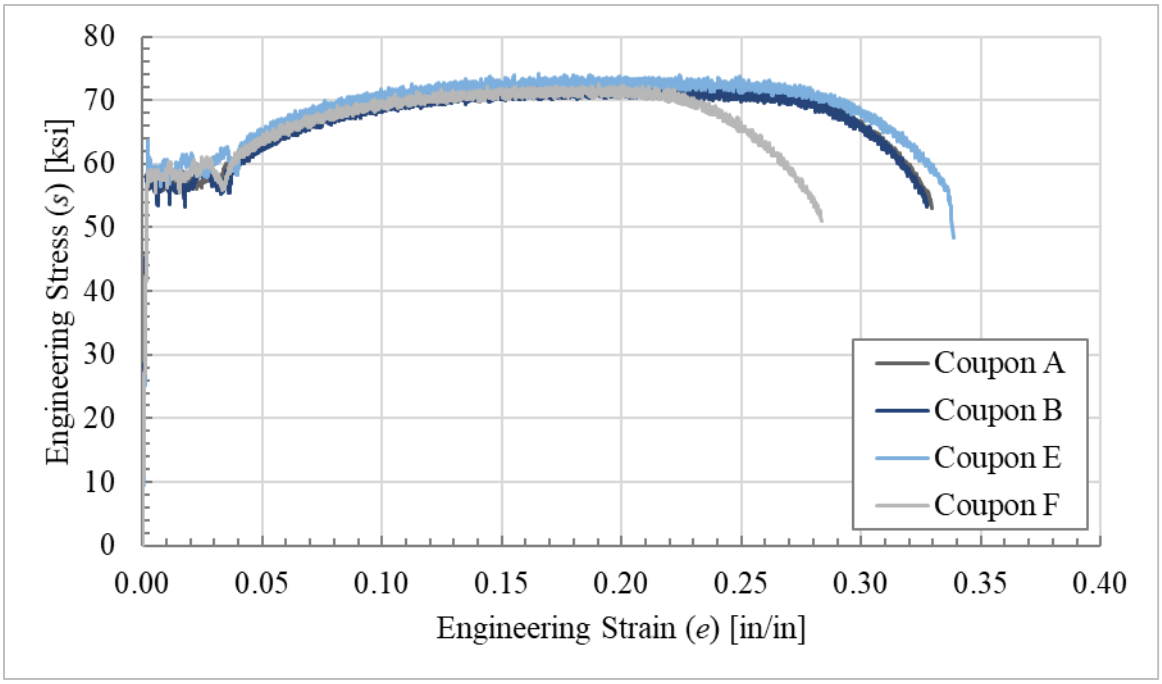

Figure A-2: Stress Strain Curves - A992 Gr. 50 W-Web Coupons

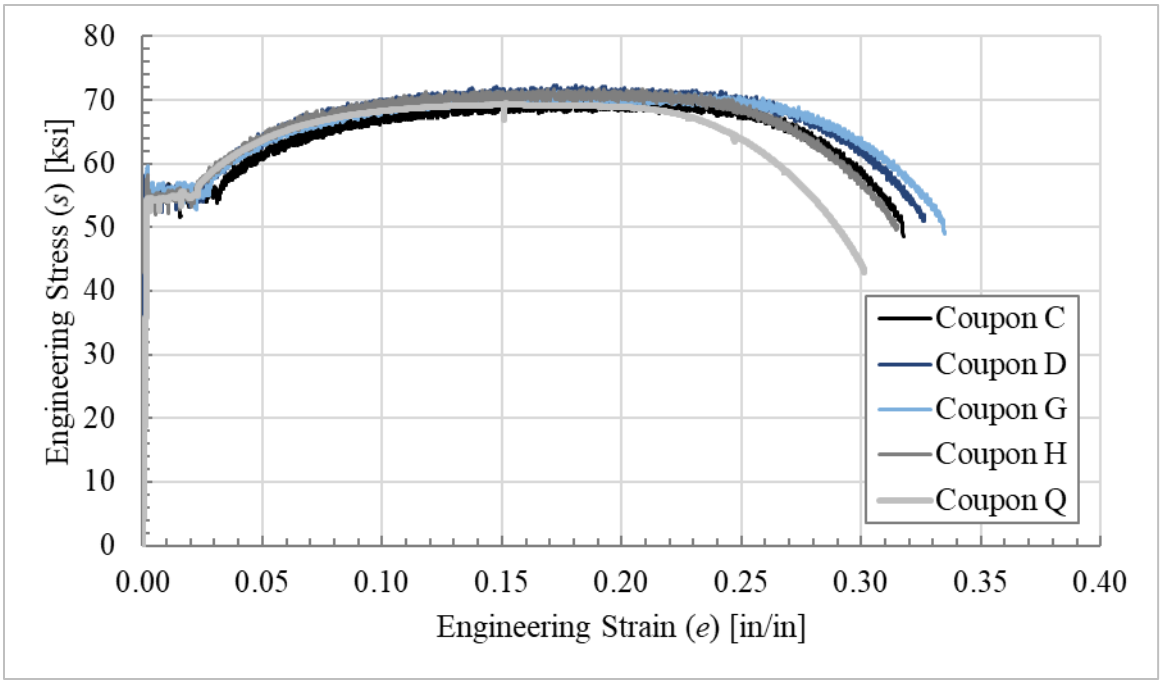

Figure A-3: Stress Strain Curves - A992 Gr. 50 W-Flange Coupons

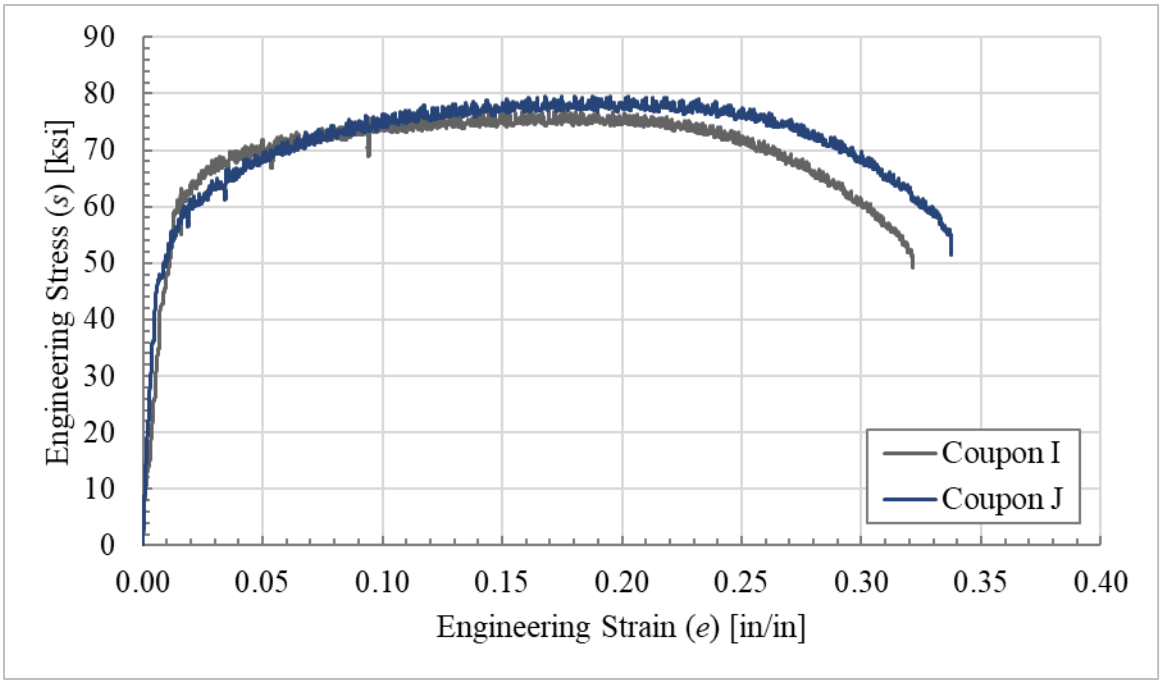

Figure A-4: Stress Strain Curves – A36 Angle Coupons

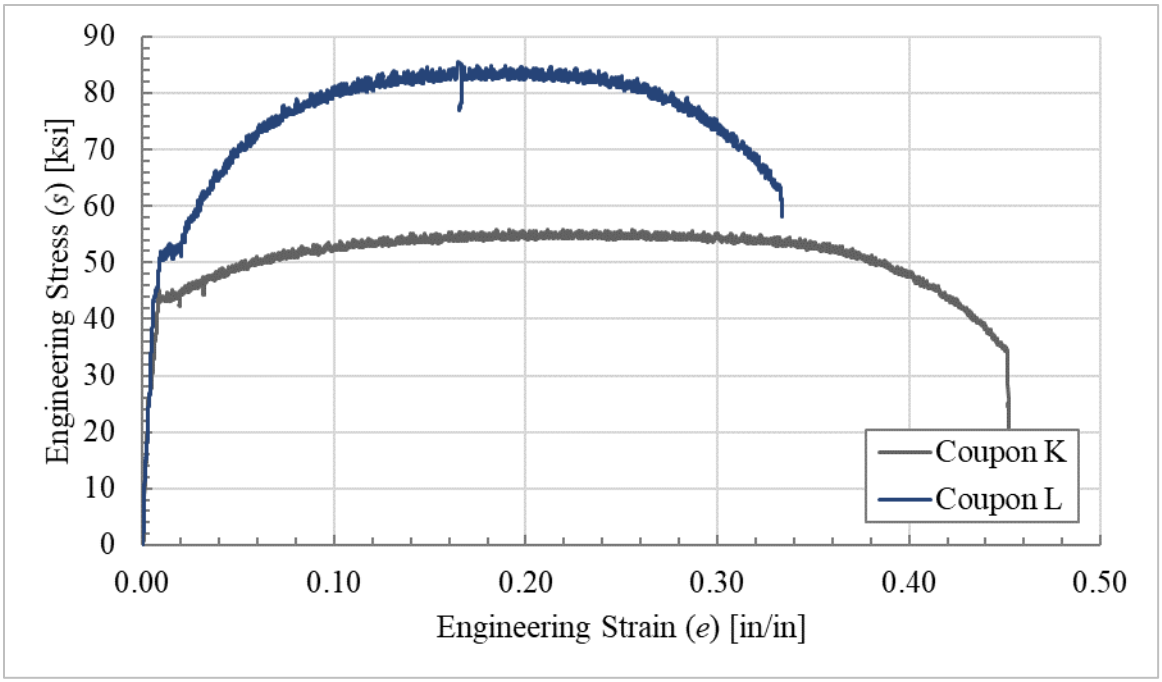

Figure A-5: Stress Strain Curves – A36 Plate Coupons

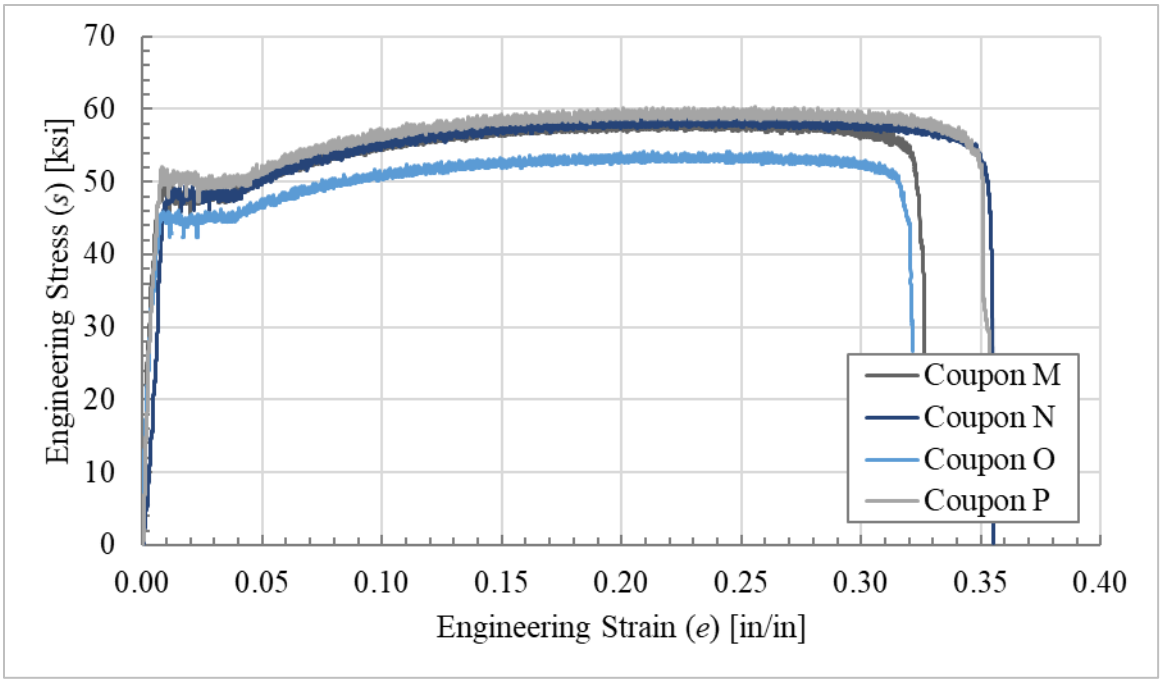

Figure A-6: Stress Strain Curves - A653 Gr. 50 Deck Coupons

APPENDIX B: FINITE ELEMENT ANALYSIS MODEL

B.1 INTRODUCTION

The first step to modeling the behavior of a steel tension coupon is to develop a finite element analysis (FEA) model. For the purposes of this dissertation, the LS-DYNA solver and LS-PrePost pre- and post-processing software were used to develop this model and the recommendations included in this chapter. Directions for using LS-PrePost were developed for Version 4.3 of the software. Alternate versions may require different steps than those recommended in the following sections.

The following sections summarize the basic process of developing a simple coupon model, running a simulation of a tension test, and interrogating the model to review and evaluate relevant results. The model and analysis techniques presented in this chapter reflect those used in the example case provided in Chapter 5. Included in the following sections are a discussion of units for FEA (Appendix Section B.2), tension coupon model geometry (Appendix Section B.3.1), boundary conditions (Appendix Section B.3.3.1), general meshing requirements (Appendix Section B.3.3.2), element formulations (Appendix Section B.4), numerical solver and typical settings (Appendix Section B.5), constitutive models (Appendix Section B.6), load application procedure (Appendix Section B.7), model outputs (Appendix Section B.8), and a brief discussion of fracture (Appendix Section B.9). The goal of this chapter to provide basic waypoints for navigating the process of developing, executing, and interrogating a typical tension coupon model. It is not intended to be a complete and thorough explanation of the topic. Additional information on LS-DYNA and LS-PrePost is included across a range of references (Livermore Software Technology Corporation, 2014) (Livermore Software Technilogy Corporation, May 2007) (Livermore Software Technology Corporation, 2012) (Livermore Software

Technology Corporation, 2004), as well as online videos, webpages, and other educational resources.

B.2 UNITS

Prior to developing an FEA model, a consistent set of units should be defined and established. Model inputs are generally unitless; thus, care must be exercised in defining inputs to ensure units are consistent across the defined geometry, material properties, and analysis controls. In defining a consistent set of units, the following general relationships in Equation B-, Equation B-2, and Equation B-3 should be obeyed (LS-DYNA Support, 2018).

$$1\ Force\ Unit = 1\ Mass\ Unit \times 1\ Acceleration\ Unit \quad \text{Equation B-1}$$

$$1\ Acceleration\ Unit = \frac{1\ Length\ Unit}{(1\ Time\ Unit)^2} \quad \text{Equation B-2}$$

$$1\ Density\ Unit = \frac{1\ Mass\ Unit}{(1\ Length\ Unit)^3} \quad \text{Equation B-3}$$

Table B-1 provides a summary of consistent unit relationships for finite element analysis. For models developed as a part of this dissertation, the units in row 11 of the table, where the base unit for mass is equal to lbf-s^2/in, were used and are reflected in the sample code blocks provided in the following sections. If an alternative unit set is chosen, values for certain terms included in the sample code blocks should be updated accordingly.

Table B-1: Consistent Units for Finite Element Analysis (LS-DYNA Support, 2018)

Mass	Length	Time	Force	Stress	Energy	Gravity
kg	m	s	N	Pa	J	9.806
kg	cm	s	1.0e-02 N	---	---	9.806e+02
kg	cm	ms	1.0e+04 N	---	---	9.806e-04
kg	cm	μs	1.0e+10 N	---	---	9.806e-10
kg	mm	ms	kN	GPa	kN-mm	9.806e-03
g	cm	s	dyne	dyne/cm^2	erg	9.806e+02
g	cm	μs	1.0e+07 N	Mbar	1.0e+07 N-cm	9.806e-10
g	mm	s	1.0e-06 N	Pa	---	9.806e+03
g	mm	ms	N	MPa	N-mm	9.806e-03
ton	mm	s	N	MPa	N-mm	9.806e+03
lbf-s^2/in	in	s	lbf	psi	lbf-in	386
slug	ft	s	lbf	psf	lbf-ft	32.17
kgf-s^2/mm	mm	s	kgf	kgf/mm^2	kgf-mm	9.806e+03
kg	mm	s	mN	1.0e+03 Pa	---	9.806e+03
g	cm	ms	1.0e+01 N	1.0e+05 Pa	---	9.806e-04

B.3 MODEL GEOMETRY, BOUNDARY CONDITIONS, AND MESHING

For the purposes of this dissertation, an eighth-symmetry model was used. Full specimens were also evaluated, providing similar results to the symmetry models when proper boundary conditions were defined. The full models were later abandoned due to the unnecessary additional computational time and resources they required. The following sections provide a brief discussion of partial and full coupon geometries in the context of tension coupon modeling, followed by a description of the eighth-symmetry modeling methodology used for the tension coupon FEA models. This discussion is used to illustrate the step-by-step true stress-strain relationship development process in Chapter 5.

B.3.1 Model Geometry

It is critical to capture the true geometry of the tested specimen to ensure it matches that used in the FEA model. Because necking and post-necking response are driven by conservation of volume, including the rate of geometric softening, $dA/d\varepsilon$, discussed in Section 2.8.2, it is critical that the computational coupon geometry matches the tested coupon geometry if a precise fit is required. If the correct geometry is not used, the resulting relationship will have some error inherent within it.

Where the coupon geometry information is unavailable, the expectations for precision and accuracy should be reduced accordingly. A potential method to deal with such a scenario would require developing a range of probable coupon geometries and use multiple models to develop a range of possible true stress-strain relationships. Then, based on evaluation of the possible solutions, a best overall fit to the family of possible relationships can be chosen. Alternative approaches are likely possible as well.

B.3.2 Full and Partial Coupon Models

The simplest approach to defining the geometry of an FEA model is typically to model the complete geometry of a given system, neglecting any possible symmetry or anti-symmetry conditions. This approach, however, is often computationally expensive and inefficient for problems where symmetries and anti-symmetries exist that can be exploited to reduce the total size of the model, subsequently reducing required computational resources and analysis time. For example, consider a standard thick plate tension coupon for ductile metals illustrated in Figure B-. This coupon exhibits three symmetry planes, two orthogonal planes parallel to the long axis of the coupon and one through the cross-section at the midline. Thin plate coupons exhibit these same symmetry planes. Cylindrical tension coupon specimens do as well, although they also exhibit radial symmetry. A discussion of radial symmetry in FEA models is not included in this dissertation, though it is widely

discussed in the context of tension response of ductile metals, particularly in early works like those published by Bridgman (Bridgman, 1952), Chen (Chen W. H., 1971), and Needleman (Needleman, 1972).

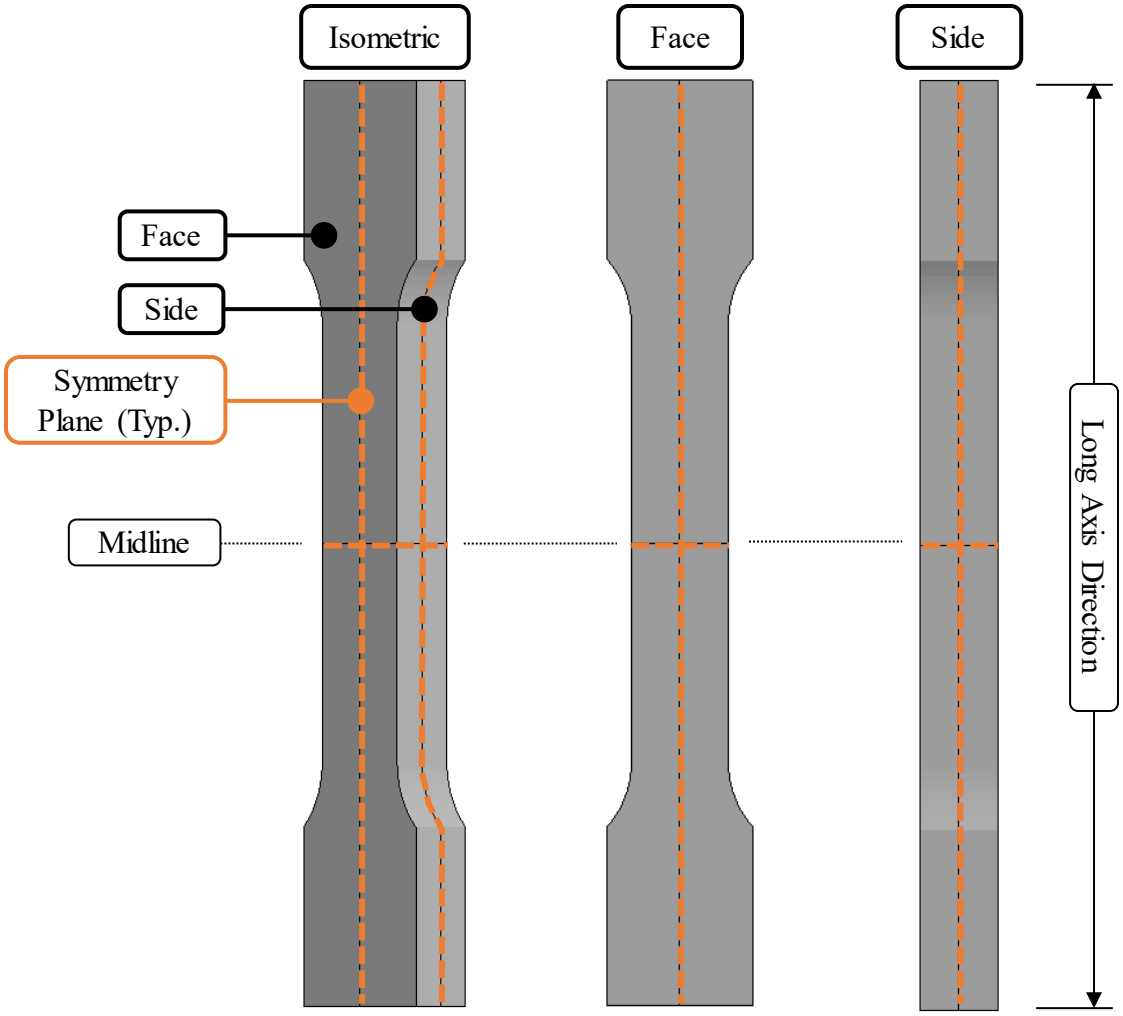

Figure B-1: Symmetry Planes in Typical Plate Coupon Specimen

In addition to considering geometric symmetries, one must consider and verify symmetry of applied loads, boundary conditions, deformations, and other relevant factors when determining whether symmetry applies within a given model. For a standard coupon tension test, the ends are loaded and displaced in the long-axis direction; thus, they are

symmetric about the midline of the specimen. In addition, considering the expected deformation of the specimen at the load application points, the ends are designed to remain elastic while developing the strength of the reduced section at the center. Therefore, no non-symmetric or other significant deformation is expected there. Accordingly, one-eighth symmetry can still be leveraged after considering load application, displacement, and boundary conditions in the tension coupon model.

While it is not necessary to account for symmetry in a FEA model, as noted previously, it can reduce the computational demands and analysis time required. For example, in the one-eighth symmetry model, there are only one-eighth the total number of elements required to capture the same behaviors as would be predicted in a full model. With computational time increasing roughly with the square of the number of elements (Thieme, 2016), an eighth-symmetry model will execute in approximately $1/64^{th}$ of the time required to analyze the equivalent full geometry model. Therefore, it is recommended, even in these simple models, to consider symmetry to reduce the overall size and associated computation time. The use of symmetry will save some time on a single model, but the effect is particularly noticeable when considering the iterative approach recommended in this dissertation, or automated iterative techniques (e.g., those discussed in Section 2.9.2). In these cases, it has the potential to significantly expedite the analysis process.

B.3.3 One-Eighth Symmetry Model

In addition to using one-eighth symmetry as described in Appendix Section B.3.1, the wide end of the coupon was reduced in length to decrease the size of the model and reflect the approximate location of the end of the grips during testing. While this step is not required, it saves from having to model a large section of elastic material that will have no appreciable effect on the overall tension performance of the specimen predicted by the FEA

model. Thus, the specimen is half length, thickness, and width, with reduced grip end as highlighted in Figure B-2.

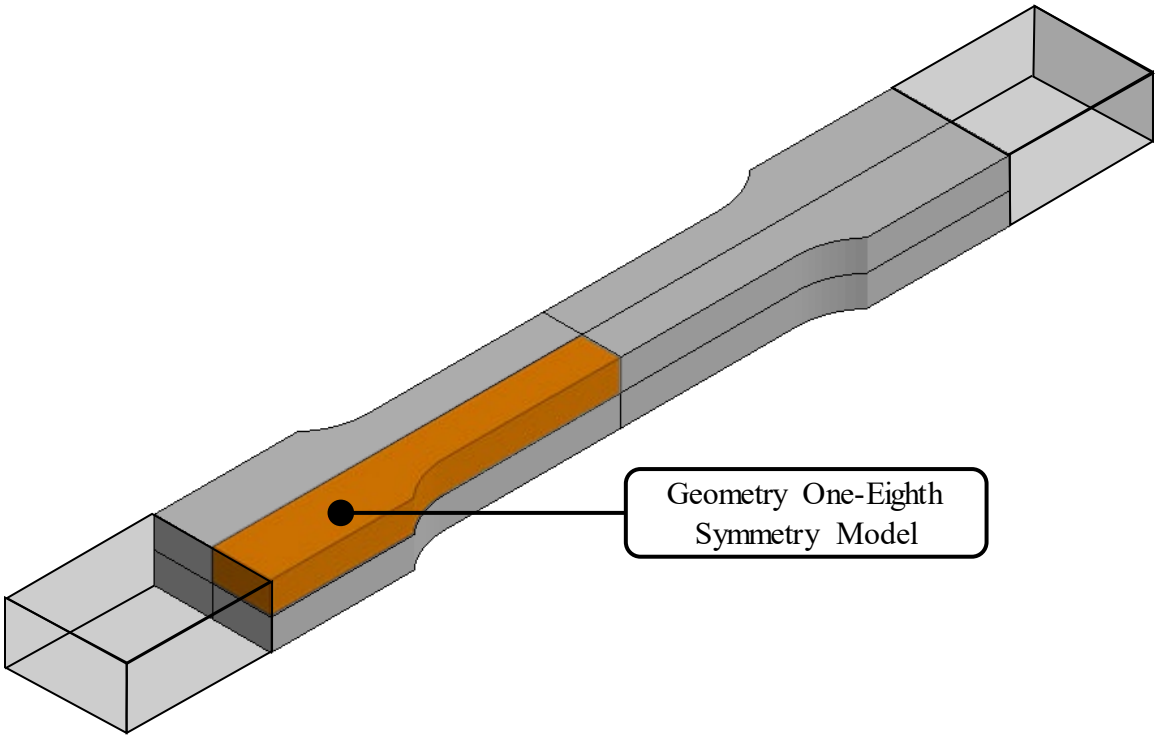

Figure B-2: Eighth-symmetry Coupon Model

B.3.3.1 *Symmetry Planes, Constraints and Boundary Conditions*

To capture the effects of symmetry, node sets were first defined for each symmetry plane, and then displacements and rotations were constrained to capture the symmetry boundary conditions. For simplicity, the model geometry was defined such that the symmetry planes lie along the orthogonal planes formed by the *x*, *y*, and *z* ordinate axes. The relevant symmetry boundaries and coordinate system used in the eighth-symmetry model are illustrated in Figure B-3. Node set constraints are summarized in Table B-2, where "DOF" refers to degree of freedom, and is followed by the coordinate direction (e.g. *x*, *y*, or *z*) for translational degrees of freedom. Rotational restraints include the "*R*" prefix prior to the relevant coordinate direction for rotations about the referenced coordinate axis.

Note that the elements themselves are not constrained. Rather, the nodes of elements (which have both translational and rotational degrees of freedom in a typical solid element) lying on a symmetry plane are constrained as summarized in Table B-2.

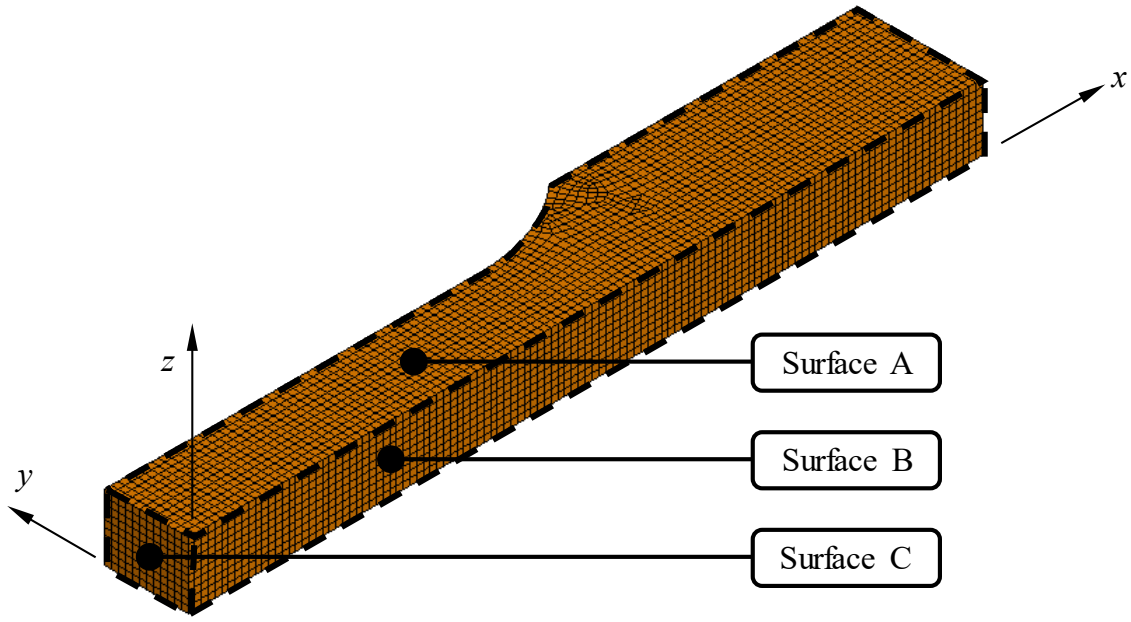

Figure B-3: Coupon Model Symmetry Surfaces and Coordinate System

Table B-2: One-Eighth Symmetry Nodal Boundary Constraints

Surface ID	**Constrained Degrees of Freedom (DOF)**					
	DOF-*x*	**DOF-*y***	**DOF-*z***	**DOF-R*x***	**DOF-R*y***	**DOF-R*z***
A			x	x	x	
B		x		x		x
C	x				x	x

Node set constraints are defined within the model using the single point constraint (SPC) function for node sets called by the keyword **BOUNDARY_SPC_SET*. This keyword allows for constraint of translational and rotational degrees of freedom in any defined coordinate system. A sample code block is subsequently provided to describe the inputs used in the eighth-symmetry analysis model with the node set ID's (nsid) replaced

by letters corresponding to the relevant symmetry surface defined previously in Figure B-3 and Table B-2. When applying this code block, surface ID's (e.g. "A", "B", "C") should be replaced by the appropriate identification numbers chosen for the predefined surface node sets. Clarifying comments are included in the code block, preceded by "$", where the "$" character is used to preface commentary text that is ignored when compiling and executing the analysis. Refer to the *LS-DYNA Keyword Manual* (Livermore Software Technilogy Corporation, May 2007) for additional information.

```
*BOUNDARY_SPC_SET
$ THROUGH-THICKNESS SYMMETRY PLANE BOUNDARY DEFINITION
$#     nsid       cid      dofx      dofy      dofz     dofrx     dofry     dofrz
        "A"         0         0         0         1         1         1         0
*BOUNDARY_SPC_SET
$ LONG AXIS CENTERLINE SYMMETRY PLANE BOUNDARY DEFINITION
$#     nsid       cid      dofx      dofy      dofz     dofrx     dofry     dofrz
        "B"         0         0         1         0         1         0         1
*BOUNDARY_SPC_SET
$ MIDLINE SYMMETRY PLANE BOUNDARY DEFINITION
$#     nsid       cid      dofx      dofy      dofz     dofrx     dofry     dofrz
        "C"         0         1         0         0         0         1         1
```

B.3.3.2 *Mesh Requirements*

A mesh sensitivity study is beyond the scope of this dissertation; however, the following section provides basic insight into general mesh-related lessons learned during this research project that specifically apply to eighth-symmetry tension coupon models for ductile metals like structural steel.

As a general rule, additional elements, particularly in areas of high stress and strain gradients (like the center of the specimen where necking occurs), can improve convergence of the model. However, generally a minimum of five elements through the thickness of the coupon—the smallest of the three major dimensions of the eighth-symmetry model—provides reasonably accurate results in terms of overall mesh convergence while

minimizing computation time. Thus, a minimum of five elements is recommended through the thickness during the early parts of the calibration process for thick and thin plate elements. For round elements, additional elements through the radius may be warranted, particularly for elements with linear edges as they must ultimately approximate the curved geometry along the surface of the specimen. Once a constitutive relationship for true stress and strain is developed, mesh refinement is recommended to verify convergence.

Another consideration, discussed further in Appendix Section B.8.3, is ensuring a node is located precisely at the point where the model will be interrogated for displacement data. Because the goal of the FEA model is to reproduce the results of a physical coupon test, the model is interrogated to produce similar load-deformation data to that measured in a real test. As a result, displacements should be extracted at the same location where the displacement gauge was applied in the experimental test. For example, for a gauge length of two inches, in a one-eighth symmetry model, the mesh should be generated such that a node is located half the displacement gauge length (i.e., one inch) away from the center of the coupon, along the long axis centerline and on the face opposite the through-thickness symmetry plane. The ID number of this node should be recorded for use in post-processing and verification of results.

Next, it is recommended that auto-meshing capabilities be relied upon wherever possible, particularly when defining the initial mesh. If, after global auto-meshing of the model is performed, further refinement or modification is desired, local mesh refinements can be done manually. This approach is typically much faster than attempting to develop a user-defined mesh for an entire model. In addition, when refining the mesh, ensure various element and node sets used in the model are updated accordingly. For example, if the mesh is divided in half as a part of a convergence study, any newly generated elements and nodes along constrained boundaries, load or displacement application points, and other similar

areas may need to be redefined in the model. Similarly, any node or element sets defined for ease of data post-processing and model output review may also need to be updated.

B.4 ELEMENT FORMULATIONS

The discussion of element formulations has the potential to be quite long due to the wide variety of element types and formulations. Therefore, detailed discussion is mostly outside of the scope of this dissertation. However, for consideration and reference, two commonly used solid element formulations were evaluated when developing the methodologies presented in this dissertation, (1) constant stress solid, and (2) fully integrated S/R (selectively reduced) solid. Both element types produced relatively similar results, particularly in pre-necking and early post-necking response. Later in the post-necking response, their predictions begin to diverge. Given their higher order, more rapidly converging results were produced using the fully integrated S/R elements (LS-DYNA ELFORM = 2.0) when compared to the constant stress solid element type (LS-DYNA ELFORM = 1.0). Nonetheless, they require additional computation time, particularly after mesh refinement. Given the limited consideration of the topic in the development of this dissertation, some experimentation with 3D solid element formulations is recommended to determine which are most appropriate for a given application.

In addition, depending on the material geometry, desired mesh, and desired behaviors that must be captured in an FEA model, different 3D solid element types may be desirable. In these cases, it is recommended as a best practice to use the same element in the material model development process as will be used in the later models. If multiple element types will be used, the constitutive relationship can be developed for each element type to ensure reliable performance in subsequent predictive models.

To apply the chosen solid element formulation in the model, the LS-DYNA keyword **SECTION_SOLID* can be used, as shown in the subsequently presented sample code block where the "X" character is included in place of the section ID defined in the model. A range of element formulations is available and can be selected using the "elform" field. Setting "elform" equal to 1 calls the constant stress solid element formulation. Setting it equal to 2, as illustrated in the following code block, calls the fully integrated S/R solid element formulation. Additional information on element formulations is included in the *LS-DYNA Keyword Manual* (Livermore Software Technilogy Corporation, May 2007).

```
*SECTION_SOLID
$ DEFINE PROPERTIES FOR SOLID ELEMENTS
$ 1 = CONSTANT STRESS SOLID ELEMENT (DEFAULT)
$ 2 = FULLY INTEGRATED SELECTIVELY REDUCED (S/R) SOLID ELEMENT
$#   secid    elform       aet
       "X"         2         0
```

In addition to defining the element type, the keyword **CONTROL_SOLID* can be used to provide a range of controls for solid element response. A sample code block using this control card is included subsequently for reference. Refer to the *LS-DYNA Keyword Manual* (Livermore Software Technilogy Corporation, May 2007) for additional information.

```
*CONTROL_SOLID
$ CONTROL SETTINGS FOR SOLID ELEMENT ANALYSIS
$#   esort   fmatrix   niptets    swlocl    psfail
         1         0         4         2         0
$#   pm1     pm2     pm3     pm4     pm5     pm6     pm7     pm8     pm9     pm10
       0       0       0       0       0       0       0       0       0       0
```

B.4.1 Alternative Element Types

While this dissertation and the proposed methodologies were developed for 3D solid elements, alternative element types such as 1D beams, or 2D plates and shells, may

be desirable to capture certain behaviors, for reduced computational demands, for specific geometries (e.g. plate structures, thin-walled members, etc.), or where warranted by other requirements. The application of the recommendations and rules presented in this dissertation to alternative element types besides 3D solids (e.g. 1D and 2D elements) is a recommended topic for future research as discussed in Section 6.3.2. Thus, the methodologies presented in this dissertation should not be applied blindly to these other element formulations without consideration of the compromises and assumptions associated with the transition from a solid 3D element to 1D and 2D element formulations.

B.5 SOLVER CONTROLS AND SETTINGS

The implicit solver was chosen for the research presented in this dissertation and is generally recommended for tension coupon FEA models used to develop material constitutive stress-strain relationships in accordance with the recommendations of Chapter 4. While an explicit solver is often used to capture large deformations, non-linear material response, material softening, and material failure in FEA, the simplicity of the tension coupon model and the use of deformation-controlled loading, discussed in Appendix Section B.6.1, allows for use of the built-in implicit solver in LS-DYNA. By using implicit analysis techniques, the calculation is essentially treated as a series of static analyses. Thus, dynamic effects, boundary deformation application rates, and other complexities that may be relevant in explicit analysis (e.g., dynamic stress-wave propagation, settling, etc.) can be avoided by using the implicit solver.

The implicit solver is evoked using the **CONTROL_IMPLICIT_GENERAL* keyword in LS-DYNA. Use of this keyword is required for all implicit analyses as it activates the implicit mode and allows the user to define appropriate solver controls including the time step size. The sample code block presented after this paragraph provides

a summary of the typical inputs for implicit analysis for a coupon tension test FEA model. Setting the "imflag" variable equal to 1 calls for the implicit analysis solver. The "dt0" field is used to define the time step. In this example, a variable is used in this location called "&TSTEP", as discussed later in this section. For information on the remaining implicit control settings, refer to the *LS-DYNA Keyword Manual* (Livermore Software Technilogy Corporation, May 2007).

```
*CONTROL_IMPLICIT_GENERAL
$ CALL IMPLICIT SOLVER AND DEFINE IMPLICIT CONTROLS INCLUDING TIMESTEP (dt0)
$#  imflag       dt0    imform      nsbs       igs     cnstn      form    zero_v
         1    &TSTEP         2         1         2         0         0         1
```

Because the implicit analysis uses timesteps to define the analysis duration, a control must be added to define the time at which the analysis is terminated. This is achieved through the use of the **CONTROL_TERMINATION* keyword in LS-DYNA and setting the "endtim" field equal to the desired termination or end time value. When defining the termination time, ensure the same units are used as those used previously in the implicit solver controls (e.g., msec, seconds, etc.). Following this paragraph, a sample code block is provided below illustrating the use of the termination control for implicit analysis where the "&TERM" variable is used to define the termination time. For information on the remaining termination control settings, refer to the *LS-DYNA Keyword Manual* (Livermore Software Technilogy Corporation, May 2007).

```
*CONTROL_TERMINATION
$ DEFINE IMPLICIT ANALYSIS TERMINATION TIME
$#  endtim    endcyc     dtmin    endeng    endmas
     &TERM         0     0.000     0.000     0.000
```

Variables are used in the preceding control keyword cards to maintain a clean analysis input file structure and allow for these controls to be rapidly edited at the top of

the input file rather than in the body, within each keyword card. These variables are defined using the **PARAMETER_EXPRESSION* keyword. As shown in the subsequently presented example code block, the time step is defined is "1E-3" or 0.001 seconds, and the termination time is 1 second. Thus, for this example, the implicit analysis will be performed considering 1000 equally spaced time steps. As shown previously, these variables can be called later by typing an ampersand, "&", and then the variable name.

```
*PARAMETER_EXPRESSION
$ DEFINE VARIABLES USED IN CONTROL AND OUTPUT CARDS
R TSTEP  1E-3
R TERM  1.0
```

B.6 MATERIAL CONSTITUTIVE MODELS

Hundreds of material constitutive models are available to capture a broad range of behaviors. For this dissertation, the simple piecewise linear plasticity model, **MAT_024* in LS-DYNA, is used for simplicity and broad applicability. It is a standard material model included with most typical FEA software. This material model is an elasto-plastic constitutive relationship, providing the ability to define any arbitrary stress-strain curve and strain rate dependency relationship. This model was chosen because it allows for the flexibility necessary to demonstrate the proposed constitutive true stress-strain relationship development process in this dissertation, though it may not be appropriate for all analyses. In fact, alternative constitutive models may be appropriate or required depending on the range of behaviors that must be captured. For example, Table B-3 provides a summary of several typical constitutive models commonly used when analyzing ductile metals like steel or aluminum for blast loads (Crawford, Magallanes, & Lan, 2006). Because a detailed discussion of material models is beyond the scope of this dissertation, refer to the *LS-DYNA*

Material Model Keyword Manual (Livermore Software Technology Corporation, 2014) or other similar FEA reference for additional information on material constitutive models.

Table B-3: Ductile Metal Material Constitutive Models and Dependencies for Blast Loading (Crawford, Magallanes, & Lan, 2006)

Category	Name	Yield Surface Basis	Strain-Rate Dependency	Thermodynamic Dependency	Material Failure
Empirically Based	Simplified von Mises	Effective Stress vs. Effective Plastic Strain	NO	NO	YES
	Modified Von Mises*		YES	NO	YES
	Johnson-Cook (JC)		YES	YES	YES
	Klopp-Clifton-Shawki		YES	YES	YES
Physics-Based	Zerilli-Armstrong	Dislocation Micromechanics	YES	YES	YES
	Mechanical Threshold Model (MTS)		YES	YES	YES

* Developed by Kargozian & Case, similar to MAT_24 in LS-DYNA

As noted previously, LS-DYNA **MAT_024*, evoked by the keyword **MAT_PIECEWISE_LINEAR_PLASTICITY*, was used to develop the rules and methodology presented in this dissertation and to demonstrate the step-by-step method for determining the true stress-strain relationship presented in Chapter 5. The sample code block, provided following this paragraph, summarizes the inputs used to define a typical ductile metal constitutive material model for FEA. In this code block, the material ID (mid) defined in the model is replaced by "X". The material defined in this example is steel; thus,

standard book values are used to define the mass density input in the field titled “ro”, the elastic modulus in field “e”, and Poisson’s ratio in field “pr”. Finally, a load curve, titled “LCID”, is used to define the stress-strain relationship. Note that, for this material model, the curve represents the plastic strain regime only, so the true stress-strain material constitutive relationship should reflect relative plastic strains. The linear-elastic properties are captured by the previously mentioned inputs (e.g. “ro”, “e”, and “pr”), and the load curve is defined with zero (plastic) strain occurring at first yield. For more information on the other inputs, refer to the *LS-DYNA Material Model Keyword Manual* (Livermore Software Technology Corporation, 2014).

```
*MAT_PIECEWISE_LINEAR_PLASTICITY
$ STEEL CONSTITUTIVE MATERIAL MODEL WITH LOAD CURVE DEFINITION
$#     mid        ro         e        pr      sigy      etan      fail      tdel
       "X"   7.33E-4 2.9000E+7     0.300                      1.0E+20     0.000
$#       c         p      lcss      lcsr        vp
         0         0    "LCID"
```

A load curve is used in this constitutive material definition because it is generally difficult to define the post-elastic stress-strain relationship using only eight points, which is the default for **MAT_24*. Thus, a separate load curve is recommended for defining the material response. As shown in the subsequently presented sample code block, a load curve is defined using LS-DYNA keyword **DEFINE_CURVE_TITLE*, followed on the next line by the title of the curve. In the following example code block, “LCID” is used as a stand-in for the load curve ID number defined in the input file. The **DEFINE_CURVE_TITLE* keyword allows for a user defined curve, in this case a plastic stress-strain material relationship. Refer to the *LS-DYNA Keyword Manual* (Livermore Software Technilogy Corporation, May 2007) for additional information on defining load curves.

```
*DEFINE_CURVE_TITLE
GENEARL DUCTILE METAL MATERIAL PLASTIC CONSTITUTIVE RELATIONSHIP CURVE
$#    lcid      sidr       sfa       sfo      offa      offo    dattyp
    "LCID"         0  1.000000  1.000000     0.000     0.000         0
$#                a1                  o1
            0.000000                  σy
                  εp1                 σp1
                  εp2                 σp2
                  εp3                 σp3
                    …                   …
                εp(n-1)             σp(n-1)
                  εpn                 σpn
```

B.6.1 Discretization

The discretion used when inputting the material model true stress-strain relationship is important and should be done with care. First, the curve should be discretized to ensure critical features of the material constitutive relationship are captured with adequate resolution. Overly coarse fits can create issues, particularly in piecewise linear models. Figure B-4 illustrates an example of a series of piecewise linear segments of the same true stress strain relationship, where δ refers to the constant discretization interval chosen for the piece-wise linear true stress-strain relationship. Interrogating these piece-wise linear true stress-strain relationships, δ, with respect to Considère's Construction (Derivative Rule #1 in Section 3.2) reveals a range of step functions for the first derivative, $d\delta$, as shown in Figure B-5. Investigating closer, as illustrated in Figure B-6, the predicted necking strain for each of these true stress-strain relationships ranges from approximately 0.16 to 0.21. This broad range will produce significantly different results when executed in a material model. Therefore, care should be taken to discretize the curve to capture necessary behaviors, such as the onset of necking, as precisely as is necessary for a given application.

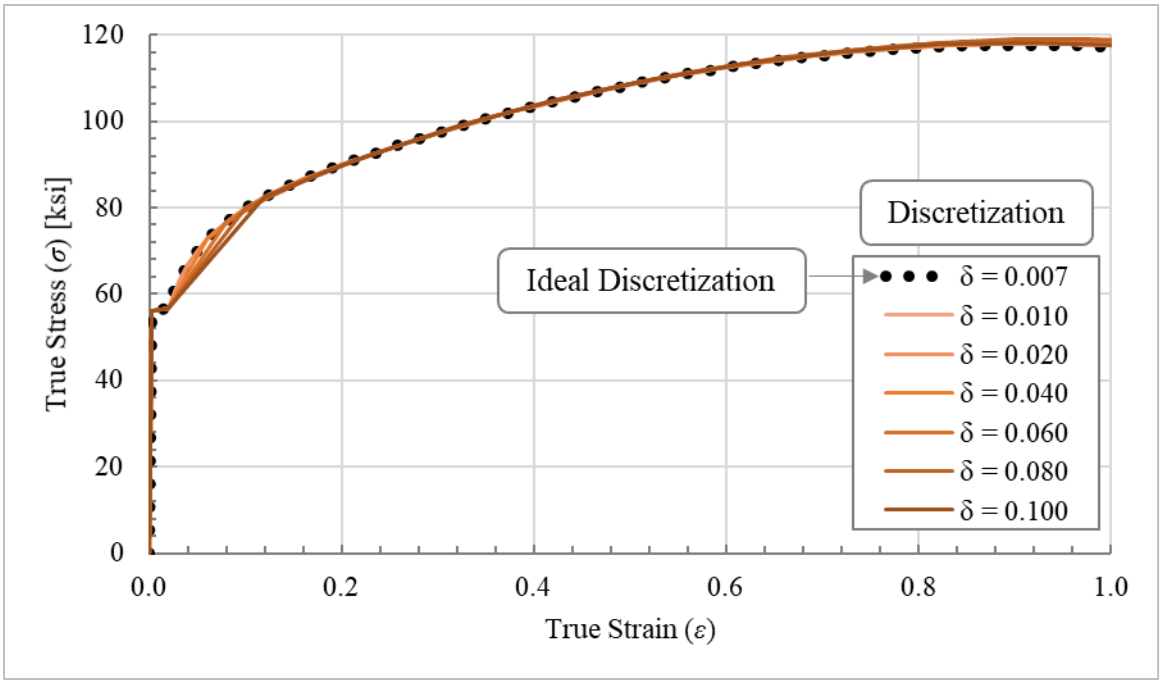

Figure B-4: Varying Discretization of True Stress-Strain Relationship

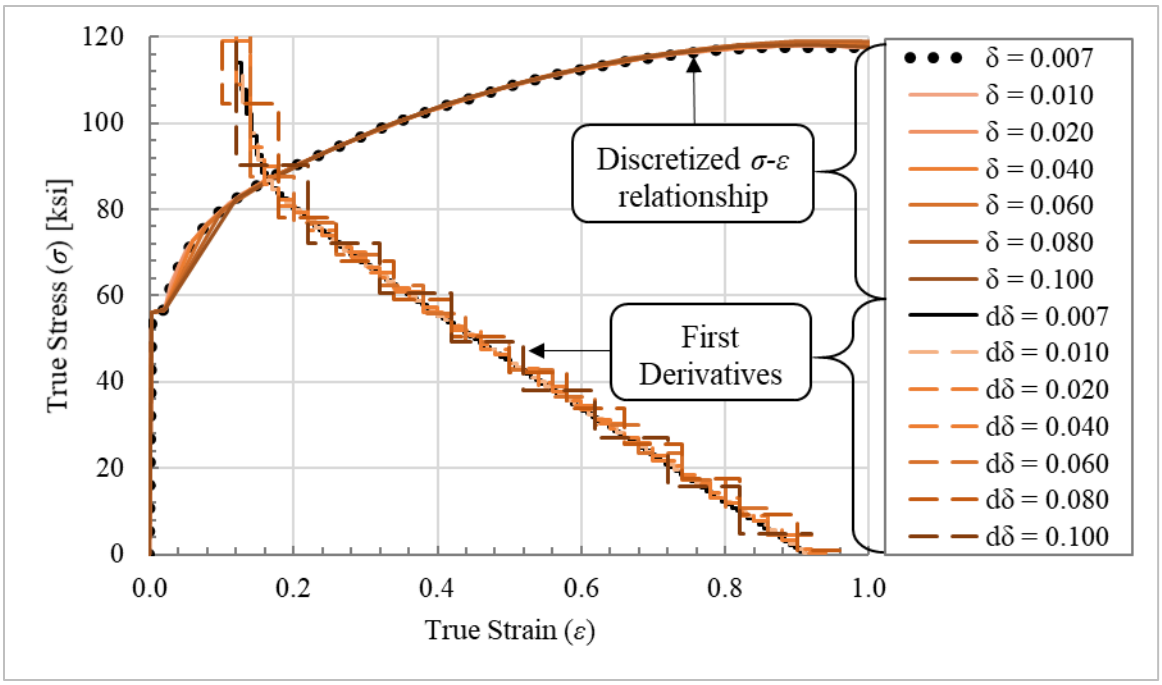

Figure B-5: Discretization Effects on First Derivative

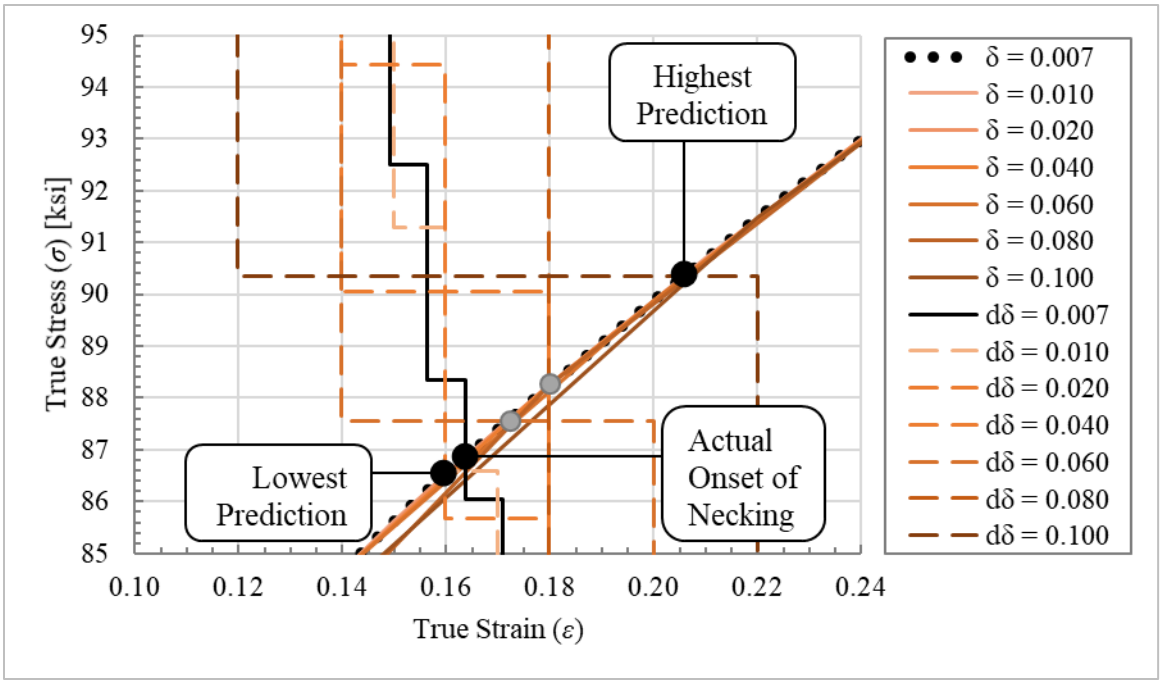

Figure B-6: Discretization Effects on Prediction of Onset of Necking

In addition, investigate the software tool (e.g. LS-DYNA) to determine if automated rediscretization of data is done when compiling and running the analysis. For example, when using the keyword **DEFINE_CURVE* in LS-DYNA, the input curve is internally discretized with equal intervals along the abscissa for fast evaluation in constitutive models. Thus, take care to avoid excessive discretization and ensure the discretized curve is being applied to the model as expected. Refer to the *LS-DYNA Keyword Manual* (Livermore Software Technilogy Corporation, May 2007) for additional information.

B.7 LOAD APPLICATION PROTOCOL

In the FEA model of a standard tension coupon test, “loads” can be applied in two different ways. The first, direct force application, is generally not recommended because of the softening behavior that occurs at the onset of necking, where the maximum

engineering stress and maximum load resistance occurs. If a prescribed monotonically increasing force is applied in the model, there is no way for the model to achieve equilibrium beyond this point of maximum load in an implicit analysis. Conversely, it is possible to achieve equilibrium and measure response beyond the ultimate load using an explicit analysis approach; however, the analysis will not produce meaningful or useful results as equilibrium will be achieved due to inertial effects resulting in the coupon ends quickly accelerating apart as the applied load is increased.

The second method for "load" application in the model is through a prescribed relative displacement between the ends of the coupon specimen. The prescribed motion is evoked using LS-DYNA keyword **BOUNDARY_PRESCRIBED_MOTION_SET_ID*, as illustrated in the following sample code block included, where the "nsid" field is used to capture the node set where a given motion is imposed, and the "dof" field is used to define the direction of the imposed motion. In this case, the value of 1 for the "dof" indicates displacement in the *x*-translational degree of freedom. Values of 2 and 3 would be used to define translation in the *y*- and *z*-directions, respectively. Other translational or rotational degrees of freedom can be evoked using this field. Next, the type of boundary motion is defined in the "vad" field. In this example, the value of 2 is used to impose a displacement motion. The motion is defined by the load curve "LCID" in the "lcid" field, the scale factor for the load curve is applied in the "sf" field. In this case, a variable is used by inputting "&DISP". This variable is defined at the beginning of the input file for ease of use and represents the maximum displacement of the coupon in the chosen unit system. For information on other settings, as well as the remaining entry fields, refer to the *LS-DYNA Keyword Manual* (Livermore Software Technilogy Corporation, May 2007).

```
*BOUNDARY_PRESCRIBED_MOTION_SET_ID
$ DEFINE BOUNDARY MOTION FOR EQUIVALENT "LOAD" APPLICATION
$#      id                                                                heading
          Top Pull of Coupon in X-Direction
$#    nsid       dof       vad      lcid        sf       vid     death     birth
       "X"         1         2    "LCID"     &DISP         0 1.000E+28     0.000
```

Because the scale factor field is used to define the maximum displacement, the load curve "LCID" is defined such that it is unitless and has a maximum value of one. Refer to the *LS-DYNA Keyword Manual* (Livermore Software Technilogy Corporation, May 2007) for additional information on load curve definitions.

```
*DEFINE_CURVE_TITLE
Load Curve Title
$#    lcid      sidr       sfa       sfo      offa      offo    dattyp
    "LCID"         0  1.000000  1.000000     0.000     0.000         0
$#                a1                  o1
              0.000               0.000
           1.000000            1.000000
```

Finally, the node set to which the imposed boundary displacement is applied should encompass all nodes on the grip end, as shown in Figure B-7. When refining the mesh, take care to redefine this node set as all nodes on the grip end must be displaced to avoid spurious results.

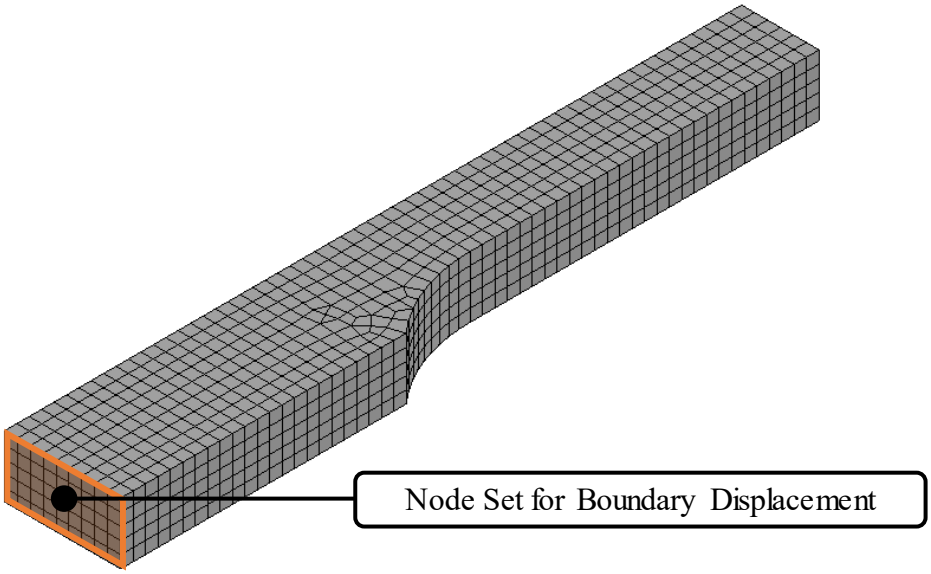

Figure B-7: Node Set for Imposed Boundary Displacement

B.8 OUTPUTS AND OUTPUT CONTROLS

A wide range of model outputs and output controls are available in LS-PrePost and LS-DYNA. These parameters allow a user to output desired results for model review, troubleshooting, and analysis. The following sections describe the main output controls used in developing the models and methodologies presented in this dissertation. Additional or alternative output controls may be warranted to capture other data when developing a tension coupon model.

B.8.1 Stresses and Strains

An important visual approach to verifying a model is producing accurate results can be to view element stresses and strains throughout the various steps of the analysis. Visualization of stress and strain data can be done by using the fringe plot feature in LS-PrePost. Figure B-8 provides an illustration of a series of fringe plots of von Mises stress for a sample coupon model, accessed by selecting “MFPost” and then “FriComp” and selecting “Von Mises Stress”. Note the stress gradient along the length that forms prior to

necking, and the concentration of stresses in the necked region once necking has occurred. This stress distribution follows expected behavior for a tension coupon and helps verify that results are reasonable. A similar relationship could be illustrated for strains.

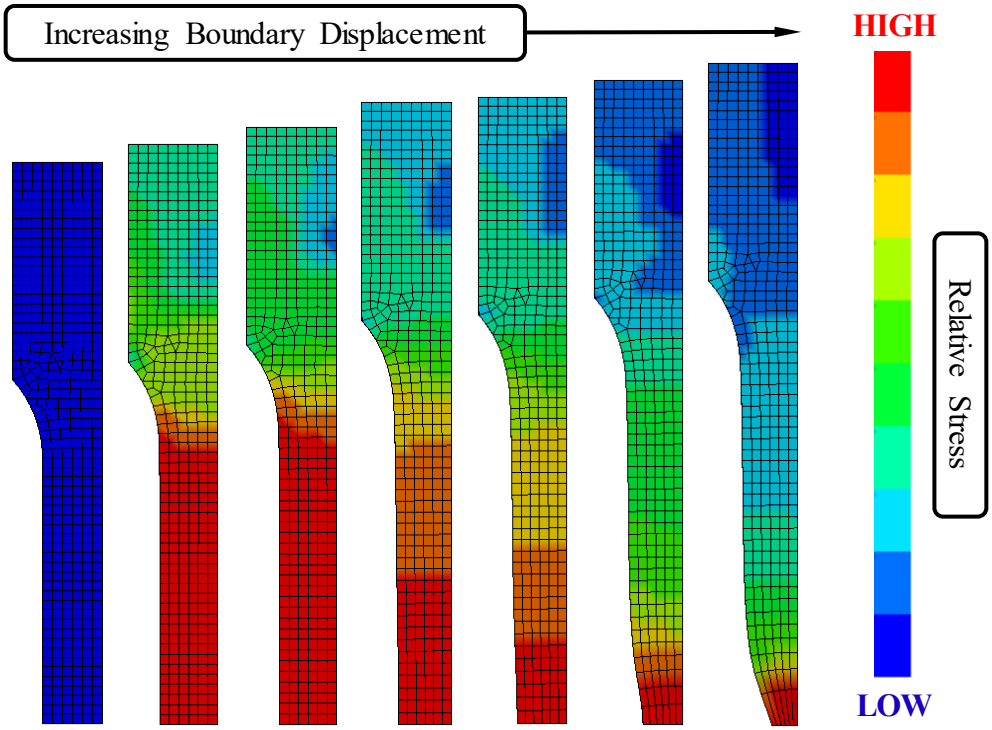

Figure B-8: Fringe Plots of von Mises Stress for Model Evaluation

B.8.2 Energies

Kinetic, internal (e.g., plastic strain), and total energies can be viewed after a model is developed to verify no spurious energy is generated or lost in the model. Energies can be viewed by selecting the MFPost button, then Histories, then selecting and plotting the desired energy histories. Figure B-9 provides a sample plot of kinetic, internal, and total energy for a tension coupon model. Because this is an implicit analysis, no kinetic energy is measured throughout the entire analysis. Therefore, the internal (plastic strain) energy is equal to the total energy through the entire analysis. Energy increases as the analysis

progresses due to the imposed boundary displacement of the end of the coupon specimen. Thus, all displacement energy input is converted directly to plastic strain energy in the coupon and the results obey Hill's stability criteria from Section 3.3.

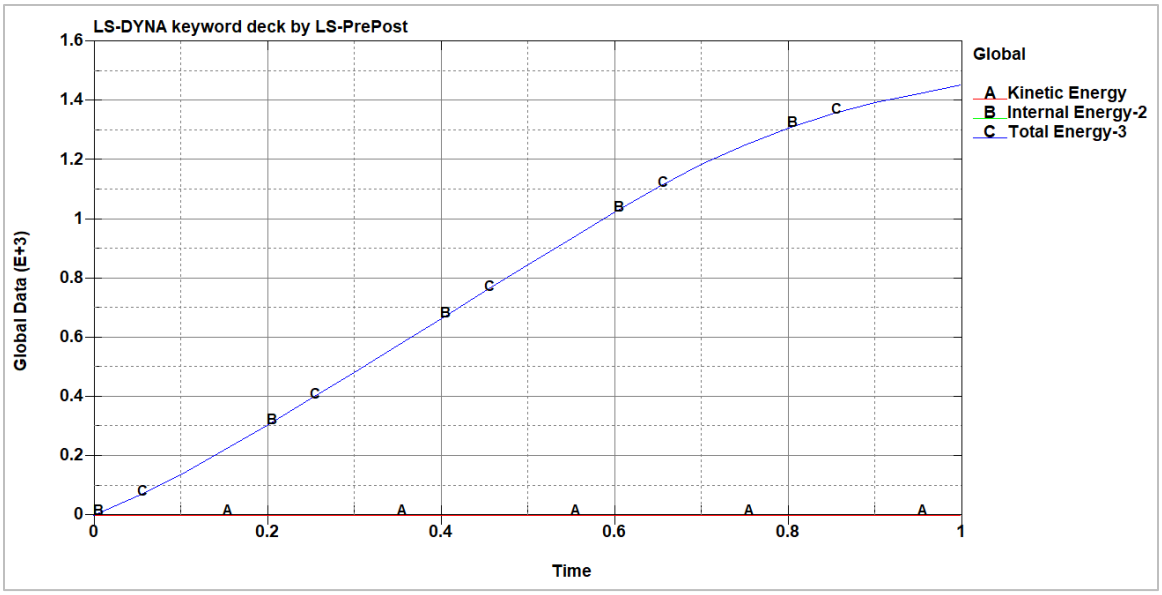

Figure B-9: Energy Plot

B.8.3 Load-Displacement History

The load-displacement history from the model is captured by cross-plotting two sets of data: (1) the boundary load (force) data, and (2) the displacement of the node at the extensometer gauge point. By calculating and plotting these data, a virtual load-deformation relationship corresponding to what is measured during the real tension coupon test can be developed and visualized.

The load history can be captured using the **DATABASE_BNDOUT* keyword, as shown in the following sample code block, where "&TSTEP" calls a variable defined earlier in the input file used to set the time step for the analysis. This keyword commands LS-DYNA to store boundary condition forces and energies in ASCII format. The results are then accessed in LS-PrePost by selecting "MFPost" and then "ASCII". In the popup

window, select “bndout” and click the “Load” button. Once the relevant output data are loaded, select all nodes, click the “Total” button, select the appropriate force component(s) and click the “Plot” button. A plot of the boundary load time-history will then open in a pop-up window that can be manipulated and saved as necessary. A sample load time-history developed using this method is presented in Figure B-10.

```
*DATABASE_BNDOUT
$Boundary condition forces and energy
$#      dt    binary      lcur     ioopt
    &TSTEP         0         0         1
```

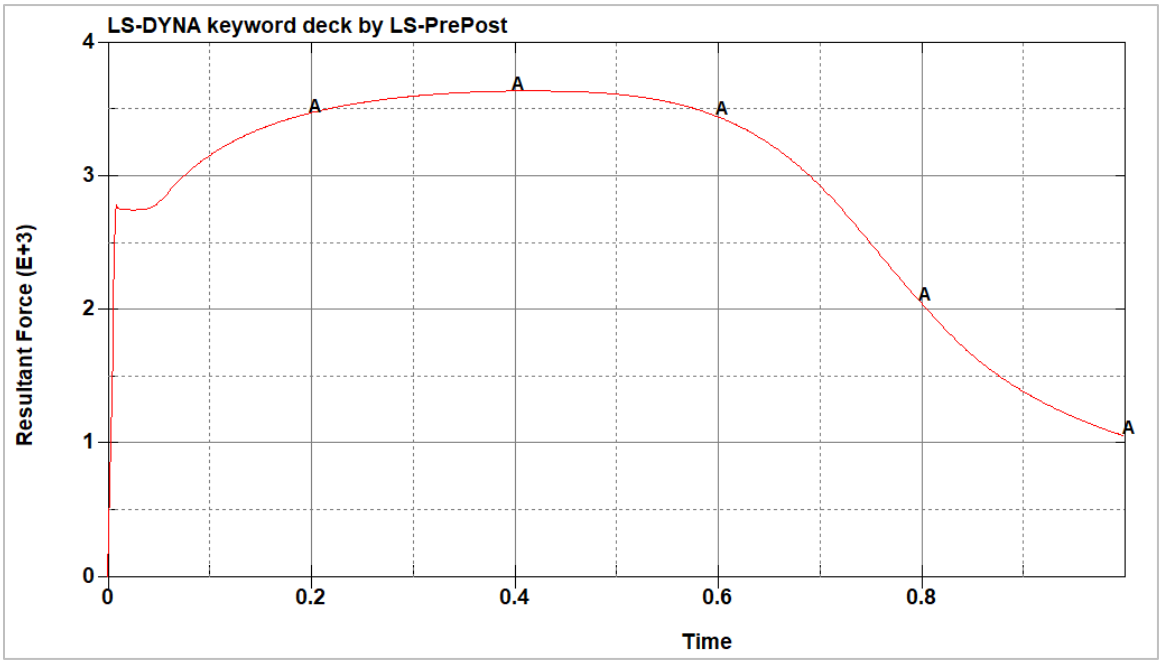

Figure B-10: Boundary Load Time-History Plot

Next, the displacement at the appropriate node where the extensometer would be attached can be recorded. First, interrogate the model and determine the ID of the node at the appropriate location, as discussed in Appendix Section B.3.3.2. Then, select “MFPost” and “History” to access the history data for the model. Next, select the “Nodal” radio button, select the appropriate displacement quantity (e.g., “X-displacement”), input the

appropriate node ID into the “ID” field of the “Sel.Nodes(0)” pop-up window, and click the “New” button to plot the history in a new window (allowing the force-history window to remain open). An example plot of a displacement time-history from LS-DYNA developed using this approach is provided in Figure B-11. Note that the displacement is nearly linear as this point is outside of the necked region. Thus, the point selected sees only minor deviation from perfectly linear translation due to the elastic deformations of the coupon that occur between the point of imposed displacement at the grip end and the point at which displacements are interrogated.

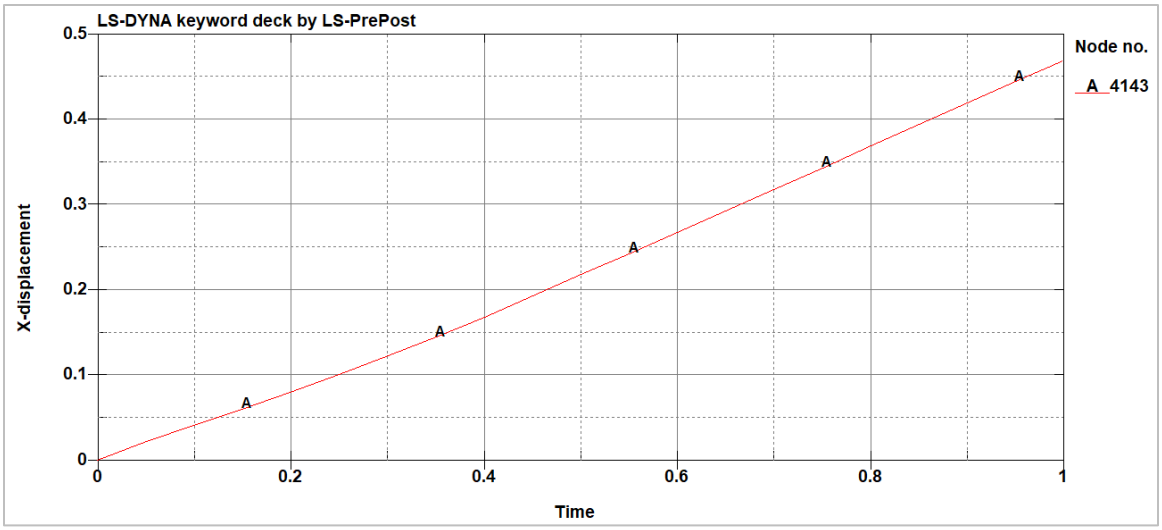

Figure B-11: Nodal Displacement Time-History Plot

Finally, the two time-histories can be cross-plotted to generate a load-displacement history for the coupon that is analogous to the load-displacement history measured in the physical coupon tension test. This cross-plotting is done by first selecting “MFPost” and then “XYPlot”. Next, in the pop-up XY Plot window select the “Window” radio button, and the “Cross” radio button. Then, select the force data for the Y-axis and displacement data for the X-axis and click “New” to generate a new plot of the force-displacement history. A sample cross-plot of the force and displacement history developed using this

approach is presented in Figure B-12. This information should be reviewed as part of the model interrogation process. If it appears reasonable, output for further interrogation and manipulation outside of LS-PrePost is recommended.

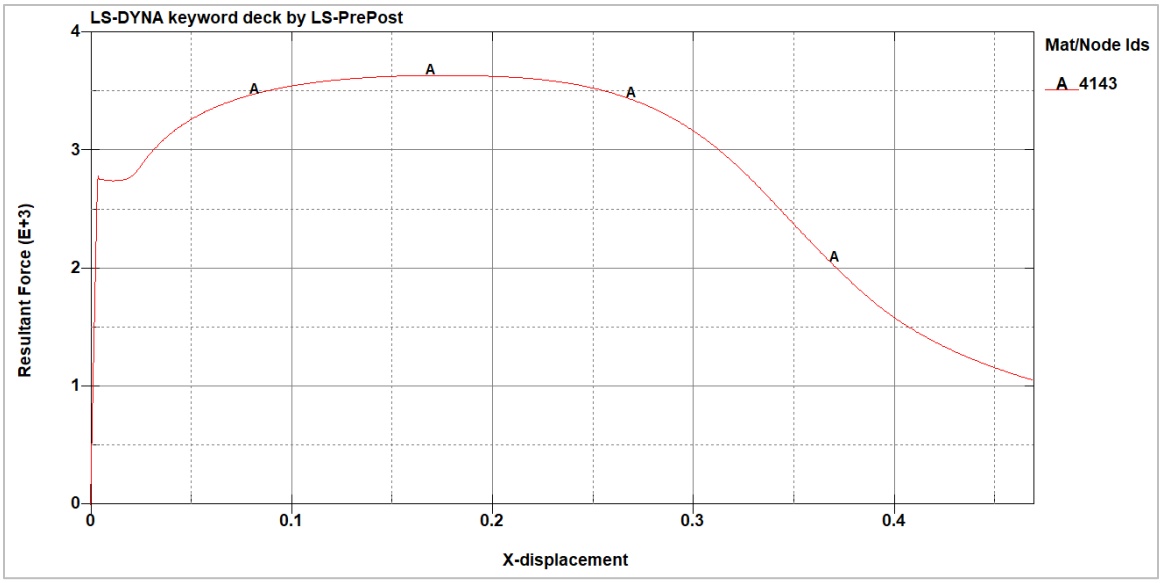

Figure B-12: Force-Displacement History Plot

B.9 FRACTURE

While a detailed discussion of fracture is beyond the scope of this dissertation, fracture can be quickly incorporated into the FEA model by adding a value for the "fail" parameter in the **MAT_24* material model definition. For example, the following code block defines the effective plastic strain at failure to 0.90. Section of an appropriate failure strain is described later in this section. When any element predicts a strain equal to or greater than this threshold, it will be deleted from the model. Once deleted, stresses are redistributed to the surrounding elements. Initial element failure and erosion generally rapidly precipitates failure in the remainder of the critical section. This is discussed in additional detail in Section 5.4.

```
*MAT_PIECEWISE_LINEAR_PLASTICITY
$ MATERIAL MODEL DEFINITION WITH EROSION STRAIN DEFINED AT 90% PLASTIC STRAIN
$#     mid        ro         e        pr      sigy      etan      fail      tdel
       "X"   7.33E-4 2.9000E+7     0.300                          0.90     0.000
$#       c         p      lcss      lcsr        vp
         0         0    "LCID"
```

When applying an effective plastic strain at failure in a coupon tension model to capture fracture, the model should be first run with an artificially high value for this parameter (e.g., a failure strain of 1e+20), to ensure that this erosion criterion is not exceeded. Then, the model can be interrogated to determine the maximum plastic strain occurring at the deformation associated with failure of the experimental coupon. This maximum strain should occur at the center element at the intersection of the three symmetry conditions in an eighth symmetry model, highlighted in Figure B-13 and discussed in Section 5.4. Then, this maximum strain can be input as the failure criterion in material model. The resulting model should then predict a rapid decrease in stress due to erosion of the elements at the critical section once this failure criteria is exceeded as shown in Figure B-14.

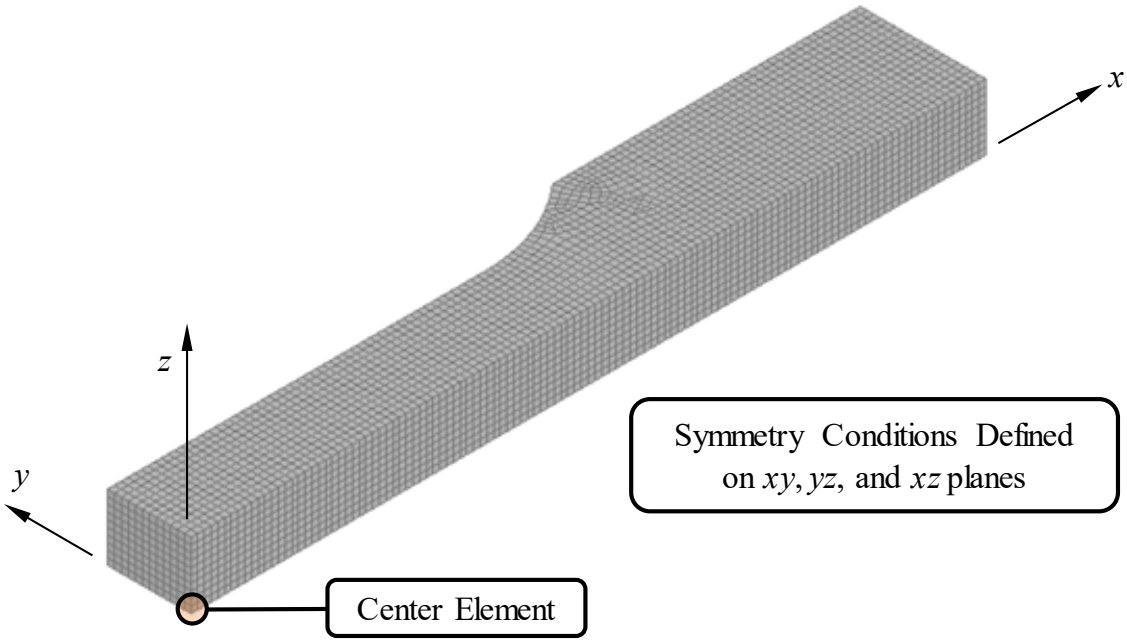

Figure B-13: Center Element Location

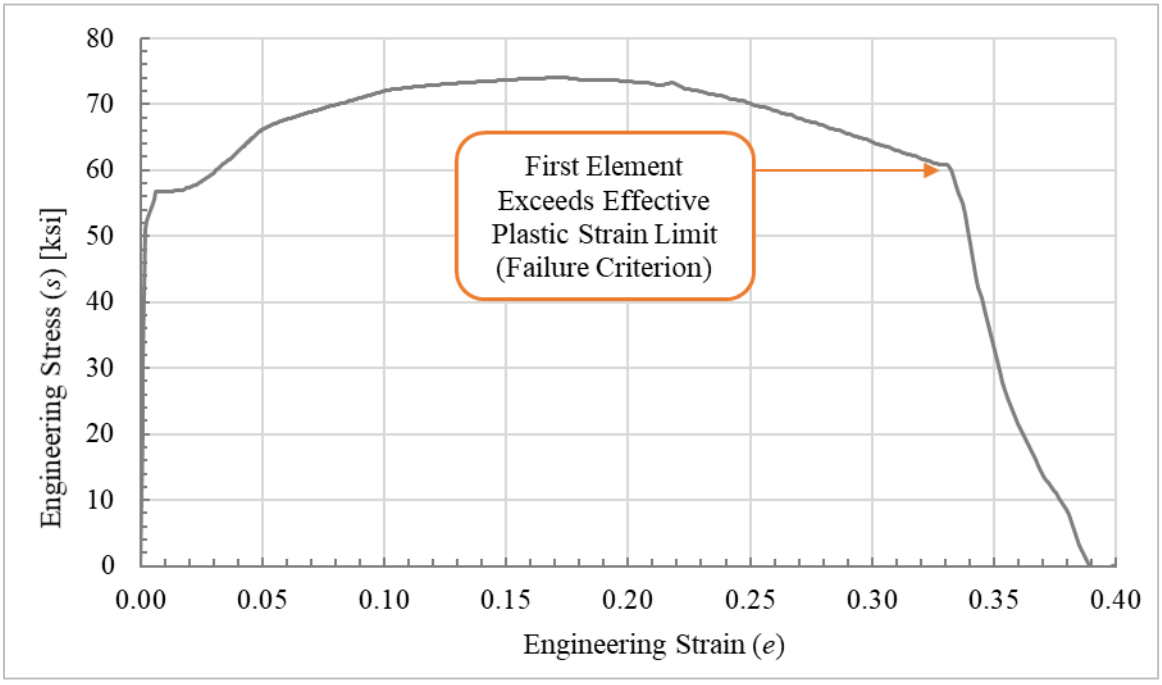

Figure B-14: Output from Model with Simple Effective Plastic Strain Failure Criterion

Alternatively, a failure model can be added to a given material model using the **MAT_ADD_EROSION* keyword card or other similar built-in failure and erosion models. Refer to the *LS-DYNA Material Model Keyword Manual* (Livermore Software Technology Corporation, 2014) for additional information in applying failure criteria to finite element analysis models.

When using either of these approaches to capture tension failure—effective plastic strain at failure in **MAT_24* or **MAT_ADD_EROSION*—the effective plastic (true) strain at fracture will typically be quite high relative to the more commonly reported engineering strain at failure. For the example case shown in Figure B-14, the effective true plastic strain used to produce the plotted engineering stress-strain data was approximately 0.90. Furthermore, it is not uncommon for the fracture strain to be on the order of 100% (1.0) strain or more, particular for highly ductile metals like stainless steel.

It should also be noted that, while the proposed approach for including failure in a coupon tension model is simple to apply, the overly simplistic nature of this plastic strain failure criterion results in a failure to capture the true complexity of the interaction between states of stress and prediction of fracture. As reported across a range of research publications (Bridgman, 1952) (Zhang & Li, 1994) (T, 1998) (Wilsdorf, 1979) (Horstemeyer & Gokhale, 1999), failure has been shown to be dependent upon a range of variables including the state of stress, stress triaxiality, and lode parameter, among others. The observed strain at failure estimated from a tension test can be used as a single case in developing these more complex models. For example, in a plastic strain versus triaxiality failure definition, the uniaxial tension coupon model can be interrogated to determine the triaxiality at the onset of rupture, as shown in Figure B-15. This information can then be used to define a single point in that failure model. Similar approaches can be used in other more complex failure models and criteria.

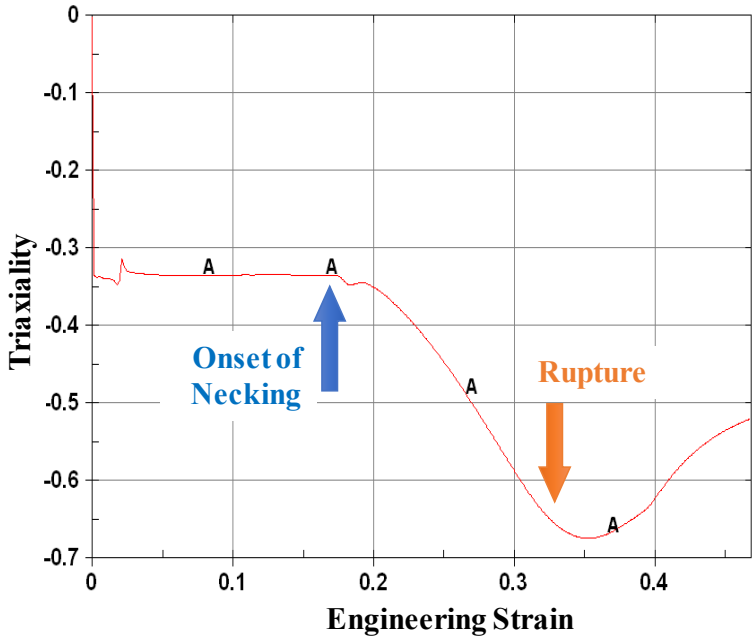

Figure B-15: Triaxiality vs. Strain Results Showing Onset of Necking and Rupture

While this is just one simple example of a more complex failure prediction approach that can be incorporated into FEA models, there are a range of failure models available. An excellent summary is provided in a DYNAmore presentation by Haufe et al. (Haufe, DuBois, Neukamm, & Feucht, 2011). For additional detailed information on failure criteria used in computational analysis of ductile metals, referenced the published work by Levanger (Levanger, 2012), Corona and Reedlunn (Corona & Reedlunn, 2013), or others.

B.10 CONCLUSIONS

This chapter included a brief summary of key steps and recommendations for developing a tension coupon model for developing the true stress-strain relationship in accordance with the recommended step-by-step approach presented in Chapter 4. These recommendations were followed and applied when developing the example case presented in Chapter 5 of this dissertation. While this chapter is not intended to provide a thorough

and complete description of the process, the goal is for it to provide adequate information and waypoints to guide a user through major steps of the process. More information on the use of LS-PrePost and LS-DYNA can be found across a range of sources including those previously referenced.

REFERENCES

Abbassi, F., Mistou, S., & Zghal, A. (2013). Failure Analysis based on Microvoid Growth for Sheet Metal during Uniaxial and Biaxial Tensile Tests. *Metals and Design*.

Aluminum Association. (2015). *Aluminum Design Manual.* Arlington, VA: Aluminum Association.

American Institute of Steel Construction. (2017). *Steel Construction Manual , 15th Ed.* Chicago, IL: AISC.

American Iron and Steel Institute. (2017). *Cold-Formed Steel Design Manual.* Washington, DC: AISI.

American Society for Testing and Materials. (2015). *ASTM A370-17a: Standard Test Methods and Definitions for Mechanical Testing of Steel Products.* West Conshohocken: ASTM.

American Society for Testing and Materials. (2016). *ASTM E8-16a: Standad Test Methods for Tension Testing of Metallic Materials.* West Conshohocken: ASTM.

American Society of Civil Engineers. (2016). *ASCE/SEI7-16 Minimum Design Loads and Associated Criteria for Buildings and Other Structures.* Reston, VA: ASCE.

Arasaratnam, P., Sivakumaran, K. S., & Tait, M. J. (2011). True Stress-True StrainModels for Structural Steel Elements. *International Scholarly Research Network: ISRN Civil Engineering, 2011*, 1-11.

Ashby, M. F., & Jones, D. R. (2006). *Engineering Materials: An Introduction to Microstructures, Processing and Design; Third Edition.* New York, NY: Butterworth-Heinemann.

Askeland, D. R., & Fulay, P. P. (2004). *Essentials of Materials Science and Engineering.* Belmont, California: Wadsworth Publishing Company Inc.

Askeland, D. R., Fulay, P. P., & Wright, W. J. (2011). *The Science and Engineering of Materials; Sixth Edition.* Stamford, Connecticut: Cengage Learning.

ASM International. (2002). *Atlas of Stress-Strain Curves; Second Edition.* Materials Park, Ohio: ASM International.

Avramovic-Cingara, G., Saleh, C. R., Jain, M. K., & Wilkinson, D. S. (2009). Void Nucleation and Growth in Dual-Phase Steel 600 during Uniaxial Tensile Testing. *Metallurgical and Materials Transactions, 40A*(December), 3117-3127.

Beer, F. P., Johnston, Jr., E. R., & DeWolf, J. T. (2002). *Mechanics of Materials: Third Edition.* New York: McGraw Hill.

Benzerga, A. A., Leblond, J.-B., Needleman, A., & Tvergaard, V. (2016). Ductile Failure Modeling. *International Journal of Fracture*, 29-80.

Boresi, A. P., & Schmidt, R. J. (2003). *Advanced Mechanics of Materials: Sixth Edition.* Hoboken: John Wiley & Sons, Inc.

Boyer, H. F. (1987). *Atlas of Stress-Strain Curves.* Metals Park, Ohio: ASM International.

Bridgman, P. W. (1952). *Studies in Large Plastic Flow and Fracture with Special Emphasis on the Effects of Hydrostatic Pressure.* McGraw.

Brockenbrough, R. L., & Merritt, F. S. (1972). *Structural Steel Designer's Handbook.* New York: McGraw-Hill, Inc.

Brünig, M. (1998). Numerical Analysis and Modeling of Large Deformation and Necking Behavior of Tensile Specimens. *Finite Element Analysis and Design, 28*, 303-319.

Cabezas, E. E., & Calentano, D. J. (2004). Experimental and Numerical Analysis of the Tensile Test using Sheet Specimens. *Finite Element Analysis and Design, 40*, 555-575.

Cadoni, E., & Forni, D. (2015). Strain Rate Effects on Reinforcing Steels in Tension. *EPJ Web of Conferences 94*.

Callister, Jr., W. D. (2007). *Materials Science and Engineering an Introduction: Seventh Edition.* New York: John Wiley & Sons, Inc.

Campbell, F. C. (2012). *Fatigue and Fracture - Understanding the Basics.* Materials Park, Ohio: ASM International.

Celentano, D. J., Cabezas, E. E., & Garcia, C. M. (2005). Analysis of the Bridgman Procedure to Characterize the Mechanical Behavior of Materials in the Tensile Test: Experiments and Simulation. *Journal of Applied Mechanics, 72*(January), 149-152.

Chen, W. H. (1971). Necking of a Bar. *International Journal of Solids Structures, 7*, 685-717.

Chen, Z., & Dong, X.-H. (2009). The GTN Damage Model Based on Hill'48 Anisotropic Yield Criterion and its Application to Sheet Metal Forming. *Computational Materials Science, 44*(3), 1013-1021.

Cheng, G., Hu, X. H., Choi, K. S., & Sun, X. (2017). Predicting Grid-Size-Dependent Fracture Strains of DP980 with a Microstructure-based Post-Necking Model. *International Journal of Fracture, 207*, 211-227.

Choung, J. M., & Cho, S. R. (2008). Study on True Stress Correction from Tensile Tests. *Journal of Mechanical Science and Technology, 22*, 1039-1051.

Considère, A. (1885). Annales des Ponts et Chaussées. *Annales des Ponts et Chaussées, 9*, 574-775.

Coppieters, S., & Kuwabara, T. (2014). Identification of Post-Necking Hardening Phenomena in Ductile Sheet Metal. *Experimental Mechanics, 54*, 1355-1371.

Coppieters, S., Cooreman, S., Sol, H., Van Houtte, P., & Debruyne, D. (2011). Identification of the Post-Necking Hardening Behavior of Sheet Metal by Comparison of the Internal and External Work on the Necking Zone. *Journal of Materials Processing Technology, 211*, 545-552.

Corona, E., & Reedlunn, B. (2013). *Sandia Report SAND2013-7989: A Review of Macroscopic Ductile Failure Criteria.* Albuquerque, NM: Sandia National Labroatories.

Courtney, T. H. (1990). *Mechanical Behavior of Materials.* New York: McGraw-Hill.

Crawford, J. E., Magallanes, J. M., & Lan, S. (2006). *Evaluation of the State of the Art Pertaining to Structural Steel Applications in Blast-Resistant Design.* Burbank: Karagozian & Case.

Davis, J. (2004). *Tensile Testing.* Materials Park: ASM International.

Dieter, Jr., G. E. (1961). *Mechanical Metallurgy.* New York: McGraw-Hill Book Company.

Drucker, D. C. (1959). A Definition of a Stable Inelastic Material. *ASME Journal of Applied Mechanics, 26*, 101-195.

Duan, X., Jain, M., Metzger, D. R., & Wilkinson, D. S. (2007). A Unified FiniteElement Analysis Approach for the Study of Postyielding Deformation Behavior of Formable Sheet Materials. *Journal of Pressure Vessel Technology, 129*, 689-697.

Garcia-Garino, C., Gabaldon, F., & Goicolea, J. M. (2006). Finite Element Analysis of the Simple Tension Test in Metals. *Finite Element Analysis and Design, 42*, 1187-1197.

Gurson, A. L. (1972). Continuum Theory of Ductile Rupture by Void Nucleation and Growth: Part I - Yield Criteria and Flow Rules for Porous Ductile Media. *Journal of Engineering Materials and Technology, 1977*(99), 2-15.

Hadjioannou, M. (2015). *Large-Scale Testing and Numerical Simulations of Composite Floor Slabs Under Progressive Collapse Scenarios.* University of Texas at Austin, Civil Engineering Department. Austin: University of Texas at Austin.

Haufe, A., DuBois, P., Neukamm, F., & Feucht, M. (2011). *DYNAmore | LS-DYNA Developer Forum.* Retrieved September 30, 2018, from https://www.dynamore.de/de/download/papers/forum11/entwicklerforum-2011/haufe-gissmo.pdf

Hayden, H. W., & Floreen, S. (1969). Observations of Localised Deformation during Ductile Fracture. *Acta Metall, 17*, 213-214.

Hayden, H. W., Moffatt, W. G., & Wulff, J. (1965). *The Structure and Properties of Materials: Vol. III Mechanical Behavior.* New York: Wiley.

Hill, R. (1952). On Discontinuous Plastic States, with Special Reference to Localized Necking in Thin Sheets. *Journal of the Mechanics and Physics of Solids, 1*, 19-30.

Hill, R. (1958). General Theory of Uniqueness and Stability in Elastic-Plastic Solids. *Journal of the Mechanics and Physics of Solids, 6*, 236-249.

Hill, R. (1961). Bifurcation and Uniqueness in Nonlinear Mechanics of Continua. In *Problems of Continuum Mechanics* (pp. 155-164). Philadelphia, PA: Society of Industrial and Applied Mathematics.

Horstemeyer, M. F., & Gokhale, A. M. (1999). A Void-Crack Nucleation Model for Ductile Metals. *International Journal of Solids and Structures, 36*, 5029-5055.

Hyun, H. C., Kim, M., Bang, S., & Lee, H. (2014). On Acquiring True Stress-Strain Curves for Sheet Specimens using Tensile Test and FE Analysis based on a Local Necking Criterion. *Journal of Material Research, 29*, 695-707.

International Code Council. (2018). *International Building Code.* Lenaxa, KS: ICC.

Jia, L.-J., & Kuwamura, H. (2014). Ductile Fracture Simulation of Structural Steels under Monotonic Tension. *Journal of Structural Engineering*(May).

Jia, N., Cong, Z. H., Sun, X., Cheng, S., Nie, Z. H., Ren, Y., . . . Wang, Y. D. (2009). An In Situ High-Energy X-ray Diffraction Study of Micromechanical Behavior of Multiple Phases in Advanced High-Strength Steels. *Acta Materialia, 57*, 3965-3977.

Joun, M., Choi, I., Eom, J., & Lee, M. (2007). Finite Element Analysis of Tensile Testing with Emphasis on Necking. *Computational Material Science, 41*, 63-69.

Joun, M., Eom, J., & Lee, M. (2008). A New Method for Acquiring True Stress-Strain Curves over a Large Range of Strains using a Tensile Test and Finite Element Method. *Mechanics of Materials, 40*, 586-593.

Kamaya, M., Kitsunai, Y., & Koshiishi, M. (2015). True Stress-Strain Curve Acquisition for Irradiated Stainless Steel including the Range Exceeding Necking Strain. *Journal of Nuclear Materials, 465*, 316-325.

Kim, J. H., Serpantié, A., Barlat, F., Pierron, F., & Lee, M. G. (2013). Characterization of the Post-Necking Strain Hardening Behavior using the Virtual Fields Method. *International Journal of Solids and Structures, 50*, 3829-3842.

Kontou, E., & Farasoglou, P. (1998). Determination of the True Stress-Strain Behavior of Polypropylene. *Journal of Materials Science, 33*, 147-153.

Kõrgesaar, M. (2015). Assumptions and reality: Stress states in uniaxial tension test. *Analysis and Design of Marine Structures*, 359-364.

LeRoy, G., Embur, J. D., Edwards, G., & Ashby, M. F. (1981). A Model of Ductile Fracture Based on the Nucleation and Growth of Voids. *Acta Metall, 29*, 1509-1522.

Levanger, H. (2012). *Simulating Ductile Fracture in Steel using the Finite Element Method: Comparison of Two Models for Describing Local Instability due to*

Ductile Fracture. Oslo, Norway: Faculty of Mathematics and Natural Sciences | University of Olso.

Li, S., Wang, T., Tan, Q., Li, R., Wang, Y., Wang, X., . . . Wang, Y. (2018). A Brittle Fracture Mechanism in Thermally Aged Duplex Stainless Steels Revealed by In Situ High-Energy X-ray Diffraction. *Materials Science & Engineering A, 739*, 264-271.

Lian, J., & Zhou, D. (1989). Diffuse Necking and Localized Necking under Plane Stress. *Material Science and Engineering, A111*, 1-7.

Ling, Y. (1996). Uniaxial True Stress-Strain after Necking. *AMP Journal of Technology, 5*, 37-48.

Livermore Software Technilogy Corporation. (May 2007). *LS-DYNA® Keyword User's Manual Volume I: Version 971.* Livermore, California: LSTC.

Livermore Software Technology Corporation. (2004). *LS-PrePost Training.* Livermore, California: 8th International LS-DYNA Users Conference Post Conference Training.

Livermore Software Technology Corporation. (2012). *LS-PrePost Online Documentation*. (LSTC) Retrieved November 11, 2018, from http://www.lstc.com/lspp/

Livermore Software Technology Corporation. (2014). *LS-DYNA® Keyword User's Manual Volume II Material Models: LS-DYNA R71 (revision: 5442).* Livermore, California: LSTC.

LS-DYNA Support. (2018). *Consistent Units*. (LSTC Inc. and DYNAmore GmbH) Retrieved November 10, 2018, from https://www.dynasupport.com/howtos/general/consistent-units

Luecke, W. E., McColskey, J. D., McCowan, C. N., Banovic, S. W., Fields, R. J., Foecke, T., . . . Gayle, F. W. (2005). *NIST NCSTAR 1-3D Federal Building and Fire Safety Investigation of the World Trade Center Disaster: Mechanical Properties of Structural Steels.* Washington, DC: U.S. Department of Commerce.

Majzoobi, G.-H., Fariba, F., Pipelzadeh, M. K., & Hardy, S. J. (2015). A new approach for the Correction of Stress-Strain Curves after Necking in Metals. *Journal of Strain Analysis, 50(2)*, 125-137.

Marshall, E. R., & Shaw, M. C. (1952). The Determination of Flow Stress from a Tensile Specimen. *Transactions of the American Society for Metals, 44*, 705-725.

Masud, A., & Chudnovsky, A. (1999). A Constitutive Model of Cold Drawing in Polycarbonates. *International Journal of Plasticity, 15*, 1139-1157.

McEvily, A. J. (2013). *Metal Failures: Mechanisms, Analysis, Prevention.* Hoboken, New Jersey: John Wiley & Sons, Inc.

Momoh, M. I., Donatus, U., & Alaneme, K. K. (2016). Fractographic Analysis of Tensile Failure in Dual Phase Medium Carbon Low Alloy Steels. *Journal of Physical Science, 27*(1), 103-110.

Möser, M. (1987). Chapter 15 - Fractography with the SEM (Failure Analysis). In *Materials Science Monographs 40: Electron Microscopy in Solid State Physics* (pp. 366-385). New York, New York: Elsevier.

Needleman, A. (1972). A Numerical Study of Necking in Circular Cylindrical Bars. *Journal of Mechanics and Physics of Solids, 20*, 111-127.

Needleman, A., & Rice, J. R. (1978). Limits to Ductility set by Plastic Flow Localization. In *Mechanics of Sheet Metal Forming* (pp. 237-267). New York, New York: Plenum Publishing Corporation.

Precision Kidd Steel Company, Inc. (2010). *The Cold Drawing Process for Steel Bars and Wire*. (Precision Kidd Steel Company, Inc.) Retrieved October 6, 2018, from https://www.precisionkidd.com/technology.htm

Rajendran, A. M. (1992). *WL-TR-92-4006 High Strain Rate Behavior of Metals, Ceramics, and Concrete.* Wright-Patterson Air Force Base, Ohio: Materials Directorate | Wright Laboratory | Air Force Systems Command.

Ramazani, A., Schwedt, A., Aretz, A., Prahl, U., & Bleck, W. (2013). Characterization and Modelling of Failure Initiationin DP Steel. *Computational Materials Science, 75*, 35-44.

Rice, J. R. (1976). The Localization of Plastic Deformation. *Theoretical and Applied Mechanics (Proceedings of the 14th International Congress on Theoretical and Applied Mechanics), 1*, 207-220.

Roylance, D. (2001). *Stress-Strain Curves.* Cambridge: Department of Materials Science and Engineering, Massachusetts Institute of Technology (MIT).

Scheider, I., Brocks, W., & Cornec, A. (2004). Procedure for the Determination of True Stress-Strain Curves from Tensile Tests with Rectangular Cross-Section Specimens. *Journal Of Engineering Materials and Technology, 126*, 70-76.

Scheyvaerts, F., & Pardoen, T. (2010). A New Model for Void Coalescence by Internal Necking. *International Journal of Damage Mechanics, 19*(January), 95-126.

Scheyvaerts, F., & Pardoen, T. (2010). A New Model for Void Coalescence by Internal Necking. *International Journal of Damage Mechanics, 19*, 95-126.

Shen, W. Q., & Jones, N. (1993). Uniaxial True Stress-True Strain Curve for a Ductile Metal. *Nuclear Engineering and Design, 140*, 153-158.

Sierakowski, R. L. (1997). Strain Rate Behaviors of Metals and Composites. *IFG.*

Steinbrunner, D. L., Matlock, D. K., & Krauss, G. (1988). Void Formation During Tensile Testing of Dual Phase Steels. *Metallurgical Transactions A, 19A*(March), 579-589.

Structural Stability Research Council. (2010). SSRC Technical Memorandum No. 1: Tension Testing. In *Guide to Stability Design Criteria for Metal Structures, Sixth Edition* (pp. 1002-1006). Hoboken, New Jersey: John Wiley & Sons, Inc.

Sun, X., Choi, K. S., Liu, W. N., & Khaleel, M. A. (2009). Predicting Failure Modes and Ductility of Dual Phase Steels using Plastic Strain Localization. *International Journal of Plasticity, 25*, 1888-1909.

Swift, H. W. (1952). Plastic Instability Under Plane Stress. *Journal of the Mechanics and Physics of Solids, 1*, 1-18.

T, P. F. (1998). A View on Ductile-Fracture Modeling. *Fatigue & Fracture of Engineering Materials & Structures, 21*, 1105-1122.

Tao, H., Zhang, N., & Tong, W. (2009). An Iterative Procedure for Determining Effective Stress-Strain Curves for Sheeet Metals. *International Journal of Mechanical Material Design, 5*, 13-27.

Tardif, N., & Kyriakides, S. (2012). Determination of Anisotropy and Material Hardening for Aluminum Sheet Metal. *International Journal of Solids and Structures, 49*, 3496-3506.

Tegart, W. (1966). *Elements of Mechanical Metallurgy.* New York, New York: Collier-Macmillan.

Thieme, C. (2016). *Whitepaper: How to Create a Good Quality FE Model.* MSC Software.

Thomson, R. D. (1985). *Ductile Fracture by Void Nucleation, Growth and Coalescence.* The University of Glasgow.

Tipper, C. F. (1949). The Fracture of Metals. *Metallurgia, 39*, 133-137.

Tuğcu, P., & Neale, K. W. (1987). Necking and Neck Propagation in Polymeric Materials under Plane-Strain Tension. *International Journal of Solids Structures, 23*(7), 1063-1085.

Tvergaard, V. (1981). Influence of Voids on Shear Band Instabilities under Plane Strain Conditions. *International Journal of Fracture, 17*, 389-407.

Tvergaard, V. (1982). On Localisation in Ductile Materials Containing Spherical Voids. *International Journal of Fracture, 18*, 237-252.

Tvergaard, V., & Needleman, A. (1984). Analysis of the Cup-Cone Fracture in a Round Tensile Bar. *Acta Metallurgica, 32*(1), 157-169.

Tvergaard, V., Needleman, A., & Lo, K. K. (1981). Flow Localization in the Plane Strain Tensile Test. *Journal of the Mechanics and Physics of Solids, 29*(2), 115-142.

Ugural, A. C., & Fenster, S. K. (2003). *Advanced Strength and Applied Elasticity: Fourth Edition.* Upper Saddle River: Prentice Hall.

Wang, W., Ma, Y., Yang, M., Jiang, P., Yuan, F., & Wu, X. (2018). Strain Rate Effect on Tensile Behavior for a High Specific Strength Steel: From Quasi-Static to Intermediate Strain Rates. *MDPI Metals*.

Wang, Y. D., & Ren, Y. (2007). *Investigations of Mechanical Behaviors of High-Strength Steel by Synchrotron High-Energy X-ray Diffraction Technique.* Technical Report to the Pacific Northwest National Laboratory.

Wang, Y.-d., Xu, S.-h., Ren, S.-b., & Wang, H. (2016). An Experimental-Numerical Combined Method to Determine the True Constitutive Relation of Tensile Specimens after Necking. *Advances in Materials Science and Engineering, 2016*, 1-12.

Ward, I. M., & Sweeney, J. (2013). *Mechanical Properties of Solid Polymers: Third Edition.* West Sussex, United Kingdom: John Wiley & Sons Ltd.

Wilsdorf, H. F. (1979). The Ductile Fracture of Metals: A Microstructural Viewpoint. *Material Science and Engineering, 59*, 1-39.

Wouters, R., & Froyen, L. (1996). Scanning Electron Microscope Fractography in Failure Analysis of Steels. *Materials Characterization, 36*, 357-364.

Zhang, K. S., & Li, Z. H. (1994). Numerical Analysis of the Stress-Strain Curve and Fracture Initiation for Ductile Material. *Engineering Fracture Mechanics, 49*(2), 235-241.

Zhang, Z. L., Hauge, M., Ødegard, J., & Thaulow, C. (1999). Determining Material True Stress-Strain Curve from Tensile Specimens with Rectangular Cross-Section. *International Journal of Solids and Structures, 36*, 3497-3516.

Zhu, Y. (2017). *Studies on Strain Localization, Ductile Fracture and Damage in Structural Metals.* University of Texas at Austin.